Development of Techniques for Time-Lapse Imaging of the Dynamics of Glial-Axonal Interactions in the Central Nervous System

Kalliopi Ioannidou BSc (Hons), MSc (Hons)

A thesis submitted in fulfilment of the requirements of the University of Glasgow for the degree of Doctor of Philosophy

College of Medical, Veterinary and Life Sciences

Institute of Infection, Immunity and Inflammation

University of Glasgow

May 2012

“Δῶς μοι πᾶ στῶ καὶ τὰν γᾶν κινάσω”

“Give me a place to stand and a lever long enough and I will move the world”

Archimedes, 220 BC

Acknowledgements

Completing my PhD degree is probably the most challenging and an unforgettable experience so far. Well, the list of the people I want to thank will not fit to a single Acknowledgement section. It would not have been possible to write this doctoral thesis without the help and support of the kind people around me, to only some of whom it is possible to give particular mention here.

I would like to express my deep and sincere gratitude to my primary supervisor, Professor Sue Barnett for the opportunity she offered me to join her active group. I am very much thankful to her for picking me up as a student at the critical stage of my PhD. I would like to gratefully acknowledge her enthusiastic supervision during this work. She provided the vision, valuable suggestions and direction necessary for me to proceed through my PhD. But this thesis would not have been possible without the help, guidance and patience of my second supervisor, Dr Julia Edgar. She did not only teach me many things in the lab but also she gave me the inspiration to always improve. Her good advice and deep knowledge, has been invaluable on both an academic and a personal level. She was and remains my best role model for a scientist, mentor and teacher.

I warmly thank Professor Kurt Anderson for guiding my first steps in Imaging, the insightful discussions, his feedback and for always being there when I needed his help. I am deeply grateful to David Strachan for his essential assistance with image analysis, the experimental setup and technical issues on multiphoton microscopy. His endless sense of humour helped me a lot to work for hours together tirelessly. I would like to thank Dr Ewan McGhee for his valuable help on image analysis. I am also extremely indebted to Tom Gilbey and Margaret O' Prey for their advice on image acquisition and to Jonathan Coles for advice on *ex vivo* imaging. My special thanks go to Iain White for his technical help and suggestions in formatting the entire thesis. I would also like to thank Professor Chris Linington for his positive feedback, critical review comments and useful advice throughout my PhD.

This list is incomplete without acknowledging all my colleagues of the Glial Biology and Applied Neurobiology Group and especially Susan, Besma, Jen, Rebecca, Hulya, Gemma, Jennifer and Fredrik for not only providing a stimulating and fun-filled environment, but for their constant support and above all for their genuine friendship. I would also like to extend huge, warm thanks to my current colleagues in Radiation Oncology, Colin, Sharon

and Mathias for their understanding, help and advice on my thesis. This thesis would also not be possible without the love and support of many Glasgow-friends who made me feel at home away from home.

Last but not least, I wish to thank my Mum and Dad for encouraging me to reach for my dreams. Their love provided my inspiration and was my driving force. I owe them everything.

I dedicate this thesis to my parents and my loving brother.

Author's Declaration

I declare that, except where explicit reference is made to the contribution of others, this dissertation is the result of my own work and has not been submitted for any other degree at the University of Glasgow or any other institution.

Signature

Printed name

Abstract

Background: Myelination is an exquisite and dynamic example of heterologous cell-cell interaction, which consists of the concentric wrapping of multiple layers of oligodendrocyte membrane around neuronal axons. Understanding the mechanism by which oligodendrocytes ensheath axons may bring us closer to designing strategies to promote remyelination in demyelinating diseases. The main aim of this study was to follow glial-axonal interactions over time both *in vitro* and *ex vivo* to visualise the various stages of myelination.

Methodology/Principal findings: Two approaches have been taken to follow myelination over time i) time-lapse imaging of mixed CNS myelinating cultures generated from mouse spinal cord to which exogenous GFP-labelled murine cells were added, and ii) *ex vivo* imaging of the spinal cord of *shiverer* (*Mbp* mutant) mice, transplanted with GFP-labelled murine neurospheres. The data demonstrate that oligodendrocyte-axonal interactions are dynamic events with continuous retraction and extension of oligodendroglial processes. Using cytoplasmic and membrane-GFP labelled cells to examine different components of the myelin-like sheath, evidence from time-lapse fluorescence microscopy and confocal microscopy suggest that the oligodendrocytes' cytoplasm-filled processes initially spiral around the axon in a corkscrew-like manner. This is followed subsequently by focal expansion of the corkscrew process to form short cuffs which then extend longitudinally along the axons. From this model it is predicted that these spiral cuffs must extend over each other first before extending to form internodes of myelin.

Conclusion: These experiments show the feasibility of visualising the dynamics of glial-axonal interaction during myelination over time. Moreover, these approaches complement each other with the *in vitro* approach allowing visualisation of an entire internodal length of myelin and the *ex vivo* approach validating the *in vitro* data.

Table of Contents

Acknowledgements ii

Author's Declaration iv

Abstract v

1. Introduction 1

1.1 Central Nervous System: Cells and Structures 1

1.2 Why myelin is important 1

1.3 The beginning of the concept of glial cells 2

1.4 Astrocytes 3

1.5 Oligodendrocytes 5

1.5.1 Origin and Differentiation 6

1.5.2 Developmental stages of the oligodendrocyte lineage 8

1.6 Role of CNS glia in axonal integrity and trophic support 13

1.7 Myelin: Anatomy of an insulating sheath 15

1.7.1 Myelin lipids 16

1.7.2 Systemic analysis of the CNS myelin protein composition 17

1.8 White matter disorders: leukodystrophies and multiple sclerosis 19

1.9 Basic Structural analysis of the myelin sheath in the CNS 20

1.10 Classical electron microscopic studies on the relationship between axons and oligodendrocytes during initial ensheathment and myelination 21

1.10.1 Oligodendroglial ensheathment of axons 22

1.10.2 Initial stages of myelination from further electron microscopy studies 24

1.11 First studies using time-lapse imaging: a reliable approach to follow oligodendrocytes ensheathment and initial stages of myelination *in vitro* 26

1.12 Use of fluorescence technology and confocal microscopy to study myelination *in vivo* 29

1.12.1 Confocal microscopy 29

1.12.2 Multiple-photon Excitation Fluorescence Microscopy 29

1.12.3 Advantages of multiphoton imaging 31

1.12.4 Limitations of multiphoton imaging 32

1.12.5 Use of Transgenic animal models to study myelination 33
1.13 *In vivo* imaging of the mouse spinal cord 35
1.14 Proposed models of myelination.....36
1.15 Regulation of oligodendrocytes' myelination potential.....39
1.16 *In vitro* Modelling of CNS Myelination 41
1.17 Mutant/Transgenic Mice.....43
1.18 *shiverer (shi)* mice 43
1.19 Identification of stem cells grown as neurospheres 45
1.20 Hypothesis 46
1.21 Aim of thesis.....46
2. Methods and Materials.....47
2.1 Animals-Animal Care.....47
2.2 Breeding Transgenic mice.....47
2.2.1 *Shiverer (shi/shi)* mice 48
2.3 Imaging neurons and glial cells in transgenic mice expressing multiple spectral variants of GFP 49
2.4 Isolation and culture of GFP-labelled and wild type neurospheres.....50
2.5 Astrocytes derived from neurospheres 51
2.6 Myelinating cultures.....52
2.7 Time-lapse.....53
2.8 PLL-coated coverslips.....54
2.9 Preparation of APES [3(aminopropyl)triethoxysilane]-coated slides 54
2.10 Quantitative analysis of axonal density 54
2.11 Myelin quantification.....55
2.12 Infection of wild type neurospheres with lentiviruses.....55
2.12.1 Description of fGFP:.....57
2.12.2 Viral vector production 58
2.13 Transplantation of spinal cord neurospheres 59
2.13.1 Anaesthesia 59
2.13.2 Laminectomy.....60

2.13.3 Recovery after Surgery 61

2.14 Tissue processing and immunohistochemistry 64

2.15 Immunohistochemistry and antibodies for myelinating cultures 65

2.16 Maintaining live cells for time-lapse imaging 69

2.17 Maintenance of the explants for *ex vivo* imaging 69

2.18 Stabilisation of the spinal cord for imaging with multiphoton microscope 70

2.19 Detailed image analysis 71

2.20 Confocal imaging 71

2.21 Imaging using multiphoton microscopy 76

2.22 Time-lapse microscopy 77

2.23 *In vivo* imaging after transplantation of GFP-labelled neurospheres into *shiverer* mice 78

2.24 Statistics 79

2.25 Neurosphere media preparation 80

2.26 Setting up the theatre for surgery 82

3. Assessment of the stages of glial-axonal interactions culminating in myelination in mouse mixed spinal cord cell cultures 84

3.1 Introduction 84

3.1.1 Background 84

3.1.2 Aims of the chapter 87

3.2 Materials and Methods 88

3.2.1 Myelinating cultures 88

3.2.2 Astrocytes derived from neurospheres 88

3.2.3 Infection of wild type neurospheres with lentiviruses 89

3.2.4 Time-lapse imaging 89

3.3 Results 91

3.3.1 Characteristics of mouse myelinating cultures after fixation and immunostaining 91

3.3.2 Assessment of initial contact between oligodendrocytes and neurites in fixed cultures 93

3.3.3 The oligodendroglial-axonal unit in fixed cultures 95

3.3.4 Structural observations of initial and intermediate stages of ensheathment as assessed in fixed cultures 97

3.3.5 Visualisation of the stages of myelination after the addition of cytoplasmic GFP labelled cells in fixed cultures 99

3.3.6 Assessment of later stages of ensheathment of the axon with oligodendrocyte processes in fixed cultures 104

3.3.7 Details of myelin assembly assessed in fixed cultures 105

3.3.8 Disposition of Caspr in the node of Ranvier in wild type myelinating cultures with exogenous cGFP-lebelled cells is observed in fixed cultures 108

3.3.9 Time-lapse visualisation of a GFP-positive process along an axonal fascicle... 111

3.3.10 Visualisation of oligodendrocyte-oligodendrocyte interactions using time-lapse 113

3.3.11 Visualisation of glial-axonal contact *in vitro* using time-lapse imaging.....113

3.3.12 Elongation of a neurosphere-derived labelled cell.....116

3.4 Discussion 119

4. Time-lapse imaging of the dynamics of glial-axonal interactions after the addition of GFP-expressing neurospheres into *shiverer* myelinating cultures.....124

4.1 Introduction 124

4.1.1 Background 124

4.1.2 Aims of the chapter 126

4.1.3 Materials and Methods 127

4.2 Results 128

4.2.1 Visualisation of cGFP-expressing oligodendroglia-like cells in *shiverer* myelinating cultures 128

4.2.2 *In vitro* time-lapse imaging of OPCs in *shiverer* myelinating cultures 130

4.2.3 Assessment of the close contact between the exogenous cGFP cells with the *shiverer* axons 132

4.2.4 *In vitro* time-lapse of cGFP oligodendrocyte-like cells in *shiverer* cultures 134

4.2.5 *In vitro* time-lapse of fGFP-expressing cells into *shiverer* myelinating cultures 136

4.2.6 *In vitro* time-lapse imaging of assembly of myelin-like membrane using fGFP-labelled neurospheres 138

4.2.7 *In vitro* time-lapse imaging of myelin-like sheath formation using fGFP-labelled cells....142

4.2.8 *In vitro* time-lapse imaging of the membrane changes of fGFP-positive cells....145

4.2.9 *In vitro* time-lapse imaging of membrane extension over *shiverer* axons...148

4.2.10 *In vitro* time-lapse imaging of fGFP-positive oligodendrocyte-like cells and its membrane protrusions....149

4.2.11 *In vitro* time-lapse imaging of fGFP and cGFP-dsRed-positive oligodendroglial-like cells....153

4.3 Discussion....156

5. Multiphoton imaging of transplanted cGFP neurospheres into the fixed spinal cord of *shiverer* mice....160

5.1 Introduction....160

5.1.1 Background....160

5.1.2 Aims of the chapter....162

5.1.3 Materials and Methods....163

5.2 Results....165

5.2.1 Multipotential ability of striatum-derived neurospheres to generate glial cells....165

5.2.2 Transplantation of cGFP neurospheres into the non-labelled hypomyelinated tracks of *shiverer* mouse....167

5.2.3 Imaging of a fixed spinal cord 3, 7 and 14 days post-transplantation of cGFP neurospheres using multiphoton microscopy....170

5.2.4 The complex morphology of cGFP-positive cells can be discerned using multiphoton microscopy of fixed spinal cord....172

5.2.5 cGFP neurospheres survived, integrated and differentiated into glial cells in the white matter of the *shiverer* mouse spinal cord....175

5.2.6 Myelin-like sheaths were produced by cGFP transplanted cells in the spinal cord of *shiverer* mice....179

5.2.7 Time-course analysis of the myelination capacity of the transplanted cells 3, 8, 14 and 28 days post-transplantation....181

5.2.8 Distribution of the cGFP transplanted neurospheres into the spinal tissue of *shiverer* mouse....183

5.2.9 Examination of tissue sections of imaged spinal cord....186

5.3 Discussion....188

6. *Ex vivo* studies of the dynamics of the glial-axonal interactions in the CNS 192

6.1 Introduction 192

6.1.1 Background 192

6.1.2 Aims of the chapter 194

6.1.3 Materials and Methods 195

6.2 Results 197

6.2.1 *Ex vivo* imaging of cGFP neurospheres after transplantation into *shiverer* mice 197

6.2.2 *Ex vivo* time-lapse of cGFP-expressing cells revealed their dynamic behaviour 199

6.2.3 *Ex vivo* time-lapse of cGFP transplanted cells showed changes in distribution and intensity of the GFP signal 201

6.2.4 *Ex vivo* imaging of cGFP-labelled cells resembling oligodendrocytes using two-photon microscopy 203

6.2.5 *Ex vivo* time-lapse of fGFP-transplanted cells into *shiverer* spinal cord 205

6.2.6 Next step: Visualisation of axons in the dorsal columns of the spinal cord of *Thy1*-CFP mouse 207

6.2.7 Establishing parameters for simultaneous visualisation of CFP and cGFP .209

6.2.8 *Ex vivo* imaging of GFP-labelled cells after transplantation into the white matter of *Thy1*-CFP**shi/shiv* mice 211

6.2.9 *Ex vivo* time-lapse of glial-axonal interactions between cGFP-labelled cells and CFP-positive axons 212

6.2.10 *Ex vivo* time-lapse of fGFP-labelled cells after transplantation into the spinal cord of *Thy1*-CFP**shi/shiv* mice 216

6.2.11 *In vivo* imaging of the dynamics of cGFP-transplanted cells after transplantation into the spinal cord of *shiverer* nice 217

6.3 Discussion 220

7. Discussion 224

Future work 232

Aim 1: How do novel myelin gene mutations affect the dynamic stages of early glial-axonal interaction?.....232

Aim 2: Identification of the mechanism of wave formation and membrane rafts.....233

Aim 3: Can wave formation be visualised in live imaging of a mouse?.....233

References.....236

List of Figures

Figure 1.1 Schematic of an oligodendrocyte extending many processes.....5

Figure 1.2 Schematic representation of the developmental stages of cells of the oligodendrocyte lineage 12

Figure 1.3 Schematic depiction of an oligodendrocyte myelinating an axon 18

Figure 1.4 a-f Schematic illustrations suggesting the origin and direction of a vermicular process by interruption of the smooth axial flow of the ensheathing cytoplasm. 23

Figure 1.5 Schematic representation of an E-type glial unit 25

Figure 1.6 Schematic representation of the mechanism of myelin-sheath formation by the oligodendrocyte plasma membrane.....28

Figure 1.7 Fluorophore excitation in multiphoton microscopy 30

Figure 1.8 Imaging fluorescent proteins using laser-scanning microscopy.....32

Figure 1.9 Two models of myelination 38

Figure 2.1 *Shiverer* mouse 48

Figure 2.2 Emission and excitation spectra.....50

Figure 2.3 Schematic drawing of the plasmid vector construct used in this study 56

Figure 2.4 Preparation of the theatre 59

Figure 2.5 Laminectomy and Injection 61

Figure 2.6 *shiverer* recover quickly after the surgery 62

Figure 2.7 Perfusion of a mouse 64

Figure 2.8 Maintenance and superfusion of explants for *ex vivo* imaging.....70

Figure 2.9 Emission and excitation spectra of fluorophores used 74

Figure 2.10 Nikon (TE2000) time-lapse inverted microscope. 78

Figure 3.1 Wild type neurospheres infected with lentivirus carrying the GFP-IRES-dsRed gene 90

Figure 3.2 Myelination in mouse culture is slightly enhanced when spinal cord cells are plated on an astrocyte monolayer.....92

Figure 3.3 Static observations of initial glial-axonal contact using fluorescent microscopy... 94

Figure 3.4 Static images of myelination from mouse cultures using differentiation markers and confocal microscopy.....96

Figure 3.5 *In vitro* observations of initial and intermediate stages of ensheathment.....98

Figure 3.6 cGFP labelled neurospheres differentiated into cells with a typical morphology of an oligodendroglial cell 101

Figure 3.7 3D reconstructed images to examine the morphology of PLP/DM20-positive membrane domains 102

Figure 3.8 cGFP labelled neurospheres generated oligodendrocytes which produce a spiralled cell process around neurites 103

Figure 3.9 Examination of the cGFP-positive oligodendroglial processes at later time points *in vitro* 106

Figure 3.10 Evidence that oligodendrocytes form spiral processes around neurites 107

Figure 3.11 Distribution of cGFP expression on either side of a presumptive node of Ranvier 109

Figure 3.12 Caspr disposition at glial-axonal contact.....110

Figure 3.13 Time-lapse visualisation of a GFP-positive process along an axonal fasicle..... 112

Figure 3.14 Two or more oligodendrocyte-like cells contacting the same neurite bundles or different neurite bundles, appeared to make contact with each other on the same or either side of the axons, remodelling their processes.....114

Figure 3.15 Time-lapse imaging of glial-axonal interaction.....115

Figure 3.16 Time-lapse imaging of a cell process' elongation 117

Figure 4.1 Time-lapse imaging of cGFP-positive OPC-like cells added to *shiverer* myelinating cultures.....129

Figure 4.2 *In vitro* time-lapse imaging of cGFP labelled OPC-like cells in *shiverer* myelinating cultures reveal dynamic cellular interactions.....131

Figure 4.3 Bright field time-lapse imaging of cGFP-positive OPC-like cells in *shiverer* myelinating cultures 133

Figure 4.4 Time-lapse imaging of cGFP oligodendrocyte-like cells in *shiverer* myelinating cultures 135

Figure 4.5 Time-lapse of fGFP-positive membranous flap 137

Figure 4.6 Imaging of fGFP-positive membranous features in *shiverer* myelinating cultures 139

Figure 4.7 Time-lapse imaging of the putative assembly of myelin membrane 141

Figure 4.8 Time-lapse imaging of myelin-like sheath formation from exogenous fGFP-positive neurospheres 143

Figure 4.9 Time-lapse imaging of the elongation of a putative fGFP labelled myelin-like sheath 144

Figure 4.10 Time-lapse imaging of myelin-like sheath extension. 145

Figure 4.11 Time-lapse imaging of membrane extension of fGFP-positive cells 147

Figure 4.12 Time-lapse imaging of membrane extension.....150

Figure 4.13 Time-lapse imaging of membrane protrusions of fGFP-positive cells in *shiverer* cultures 152

Figure 4.14 Time-lapse imaging of fGFP and cGFP-dsRed-positive oligodendroglial-like cells 154

Figure 5.1 Neurospheres differentiated into glial cells when cultured in differentiation medium *in vitro* 166

Figure 5.2 Detection of cGFP-expressing cells at the point of transplantation using the OV100 microscope.....168

Figure 5.3 Transplanted cGFP-positive cells populated the spinal cord dorsal columns ..169

Figure 5.4 Transplanted cGFP-positive neurospheres survived and acquired a differentiated morphology 171

Figure 5.5 Morphological comparison of the differentiation of cGFP transplanted cells at increasing times post-transplantation 174

Figure 5.6 cGFP-positive transplanted cells expressed markers of the oligodendroglial lineage 7 and 14 days post-transplantation 176

Figure 5.7 cGFP-positive transplanted cells near the transplantation site differentiated into astrocytes 177

Figure 5.8 Expression of the GFAP marker in relation to the injection site.....178

Figure 5.9 Immunohistochemistry of transplanted neurospheres showed that cGFP - positive cells differentiate into oligodendroglia.....180

Figure 5.10 Immunohistochemistry of transplanted cGFP cells showed different stages in MBP expression 182

Figure 5.11 Distribution of cGFP-positive transplanted cells in the *shiverer* spinal tissue 15 days post-transplantation.....184

Figure 5.12 cGFP-expressing cells' topography 15 days post-transplantation.....185

Figure 5.13 Transplanted cells were found throughout the dorsal columns of the transplant recipient 186

Figure 5.14 Transplanted cells associated with axons throughout the white matter of the transplant recipient. 187

Figure 6.1 *ex vivo* imaging of a spinal cord 14 days post-transplantation illustrated cGFP differentiated cells bearing complex morphology.....198

Figure 6.2 Time-lapse of ex vivo spinal cords revealed that exogenous cells were motile..... 200

Figure 6.3 Longer term time-lapse of an *ex vivo shiverer* spinal cord showed changes in the intensity signal of the cGFP-expressing cells 202

Figure 6.4 *ex vivo* imaging of cells resembling oligodendrocytes 10 days post-transplantation into a *shi/shi* spinal cord.....204

Figure 6.5 *ex vivo* time-lapse of fGFP-tagged cells after transplantation into *shiverer* spinal cord 206

Figure 6.6 e*x vivo* imaging of axons in the dorsal columns of the spinal cord of a *Thy-1* CFP-mouse using multiphoton microscopy 208

Figure 6.7 Simultaneous imaging of CFP-positive axons and cGFP-labelled cells 210

Figure 6.8 *ex vivo* imaging of spinal cords from Thy1-CFP*shi/shiv mice transplanted with cGFP and fGFP-labelled cells respectively.....212

Figure 6.9 *ex vivo* imaging of glial-axonal interactions 15 days post-transplantation into a *Thy1*-CFP**shi/shiv* mouse.....214

Figure 6.10 cGFP-labelled cells' processes were highly motile.....215

Figure 6.11 *ex vivo* imaging of fGFP-labelled cells and CFP-positive axons 8 days post-transplantation.....218

Figure 6.12 *in* vivo imaging of cGFP-labelled cells 9 days post-transplantation.....219

Figure 6.14 *Ex vivo* imaging of cGFP-labelled cells and CFP-positive axons 7 days post-transplantation.....222

Figure 7.1 Confocal images of transplanted cGFP-expressing cells in the shiverer spinal cord.....227

Figure 7.2 Schematic of initiate and intermediate stages of ensheathment.....231

List of Tables

Table 2.1 Primary antibody list.....67

Table 2.2 Secondary antibody list.....68

Table 2.3 Excitation (ex) and emission (em) of generally used fluorochromes in order of their ex wavelength.....75

Abbreviations

1D-UP-LC	1D ultra performance liquid chromatography
ALS	Amyotrophic lateral sclerosis
APES	3(aminopropyl)triethoxysilane
ASDs	autism spectrum disorders
BBB	blood brain barrier
CFP	cyan fluorescent protein
CNP	2',3'-cyclic nucleotide 3'-phosphodiesterase
CNS	central nervous system
CNTF	ciliary neurotrophic factor
DIV	days *in vitro*
DRG	dorsal root ganglia
EAE	experimental autoimmune encephalomyelitis
ECM	extracellular matrix
EGF	epidermal growth factor
FGF	fibroblast growth factor
FLIM	fluorescence lifetime imaging
GalC	galactosylceramides
GFAP	glial fibrillary acidic protein
GFP	green fluorescent protein
IGF-I	insulin-like growth factor-1
jp	myelin synthesis deficiency
LIF	leukemia inhibitory factor
LV	lentiviral
MAG	myelin associated glycoprotein
MAL	myelin and lymphocyte protein
MAPK	mitogen-activated protein kinase
MBP	myelin basic protein
MDL	major dense line

MOG	myelin oligodendrocyte glycoprotein
MS	multiple sclerosis
msd, A242V	*mjimpy-msd*
NAA	N-acetylaspartate
NRG1/III	neuregulin-1 type III
NSCs	neural stem cells
OPCs	oligodendrocyte progenitor cells
PDGF	platelet derived growth factor
PDGF-a	platelet-derived growth factor a-receptor
pEGFP-F	farnesylated enhanced green fluorescent protein
PI3K	phosphoinositide 3-kinase
PIP2	phosphatidylinositol 4,5-bisphosphate
PIP3	3,4,5-trisphosphate
PLL	Poly-L-Lysine
PLP/DM20	proteolipid proteins
PMD	Pelizaeus-Merzbacher disease
PNS	peripheral nervous system
pro-OL	pro-oligodendrocyte
qk.	quaking
rsh, I186T	*rumpshaker*
shi	*shiverer*
shiv/shiv	homozygous *shiverer* mice
SIRT2	NAD+-dependent deacetylase sirtuin 2
SNAREs	*N*-ethylmaleimidesensitive factor attachment protein receptor proteins
SPG-2	spastic paraplegia type 2
SQS	squalene synthase
SVZ	subventricular zone
T3	3,5,3-tri-iodothyronine
Tr	trembler
twi	twitcher

1. Introduction

1.1 Central Nervous System: Cells and Structures

The nervous system is the major communications network of the body. In all vertebrates, its normal function is exquisitely dependent on the maintenance of structural integrity, as well as a host of complex metabolic processes (Robbins et al 2005). As a key homeostatic regulatory and coordinating system, it detects, interprets, and responds to changes in internal and external stimuli. The brain and the spinal cord comprise the central nervous system (CNS) and the connecting nerve processes to effectors and receptors serve as the peripheral nervous system (PNS).

Two main cell types make up the CNS: the neurons, which are involved in electrical transmission and information processes and the glial cells. In all areas of the CNS the glial cells interact with neurons, having a dynamic role in development and in the normal function of the mature system. The term “glial cell” represents a broad category of cells that comprises many sub-types (Jessen 2004). In the CNS the major glial cells are oligodendrocytes and astrocytes and within the PNS the major glial cell is the Schwann cell.

1.2 Why myelin is important

Myelination is a fundamental biological process in the developing vertebrate nervous system. Myelin is the lipid-rich multi-lamellar assembly of membrane processes extending from oligodendrocytes in the CNS, forming an insulating sheath around nerve axons. The myelin sheath is a dynamic system that communicates with both the underlying axon and the external environment and enables rapid transmission of nerve impulses by saltatory conduction [reviewed in (Harauz et al 2009)]. The myelin sheath is formed by the spiral wrapping of the oligodendrocyte’s plasma membrane extensions around the axon (Peters 1960, Remahl & Hildebrand 1990). Myelin sheaths foster rapid and efficient conduction of electrical impulses along axons. The development of the myelin sheath has allowed for the evolution of highly complex but compact nervous systems (Franklin & Ffrench-Constant

2008). However, the specialised process of wrapping and compaction of the myelin sheath is not well understood (Bauer et al 2009).

Myelin contains an array of proteins (Werner & Jahn 2010); myelin basic protein (MBP) and the proteolipid proteins (PLP/DM20) being the two major CNS myelin proteins. Before final maturation and myelin formation, oligodendrocytes go through many stages of development which have been characterised by a panel of antigenic markers, by their morphological phenotypes and their mitotic and migratory properties (Li et al 2007b, Raff et al 1983c).

1.3 The beginning of the concept of glial cells

While neurons have been extensively studied over the years, it is relatively more recently that researchers have turned their focus on to glia cells. Virchow first introduced the concept of neuroglia in a lecture in Berlin University, in 1856, 150 years ago. In that lecture, Virchow made public his earlier thoughts on the brain connective tissue, the "nervenkitt" (nerve glue) or nerve-cement (Baumann & Pham-Dinh 2001). For Virchow, neuroglia was a connective material and against the concept of nervous elements. However, glial elements were documented in 1838, when Robert Remak described a sheath around single fibres. In addition, some years later in 1851, Heinrich Müller discovered radial fibres in the retina (Kettenmann & Verkhratsky 2008). The characterisation of the major glial cells was the outcome after several microscopic studies and techniques of metallic impregnation developed by Ramon y Cajal and Rio Hortega (Baumann & Pham-Dinh 2001).

There are three types of glia cells in the CNS: astrocytes, oligodendrocytes and microglia constituting the majority of cells in the nervous system. Despite their number and their role during development, their active participation in the physiology of the brain and the spinal cord and the consequences of their dysfunction on the pathology of the nervous system is only in recent years being recognised. Their role is very important and diverse. Generally, glial cells are necessary for correct neuronal development and function and they have to be able to respond to changes in the cellular and extracellular environment rapidly. Furthermore, there is now growing recognition that glia, possibly through a glial network,

may have communication skills that complement those of the neurons themselves (Baumann & Pham-Dinh 2001).

Astrocytes are a very heterogeneous population of cells which interact with neurons and blood vessels. These cells detect neuronal activity and can modulate neuronal networks and will be discussed further in section 1.4. Oligodendrocytes and Schwann cells form myelin and therefore are prerequisites for the high conduction velocity of axons in vertebrates. Microglia cells are the immune cells of the CNS and respond by a process called activation to any change in the environment. They are therefore considered as pathological sensors of the brain. They migrate to the site of injury, can proliferate, phagocytose and interact with the peripheral immune system by antigen presentation (Kettenmann & Verkhratsky 2011).

1.4 Astrocytes

Astrocytes are the major support cells in the CNS providing physical and metabolic support (Robbins et al 2005). In addition, astrocytes are thought to play an important role in neuronal communication, blood brain barrier (BBB), myelination and scar formation after injury (Silver & Miller 2004, Sofroniew & Vinters 2010, Sorensen et al 2008). Astrocytes are the most abundant cell type in the CNS and exist as different subtypes, such as fibrous and protoplasmic, based on morphologic and antigenic criteria. However, these subtypes are thought to spatially segregate primarily according to their location in either grey or white matter (Hochstim et al 2008).

Astrocytes are defined by their stellate morphology and expression of glial fibrillary acidic protein (GFAP) (Eng et al 1971). They have been termed ‘support cells’ and in the normal adult brain are thought to have a relatively passive role in the CNS. However, astrocytes are emerging as key players in many aspects of CNS diseases and injury. More specifically, their diverse roles extend from energy metabolism and neurotransmitter homeostasis, myelination and axonal outgrowth to maintenance of the BBB and synaptogenesis (Liberto et al 2004, Nair et al 2008, Silver & Miller 2004, Sorensen et al 2008, Ullian et al 2001, Watkins et al 2008). The term phenotype is used to represent the various properties of astrocytes that change after injury and includes their morphological,

antigenic and physiological characteristics. The phenotypic status of astrocytes has been an intriguing and widely discussed issue as they appear to play an important role in the pathology of many neurological diseases (Nash et al 2011a).

An indication that astrocytes can influence processes such as myelination has come from recent work in the lab. Using a mixed culture of dissociated rat embryonic spinal cord cells plated on a monolayer of astrocytes derived from stem cells, termed "myelinating cultures" it was shown that astrocytes have a direct role in promoting myelination (Sorensen et al 2008). In fact, myelination is poor on monolayers of other supporting glia, such as olfactory ensheathing cells or Schwann cells, suggesting that astrocytes promote myelination either by releasing a soluble factor or by cell–cell contact. More recently, it has also been suggested that the astrocyte phenotype can influence the ability of oligodendrocytes to myelinate axons. Astrocytes can exhibit a continuum of phenotypes ranging from quiescent/resting to reactive (Liberto et al 2004, Sofroniew & Vinters 2010, Williams et al 2007). Myelination was poor when the myelinating cultures were plated on quiescent astrocytes, but enhanced when they were plated on a more reactive/activated phenotype (Nash et al 2011b).

This ability of astrocytes to influence myelination was proposed by others. Indeed, in 1904 it was suggested that hypertrophic-reactive astrocytes were a pathological feature of multiple sclerosis (MS) and it was hypothesised that they had an important role in the disease (Muller, 1904). A similar hypothesis was raised by Wu & Raine (1992) from studies of human MS lesions. In this study the authors demonstrated a correlation between hypertrophic astrocytes and MS pathology (Wu & Raine 1992). Several other reviews have discussed the role of astrocytes in MS (Lassmann 2005, Nair et al 2008, Sofroniew & Vinters 2010, Williams et al 2007) and have detailed the importance of astrocyte-secreted factors that either promote or impede myelination (Moore et al 2011). It has also been shown from immunohistochemical studies of the developing rat spinal cord that a temporary increase in GFAP-positive cells correlated with an increase in immunoreactivity with the late myelin marker MBP, suggesting that this increase of GFAP-positive cells accompanying myelination is necessary for normal myelin development (Dziewulska et al 1999). Other *in vitro* studies have confirmed the role of astrocytes in myelination. For instance, Barres and colleagues demonstrated that astrocytes secrete factors that influence the rate of myelin ensheathment *in vitro* (Watkins et al 2008). This highlights the

importance astrocytes have on influencing myelination and the use of myelinating cultures may provide a way to define the differing phenotypes of astrocytes (Nash et al 2011a).

1.5 Oligodendrocytes

The term *oligodendroglia* was introduced by Rio Hortega to describe those neuroglial cells that show few processes in material stained by metallic impregnation techniques. The oligodendrocyte is mainly a myelin-forming cell, but there are also satellite oligodendrocytes that may not be directly connected to the myelin sheath, and may serve to regulate the microenvironment around neurons. An oligodendrocyte extends many processes, each of which contacts and repeatedly envelopes a stretch of axon with subsequent condensation of this multi-spiral membrane, leading to the formation of myelin (Li et al 2007b). On the same axon, adjacent myelin segments belong to different oligodendrocytes. The number of processes that form myelin sheaths from a single oligodendrocyte varies (Fig. 1.1) according to the area of the CNS and possibly the species, from 40 in the optic nerve of the rat to 1 in the spinal cord of the cat (Baumann & Pham-Dinh 2001).

Figure 1.1 Schematic of an oligodendrocyte extending many processes

Each of the oligodendroglial plasma processes contacts and repeatedly envelopes a stretch of axon with subsequent condensation of this multi-spiral membrane-forming myelin. The number of processes that form myelin sheaths from a single oligodendrocyte varies in the CNS.

Rio Hortega classified oligodendrocytes in four categories, in relation to the number of their processes, according to their morphology and the size or thickness of the myelin sheath they form. Butt (Butt et al 1998) also distinguished four types of myelinating oligodendrocytes, from small cells supporting the short, thin myelin sheaths of 15-30 small diameter axons (type I), through intermediate types (II and III), to the largest cells forming the long, thick myelin sheaths of 1-3 large diameter axons. Morphological heterogeneity is, in fact, a recurrent theme in the study of inter-fascicular oligodendrocytes. Before their final maturation involving myelin formation, oligodendrocytes go through many stages of development. Their characterisation is often insufficient by morphological criteria alone. A number of distinct phenotypic stages have been identified both *in vivo* and *in vitro*, based on the expression of various specific antigenic markers (Baumann & Pham-Dinh 2001).

1.5.1 Origin and Differentiation

In the mammalian cortex, both neurons and glia arise from the proliferating neuroepithelial cells of the telencephalic ventricular and subventricular zone (SVZ). The SVZ is a mosaic of multipotential and lineage restricted precursors, where environmental cues influence both fate and choice of all surviving cells (Doetsch et al 1997, Jensen & Raff 1997, Levison & Goldman 1993). A number of trophic factors influence the actual developmental fate of a progenitor or a multipotent stem cell from the SVZ. Oligodendrocyte progenitor cells (OPCs) migrate extensively throughout the CNS before their final differentiation into myelin-forming oligodendrocytes (Calver et al 1998).

During development, OPCs are heterogeneous in their spatiotemporal origin and arise from multiple regions of the ventricular zone in a sequential manner. The first wave of OPCs that populate the forebrain originates from the medial ganglionic eminence and anterior entopeduncular area. These OPCs are followed by a second wave from the lateral

ganglionic eminence and caudal ganglionic eminence. Finally, a third collection of OPCs originates within the postnatal cortex. These respective populations are identified not only by their spatiotemporal differences but also by their differential transcription factor expression (Kessaris et al 2006). Although these studies suggest the presence of heterogeneous OPC populations, the majority of the OPCs differentiate into oligodendrocytes and myelinate axons regardless of their origin. Despite originating from multiple regions at different times throughout development, OPCs are found evenly distributed throughout the adult brain in both grey and white matter alike.

Additionally, compensatory mechanisms are observed when specific OPC populations are eliminated, whereby OPCs from different regions replace eradicated cells, resulting in normal oligodendrocyte and myelin phenotype (Kessaris et al 2006, Kirby et al 2006). Given the interchangeable nature of these OPCs, despite spatiotemporal differences and the lack of evidence for adult OPCs originating from a separate lineage, it is reasonable to assume that insight into the mechanisms responsible for differentiation during development, may provide valuable information concerning the presence and potential utility of the adult OPCs (Chan et al 2010).

Moreover, as in other developmental systems, oligodendrocytes have to extend processes in a similar fashion to the extension of neurites from neuronal cell bodies. As for neurons, a number of extracellular matrix (ECM) molecules play an instructive role in the control of migrating oligodendrocytes. OPCs as they migrate extend processes that appear to sample the extracellular environment for motility and guidance factors. Platelet derived growth factor (PDGF), a mitogenic and migratory factor, acts through OPC-expressed PDGF-receptor (PDGFR) to initiate and promote migration through extracellular regulated kinase signalling and un undetermined pathway that couples Fyn kinase to Cdk5 phosphorylation of WAVE2 (Frost et al 2009, Miyamoto et al 2008). Migration can be maintained through voltage operated calcium channels and intracellular calcium signals, while chemoattractive or chemorepulsive factors such as Selaphorin 3F or netrin, direct OPCs towards their targets (Paez et al 2009, Simpson & Armstrong 1999, Spassky et al 2002). Many other growth factors, [basic fibroblast growth factor (FGF), FGF2], insulin-like growth factor I, neurotrophin-3] have been found to be involved in the proliferation, differentiation, and maturation of the oligodendrocyte lineage.

Recently, microRNAs (miRs) were shown to be necessary and sufficient to promote oligodendrocyte differentiation. In particular, miR-219, arrests proliferation, suppresses expression of OPC-related genes and activates expression of pro-oligodendrocyte genes. Hence, miRs might effectively coordinate the rapid transition from mitotically active OPCs to pro-oligodendrocytes (Dugas et al 2010, Zhao et al 2010).

The signals that tell an OPC to stop migrating in the forebrain are unknown. However, in the developing spinal cord, CXCR2 controls positioning of OPCs by arresting their migration (Padovani-Claudio et al 2006, Tsai et al 2002). Established pathways associated with OPC maturation include thyroid hormone signalling. OPCs exposed to 3,5,3-tri-iodothyronine (T3) in culture rapidly differentiate into MBP-expressing oligodendrocytes (Barres et al 1994). OPC differentiation can proceed in the absence of T3, however T3 regulates the onset of oligodendrocyte maturation and is required to achieve the appropriate number of myelinating oligodendrocytes (Rodriguez-Pena 1999). Other pathways may serve to delay OPC maturation in development and remyelination. Activation of the canonical Wnt signalling pathway, via β-catenin stabilisation and transcription factor 4 (Tcf4)-mediated gene activation, may serve as an important inhibitory mechanism for repressing oligodendrocyte differentiation and therefore suppressing Wnt-signalling might be necessary for OPCs to mature into pro-oligodendrocytes (Ye et al 2009).

Most of these studies have been performed *in vitro*. It is extremely difficult to extrapolate to *in vivo* conditions, as multiple factors may act in concert to achieve the exquisitely fine regulation of the complex process of oligodendrocyte development and myelination (Franklin & Hinks 1999). Combinations of factors often produce effects that are significantly different from those seen with any one factor alone. Furthermore, these factors have multiple effects during development.

1.5.2 Developmental stages of the oligodendrocyte lineage

Oligodendrocytes originate from migratory and mitotic precursors, then progenitors and finally mature progressively into myelin-forming cells (Fig. 1.2). Differentiation of the mitotically active OPC into an oligodendrocyte capable of myelinating, a pro-

oligodendrocyte or pro-OL requires cell cycle withdrawal, down regulation of OPC genes (such as PDGFR) and the upregulation of oligodendrocyte genes necessary for the upcoming events of process extension and elongation, myelin synthesis and compaction (Potter et al 2011). The sequential expression of developmental markers, identified by a panel of cell specific antibodies, divides the lineage into distinct phenotypic stages (Hardy & Reynolds 1993, Pfeiffer et al 1993). However, the specific antigenic components characterising cells of the oligodendroglial lineage as some of them are myelin components, may be present in other cell types or other tissues.

In vitro studies have shown that oligodendrocyte development proceeds through a series of stages, each marked with a distinct morphology, expression of surface antigens, and response to growth factors (Grinspan et al 2000). One of the earliest stages of the oligodendrocyte lineage identified in culture, is the oligodendrocyte pre-progenitor (also termed "pre-O2A"), identified by a variety of groups (Ben-Hur et al 1998, Grinspan et al 1990, Hardy & Reynolds 1991, Marmur et al 1998). These cells have been isolated from rat forebrain immediately after birth. They are small, round, and process-bearing and express the heavily sialylated, embryonic form of NCAM (PSA-NCAM), vimentin and PDGF-a receptors.

Oligodendrocyte precursor cells are the next stage in the lineage. These cells are defined by the expression of a surface ganglioside, recognised by the A2B5 antibody (Raff et al 1983c). In serum-free medium and at low density, they differentiate into oligodendrocytes. However, in serum they appear small and stellate and express an unusual combination of antigens, including GFAP, a characteristic intermediate filament of astrocytes (Bignami & Dahl 1974), and A2B5 (Raff et al 1983a). These A2B5-positive/GFAP-positive cells have been termed "type 2 astrocytes" to distinguish them from the flatter, larger A2B5-type 1 astrocytes (Raff et al 1983a). Nestin is another protein for classification whose expression specifically distinguishes neuroepithelial stem cells from other more differentiated cells in the neural tube. PDGF-a transcripts are detected at very early stages of the developmental maturation of oligodendrocytes (Richardson et al 2000). Thus, progenitors were known as O-2A cells for several years because of these properties.

As the cells differentiate from precursors to the mature oligodendrocyte, they acquire immunoreactivity with the O4 antibody (Sommer & Schachner 1982). The monoclonal

antibody O4 (Sommer & Schachner 1981) marks a specific pre-oligodendrocyte stage of oligodendrocyte maturation. It reacts also with sulfatides. Mature oligodendrocytes, which do not differentiate into astrocytes, are immunoreactive with antibodies against galactocerebroside (GalC) and various myelin proteins (Bansal et al 1992, Warrington & Pfeiffer 1992). Myelin proteins, which comprise 30% dry weight of myelin, are the specific components of myelin and oligodendrocytes (Campagnoni & Macklin 1988). The major CNS myelin protein-markers such as MBP and PLP/DM20 are widely used to identify late stage oligodendrocytes. Several glycoproteins such as myelin associated glycoprotein (MAG) and myelin oligodendrocyte glycoprotein (MOG) are also present in myelin.

1.5.2.1 Myelin Basic Protein (MBP)

MBP is one of the major proteins of the CNS myelin. There are multiple isoforms produced by differential splicing of a single mRNA transcript arising from one of three transcription start sites of the gene complex called golli (gene of oligodendrocyte lineage). There are many isoforms of different molecular masses. Direct evidence that MBPs play a major role in myelin compaction in the CNS was provided from studies of the *shiverer* mutant mouse, which is characterised by a large deletion of the MBP gene and in which the major dense line (MDL) is absent from myelin (Roach et al 1985). *shiverer* mice have only one or two layers of poorly compacted myelin, which can be rescued by MBP-producing cells (Windrem et al 2004). Because of its major importance, MBP has been called the "executive" protein of myelin by Moscarello (1997). *In vivo*, oligodendrocytes do not produce the extensive MBP-containing membrane sheets observed in culture, since the oligodendrocyte processes do not produce large amounts of membrane until after contact with axons, during axonal ensheathment. MBP is observed only in oligodendrocytes that have migrated into axonal pathways and it is produced just before the commencement of axonal ensheathment (Asou et al 1995a, Butt et al 1997). At this stage, the oligodendrocyte produces many filopodia which associate with numerous axons. Some may function as sensors to locate mature target axons for myelination, while others perform ensheathment of the axon and myelination (Ogawa et al 2004). In mature myelinating oligodendrocytes, MBP redistributes from the soma and primary processes

into the myelin sheaths, reflecting a change in the site of MBP mRNA expression (Barbarese et al 1999). Cytosol is present in the first few layers before compaction and appearance of the MDL occur. These early ensheathments actively elongate and undergo extensive remodelling. Varicosities are also observed in immature myelin sheaths indicating the presence of cytosol (Hartman et al 1982) [reviewed in (Harauz et al 2009)].

1.5.2.2 Proteolipid protein (PLP)

Gene expression of the PLP is considered as a marker of developmental maturation of myelinating glial cells in the CNS. PLP is an integral membrane protein, composed of 276 amino acids. PLP and DM20 are encoded by the highly conserved X-linked *PLP1* gene, which is expressed in the CNS, predominately in oligodendrocytes. These protein isoforms are generated by alternate splicing of *PLP1* pre-mRNA arising from differential usage of alternative splice sites in exon 3 (Milner et al 1985, Nave et al 1987, Simons et al 1987). *PLP1* expression in the CNS commences prior to myelination, with the classical DM20 gene product dominating at this stage (Kronquist et al 1987, LeVine et al 1990, Schindler et al 1990, Timsit et al 1992). As oligodendrocytes contact and myelinate axons, *PLP1* gene expression increases and PLP becomes the predominant isoform (Kidd et al 1990, Trapp et al 1997). As a structural protein PLP has an important role in the correct apposition of the extracellular leaflets of the membrane, stabilising the multi-layered myelin membrane structure upon compaction [reviewed in (Gruenenfelder et al 2011)].

Biogenesis of the myelin sheath requires extensive membrane expansion involving targeted fusion of transport vesicles. Lately, studies have focused on proteins regulating key steps of membrane fusion within myelin membrane trafficking pathways. There is accumulating evidence that oligodendrocytes, which simultaneously assemble myelin sheaths at multiple subcellular sites, use endosomes as local internal membrane sorting and storage compartments, from which membrane is rapidly recruited to the sites of membrane growth controlled by neuronal signalling. For example, soluble neuronal signals trigger exocytosis of PLP from late endosomal membrane stores (Trajkovic et al 2006, Winterstein et al 2008). Vesicular and target membrane-localised N-ethylmaleimidesensitive factor attachment protein receptor proteins (SNAREs) (Jahn & Scheller 2006) interact to form an

intertwined helical bundle consisting of four coiled-coil domains (SNARE motifs) pulling the opposing membranes together and exerting the force required for fusion (Li et al 2007a). In particular, VAMP3 and VAMP7 colocalise with the PLP in recycling endosomes and late endosomes/lysosomes, respectively contributing to myelin biogenesis by delivering cargo to the myelin membrane. PLP initially travels from the Golgi to recycling endosomes before arriving at the plasma membrane in a VAMP3-dependent manner. On endocytosis, PLP is stored in late endosomes/lysosomes and delivered back to the myelin domain of the plasma membrane by VAMP7-dependent exocytosis in studies from co-cultures of mouse oligodendrocytes onto primary cortical neurons (Feldmann et al 2011). However, how myelinating cells achieve the specific targeting and fusion of vesicles transporting myelin components required for the expansion of the myelin membrane, is unknown**.**

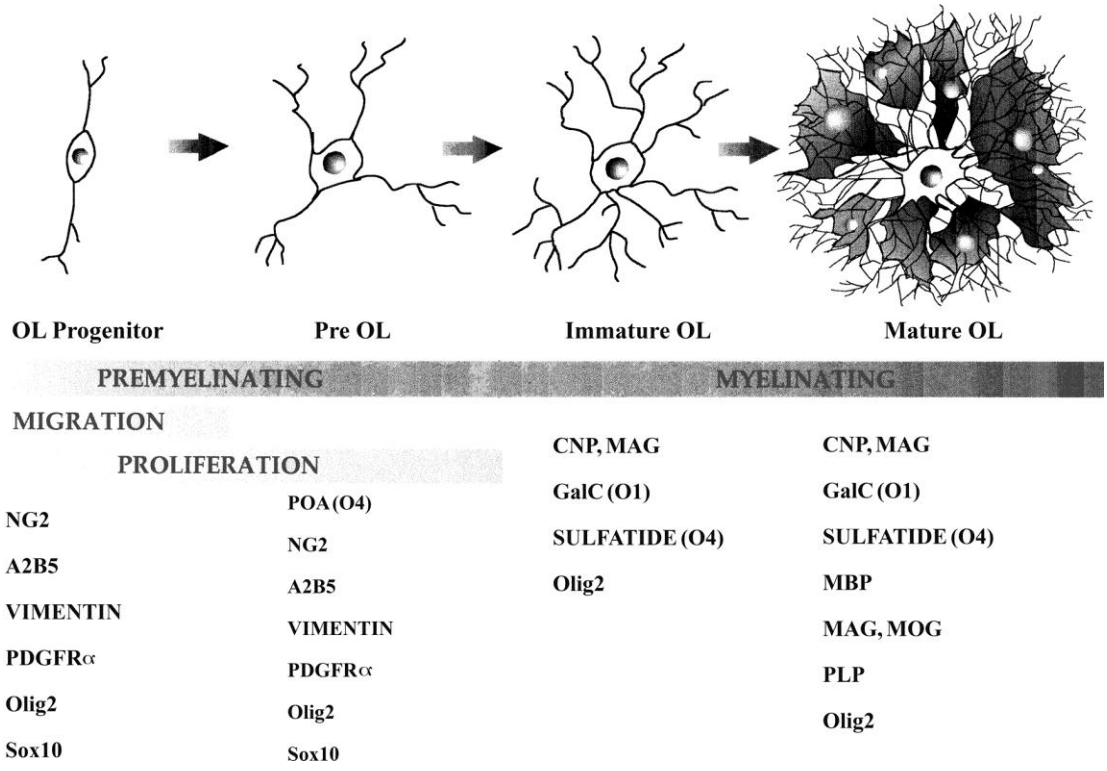

Figure 1.2 Schematic representation of the developmental stages of cells of the oligodendrocyte lineage

Schematic drawing of the morphological and antigenic progression from precursor cells to myelinating mature oligodendrocytes, through progenitors, pre-oligodendrocytes and immature non-myelinating oligodendrocytes [from (Back et al 2007)].

1.6 Role of CNS glia in axonal integrity and trophic support

In recent years, much research has focused on axonal injury. Primary alterations of glial-axonal interactions can have an unfavourable secondary consequence on the axons, revealing that white matter glia are important for axonal integrity (Edgar & Nave 2009). Many examples which elucidate the role of CNS glia in preserving axonal function have been reported. For instance, axonal swelling, loss of axonal transport and Wallerian degeneration has been reported in mice in which mutant oligodendrocytes lack certain proteins or metabolic functions. PLP/DM20, 2',3'-cyclic nucleotide 3'-phosphodiesterase (CNP) (Edgar et al 2009, Lappe-Siefke et al 2003) or MAG deficiency could lead to loss of signalling and therefore dysregulation of motor protein function and loss of axonal cytoskeletal stabilisation (Nguyen et al 2009). Moreover, deprivation of key molecules may prevent the oligodendrocyte from supplying metabolites such as glucose, to the axon (Nave 2010b).

The underlying mechanism by which glial cells contribute to the support and maintenance of axons on one hand, but also can mediate axonal damage on the other, is still not known. However, it is thought that oligodendrocytes could supply the axons with essential metabolites, through the non-compact myelin, that is to say cytoplasm filled channels connecting the oligodendrocyte cell body with the oligodendrocyte processes at the glial-axonal junction. Moreover, since oligodendrocytes are coupled with astrocytes by gap junctions which are connected to blood vessels, the non-compact myelin could serve as a route for metabolites from the BBB to the axon (Orthmann-Murphy et al 2008). In addition to simple diffusion, cytosolic “perfusion” could attenuate concentration differences of metabolites with high axonal turnover (Nave 2010b). Similar to fast axonal transport, glia intracellular transport may depend on tubular tracks and the fine architecture of this channel system (Nave 2010b). Changes of this possible oligodendroglial transport could cause deprivation of the axonal energy metabolism and consequently axonal deficiency (Edgar & Nave 2009, Nave 2010a).

Moreover, glia ensheathment triggers changes in the membrane architecture of the enwrapped axon, which could prepare the axon for long-term metabolic interactions with glia. However, the myelin sheath itself could be a “double-edged sword” (Nave 2010b). It has been suggested that the nearly complete insulation of axons by myelin, could restrict

their access to extracellular metabolic substrates (Edgar & Nave 2009, Nave 2010a). The myelin sheath could create a diffusion barrier for ions and small molecules and is interrupted only by the nodes of Ranvier, which are less than a micron in length and are often several hundred microns apart (Nave 2010b). The oligodendroglial turnover of N-acetylaspartate (NAA), a metabolite synthesised in neuronal mitochondria, is evidence that axons and oligodendrocytes can exchange small metabolites. In oligodendrocytes, NAA is hydrolysed to aspartate and acetate-a process required for myelin lipid synthesis during development. The flux of NAA between axons and oligodendrocytes is therefore extensive at least during development. It might seem that exchange of small metabolites would occur in both directions, provided the necessary transporters are in place (Moffett et al 2007).

Myelinating glial cells may be able to compensate for the physical insulation of the axon by providing a suitable extracellular milieu (Nave 2010a). The channel system may be used to physically connect the glial cytosol to the inner collar and paranodal loops that face the periaxonal space. Moreover, the myelin-forming cell could supply the underlying axon by transfer of oligodendrocyte cytoplasm to the axon by invagination of the axolemma or through secretion of a diffusible factor (Edgar & Garbern 2004). Therefore, a trophic action of PLP/DM20 and CNP for instance could be mediated directly, or through downstream factors that traverse the oligodendroglial/axolemmal membrane, diffuse across the periaxonal space or are transferred directly in oligodendrocyte cytoplasm to the axon (Edgar & Garbern 2004). Also the fact that *Plp* and *Cnp* knockout mouse are of a late onset phenotype suggests that either axonal requirements change over time or deficits in myelin-axonal signalling accumulate until a threshold is reached, where axonal degeneration begins (Edgar & Garbern 2004).

The perception of myelin has gradually changed from that of an inert membrane sheath to that of a metabolically active glial organelle that provides both axonal insulation and neuroprotection (Nave 2010b). Taken into consideration that neurodegeneration can result from primary oligodendrocyte dysfunction that barely alters the myelin phenotype, it is possible that oligodendrocytes also have important bystander effects in neurodegenerative diseases that are not associated with demyelination. The hypothetical relevance of "oligodendroglial support as a disease-modifying factor" should be experimentally addressed with the large number of neuronal and glial mouse mutants that have been generated (Nave 2010a, Nave 2010b).

1.7 Myelin: Anatomy of an insulating sheath

Myelin, termed by Virchow, is a spiral structure constituted of extensions of the plasma membrane of the myelinating oligodendrocytes in the CNS. Myelin, is contained in the glial sheath around axons and is one of the defining features of jawed vertebrates (gnathostomes). The compacted myelin sheath with multiple layers of membranes around most axons constitutes the most abundant membrane structure in the vertebrate nervous system. Several structural features characterise myelin.

Generally, it is described as a periodic ultra-structure, with alternating concentric electron-dense and light layers. The major dense line (dark layer) forms as the cytoplasmic surfaces of the expanding myelinating processes of the oligodendrocyte are brought into close apposition. Electron dense layers represent the closely apposed hydrophilic ends of extracellular membranes (intraperiod lines) and the tight apposition of cytoplasmic membranes (MDL) (Saher et al 2011). The distance between the midpoints of two successive major dense lines represents one myelin period. By X-ray diffraction of unmixed tissue of young adult mice, PNS myelin has a period of 17.45 nm, whereas the period of CNS myelin is about 10% smaller , that is to say 15.65 nm (Agrawal et al 2009). The unique structure of compact myelin reduces the capacitance of the axonal surface and increases the trans-membrane resistance (Hartline & Colman 2007). Myelinated sheath segments, termed internodes, which appear to be 150-200 µm in length, are interrupted by small gaps, the nodes of Ranvier [reviewed in (Rasband 2006, Salzer et al 2008)]. At these specialised domains, sodium channels are clustered and action potentials are generated for saltatory impulse conduction. Flanking each internode, paranodal loops partially seal the internodal periaxonal space from the outside milieu and represent uncompacted myelin. In addition to paranodal loops, non-compact myelin comprises the adaxonal layer of internodal myelin, as well as the abaxonal myelin layer and Schmidt-Lanterman incisures of PNS myelin. Non-compacted myelin contains some cytoplasm and may facilitate the transport of metabolites, proteins and ions (Nave 2010a).

1.7.1 Myelin lipids

Its unique composition (rich in lipids that constitute about 70% to 80% of its dry weight and low water content) and its unique segmental structure support the fast nerve conduction in the thin fibres in the vertebrate system. High-speed conduction, fidelity of transfer of signalling over long distances, and space economy are the three major advantages conferred to the vertebrate nervous system by the myelin sheath, in contrast to the invertebrate nervous system, where rapid conduction is accompanied by increased axonal calibres (Michailov et al 2004). The molecular composition of myelin differs from other plasma membranes. Moreover, CNS myelin contains the exceptional molar ratio of cholesterol: phospholipid: galactolipid: plasmogen of 3:3:2:1 to 4:3:2:1 (Morell & Jurevics 1996) which distinguishes myelin from other cellular membranes. The abundance of cholesterol within a membrane affects its biophysical properties, including fluidity and curving (Huttner & Zimmerberg 2001). Cholesterol has been identified as unusually enriched in myelin from other cellular membranes and constitutes 24-28% of the total myelin lipids (Norton & Poduslo 1973). Cholesterol assembles with galactolipids and plasmogens within the plane of the membrane, but how they are enriched to the levels found in myelin, is unknown.

The content of 20% to 30% galactolipids comprises galactosylceramides (GalC) and their sulfated derivatives, sulfatides. It has been suggested that lipids are targeted to future myelin membrane by their association with myelin-bound proteins, such as GalC association with myelin and lymphocyte protein (MAL) (Frank et al 1999). Galactolipids are almost exclusively located at the extracellular leaflet of the membrane, facing the intraperiod lines (Eckhardt 2008). Glycosphingolipids, especially when esterified with saturated long fatty acid chains, together with cholesterol promote the formation of membrane subdomains, termed membrane lipid rafts (Ikonen & Jansen 2008). The specific composition of lipids is assumed to favour an increased lateral compaction of the fatty acid chains that is likely to contribute to the insulator function of myelin. Additionally, it has been suggested that membrane lipid rafts might be one type of transport unit that delivers myelin proteins and lipids to the growing myelin sheath (de Vries & Hoekstra 2000, Kramer et al 2001).

1.7.2 Systemic analysis of the CNS myelin protein composition

In order to understand the myelin biogenesis and pathology, a comprehensive knowledge of the proteins associated with myelin is essential. Recent studies applying nanoscale 1D ultra performance liquid chromatography (1D-UP-LC) separation coupled to detection with a quadrupole time-of-flight (Q-TOF) mass spectrometer (Patzig et al 2011) have confirmed and expanded the previous myelin protein compendia in PNS. The proteins are candidates for performing important functions in myelin biogenesis and integrity, molecular interactions between myelinating glial and neighbouring cells and white matter homeostasis. By gene ontology terms, many myelin-associated proteins in CNS are implicated in catalytic activities (48%), the cytoskeleton (20%), protein transport (21%), vesicular trafficking (6.8%), cell adhesion (6.3%), phospholipid binding (4.2%) or glycolysis/gluconeogenesis (5.1%) (http://david.abcc.ncifcrf.gov).

In a study on CNS myelin, identified peptides were annotated to a total of 294 myelin-associated proteins. Interestingly, PLP, MBP and CNP constituted only 17%, 8% and 4% of the total CNS myelin-associated proteins respectively. All previously known proteins together constituted 35%, while newly identified myelin-associated proteins accounted for 65%. Among the newly detected proteins are those of quite various anticipated functions, such as the NAD+-dependent deacetylase sirtuin 2 (SIRT2) (Werner et al 2007), cytoskeletal proteins of the septin family (Buser et al 2009), regulators of intracellular vesicle transport in the secretory pathway, such as cdc42 and Rac1 (Thurnherr et al 2006), the paranodal transmembrane glycoprotein Opalin/TMEM10 with a suggested signalling or adhesive function (Golan et al 2008). The above quantifications take into question previous estimates based on conventional techniques. It is remarkable that the abundance of PLP and MBP was previously overestimated at 30-45% and 22-35% respectively, because low abundant proteins did not constitute significant bands, due to limitations in the resolving power of the 1D gel separation and in the dynamic range of protein staining. Although the modern LC-MS-based approaches are technically more demanding than gel-based studies, they appear to be appropriate for tackling the myelin proteome as they cover several orders of magnitude of protein abundance and detect highly basic, hydrophobic, and membrane-spanning proteins (Jahn et al 2009).

CNS myelin is produced by oligodendrocytes in a process (Fig. 1.3) comprising the following phases: a) Selection of an axonal segment by an oligodendroglial process, b) Initiation, specialisation and stabilisation of glial-axonal interactions at the nodes, paranodes and internodes, c) Specialisation of the sheath's lipid and protein composition relative to the oligodendroglial plasma membrane, d) Radial expansion-regulated increase in layer number, e) Intra- and extra- cellular compaction, f) Longitudinal expansion of myelin segments coinciding with axonal elongation during body growth (Sherman & Brophy 2005). The delicate arrangement with one oligodendroglial cell body maintaining up to 60 comparatively large myelin sheaths via tenuous connections may explain the sensitivity to disease (Werner & Jahn 2010). Once myelinated, axons become dependent on glial support (Nave & Trapp 2008).

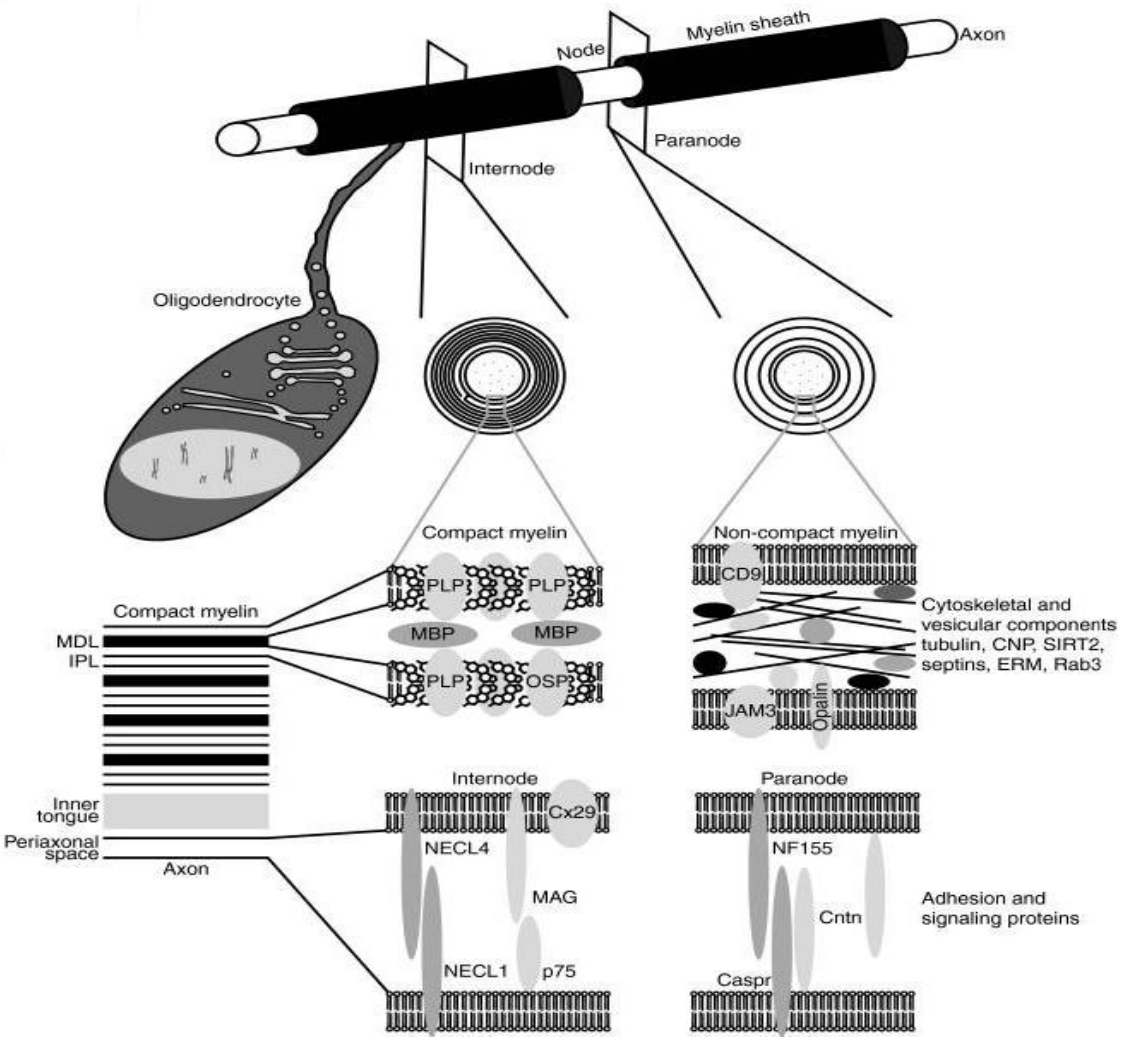

Figure 1.3 Schematic depiction of an oligodendrocyte myelinating an axon

Cross-sections in the intermodal and paranodal segments and subcellular localisation of myelin proteins, MBP and PLP. Other structural proteins, adhesion and signalling proteins and cytoskeletal components are depicted in grey [from (Jahn et al 2009)].

1.8 White matter disorders: leukodystrophies and multiple sclerosis

The importance of myelin forming correctly in human development is highlighted by its involvement in an array of different neurological diseases or disorders that impair oligodendrocyte generation, differentiation or myelin production and maintenance. Inherited myelin diseases, called leukodystrophies are associated with dysmyelination (improper formation of myelin), hypomyelination (inadequate levels of myelin), or demyelination (loss or breakdown of myelin). This heterogeneous group of diseases is characteristised by the loss of motoric, sensory and mental capabilities and the susceptibility to seizures.

Some level of dysmyelination or hypomyelination present during fetal life or early infancy, as observed in the connatal form of Pelizaeus-Merzbacher disease (PMD) in which a major component of the myelin sheath, PLP/DM20, is abnormal. A large variety of *PLP1* point mutations and gene duplications have been described (Sarret et al 2010). Demyelinating leukodystrophies are also characteristic of metabolic diseases such as Krabbe's disease, in which the lysosomal enzyme GalC is defective, resulting in accumulation of psychosine, a metabolite toxic to oligodendrocytes (Pastores 2009).

Inflammatory demyelinating diseases, in which oligodendrocytes are targeted by the immune system, are exemplified by MS, the most common cause of neurological dysfunction in young adults (Compston & Coles 2002). MS is generally thought to result from an autoimmune inflammatory response towards components of the myelin sheath (Steinman et al 2002), resulting in areas of demyelination or plaques. As the disease progresses, a spectrum of pathologies are observed in which some white matter areas contain evidence of remyelinating axons, while others are almost completely demyelinated. It is thought that sustained loss of myelin results in axonal dysfunction and neuronal death

and underlies the irreversible neurological impairments of MS (Hauser & Oksenberg 2006). The variability in remyelination of MS lesions lead to the notion that dysregulation of myelin repair is a factor that could account for disease progression (Franklin & Ffrench-Constant 2008).

1.9 Basic Structural analysis of the myelin sheath in the CNS

It is the purpose of this thesis to focus on the process of myelination starting with a description of the initial studies, using electron microscopy, in order to present what is currently known about the formation of the myelin sheath in the CNS. The theory of spiral wrapping by a single cell process is generally accepted as the main process by which myelin is formed in the vertebrate CNS, both in myelinogenesis and in remyelination. However, occasionally, profiles of the myelin sheath were observed which although they were not opposite to the spiral-wrapping theory, required a more detailed analysis and deeper understanding than the simple wrapping of a myelin-forming cell process around an axon. These profiles were mainly frequent under pathological or experimental conditions. They include isolated cytoplasmic islands within incompletely fused major dense lines (Hirano & Dembitzer 1967), unconnected cell processes between the innermost myelin lamellae and the axons and double, concentric sheaths surrounding a single axon.

There have been described various configurations of the developing myelin sheath. In the detailed report by Hirano & Dembitzer (Hirano & Dembitzer 1967) a form, described as type A, was characterised by a single, continuous spiral. It was the most common form and consisted of several lamellae around the axon. The only cytoplasm visible in the myelin-forming cell was in the inner and outer loops which lacked any organelles. In type B, the only difference from type A was the presence of organelles such as mitochondria and dense bodies in the inner and /or outer loops. In Type C, in addition to the inner and outer loops, occasional islands of cytoplasm were seen among the myelin lamellae themselves. These cytoplasmic islands represented unfused portions of the MDL. In type D, a cell process was observed unconnected to either the myelin sheath or the axon, between the innermost myelin lamella and the axon. In type E, two distinct, concentric myelin sheaths,

both spiralling in the same or opposite directions with equal or unequal number of turns, were formed by two cell processes around a single axon (Hirano & Dembitzer 1967).

The variety of profiles of the myelin sheath, seen in electron microscopy, helped at that stage to explain the general model of central myelin described by Bunge et al., 1961. The myelin sheath was described as a shovel-shaped myelin sheet surrounded by a thicker, continuous rim of cytoplasm. In cross section through a myelinated fibre, the outer and inner cytoplasmic rims were represented by the outer and inner cytoplasmic loops respectively. In conclusion the inner, outer and lateral loops are continuous with the perikaryon of the oligodendrocyte, at least during myelin formation. Moreover, the outer loops in the CNS cannot rotate around the axon since they are connected to the glial cells which are effectively anchored due to their multiple processes. It should be pointed out that all the aforementioned variations were observed during the recovery stage of a white matter lesion. These variations may occur in normal myelinogenesis, but were frequently observed only in a chronic lesion (Hirano & Dembitzer 1967).

1.10 Classical electron microscopic studies on the relationship between axons and oligodendrocytes during initial ensheathment and myelination

The morphology of the oligodendroglial-axon unit during ensheathment and initial myelination in the developing feline spinal cord and corpus callosum white matter was examined by electron microscopy. Serial sections from many stages of development initially suggested the presence of four basic types of oligodendrocytes (I-IV). From several studies it was documented that oligodendroglial cells relate to a single large axon, as well as multi-branched varieties associate with several small axons (Del Rio-Hortega, 1928; Penfield, 1932; Plenk, 1934). Other studies promoted the view that each oligodendrocyte creates several myelin sheaths, scattered among different axons at some distance from the cell body (Raine, 1984; Wood and Bunge, 1984). It was also estimated that the number of axons per oligodendrocyte may be 30-60 (Peters and Proskauer, 1969; Matthews and Duncan, 1971). In the CNS, the axon diameter at which myelination

commences varies between 0.2 μm and 1.2 μm (Remahl & Hildebrand 1982), depending on the developmental stage and fibre tract.

1.10.1 Oligodendroglial ensheathment of axons

The distribution of ensheathing cytoplasm-filled membrane cannot be explained by a simple spiral wrapping or rotation hypothesis. Classical analysis of serial electron micrographs of early neonatal rat spinal cord white matter revealed evidence related to the distribution of ensheathing cytoplasm and membrane compaction during myelin formation along a developing internode (Knobler et al 1974). These features reflect simple forms of ensheathment by spirals of oligodendroglial cytoplasm. Specifically, these wormlike "vermicular" oligodendroglial processes originate from one of the spirally arranged layers ensheathing the axon. The different origin and direction of a vermicular process is depicted in schematic illustrations as interruptions of the smooth axial flow of the ensheathing cytoplasm (Fig. 1.4a-f). Particularly, the ensheathing cytoplasm flows smoothly until interrupted by the presence of additional processes, at which point the axial advance bifurcates (Knobler et al 1974).

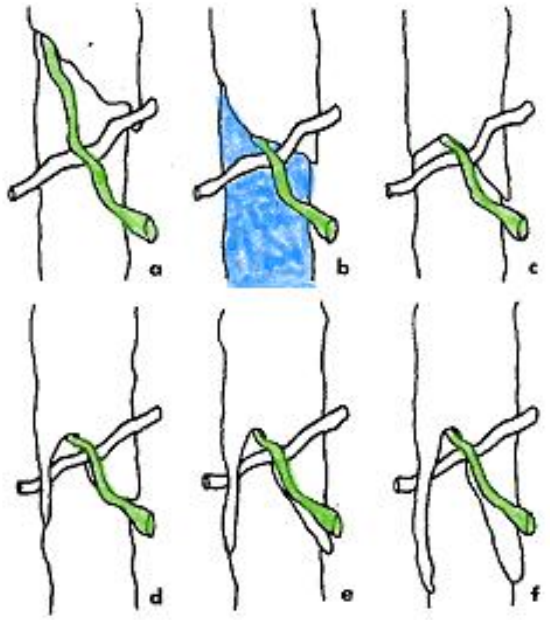

Figure 1.4 a-f Schematic illustrations suggesting the origin and direction of a vermicular process by interruption of the smooth axial flow of the ensheathing cytoplasm.

The ensheathing cytoplasm flows smoothly (a,b), until interrupted by the presence of additional processes (green) (c), at which point the axial advance diverges (d,e,f). Axon is coloured blue. [Modified from (Knobler et al 1974)].

Additionally, there is a variation in the length and consequently the number of turns around the axon at different levels along the length of the internode, which was similar to previous observations in the PNS (Webster 1971). These observations led to the hypothesis that the cytoplasmic sheath might occur at different rates within the same internode, rather than as a uniform advancement of a cytoplasmic sheet. Moreover, Knobler proposed that the leading edges of both the inner and outer layers of the sheath are capable of advancing to support additional axonal ensheathment. It was suggested that the vermicular processes might change in shape, becoming wide and forming a structure which would eventually turn around the axon and become a lamella. In other words, the initial flattened u-shaped structure gradually changes to a small circular profile (Knobler et al 1974).

In the same work further analysis documented a bidirectional nature to the oligodendroglial ensheathment of some axons during myelination. This was associated with the extension of

the vermicular processes or “plates” on the axonal perimeter from one of the ensheathing layers. The presence of vermicular processes was evidence that myelin formation is not uniform at all points along a developing internode. These findings suggested that the growth of early axonal ensheathment and compaction arises in a random fashion, consistent with helical extension around the axon, like the thread of a screw, rather than concentric spiralling of a uniform sheet of cytoplasm. The amount and form of the ensheathment may vary in accordance with the dimensions of the progressive waves of cytoplasm-filled membrane including “uniform” layers through vermicular processes that ultimately become full layers of ensheathment (Knobler et al 1976).

1.10.2 Initial stages of myelination from further electron microscopy studies

In work by Remahl and Hilderbrand (1990) glial cells were identified with uncompacted cytoplasmic ensheathments (E-sheaths) or compacted myelin sheaths (M-sheaths). E-sheaths were composed of an uncompacted cytoplasmic lamella that at least at some point formed one complete turn around the axon, whereas M-sheaths were composed of compact myelin displaying at least one major and minor dense line (Remahl & Hilderbrand 1990). Immature glial cells lacking the cytological features of typical oligodendrocytes initially associated with several axons and provided them with cytoplasmic sheaths. An E-type glial unit may be represented by two axons. In Fig. 1.5 A and B both axons are ensheathed by short (4-6 um) cuffs of glial cytoplasm (Fig. 1.5A and B).

Serial section analysis of units which had begun formation of compact myelin indicated that individual oligodendrocytes were associated with single myelin sheath (type M). Although both E-and M-sheaths did not exist in the same glial unit, some M-sheaths included E-segments. Furthermore, there was a close relation between the perikaryon and the myelin sheath that extended along the whole cell body. These observations suggested that early spinal cord oligodendrocytes might change from a polyaxonal to a monoaxonal association after initial ensheathment and before formation of compact myelin (Remahl & Hilderbrand 1990).

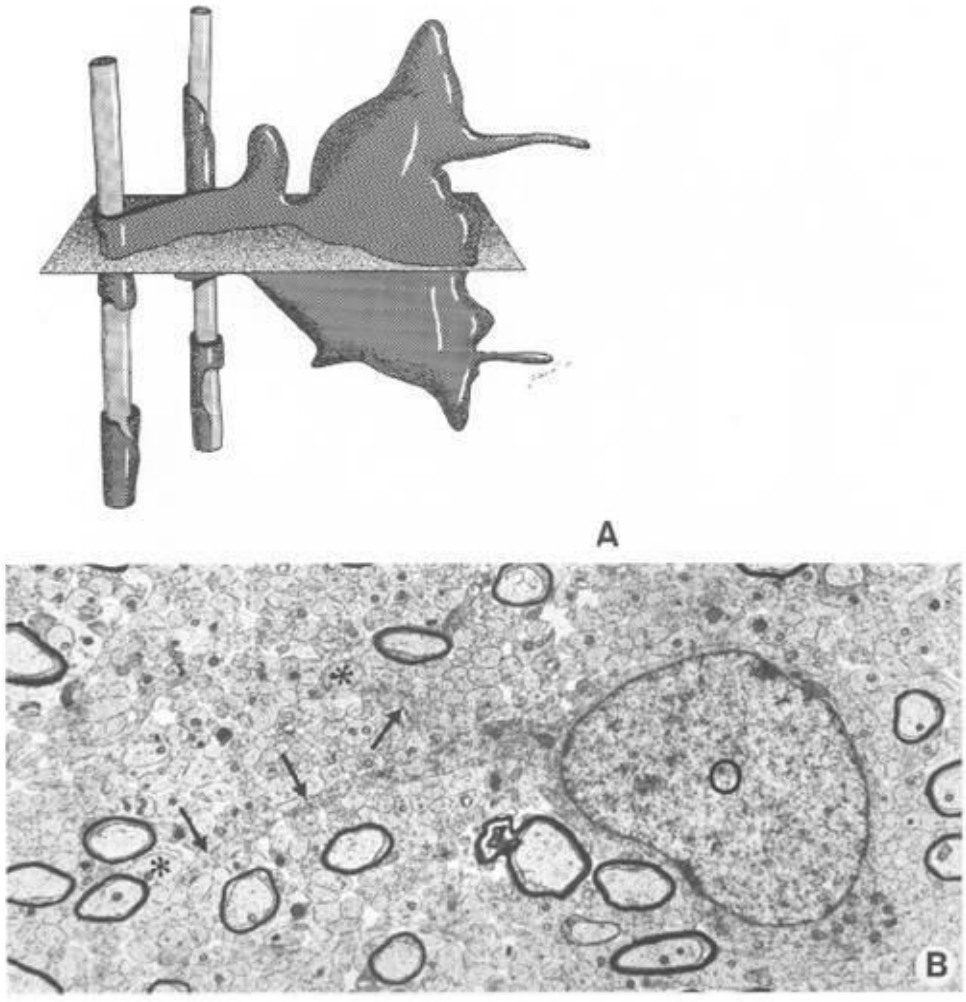

Figure 1.5 Schematic representation of an E-type glial unit

A) An E-type glial unit is drawn with two axons, which are ensheathed by short cuffs of glial cytoplasm. In the same schematic, additional cytoplasmic cuffs are shown, not deriving from the same oligodendrocyte. B) Electron micrograph corresponds to the schematic. The two axons (*) are contacted by long and slender processes (arrows) emanating from the oligodendroglial perikaryon (O) x10.000 [from (Remahl & Hildebrand 1990)].

Electron micrographs have shown that as a first stage of myelination axons become ensheathed by one to three uncompacted glial lamellae (E-sheaths). These early glial sheaths of developing CNS axons actively elongate and undergo extensive remodelling

before compaction (Remahl & Hildebrand 1990). It was shown that initial ensheathment of immature axons is preceded and partly paralleled by the occurrence of inta-axonal clusters of vesiculotubular profiles. It was suggested that these might reflect on-going membrane deposition to the axolemma by an exocytosis mechanism (Hildebrand & Waxman 1984, Waxman & Black 1985). Similar vesiculotubular clusters occur in growth cones (Williams et al 1986). As far as the initial length of E-sheaths is concerned, when one turn has been wrapped around the axon and later just before compaction into myelin, data indicated that there is a wide length range. Moreover, short E-sheaths develop into long ones through active elongation (Fraher et al 1988, Seggie & Berry 1972). With respect though to limited naked axonal space between individual E-sheaths to grow into long ones, there is a possibility that some short E-sheaths might be eliminated, so that those which persist can elongate. This elimination could be combined with the retraction of the glial cell-oligodendrocyte process as has been observed *in vitro* (Knapp et al., 1987, Lumsden et al., 1971). The transition from E to M sheath seems to occur after formation of maximally three layers of glial lamella. Some sheaths with compact myelin exhibit E-M-E sheaths, some E-M-features and some present M-features. As a final stage of myelination, steps as gradual spreading of compaction towards the sheath ends, formation of axoglial junctions and emergence of nodes of Ranvier, seem to take place (Remahl & Hildebrand 1990).

To conclude, the CNS axon during myelination displays a chaotic mixture of naked portions and portions with E- or M-sheaths (Storts & Koestner 1969). Consequently, the shift from a completely unmyelinated status is gradual and non-uniform and therefore it is inaccurate to describe such axons as entirely unmyelinated, ensheathed or myelinated. (Remahl & Hildebrand 1990).

1.11 First studies using time-lapse imaging: a reliable approach to follow oligodendrocytes ensheathment and initial stages of myelination *in vitro*

Little is known about the timing of the induction of differentiation of oligodendrocytes and how they form myelin. Furthermore, the initiation and precise mechanism of myelination in CNS still remains a puzzle (Asou et al 1994). Time-lapse video microscopy allowed the

investigation of early interactions between an oligodendrocyte and an axon, shedding some light on the unanswered questions of myelinogenesis before myelin compaction (Almeida et al 2011, Czopka & Lyons 2011).

Preliminary studies utilising video-enhanced differential interference microscopy for analysis *in vitro* using rat cultures, showed the initial stages of contact which included the formation of a lamellipodium process at the end of an oligodendrocyte process. It was proposed that at the first step in myelination, the axon becomes ensheathed by lamellipodial processes of an oligodendrocyte process through a single turn around the axon (Asou et al 1995b). That agreed with previous studies by Remahl and Hildebrand on the relationship between axons and oligodendrocytes during initial myelination which demonstrated that early glial sheath of developing CNS axons actively elongates and undergoes extensive remodelling before compaction. So, oligodendrocytes formed small ruffling lamellipodial membranes with fine filopodia. It appeared that this process contacted the axon several times and later retracted. From these initial observations, this retractive behaviour was repeated at least three times at 10 min intervals in real time before the onset of myelination. After that, the ruffling lamellipodia underwent a change in the morphology to a "veil-like flattened balloon". The filopodia and lamellipodium underwent further morphological changes prior to the onset of the myelination (Asou et al 1995b). The arms of the filopodia waved from side to side as if to "measure" the length of myelin required enveloping the axon. Simultaneously, the neural cell body and the axon also moved forward.

In the second stage of these observations by Asou, the lamellipodium appeared to thicken and anchor to the axon. Then, when lamellipodial ruffling occurred, the angle between the anchoring filopodium and axon changed depending on the direction of lamellipodial movement and the lamellipodium, which was folded in layers, wrapped around the axon like a transverse wave in one motion. A slender protrusion appeared as a result of the aforementioned morphological changes of the lamellipodium after one turn around the axon. Finally, the axons become ensheathed by one to three uncompacted glial membrane layers (E-sheath), which are oligodendrocyte lamellal leaflets (Asou et al 1995b) (Fig. 1.6). It was concluded that the membrane activities involved in the lamellipodial ruffling may be associated with movement of new surface membrane, resulting from the fusion of shuttle vesicles with the plasma membrane (Bretscher 1984).

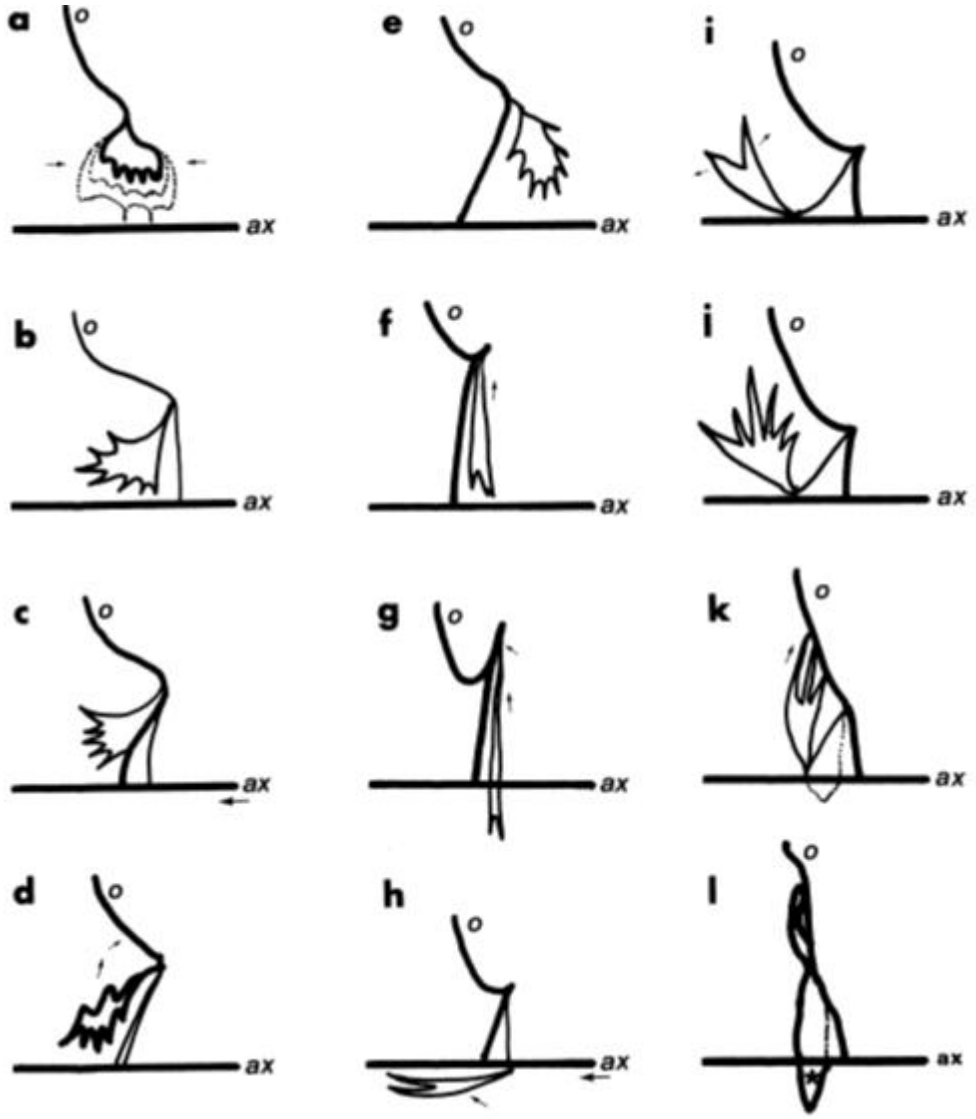

Figure 1.6 Schematic representation of the mechanism of myelin-sheath formation by the oligodendrocyte plasma membrane

A thick filopodium is formed and contacts with the axon and begins to ripple, subsequently forming a large veil-like morphology (a). The arms of the filopodium actively waved from side to side and veil-like structure (b and c) that waved from left to right according to the axonal motile (d and e). Ruffling of a sheath-like lamellipodial process is immediately induced, and the lamellipodium wraps around the axon in a crooked “J-wave” (f-g). The folded sheath-like lamellipodium extends underneath the axon (h), and then the motile complex structure (arrow) formed by the lamellipodial process after wrapping around the axon is rearranged (i), leaving a thin filopodial protrusion (j). A protrusion having a slender, pointed morphology, which may result from persistent elongation of the

lamellipodium, is formed and surrounds the axon (k-l, asterisk). (o, oligodendrocyte process; ax, axon). [From (Asou et al 1995b)].

1.12 Use of fluorescence technology and confocal microscopy to study myelination *in vivo*

1.12.1 Confocal microscopy

A confocal microscope excites fluorescence in a large, non-sectioned volume but only collects the signal from a thin slice of this by the confocal pinhole filtering the out-of-focus light. A set of conjugate apertures, one for illumination and one for detection of the scattered or fluorescent light function as spatial filters. There are two enhancements of the imaging characteristics of a confocal microscope as compared with standard light microscopes: (1) enhanced lateral resolution, and (2) enhanced axial resolution. It is the latter effect which lends itself to the optical sectioning of thick specimens. The increased axial resolution results in a strong rejection of light from regions outside of the focal plane. The main advantage of a confocal microscope is its ability to optically section thick specimens. Contrast is provided from differential scattering due to differences in refractive index between various cellular and extracellular features in the field. The microscope objective of a confocal microscope illuminates the specimen with a double inverted cone of light. Photobleaching of fluorophores occurs in the entire inverted illumination cone of light as well as in the focal volume.

1.12.2 Multiple-photon Excitation Fluorescence Microscopy

This technique also referred to as non-linear, multiphoton, or two-photon laser scanning microscopy, is an alternative to confocal and deconvolution microscopy and uses non-linear optical effects to achieve optical sectioning. Two-photon excitation is a relatively old theoretical concept in quantum optics and it was first proposed by Maria Goeppert-Mayer in her doctoral dissertation (Fundamentals and Applications in Multiphoton

Excitation Microscopy). The sample is illuminated with a wavelength around twice the wavelength of the absorption peak of the fluorophore being used. For example, in the case of fluorescein which has an absorption peak around 500 nm, 1000 nm excitation could be used. Essentially, no excitation of the fluorophore will occur at this wavelength. However, if a high peak-power, pulsed laser is used (so that the mean power levels are moderate and do not damage the specimen), two-photon events will occur at the point of focus. At this point the photon density is sufficiently high that two photons can be absorbed by the fluorophore essentially simultaneously (www.microscopyu). Two photons of about equal energy (from the same laser) interact with a molecule, producing an excitation equivalent to the absorption of a single photon processing twice the energy. If the excited molecule is fluorescent, it can emit a single photon of fluorescence as if it were excited by a single higher energy photon. This event depends on the two photons both interacting with the molecule nearly simultaneously (~10^{-16} s), resulting in a quadratic dependence on the light intensity rather than the linear dependence of conventional fluorescence (Zipfel et al 2003). In this way, fluorophore excitation will only occur at the point of focus (Fig. 1.7), where it is needed, thereby eliminating excitation of out-of-focus fluorophore and achieving optical sectioning.

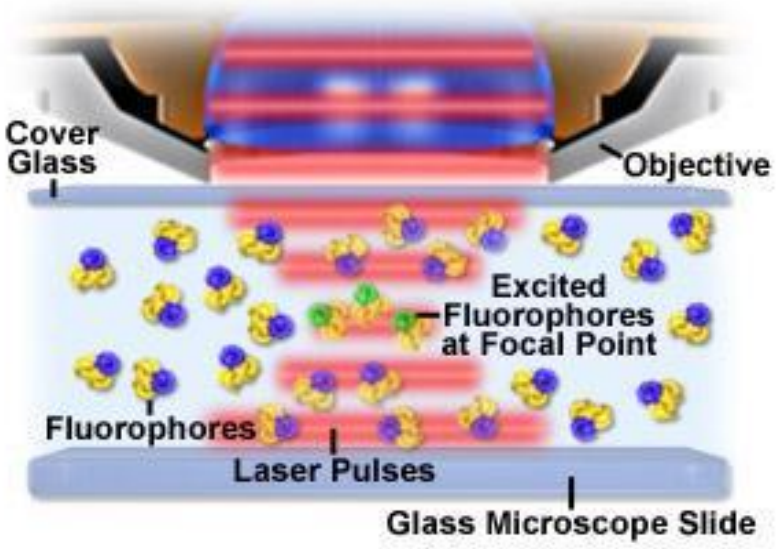

Figure 1.7 Fluorophore excitation in multiphoton microscopy

The picture illustrates diagrammatically the generation of two-photon excitation in a fluorophore-containing specimen at the microscope focal point. Above the focal point, the

photon density is not sufficiently high for two photons to pass within the absorption cross-section of a single fluorophore at the same instant. At the focal point, the photons are so closely spaced that it is possible to find two of them within the absorption cross-section of a single fluorophore simultaneously. From www.microscopyu.com.

1.12.3 Advantages of multiphoton imaging

The narrow localisation of two-photon excitation to the illumination focal point is the basis for the technique's most significant advantages over the confocal microscopy. In a confocal microscope, although fluorescence is excited through the illuminated volume of the specimen, only signal originating in the focal plane passes through the confocal pinhole, allowing background-free data to be collected (Fig. 1.8). By contrast, two-photon excitation only generates fluorescence at the focal plane, and since no background fluorescence is produced, a pinhole is not required. The most powerful advantage of two-photon excitation microscopy is its ability to provide superior optical sectioning at greater depths, in thick specimens-tissues, than is possible by other methods, such as confocal microscopy. Three physical mechanisms exist that function in combination to allow the increased depth of penetration and effectiveness in thick specimens: 1) Absence of out-of-focus absorption, allows more of the excitation light photons to reach the desired specimen level. Moreover, the excitation source is not attenuated by absorption by fluorophore above the plane of focus. 2) The red and infrared light, employed in two-photon excitation, undergoes less scattering than light that is bluer in colour (shorter wavelengths). 3) The effects of light scattering are less detrimental to the tissue using two-photon microscopy than using confocal microscopy (Fundamentals and Applications in Multiphoton Excitation Microscopy).

Multiphoton excitation has the advantage of less overall photobleaching and less damage to the tissue by repeated illumination because, when creating a three-dimensional stack of images along the z-axis, each focal plane is excited only once. By contrast, in confocal microscopy all focal planes are exposed to excitation light each time an optical plane is collected. Confocal scanning can lead to extensive photobleaching and a greater chance of toxicity if multiple z-stacks are taken repeatedly over time (Hadjantonakis et al 2003).

1.12.4 Limitations of multiphoton imaging

Multiphoton microscopy might have lower resolution than imaging with confocal microscopy, with a particular fluorophore. This loss in resolution can be eliminated by the use of a confocal aperture at the expense of a loss in signal. Generally, multiphoton microscopy is an expensive technique that works only with fluorescence imaging. In some cases, the laser power can burn the sample. Also, thermal damage can occur in specimens if they contain chromophores that absorb the excitation wavelengths, such as the pigment melanin. Moreover, inverted multiphoton microscopes can possibly make imaging of a tissue, for example spinal cord, extremely difficult because the heart rate and breathing affects the acquisition of steady images, producing artefacts. Additionally, certain tissue characteristics may impose limitations on penetration in either heavily pigmented tissue, such as liver, or highly scattering tissue, such as skin (Multiple-photon excitation fluorescence microscopy www.loci.wisc.edu).

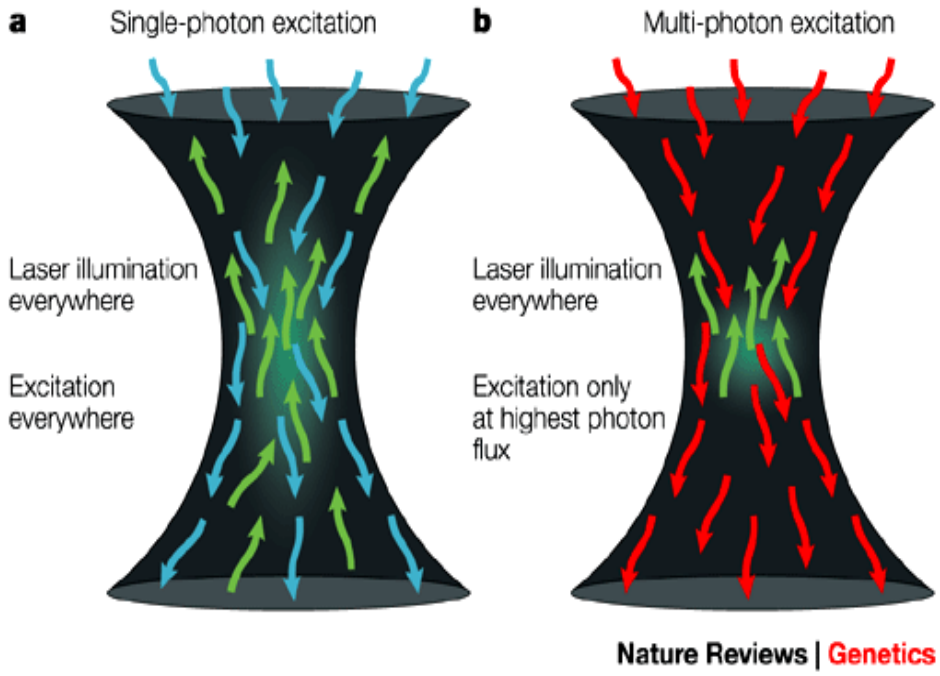

Figure 1.8 Imaging fluorescent proteins using laser-scanning microscopy

For a fluorescent protein such GFP (panel a), a blue photon (blue arrows) is absorbed and a green photon (green arrows) is emitted. In multiphoton excitation, the single high-energy photon is replaced by the quasi-simultaneous absorption of two (two-photon excitation) or

three (three-photon excitation) lower-energy near-infrared photons. So, for GFP, rather than a single blue excitation photon, two near-infrared photons (red arrows) can be used to excite the fluorochrome, which leads to the emission of a green photon (panel b) [From (Hadjantonakis et al 2003)].

1.12.5 Use of Transgenic animal models to study myelination

The use of transgenic animal models that express green fluorescent protein (GFP) has been employed to directly visualise and analyse dynamic developmental processes. Several lines expressing GFP specifically in the nervous system have been used to investigate the regulation in axonal growth during development and generation (Goldman et al 2001, Udvadia et al 2001). Additionally, generated transgenic mice in which red, green, yellow, or cyan fluorescent proteins, together termed XFPs, all from the *thy-1* promoter were selectively expressed in neurons. All four generating transgenic mice that expressed GFP or one XFPs labelled neurons in their entirety, including axons, nerve terminals, dendrites, and dendritic spines (Feng et al 2000).

Stable transgenic zebrafish that express GFP in oligodendrocytes has been a valuable tool to visualise complex myelination and demyelination processes *in vivo* that could be recorded under time-lapse confocal microscopy. Two promoters have been used to obtain oligodendrocyte-specific EGFP expression, the zebrafish P0 and the mouse PLP. Transgenic mouse lines that express GFP under the control of the PLP promoter have been extensively used for population analysis of oligodendrocytes *in vivo* (Fuss et al 2000). From studies in the zebrafish CNS, it was shown *in vivo* that radial glial cells may give rise to oligodendrocytes and also EGFP-expressing cells with polygonally shaped cell bodies, resembling immunopositive oligodendrocyte cells, extended processes suggesting the first manifestation of internode formation around the axons (Yoshida & Macklin 2005).

Taking a step further in myelination studies, it was crucial to investigate the behaviour of OPCs as they migrate and make contacts with axons *in vivo.* The created transgenic zebrafish that express fluorescent proteins in oligodendrocyte-lineage cells in combination with time-lapse imaging, during normal development, showed dynamic oligodendrocyte progenitor behaviour. Additionally, the advances in labelling methods, where a new line

was used expressing a membrane-localised EGFP, made possible to see processes that were not visible with cytosolic EGFP (Kirby et al 2006). The transgenic line Tg (nkx2.2a: megfp) expresses a membrane-tethered enhanced green fluorescent protein (mEGFP) under control of nkx2.2a regulatory sequences, carried on a bacterial artificial chromosome (BAC). The transgene expresses EGFP in a pattern similar to nkx2.2a RNA, marking a subset of oligodendrocyte-lineage cells (Kirby et al 2006).

MBP, the second most abundant protein in CNS myelin, is responsible for the adhesion of the cytosolic surfaces of multi-layered compact myelin (Boggs 2006, Brosamle & Halpern 2002, Harauz & Musse 2007). MBP is expressed specifically in the myelinating oligodendrocytes in the CNS, in the zebrafish. To investigate the mechanisms of myelination *in vivo* a new transgenic line of zebrafish Tg (mbp:egfp) was generated expressing EGFP under the control of the mbp promoter having several advantages. Therefore, faithful EGFP expression was observed in the oligodendrocytes of embryonic and adult transgenic zebrafish. Oligodendrocyte processes surrounding the axon bundles were clearly visualised throughout the post-embryonic stages (Jung et al 2010).

Time-lapse recordings in zebrafish showed migrating OPCs forming numerous highly branched filopodium-like processes, making contacts with the axons. Moreover, OPC process extension and retraction persisted for several hours and occurred after apparent contacts between neighbouring OPCs (Kirby et al 2006). Generally, uniform myelination requires such a distribution of oligodendrocytes in sufficient numbers to wrap the entire length of the targeted axons. OPC migration and division and the signals that regulate these mechanisms, influence importantly the oligodendrocyte distribution (Barres & Raff 1994). Consequently, the dynamic process activity may also function as a surveillance mechanism to recognise the presence or absence of nearby oligodendrocyte-lineage cells.

One of the most remarkable characteristics of myelin forming cells is that as oligodendrocyte-lineage cells develop, they produce numerous, fine, membrane processes that eventually wrap axons (Baumann & Pham-Dinh 2001, Pfeiffer et al 1993). Distinct process morphologies and formation of extensive membranes are evident in fixed tissues and cell culture and they seem to exemplify progressive oligodendrocyte maturation from pre-myelinating to myelinating phenotypes. Process remodelling, as observed in time-lapse

studies, is associated with post-mitotic cells and is considered to reveal a mechanism for axon identification and contact (Kirby et al 2006).

To conclude, oligodendrocyte precursor cell division, migration and regular alignment along the axons have been recently visualised *in vivo* in zebrafish (Kirby et al 2006), which today complement rodents as an important model organism for myelin research.

1.13 *In vivo* imaging of the mouse spinal cord

Despite the valuable knowledge of imaging of oligodendrocyte behaviour, the axonal biology and knowledge of axons' dynamic behaviour and signalling to the oligodendrocytes is important to untangle the challenging processes of myelination, degeneration and regeneration. In recent years, the advent of two-photon microscopy (Denk et al 1990) and the generation of transgenic animals which express fluorescent proteins driven by tissue-specific promoters (Feng et al 2000, Tsien 1998) have allowed the direct observation of cells and their behaviours under both physiological and pathological conditions *in vivo* (Davalos et al 2008).

However, limited work has been performed on imaging the intact living spinal cord. The close proximity of the animal's heart and lungs to the spinal column results in artefacts generated by the heartbeat and breathing movements, which significantly impede the acquisition of steady images from the spinal cord of anesthetised mice. As a result, imaging studies have been predominantly performed on *ex vivo* spinal cord slices. Recently, a method to image single axons in the mouse spinal cord was described which has previously been used to demonstrate single axon degeneration and regeneration for the first time *in vivo* (Kerschensteiner et al 2005, Misgeld et al 2007). However, this method required a series of surgically invasive techniques, such as multiple serial laminectomies combined with a temperature-controlled perfusion system and animal intubation, as well as extensive image post-processing to remove out-of focus frames and reconstruct aligned low-noise images (Misgeld et al 2007). Moreover, this method required the interruption of the animal's respiration during image acquisition and was performed on a transgenic line with sparsely labelled axons that made imaging and reconstruction of a single axon per field of view possible in the living mouse (Kerschensteiner et al 2005, Misgeld et al 2007).

In 2005, it was the first time that single sensory axons were *in vivo* imaged in the mouse spinal cord (Kerschensteiner et al 2005). Individual axons in the spinal cord of living mice were visualised, using a transgenic mouse line (GFP-S mice), in which a neuron-specific fragment of the *Thy-1* promoter drives cytoplasmic expression of high levels of GFP in subsets of neurons, including sensory neurons in the dorsal root ganglia (DRG). After documenting the morphology of a GFP-labelled axon and its position in relation to nearby blood vessels by fluorescence microscopy, repetitive imaging was able to be performed to study axonal changes following injury. *In vivo* imaging is a very useful as many limitations of conventional tracing methods could be overcome because the mechanistic insight can be inferred from time-resolved observations. Besides the description of pathological processes, *in vivo* microscopy is used to monitor the efficacy and mechanism to prevent degeneration or to promote regeneration. Imaging how axons respond to injury can be useful for numerous white matter pathologies such as multiple sclerosis and amyotrophic lateral sclerosis (ALS) (Kerschensteiner et al 2005).

1.14 Proposed models of myelination

Electron microscopy studies and time-lapse imaging of GFP-labelled oligodendrocytes *in vivo* (Kirby et al 2006) and *in vitro* (Watkins et al 2008) have helped to elucidate the mechanisms of glial-axonal interactions during the initial stages of myelination. Nonetheless, the processes of axonal ensheathment and myelin compaction are still not fully understood. More than half a century ago, the assembly of myelin membrane layers was described and still represents the current myelination model (Bunge et al 1989). There, an intermodal length of axon is enclosed by the plasma membrane of the myelinating cell. The inner glial process migrates underneath an already existing myelin layer to achieve myelin thickening.

Two models have dominated over the past few years (Fig. 1.9). First, it has been proposed that the leading edge of the myelin sheath, which aligns along the axon in a sheet-like manner, forms an initial wrap, which then moves underneath the growing sheet to form the next wrap (Bauer et al 2009) and described as a “carpet crawler” model in (Bauer et al 2009). In the second model, a narrow oligodendrocyte cell process spirals around the axon

and when a sufficient number of wraps have been generated by turns around the axon, the spirals extend laterally into overlapping sheets (Pedraza et al 2009) and is described as a "serpent" model. It has also been suggested that these two models are not mutually exclusive and it is likely that intermediate mechanisms might be involved (Bauer et al 2009).

Recently, CNS high-resolution live confocal imaging using murine organotypic cerebellar slice cultures lead to another mechanism being proposed, "the liquid croissant model". According to this model, myelin formation occurs by "pouring out" of myelin into a triangular shaped oligodendrocyte process that attaches at possible adhesion sites to the axon. While this pouring process continues, myelin spreads sideward potentially being guided by axonal membrane proteins that move around the axolemma in a coordinated fashion. Myelin thickening is thus achieved by new layers forming on top of the inner one, resulting in a bidirectional coiled turn of myelin layers along the axon, resembling the bidirectional dough edges of a croissant. This model differs from the established models exhibiting not a smooth but uneven, regularly coiled surface contour that forms during myelination. The myelin outer tongue most likely gives rise to the confocal microscopic observations of coiled myelin turnings. It was suggested that an active axonal participation may also help to resolve the theoretically suspected energy concerns in the "carpet crawler" model (Sobottka et al 2011).

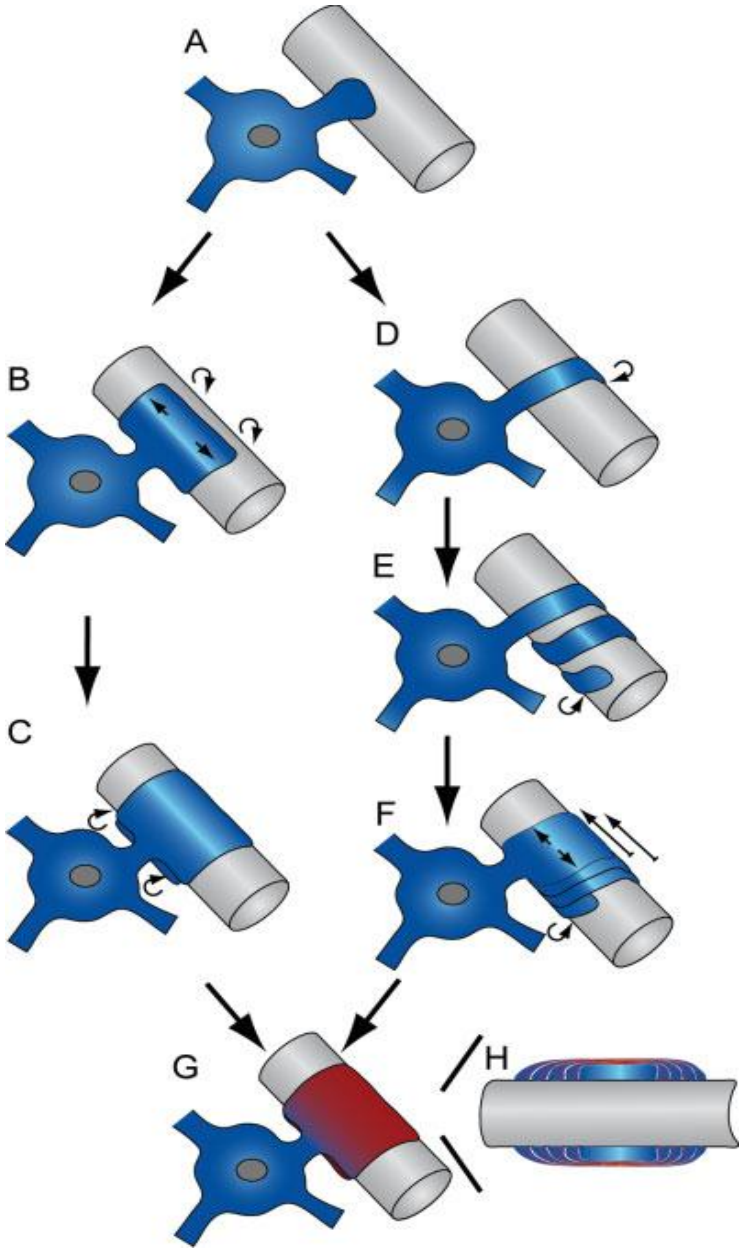

Figure 1.9 Two models of myelination

After contact formation of an oligodendrocyte process with an axon (A), the process could flatten into a broad sheet, wrap around the axon (B), and then moves underneath (C) to form the multiple layers of the mature myelin sheath (G). In the second model, the process could wrap around the axon-like twine around a post (D), and once the appropriate number of wraps has formed, flatten out and move laterally (E, F) to conclude sheath formation. H) Illustrates a longitudinal section through a myelinated axon with the different layers of the compact myelin sheath, with cytoplasm-containing paranodal loops at either side [from (Bauer et al 2009)].

1.15 Regulation of oligodendrocytes' myelination potential

The ensheathment of axons by myelin, a spiral extension of the glial cell membrane, is generally considered one of the most complex cellular interactions in the nervous system. In mixed brain cultures, glial cells only wrap axons but never dendrites (Lubetzki et al 1993), suggesting a continued role of axon-specific myelination signals. So, myelination is physiologically controlled by axon caliber, which likely stands for growth factor signals on the axonal surface (Michailov et al 2004, Raval-Fernandes & Rome 1998), and by factors secreted from astrocytes (Ishibashi et al 2006, Nash et al 2011b). In the PNS, neuregulin-1 type III (NRG1/III) is an axonal growth factor that activates ErbB receptor tyrosine kinases on glial cells and is required for Schwann cell survival, differentiation and myelination (Jessen & Mirsky 2005, Nave & Salzer 2006, Taveggia et al 2005). Unexpectedly, in the CNS, the corresponding signals that induce myelin formation appear to be very different. Specifically, axonal NRG1 and oligodendroglial ErbB receptors are not required for CNS myelination (Brinkmann et al 2008).

Despite the striking differences of axon-glia signalling at the ligand/receptor level, essential downstream mechanisms appear preserved in the evolution of myelinating glia in PNS and CNS. Experiments *in vitro* have suggested an important regulatory function for phosphoinositide 3-kinase (PI3K), the enzyme converting phosphatidylinositol 4,5-bisphosphate (PIP2) into the signalling lipid phosphatidylinositol 3,4,5-trisphosphate (PIP3) in myelination by Schwann cells (Ogata et al 2004) and in oligodendrocyte survival, differentiation and myelin growth through downstream effectors of PI3K, such as AKT (Barros et al 2009) and mammalian target of rapamycin (mTOR) (Tyler et al 2009).

Recent studies have revealed that elevated levels of PIP3, generated by the cell-specific loss of *Pten*, a PIP3 antagonist, phosphatase and tensin homolog, which dephosphorylates PIP3 to PIP2 and has important regulatory functions in growth, proliferation, migration and survival of cells in the nervous system (van Diepen & Eickholt 2008), in oligodendrocytes are sufficient to trigger the formation of myelin, which emerges as a highly specialised form of glial cell growth. Mutant glial cells also spirally enwrap C-fiber axons within Remak bundles and even collagen fibrils, which lack any membrane surface. This suggests that in oligodendrocytes, elevated PI3K signalling amplifies a yet-unknown axonal myelination signal that may differ in strength between individual fibers. This evidence is of

great importance and of clinical relevance, as it might help in the development of therapies aimed at boosting CNS remyelination (Goebbels et al 2010). Conditional *Pten* mutants are relevant to several human diseases. Mutations in *Pten* have been linked to macrocephaly, mental retardation and autism spectrum disorders (ASDs) (Butler et al 2005, Herman et al 2007). Moreover, the ability of PIP3 and PTEN to control the actin cytoskeleton has been implicated in cell polarity, motility and membrane dynamics in a number of cellular systems (Charest & Firtel 2007, Kolsch et al 2008, Wu et al 2007) and could also be involved in the early steps of myelination. The activity of proteins such as Rho GTPases and Rac effectors proteins and WASP, is regulated by PIP3 and leads to the localised polymerisation of F-actin (Charest & Firtel 2007). The aforementioned proteins have been independently implicated in oligodendrocyte development, process extension, axonal sorting and myelination (Bacon et al 2007, Kim et al 2006, Thurnherr et al 2006).

Cholesterol seems to have a novel regulatory role in myelin formation. The importance of cholesterol in myelination has been studied in conditional mouse mutants that lack cholesterol biosynthesis specifically in myelinating glial cells, both oligodendrocytes in the CNS and Schwann cells in the PNS. These mutants have been obtained by inactivating the first committed enzyme of the cholesterol biosynthesis pathways, squalene synthase (SQS, *Fdft1* gene) (Saher et al 2005). Analysis of the above mutants has revealed five important roles for cholesterol: 1) Cholesterol is rate limiting for central myelination as the biogenesis of myelin requires cholesterol enrichment. 2) Oligodendrocytes are able to take up cholesterol from their surroundings and enrich it in myelin membranes. 3) Only a minimal decrease of cholesterol in CNS myelin is tolerated. By this quality control, cholesterol apparently coordinates the assembly of lipids and proteins to preserve the unique composition of CNS myelin membranes. 4) In the CNS the transcription of myelin proteins is coupled to intracellular cholesterol levels. The reduced availability of cholesterol limits the expression of myelin proteins, possibly at the transcriptional level, because mRNA levels of myelin protein genes are strongly reduced in SQS mutants (Saher et al 2005) . Also, the importance of cholesterol biosynthesis in myelin maintenance and oligodendrocyte survival has been shown by treating adult rodents with statins. Treatment with simvastatin for five weeks induces demyelination (Miron et al 2009). Simvastatin treatment decrease the number of mature oligodendrocytes and enhance the number of

oligodendrocyte precursors. The benefit for MS patients treated with statins is ambivalent (Saher et al 2011).

Many genetic conditions cause loss of myelin, however, there are a few known examples of inherited hypermyelination. In the CNS enhanced myelin sheath thickness has been seen in transgenic mice overexpressing IGF-1 (Carson et al 1993). Given that IGF-1 receptors are expressed by oligodendrocytes and signal via PI3K and MAPK (mitogen-activated protein kinase) pathways at least *in vitro* (Bibollet-Bahena & Almazan 2009), IGF-1 would be a candidate to stimulate myelin formation via PI3K downstream signalling.

1.16 *In vitro* Modelling of CNS Myelination

Since many acquired or inherited diseases affect the integrity and function of the myelin sheath, resulting in either motor or sensory neuropathies, it is interesting to have at our disposal convenient models for studying pathogeny and possible treatments of these diseases. For this purpose, various *in vivo* and *in vitro* models have been developed. However, their aims are different. In the case of animal models of demyelinating diseases, it is expected to mimic a pathological process. On the other hand co-cultures of neurons and oligodendrocytes are primarily developed to study myelination process and to replace animals in experiments of myelin destruction or functional disturbances (Callizot et al 2011).

Tissue cultures approaches have been used for the study of myelination since the mid-1950s. Although these early studies using organotypic and aggregate cultures allowed a greater understanding of myelin ultra-structure, it was the development of culture methods that allowed the isolation of oligodendrocytes (McCarthy & de Vellis 1980) and provided a new insight into how oligodendrocytes mature and produce myelin. Moreover, the identification of stage-specific markers [reviewed in (Baumann & Pham-Dinh 2001)] allowed the precise classification of oligodendroglial differentiation state. Static imaging of oligodendrocytes at different developmental stages has shown that they are morphologically diverse (Butt et al 1997, Hardy & Friedrich 1996, Reynolds & Wilkin 1988). Differentiation into pro-myelinating or pre-myelinating oligodendrocytes involves the extension of a large network of branching processes often ending with motile

lamellipodial-like structures (Asou et al 1995b, Kachar et al 1986). These structures have recently been described as oligodendrocyte-growth cones because of their similarity to axonal growth cones (Fox et al 2006).

A comparison between current techniques used to model myelination would be beneficial for approaches in the future, in order to model effectively most of the aspects of myelination. In general, oligodendroglial development, myelination and remyelination are known to be regulated by secreted factors (Allamargot et al 2001, Ishibashi et al 2006, Jean et al 2002, Piaton et al 2011), contact-mediated signals, as for example integrins (Camara et al 2009, Zonta et al 2008) and electrical activity (Stevens et al 2002, Wake et al 2011) which all require the presence of neurons and in some cases, astrocytes (Sorensen et al 2008).

The first reports of myelination in two-dimensional dissociated culture, include studies where initial CNS myelin formation was observed from preparations, derived from 11 days old chick spinal cord, after 24 days *in vitro,* with mature compact myelin visible after 30 days *in vitro* (Kim 1972). Using dissociated CNS cultures to study myelination, from E13.5 mouse spinal cord, has many advantages, as these cultures faithfully recreate CNS myelination as they comprise a mixed culture of neuron and glial populations (Thomson et al 2006). Additionally, the method allows for the preparation of a sufficiently large quantity of cultures for histochemical analysis from a relatively small number of mouse embryos (Thomson et al 2008).

A second myelinating co-culture system that has been used for decades is comprised of DRG neurons maintained in culture in the presence of nerve growth factor (NGF) to which oligodendrocytes, having been prepared independently, are added. Electron microscopy confirmed that oligodendrocytes had wrapped axons with compact myelin after 5 weeks. Moreover, these early studies demonstrated that axons promote the proliferation of embryonic and adult OPCs (Wood et al 1980, Wood & Williams 1984) and that OPCs from adult CNS can differentiated into myelin-forming oligodendrocytes (Wood & Bunge 1986b). Using this co-culture system, studies suggested that OPC mitogens, such as PDGF and FGF-2 could inhibit myelination, while soluble neuregulin increased myelin formation (Wang et al 2007). The major advantage of the oligodendrocyte-DRG co-cultures is that

oligodendrocytes can be obtained from different species, CNS regions and tissues of different ages and added to DRG neurons [reviewed in (Jarjour et al 2011)].

1.17 Mutant/Transgenic Mice

As mice with natural mutations and hypomyelinating phenotypes became available, slice cultures from new born mice were used to study the cell biology of these mutations. For example, cerebellar slices from quaking *(qk)* and jimpy [jpmsd (myelin synthesis deficiency)] and *(jp)* mice were examined using semi-thin and ultra-thin sections to assess whether myelin defects were intrinsic to the myelin or were caused, or at least influenced, by a circulating deleterious substance (Billings-Gagliardi et al., 1980). The slice technique also allows the study of myelination in cerebellar cultures using transgenic mice which otherwise die before myelination occurs. For example, transgenic mice null for Netrin-1 or DCC die within hours of birth (for non-neurological reasons) but by study of cerebellar slices from these mice, it was seen that myelination occurred with abnormalities of the paranodal loops (Jarjour et al., 2008). Direct visualisation of myelinating cells in slice cultures can be achieved using transgenic mice expressing a fluorescent protein under an oligodendrocyte promoter (e.g. PLP-GFP) (Harrer et al., 2009). Delivery of genes, e.g. GFP or sh/ mirRNAs directly to cells within slices to manipulate cell biology is also possible using lentiviruses (Zhang et al., 2011) or Semiliki Forest Virus (Haber et al., 2009).

1.18 *shiverer (shi)* mice

Mutations that specifically affect myelin synthesis or maintenance can be divided into three categories: those like *shi* and *jp*, which affect primarily oligodendrocyte function; those like trembler (*Tr)*, which affect Schwann cell function; and those like *qk* and twitcher *(twi)*, which affect both oligodendrocytes and Schwann cells and consequently affect both CNS and PNS myelination. A number of mutations have been identified in mice that affect oligodendrocyte and/or Schwann cell function, which lead to dysmyelination in the CNS and/or PNS (Molineaux et al 1986). The *shi* mutation is autosomal recessive, first observed

by Biddle et al. (1973) in the F38 generation of the Swiss Vancouver (SWV) stock mice (Chernoff 1981) and is characterised by the onset of tremors at about the 12th day of life, tonic seizures at later times and a progressive deterioration ending in an early death (Bird et al 1978, Chernoff 1981). The mutation principally affects oligodendrocyte functions and the CNS of the *shiverer* mice is almost entirely devoid of compacted myelin membrane. The complex array of phenotypic traits associated with this mutation like the failure of myelin compaction and degradation of MBP RNA and protein can be largely reversed by the integration and expression of the *Mbp* gene in *shiverer* mice (Readhead et al 1987). The *shiverer* mutation has been mapped to chromosome 18 (Sidman et al 1985) and so has the mouse *Mbp* gene (Roach et al 1985), consistent with the hypothesis that the deleted *Mbp* gene causes the *shiverer* phenotype. Analysis of *shiverer* mutant mouse DNA with probes from wild-type *Mbp* genes has revealed that the *Mbp* gene is partially deleted and several exons from the 3' portion of the gene are missing. The organisation of the *Mbp* gene has been determined by restriction endonuclease mapping, Southern transfer analysis and ultimately sequencing all exons and flanking regions (Roach et al 1985). The gene is composed of seven exons spanning 32 kb of DNA. The information encoded in exons 2 and/or 6 are specifically deleted from some forms of mature MBP mRNAs, which explains the four forms of MBP found in the rodent (Molineaux et al 1986).

From electron microscopy studies, in 18 and 38 days old *shiverer* mutants, many axons appeared unmyelinated in the cerebellum, corpus callosum and spinal cord. Those which were myelinated had no more than ten turns of myelin and this myelin was abnormal. The MDL was absent and the space between two intraperiod lines was occupied by an 8 nm thin sheath of oligodendrocyte cytoplasm. This cytoplasm was continuous with the cytoplasm contained in inner and outer tongues and in paranodal loops. The paranodal regions appeared frequently abnormal, lacking normal contact with the axons. In 90 days old mutants, most axons were surrounded by thin oligodendrocyte processes but fully normal myelin sheath, with a continuous MDL had never been observed (Privat et al 1979).

1.19 Identification of stem cells grown as neurospheres

For most of the past century, the prospect of replacing lost or damaged cells in the CNS was hampered by the opinion that the adult mammalian CNS was incapable of generating new nerve cells. This belief, like most dogmas, was essentially founded on a lack of experimental evidence to the contrary. The overturning of this "no new neuron" hypothesis began midway through the twentieth century with a series of reports documenting neurogenesis in the postnatal and adult brain, continued with the isolation and *in vitro* culture of neurogenic cells from the adult mammalian brain and culminated in the discovery of a population of multipotent, self-renewing cells in the adult CNS (that is, bona fide neural stem cells). Although a variety of techniques were initially used, the neurosphere assay rapidly emerged as the assay of choice and has since become a valuable tool for isolating and understanding the biology of embryonic CNS (Reynolds & Rietze 2005).

Murine embryonic day 0 (P0) neural stem cells (NSCs) are a unique population of cells capable of self-renewal. In addition, they produce a large number of progeny capable of differentiating into the three primary neural phenotypes-neurons, astrocytes and oligodendrocytes-found in the adult mammalian CNS. A defined serum-free medium supplemented with epidermal growth factor (EGF) is used to maintain the NSCs in an undifferentiated state in the form of clusters of cells, called neurospheres, for several culture passages. When EGF is removed and serum added to the medium, the intact or dissociated neurospheres differentiate (Louis & Reynolds 2005).

Upon passage, the generation of new or secondary spheres represents a renewal of the previous population. Under these conditions, growth factor-responsive cells can theoretically be passaged indefinitely-and in practice for at least ten passages-with little change in the proliferation or differentiation potential of early and late passed cells. This demonstration of extensive renewal and of the generation of a large number of differentiated progeny provides the strongest evidence to date that the neurosphere assay represents a bona fide methodology for isolating and propagating neural stem cells (Reynolds & Rietze 2005).

1.20 Hypothesis

There are two models describing myelination that have been proposed over the last years. My hypothesis is that the mechanism of early glial-axonal interactions culminating to myelination may be a combination of both. For this reason, a range of methodologies and modern techniques (instead of EM) were set up to visualise oligodendrocyte-axonal interactions based in tissue culture (*in vitro*) and extended to the whole animal (*ex vivo*).

1.21 Aim of thesis

The main aim of this thesis is to follow myelination over time to identify the complex process involved in the formation of the myelin sheath.

Three approaches have been taken to follow myelination over time: i) imaging of fixed murine CNS tissue or murine cell culture models of white matter, to visualise early glial-axonal interactions ii) time-lapse imaging of mixed CNS myelinating cultures generated from mouse spinal cord to which exogenous GFP-labelled murine cells were added and iii) *ex vivo* imaging using time-lapse microscopy of the spinal cord of *shiverer* (*Mbp* mutant) mice, transplanted with GFP-labelled murine neurospheres which differentiate into myelin-forming oligodendroglia.

2. Methods and Materials

2.1 Animals-Animal Care

The following mice were used and maintained in Glasgow University Veterinary Research Facility: homozygous *shiverer* mice (*shiv/shiv*) on the C3H/101 genetic background, wild type mice on the C57BL/6 (Charles River Laboratories International Inc, Ormiston, Scotland) background, mice expressing enhanced GFP under the *β-actin* promoter (Okabe et al 1997) on the C57BL/6 genetic background (C57BL/6-Tg(ACTB-EGFP)1Osb/J) and mice expressing cyan fluorescent protein (CFP) under the *Thy1* promoter. The *β-actin* promoter drives cytoplasmic expression of GFP in all cells. The *Thy1-CFP* line (Feng et al 2000) (B6.Cg-Tg(Thy1-CFP)23Jrs/J), which was originally supplied as a double transgenic, expressing GFP under the S100 promoter, was kindly provided by Professor Wesley Thompson. For some experiments the *Thy1-CFP* line was crossed with *shiverer* mice to produce Thy1-CFP**shi/shiv* mice which had both labelled axons and the *Mbp* mutation.

All experimental mice were bred at the facility. Mice had access to food and water, *ad libitum*. Furthermore, all procedures were carried out in accordance with the guidelines, set forth by the Animals Scientific Procedures Act, under a project license (No. 6003895) granted by the UK Home Office and with the approval of the University of Glasgow Ethical Review Process Applications Panel.

2.2 Breeding Transgenic mice

For all experiments, wild type females were crossed from the GFP line with a *β-actin*-GFP male; therefore the F1 generation was either wild type (not green) or hemizygous (green). Homozygous mice were not used from this cross, as this would become impossible to know the genotypes of mice used for the experiments. Likewise, CFP, *shi*/+ mice were crossed to the *shi/shi* mice, so the F1 generation was hemizygous Thy1-CFP**shi/shiv* or wild type for the *Thy1*-CFP transgene.

2.2.1 *Shiverer (shi/shi)* mice

Mouse neurological mutants provide a valuable tool for elucidating morphologic and molecular processes of normal development. The natural mouse mutations *jimpy-msd* (*msd*, A242V) and *rumpshaker* (*rsh*, I186T) had been identified in humans and model severe conatal PMD and mild and spastic paraplegia type 2 (SPG-2) respectively (Komaki et al 1999, Kramer-Albers et al 2006). *Msd* mice develop progressive tremors and seizures, causing death between the third and fourth week of life. Morphologically, myelin is almost absent in the CNS, most likely because of oligodendroglial apoptosis (Knapp et al 1986).

The *shiverer* mouse observed by Biddle et al., 1973, is characterised by a tremor (Fig. 2.1) that can first be seen at about 12-14 days of age and continues for the remainder of the mouse's short life (50-100 days). The mutant *shiverer* had been proved to be one of the more interesting of these mutants, since the lack of myelin in the CNS of this mutant is related to a deficiency in MBP (Chernoff 1981).

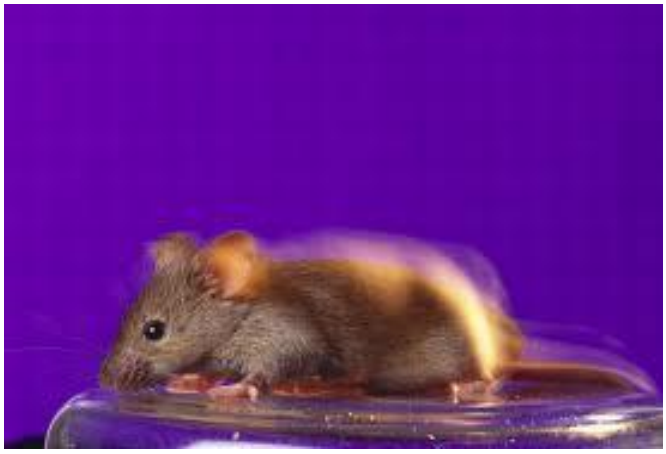

Figure 2.1 *Shiverer* mouse

The *shiverer* strain has uncontrollable boots of shivering. The first sign of abnormality is observed about 12 days of age, when a generalised tremor, resembling a shiver, accompanies movement by the animal. With age, the tremor becomes prominent in the hindquarters, and on rare occasion, paralysis of the hind limbs is observed. The tremors only appear when the animal is active, and are absent when the animal is at rest.

2.3 Imaging neurons and glial cells in transgenic mice expressing multiple spectral variants of GFP

Advance in the understanding of neural organisation and development has depended on a series of improvements in the ability to image individual neurons. The introduction of the jellyfish *Aequorea Victoria* GFP as a vital stain (Chalfie et al 1994) has significantly advanced optical microscopy of living cells (Patterson et al 2001).

GFP has some features that make it especially useful. First of all, GFP is a protein, so cells can be rendered fluorescent by introduction of a cDNA rather than the chromophore itself. Thus, the label can be rendered stable and heritable. GFP can be used to view living cells with minimal perturbation. Moreover, GFP can be fused to other proteins without loss of fluorescence (Krause et al., 2007; Sanes et al, 2000). GFP can be mutated to generate variants with altered spectral properties and improved translational efficiency, thermostability and quantum yield. It is well established that each of four spectral variants (green [GFP], yellow [YFP], cyan [CFP], and red [RFP], fluorescent proteins) satisfactorily label neurons *in vivo*. These generated GFP variants are better suited, in terms of resistance to photobleaching and quantum yield, for fluorescent microscopy than wild-type GFP and have optimised codon usage (Tsien 1998). Figure 2.2 depicts excitation and emission spectra determined for each fluorescent protein.

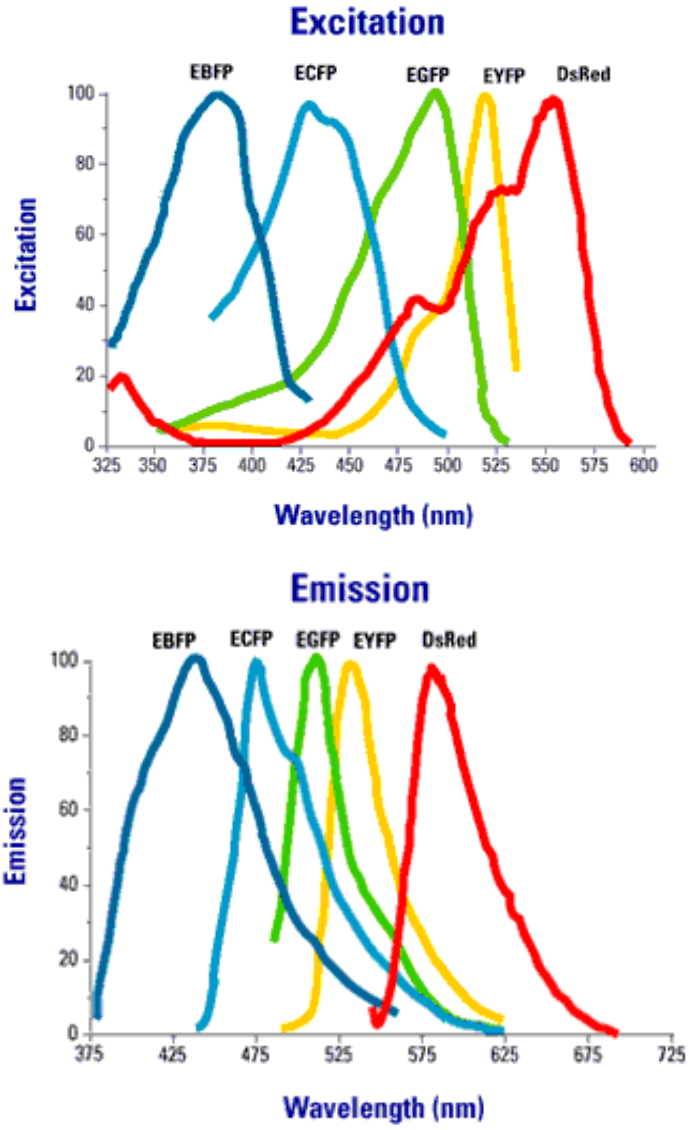

Figure 2.2 Emission and excitation spectra

Fluorescent protein spectra of the GFP variants

2.4 Isolation and culture of GFP-labelled and wild type neurospheres

Neurospheres were generated from both striata of *β-actin* GFP-transgenic mice expressing cytoplasmic GFP (cGFP) or wild type mice as previously described (Sorensen et al 2008), based on methods from Reynolds and Weiss (Reynolds & Weiss 1996, Zhang et al 1998b). Postnatal embryos P1 were decapitated, the brains excised and transferred to 5 ml of Leibovitz's-15 medium (L-15) (Invitrogen, Paisley, UK), on ice. After removing the

overlying meninges, using sterilised surgical instruments, the tissue was mechanically dissociated and triturated through a glass Pasteur pipette to produce a cell suspension. The dissociated cells were spun at 800 rpm for 5 min, the supernatant was removed and the cell pellet was reconstituted in 20 mL of neurosphere medium, consisting of DMEM/F12 (1:1, DMEM containing 4,500 mg/L glucose), supplemented with 0.105% $NaHCO_3$, 2mM glutamine, 5,000 IU/ml penicillin, 5 mg/ml streptomycin, 5.0 mM HEPES, 0.0001% bovine serum albumin, (all aforementioned from Invitrogen), 25 μg/ml insulin, 100 μg/ml apotransferrin, 60 μM putrescine, 20 nM progesterone, and 30 nM sodium selenite (from Sigma). The suspension was then placed into a 75 cm^3 tissue culture flask (Greiner, Gloucestershire, UK) and supplemented with 20 ng/ml mouse submaxillary gland epidermal growth factor (EGF, Peprotech, London, UK). Every 2-3 days, 5 ml neurosphere medium and 4 μl EGF (20 ng/ml) were added into the flask (Thomson et al 2008).

Neurospheres were passaged weekly for expansion, by mechanical dissociation in the same neurosphere medium. The cultures were incubated at 37^oC, in a humidified atmosphere of 7% CO_2/93% air, changing two thirds of the media every 2-3 days.

GFP neurospheres were used in both the *in vitro* and *in vivo* experiments. In some experiments the neurospheres were labelled with farnesylated GFP (fGFP) by lentivral transduction (lentivirus gift from Prof J Verhaagen, Netherlands Institute for Neuroscience, NIN) (see section 2.11). Triturated neurospheres were incubated with 10 μl of 2.2 x10^9 tu/ml of the viral supernatant overnight and maintained in neurosphere medium.

2.5 Astrocytes derived from neurospheres

After 7-10 days *in vitro*, large spheres were triturated, using a Pasteur pipette to produce smaller spheres/cell clusters. The spheres were differentiated into astrocytes as described in Thomson et al., (2006), by plating onto poly-lysine-coated coverslips (PLL 13 μg/ml, Sigma) in low glucose (1000 mg/ml glucose) DMEM, supplemented with 10% foetal bovine serum and 2 mM L-glutamine (DMEM-FBS 10%) (From Sigma). After 7-10 days, a confluent layer of astrocytes was formed and dissociated embryonic spinal cord cells were plated onto those, as previously described (Sorensen et al 2008).

2.6 Myelinating cultures

Myelinating cultures were generated from embryos taken from E13.5 (embryonic day E13.5) pregnant dams. Body weight is used to monitor the pregnancy status of the time-mated mice. The time-mated females were weighed on the day of plugging, then every day from E10 onwards. Between E10 and E13.5, the weight of a pregnant female mouse with more than 3 foetuses, increases 0.4-1.0 g/day. Total weight gain from day of plugging is approximately 0.8-1.0 g/foetus (Thomson *et al.*, 2008).

The method of generating myelinating cultures is based on previously published work (Sorensen et al 2008, Thomson et al 2008). Wild-type, GFP (*β*-actin) or *shiverer (shi/shi)* female mice were time-mated, with the day of plugging denoted as embryonic day 0.5 (E0.5) and embryos were collected on embryonic day 13.5 (E13.5). All culture preparation and maintenance was performed in an aseptic fashion, using laminar flow hoods, except for the tissue dissection stage, which was performed on the bench.

At E13.5, the pregnant female was killed by overdose of CO_2, followed by cervical dislocation. The abdomen was sterilised using 70% ethanol. Using sterilised scissors, the gravid uterus was removed in an aseptic fashion into a sterile plastic Petri dish, the foetuses extruded, decapitated and the umbilical cords cut. The point of decapitation of the foetus was sited just caudal to the attachment of the cerebellum, about 3 mm rostral to the cervical flexure. The bodies of the embryos were transferred in an empty chilled Petri dish, where the skin and tissue were gently removed, to reveal the spinal cord. The spinal cords were then removed and placed in a chilled small Petri dish with L-15 medium. The meninges were then stripped and the CNS spinal cords were minced using a scalpel blade and dissociated enzymatically by trypsin (100 μl of 2.5% trypsin, Invitrogen, Paisley, UK) and collagenase (100 μl of 1.33% collagenase, ICN Pharmaceuticals, UK). Enzymatic activity was stopped by the addition of 1 ml of a solution (SD) containing 0.52 mg/ml soyabean trypsin inhibitor, 3.0 mg/ml bovine serum albumin and 0.04 mg/ml DNase (Sigma, Poole, Dorset, UK) to prevent cell clumping.

The cells were triturated through a glass pipette and spun at 800 rpm, for 5 min and the pellet resuspended in 5 ml of plating medium [PM: 50 % low glucose DMEM , 25 % horse serum, 25 % HBSS (Hanks balanced salt solution without Ca^{2+} and Mg^{2+}) and 2 mM L-

glutamine, (Invitrogen)]. Cell viability was tested with Trypan Blue and cell number was estimated using a Haemacytometer. Trypan Blue stains dead or dying cells. Viable cells are able to repel the dye and do not stain.

The dissociated mixed spinal cord cells were plated onto coverslips supporting a monolayer of astrocytes or in most cases on top of PLL-coated coverslips at a density of 150,000 cells/100 µl. The coverslips were then placed in a 35 mm Petri dish and the cells were left to attach for 2 hours in the incubator, after which 300 µl of PM and 500 µl of differentiation medium DM was added (Sorensen et al 2008, Thomson et al 2006), which contained DMEM 4,500 mg/mL glucose, 10 ng/ml biotin, 0.5% hormone mixture (1 mg/mL apotransferrin, 20 mM putrescine, 4 µM progesterone, and 6 µM selenium) (formulation based on N2 mix of Bottenstein and Sato, 1979), 50 nM hydrocortisone, and 0.5 mg/ml insulin (all reagents from Sigma) was added. Cultures were maintained by replacing half of the medium with fresh medium three times a week. After 12 days in culture, insulin was excluded from the DM.

The cultures were maintained for up to 28 days, in a humidified atmosphere of 7% CO_2/ 93% air, at 37^{o}C. For time-lapse imaging in some cases, ascorbic acid (0.5 µl/1 ml) was added to the medium to enhance cell survival.

2.7 Time-lapse

For the study of glial-axonal interactions under time-lapse, several methods were used to generate the cultures: i) spinal cords at a 70:30% ratio of cells from the *β*-actin GFP mouse: wild type mouse, as a completely GFP-positive culture was visually “confusing” to follow glial-axonal contact over time. ii) cytoplasmic (c)GFP or farnesylated (f to label cell membrane) tagged neurospheres added to WT or *shiverer* myelinating cultures or iii) myelinating cultures infected with a virus containing cGFP, fGFP or a virus carrying both cGFP and dsRed.

2.8 PLL-coated coverslips

Poly-L-Lysine (PLL, Sigma P1274) was prepared to 4 mg/ml ddH_2O and stored in 67µl aliquots at -20^oC. One aliquot was diluted in 20 ml of ddH_2O (to 13.3ug/ml). Autoclaved, 13 mm coverslips were added to a 35 mm Petri dish containing 20 ml PLL (13.3ug/ml) and left for a minimum of 1 hour, but usually overnight at 37^oC for coating. The coverslips were then carefully picked out, using sterilised curved forceps and placed one per well, into a 24-well tissue culture plate, or two placed in a 35 mm Petri dish.

2.9 Preparation of APES [3(aminopropyl)triethoxysilane]-coated slides

APES (Sigma-Aldrich) slides were produced by soaking slides overnight in 5% Decon 90 (Decon Lab Ltd) and then washing them in distilled water before oven drying. The slides were dipped in methylated spirits, then 0.25% APES/methylated spirit for 2 minutes, before being rinsed in distilled water, oven dried, wrapped in foil and stored at room temperature (RT).

2.10 Quantitative analysis of axonal density

For quantitative analysis of axonal density and myelination, ten images from each coverslip were captured randomly, using Zeiss Axioplan 2 and Olympus IX70 fluorescent microscope and ISIS software and 10x magnification lens. Each experiment was performed in triplicate. For quantitative analysis of oligodendrocyte process formation and myelin membrane formation, 10 images/coverslip immunostained with the O4 antibody were also obtained.

Axonal density was measured using Image J software (NIH systems, version 1.45). The pixel value of the SMI-31 reactivity (neurites) was measured as a percentage of the total pixel value in one image (total area) and therefore the axonal density. The image was opened in Image J and split into the 3 channels (red, green and blue). The blue window and

the green window were both closed down, leaving the red channel showing the neurites open. The number of black and white pixels was obtained from the histogram selection and the percentage of black pixels was calculated (black pixels ÷ total pixels [black and white pixels] X 100 = % black pixels) for each image in Microsoft Excel.

2.11 Myelin quantification

Myelin sheaths were visualised using the AA3 primary antibody, which recognises not only the C-terminal of the PLP/DM20, but also the cell bodies of oligodendrocytes. Therefore, it was essential to manually identify and draw along the PLP/DM20 myelinated sheaths, avoiding the oligodendrocytes' cell bodies, using Adobe Photoshop (Elements 7.0) and adjusting the contrast. Brush shape size 9 was used to draw a pure blue colour (Blue: 255, Red: 0, Green: 0). The colour channels were then split, keeping this time the green channel open. The threshold of the average of the green channel was noted for each condition. A macro was generated in the lab (Myelin macro) to calculate the amount of green and blue overlap, the pixel number representing the amount of myelinated axons. These values were then exported into Microsoft Excel, where they were expressed as a percentage of the total red pixel value (SMI-31 reactivity) and therefore representation of the percentage of the myelinated axons. Each green/blue image pixel value corresponded to its own red axonal density value. The protocol is described in (Sorensen et al 2008).

2.12 Infection of wild type neurospheres with lentiviruses

Lentiviral (LV) vector systems are widely used as novel tools for the introduction of foreign genes in neural tissue, either by direct injection of the vector into the nervous system or indirect *ex vivo* gene transfer techniques. Two lentiviruses (Fig. 2.3) were used to infect wild type neurospheres, which afterwards added to the wild type or *shiverer* myelinating cultures, at various days *in vitro*.

1. LV-GFP-IRES-dsRed with a titer of $2.5x10^7$/ml (for red and green fluorescent cells)

Not concentrated virus.

2. LV-fGFP with a titer of $7.5x10^8$ /ml (for GFP in the membrane).

Concentrated virus.

Map LV-fGFP and dsRedexpress-IRIS-GFP

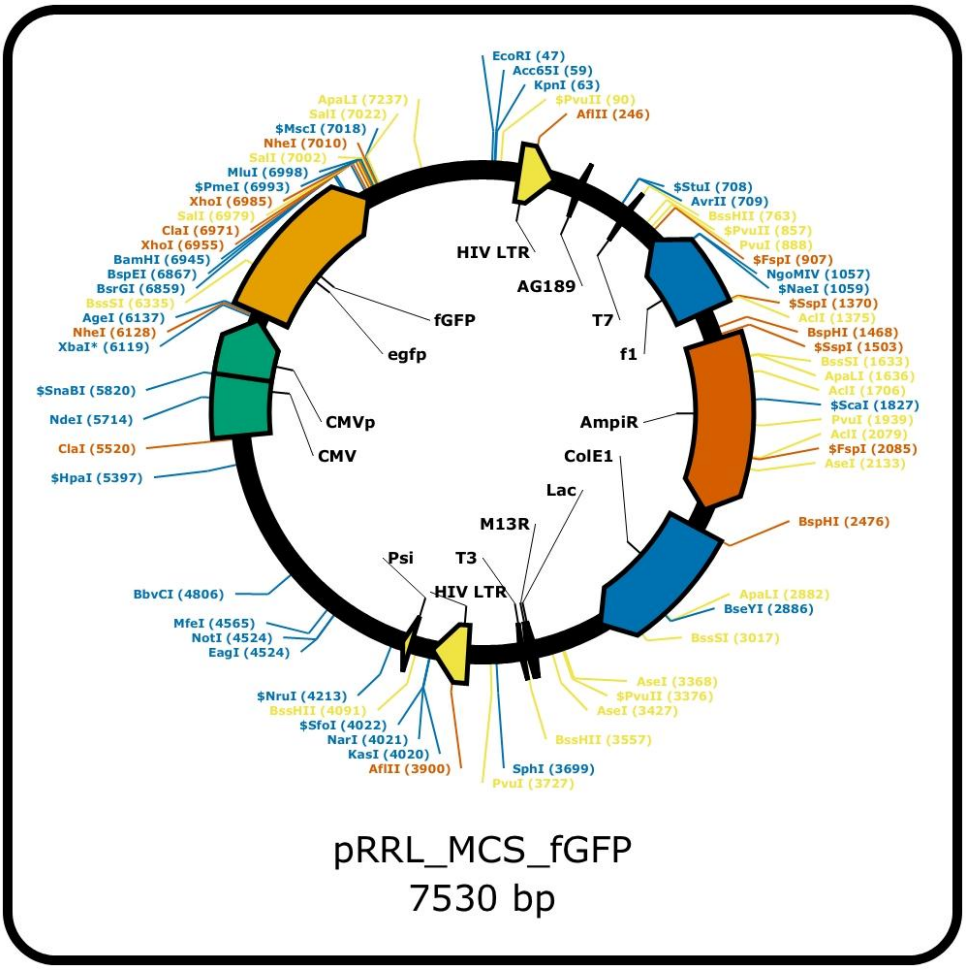

Figure 2.3 Schematic drawing of the plasmid vector construct used in this study

The lentiviral construct carries an internal cassette encoding farnesylated GFP. Transgene expression is driven by the cytomegalovirus (CMV) promoter. Transgene expression cassette was cloned in long-terminal repeats (LTRs).

2.12.1 Description of fGFP:

pEGFP-F encodes farnesylated enhanced green fluorescent protein, a modified form of EGFP that remains bound to the plasma membrane in both living and fixed cells. The abbreviation fGFP is used throughout the thesis. The vector contains the 20-amino-acid farnesylation signal from c-Ha-Ras fused to the C-terminus of EGFP. This farnesylation signal directs EGFP-F to the inner face of the plasma membrane. pEGFP-F encodes a red-shifted variant of wild-type GFP, optimised for brighter fluorescence and higher expression in mammalian cells (excitation maximum = 488 nm; emission maximum = 507 nm). The coding sequence of the EGFP gene contains more than 190 silent base changes which correspond to human codon-usage preferences. Sequences flanking EGFP-F have been converted to a Kozak consensus translation initiation site to further increase the translation efficiency in eukaryotic cells.

The vector backbone also contains an SV40 origin for replication in mammalian cells expressing the SV40 T-antigen. A neomycin resistance cassette (Neor), consisting of the SV40 early promoter, the neomycin/kanamycin resistance gene of Tn5, and polyadenylation signals from the herpes simplex virus thymidine kinase (HSV TK) gene, allows stably transfected eukaryotic cells to be selected using G418. A bacterial promoter upstream of this cassette expresses kanamycin resistance in E. coli. The pEGFP-F backbone also provides a pUC origin of replication for propagation in E. coli and an f1 origin for single-stranded DNA production.

In general, EGFP-F is designed for use as a cotransfection marker. Because it remains attached to the plasma membrane, it can be detected by fluorescence microscopy in permeabilised cells after ethanol fixation. However, in this thesis it is used to label the oligodendrocyte membrane so that the process can still be seen when compact myelin is formed. Since all the cytoplasm is extruded from the compact myelin, cGFP labelling in the cytoplasm cannot be seen in the later stages of myelination.

2.12.2 Viral vector production

The viral supernatants from cell transfected with plasmids needed to produce fGFP-encoding LV vector were generously provided by Professor Joost Verhaagen (Graduate School for Neurosciences Amsterdam, Netherlands Institute for Brain Research, Amsterdam, The Netherlands). The EGFP-F was in the lentiviral backbone pRRL-MCS. All viral stocks were kept at -80 C until use.

The wild type or *shiverer* myelinating cultures were infected with supernatant at various concentrations and GFP expression visualised in the cells using an inverted fluorescent microscope after 3 days. The spinal cord cells were infected with a MOI of 50 (usually 50 viral particles per cell). Generally, the probability that a cell will absorb n virus particles when inoculated with a MOI of m can be calculated by a Poisson distribution:

$$P(n) = \frac{m^n \cdot e^{-m}}{n!}$$

where m is the multiplicity of infection or MOI, n is the number of infectious viral particles that enter cell and $P(n)$ is the probability that a cell will get infected by $\boldsymbol{n}$ infectious virus particles.

Healthy and dense wild type neurospheres, forming many small spheres, after 10 days *in vitro,* in neurosphere medium, were plated on a 6-well plate and infected with the lentiviruses overnight. The next day the medium was aspirated and the cells were spun down at 5000 rpm for 5 min. The pellet was diluted with 4 ml of fresh neurosphere medium and 1 ml of supernatant in a small flask. After 2-3 days many labelled spheres could be seen.

2.13 Transplantation of spinal cord neurospheres

2.13.1 Anaesthesia

Neonatal *shiverer* mice 19-21 days of age were recipients of neurosphere transplantation, as described previously (Edgar et al 2004). This required good aseptic techniques. Briefly, the mice were anesthetised by inhalation of 5% isofluorane which was reduced to ~2% during surgery (Fig. 2.4 A and B), in combination with a mixture of nitrous oxide and oxygen (0.3 l/min O_2/0.7 l/min N_2O). Nitrous oxide is a weak anaesthetic agent, which has sedative, analgesic and anxiolytic properties. Because of its weak properties and when it is mixed with 50% oxygen, it rarely produces loss of consciousness. The mouse sat for 2-3 min in an empty cage while the anaesthesia took place. It was important not to disturb the animal prematurely, since that could agitate the mouse and affect the quality of the subsequent procedure. The most useful indicator to ensure that an adequate depth of anaesthesia had been attained was the toe-pinch reflex. The toe of the hind limb should be pinched firmly between the operator's fingernails.

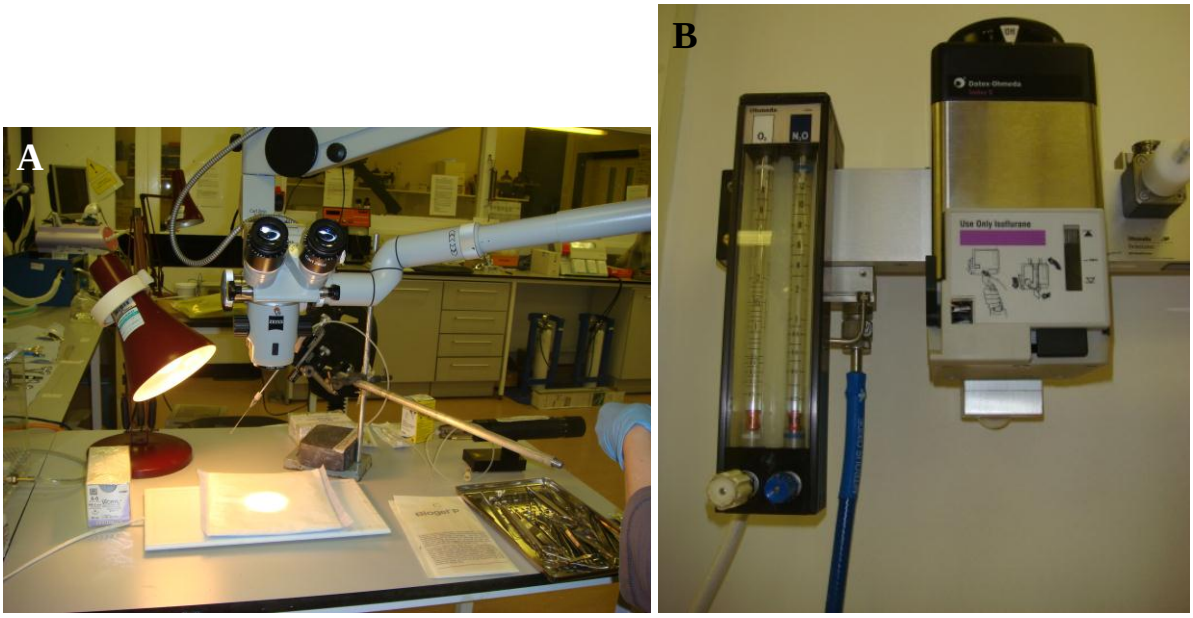

Figure 2.4 Preparation of the theatre

A) Operating microscope, CellTram Oil manual micromanipulator and sterilised surgical instruments under aseptic set up conditions. B) Mice were anesthetised by inhalation of 5%

isofluorane which was reduced to ~2% during surgery, in combination with a mixture of nitrous oxide and oxygen (0.3 l/min O_2/0.7 l/min N_2O).

For mice of approximately 10 g, 100 µl of Rimadyl–Carprofen (Pfizer Animal Health, Tadworth, Surrey UK) was administered subcutaneously (after two dilutions 1:100 in distilled water) at the start of surgery, for pain relief and to reduce any possible post-operative inflammation. There was no need to employ any other pain-relief protocol as the mice recovered quickly.

2.13.2 Laminectomy

A short vertical incision was made with a scalpel blade over the thoraco-lumbar region of the spine, from anterior to posterior. With the aid of an operating microscope, the transverse laminae of a vertebra were broken (laminectomy) to reveal the spinal cord (Fig. 2.5). A small opening was made in the dura with a sterile needle and a cell suspension of cGFP or fGFP neurospheres was injected using a CellTram Oil manual micromanipulator (Eppendorf Ltd, Cambridge, UK) at a rate of 1 µl/min, using a glass microelectrode that was inserted into the exposed spinal cord. One injection was made into the dorsal spinal cord, avoiding the midline dorsal vein. A total volume of 3-5 µl of cell suspension containing, approximately $5x10^4$ cells/µl was injected, at the depth of < 1 mm. The electrode was left in place for an additional 2 min to minimise back-flow of cells. No immunosuppressant treatment was used. Mice were sacrificed at various time points 3 days, 7-10 days, 14 days and 4 weeks (± 3 days) after transplantation.

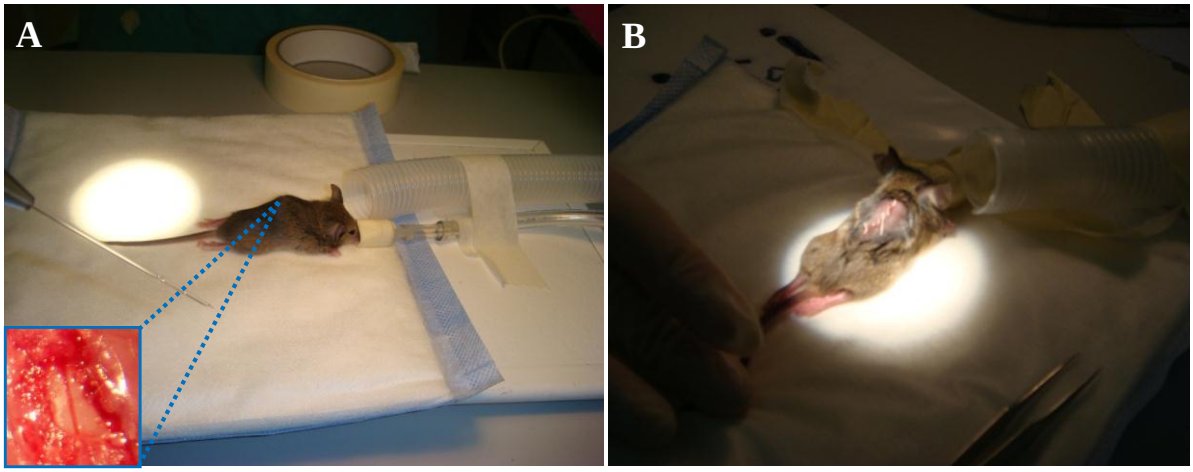

Figure 2.5 Laminectomy and Injection

A) The transverse laminae of a vertebra were broken to reveal the spinal cord and the vertebral column was exposed at T5-T9 level approximately of the thoraco-lumbar region. One injection was made into the dorsal spinal cord, avoiding the midline dorsal vein (insert). B) 5-7 sutures were made after the injection.

2.13.3 Recovery after Surgery

For all surgery, minimising stress during recovery was important; mice were kept in a thermostatically controlled heat pad and were transferred, after the surgery, to an incubator for at least two hours, before their return to the animal unit facility. It was also essential that neonatal mice were not separated too long from their mother after the surgery, as they had not been weaned and were still nutritionally dependent on their mother (Fig. 2.6). In addition, it is known that maternal deprivation enhances the neuroendocrine response to stressors (Daskalakis et al 2011, Ladd et al 1996). Physical contact not only kept them warm, in order to maintain body temperature, but maternal care during that critical period of recovery, decreased conditions of anxiety (Francis et al 1999, Ogawa et al 1994). The mice were monitored twice a day and their health and recovery status recorded on a recovery sheet.

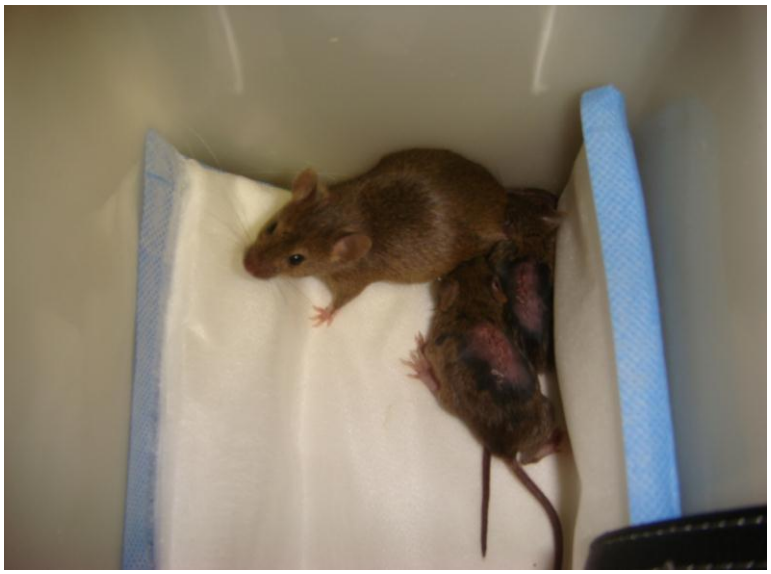

Figure 2.6 *shiverer* recover quickly after the surgery

Soft food and water were provided and *shiverer* recovered fast due to maternal care.

Recovery Sheet

Recovery animals on a severe severity band should be monitored and information recorded at least 3 times a day.

(i.e. first thing in the morning, around lunch time and last thing before leaving the department in the evening

Recovery animals on a moderate or mild severity band should be monitored twice a day

If you are concerned about the general condition of any animal, consult with the project licence holder, one of the vets or a member of Biological services staff.

Rat ID No …….. Licensee …….

Date of Operation …… Pre-op weight ……

Date	Time	Faeces	Urine	Has animal eaten any soft diet	Satisfactory recovery from surgery	Spontaneously moving about cage	Vocalisation on handling	Unresponsive when handled	Facial swelling	Comments
				yes no	good ok slow	yes no	yes no	yes no	yes no	

2.14 Tissue processing and immunohistochemistry

Animals were euthanised with CO_2 and perfused transcardially with 10 ml of saline (Fig. 2.7), followed by 20 ml of 4% paraformaldehyde.

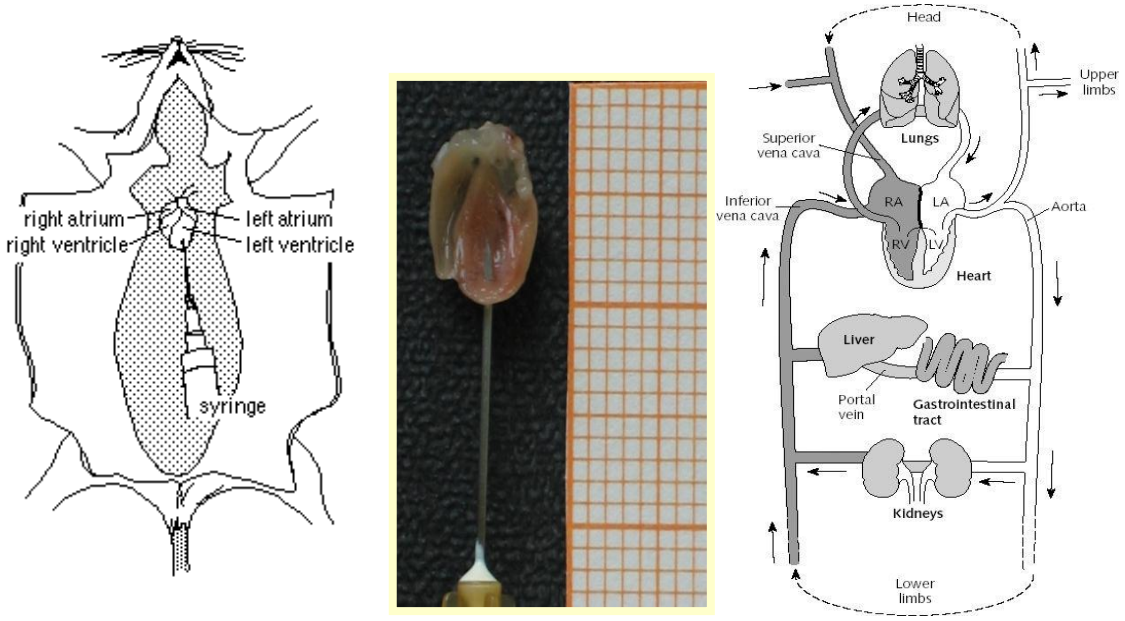

Figure 2.7 Perfusion of a mouse

The diagram illustrates the chambers of the heart and the correct positioning of the syringe in the left ventricle for perfusion. Under *in situ* conditions, vascular perfusion results in a uniform and rapid dissemination of fixative into all parts of the tissue via the vascular bed, resulting in an increased depth and rate of actual fixation. Adapted from (Zeller 2001).

The spinal cords were dissected and placed in 0.1 M glycine in PBS, then cryoprotected in 20% sucrose overnight at 4^{o}C. The spinal cords were embedded in OCT and frozen rapidly in isopentane, cooled in liquid nitrogen. The rostro-caudal segment at the lumbar thoracic junction of the spinal cord encompassing the transplant site was embedded and cryosectioned dorso-ventrally. Cryostat serial sections (10 μm) were cut, mounted onto APES-coated slides and stored at -20^{o}C. Before immunostaining, sections were air dried at RT for 10-20 min and then rehydrated in PBS for 10 min. The sections were permeabilised with methanol at -20^{o}C for 10 min and blocked with 10% normal goat serum in PBS for 1

hour at RT followed by incubation in primary antibody in the same blocking solution overnight at 4^{o}C. Antibodies used were: rabbit anti-GFP (1:1000, Abcam), mouse anti-GFP (1:250, Abcam) for GFP transplanted cells, rabbit Olig-2 (1:500, Chemicon) and rabbit PDGF-a (1:250, Pierce) for pre-myelinating oligodendrocytes, rat anti-MBP (1:500, Serotec) for mature oligodendrocytes, rabbit anti-Caspr (1:1000; gift from Elior Peles) for nodes of Ranvier, mouse anti-GFAP (1:1000, Sigma) for astrocytes and mouse anti-phosphorylated neurofilament SMI-31 or mouse anti-non phosphorylated neurofilament SMI-32 (1:1500 Affiniti) for neurites. The slides were washed three times with PBS and then incubated with appropriate fluorescent-conjugated secondary antibodies (Cambridge Biosciences) for 1 hour at RT. The slides were washed three times with PBS and then mounted in Citifluor antifade (Citifluor Ltd, London, UK) mounting medium.

2.15 Immunohistochemistry and antibodies for myelinating cultures

Immunocytochemistry was performed on differentiated cells, unfixed (O4 antibody) or fixed with 4% paraformaldehyde. Neurites/axons were visualised using a monoclonal antibody against phosphorylated neurofilaments (SMI-31, IgG1, 1:1500) or non phosphorylated neurofilaments SMI-32 (IgG1, 1:1500). Mature myelin (PLP/DM20) was detected using the AA3 antibody [1:100, anti-rat, hybridoma supernatant (Yamada et al 1999)] directed against PLP/DM20 or MBP (1:100 for cells, anti-rat, Serotec). Morphological changes and the differentiation of oligodendrocytes in spinal cord myelinating cultures were visualised using the O4 antibody [IgM, hybridoma supernatant, (Sommer & Schachner 1981)]. The integrity of the underlying astrocyte monolayer was investigated using antibodies against glial fibrillary acidic protein for astrocytes (GFAP; 1:100: anti-rabbit, Dako or anti-mouse IgG1 1:1000 Sigma). To detect GFP labelled cells rabbit anti-GFP (1:1000, Abcam) or mouse anti-GFP (1:250, Abcam) were used (see Table 2.1).

For cell surface labelling, primary antibodies (diluted in DMEM) were applied for 1 hour at RT. The cultures were washed in DMEM and briefly in phosphate-buffered saline (PBS) and were fixed in warm 4% paraformaldehyde for 20 min. After washing in PBS the appropriate secondary fluorescent-conjugated antibody (diluted in DMEM) was added for

1 hour at RT. For co-labelling with cytoskeletal and membranous antigens, cells were subsequently washed in PBS, permeabilised with methanol at -20^{o}C for 10 min and blocked with 10% normal goat serum in PBS, for 1 hour at RT. Primary antibodies, diluted in 10% normal goat serum, were incubated on the coverslips overnight, at 4^{o}C. The following day the coverslips were washed three times in PBS at RT and the appropriate fluorochrome-conjugated secondary antibodies were added for 1 hour, at RT. The coverslips were washed three times in PBS, followed by dH20 and subsequently mounted in Vectashield containing DAPI (Vector Laboratories Ltd, Peterborough, UK). However, if a blue secondary antibody was used, Vectashield without DAPI was used (see Table 2.2).

Table 2.1 Primary antibody list

Antigen	Raised in	Isotype	Dilution	Fixation method	Internal/ External	Source
AA3 (PLP)	Rat	IgG	1:100	4% PF	Internal	Hybridoma
Caspr-1	Rabbit	IgG	1:1000	4% PF	Internal	Gift from Dr Elior Peles
GFAP	Mouse	IgG1	1:1000	Ice cold methanol	Internal	Sigma
GFAP	Rabbit	IgG	1:500	Ice cold methanol	Internal	DAKO
GFP	Mouse	IgG	1:250	Ice cold methanol	Internal	Abcam
GFP	Rabbit	IgG	1:1000	Ice cold methanol	Internal	Abcam
MBP	Rat	IgG	1:100 1:500 (sections)	Ice cold methanol	Internal	Serotec
MOG	Mouse	IgG2A	1:1000	4% PF	Internal	Gift from Dr Chris. Linington
Olig-2	Rabbit	Poly-clonal	1:500	Ice cold methanol	Internal	Chemicon
O4	Mouse	IgM	1:1	N/A	External	Hybridoma
PDGF-a	Rabbit	IgG	1:250	Ice cold methanol	External	Pierce
SMI-31 phosphorylated neurofilaments	Mouse	IgG1	1:1500	4% PF	Internal	Affinity
SMI-32 non phosphorylated neurofilaments	Mouse	IgG1	1:1500	4% PF	Internal	Affinity

Table 2.2 Secondary antibody list

Antibody	Conjugate	Dilution	Source
Goat anti-mouse IgG1	FITC, TRITC	1:75	Southern Biotech
Goat anti-mouse IgG2A	FITC, TRITC	1:25, 1:50	Southern Biotech
Goat anti-mouse IgM	FITC, TRITC	1:100	Southern Biotech
Goat anti-mouse IgG	Cascade blue C-962	1:50	Southern Biotech
Goat anti-rat IgG	Alexa Fluor 594	1:1000	Invitrogen
Goat anti-rat IgG	Alexa Fluor 350	1:50	Invitrogen
Goat anti-rat IgG	FITC, Texas Red	1:100, 1:50	Southern Biotech
Goat anti-rabbit IgG	FITC, Texas Red	1:100	Southern Biotech
Goat anti-rabbit	Alexa Fluor 350	1:100	Invitrogen
Goat anti-rabbit IgG	Alexa Fluor 488	1:1000	Invitrogen

2.16 Maintaining live cells for time-lapse imaging

One of the most significant technical challenges for performing successful live-cell imaging experiments, is to maintain the cells in a healthy state and functioning normally on the microscope stage, while being illuminated in the presence of synthetic fluorophores and/or fluorescent proteins. Among the most important considerations for live-cell imaging that should be taken into serious account are temperature, oxygenation, humidity, phenomenon of osmosis, pH (medium buffering), phototoxicity, the laboratory environment, microscope focus drift, fluorescence signal strength, bleed-through, and resolution. Another important aspect of successful live imaging is a deep insight into the biology of the cells or tissue being studied.

Close control of the environment is one of the most critical factors in successful live-cell imaging experiments. In particular, the conditions under which cells are maintained on the microscope stage, although widely variable in many requirements, depending upon the tissue, often determine the success or failure of an experiment. Aspects of the environment that are readily manipulated include the physical parameters of the chamber in which the cells are grown and imaged, the localised degree of temperature control, atmospheric conditions (gas mixture and humidity), nutritional supplements and issues of osmosis of the culture medium.

2.17 Maintenance of the explants for *ex vivo* imaging

The protocol was based on studies by Kerschensteiner and colleagues (Kerschensteiner et al 2008). To keep the explants viable during the 3-5 hour imaging, it is vital to ensure sufficient O_2 and nutrient supply as well as constant pH and temperature Therefore, all procedures were performed in a combination of F12+L-glutamine, CO_2 independent medium and DMEM+ Glutamax (4 g/L D-glucose) or Neurobasal A medium (Invitrogen) that had been bubbled with 95% O_2 and 5% CO_2 for at least 15 min before imaging. During dissection, the temperature was kept low by placing the mouse on aluminium foil with ice underneath, to protect the tissue from hypoxia. During imaging the explant was superfused with pre-warmed O_2-bubbled medium (Fig. 2.8). The temperature of the explant was maintained at 35-37^{o}C using a heating stage, superfused with pre-warmed medium.

Generally the tissue was kept well oxygenated after careful dissection and established steady flow rates and temperature were established to create conditions as close to physiological as possible and to avoid any drift during recording.

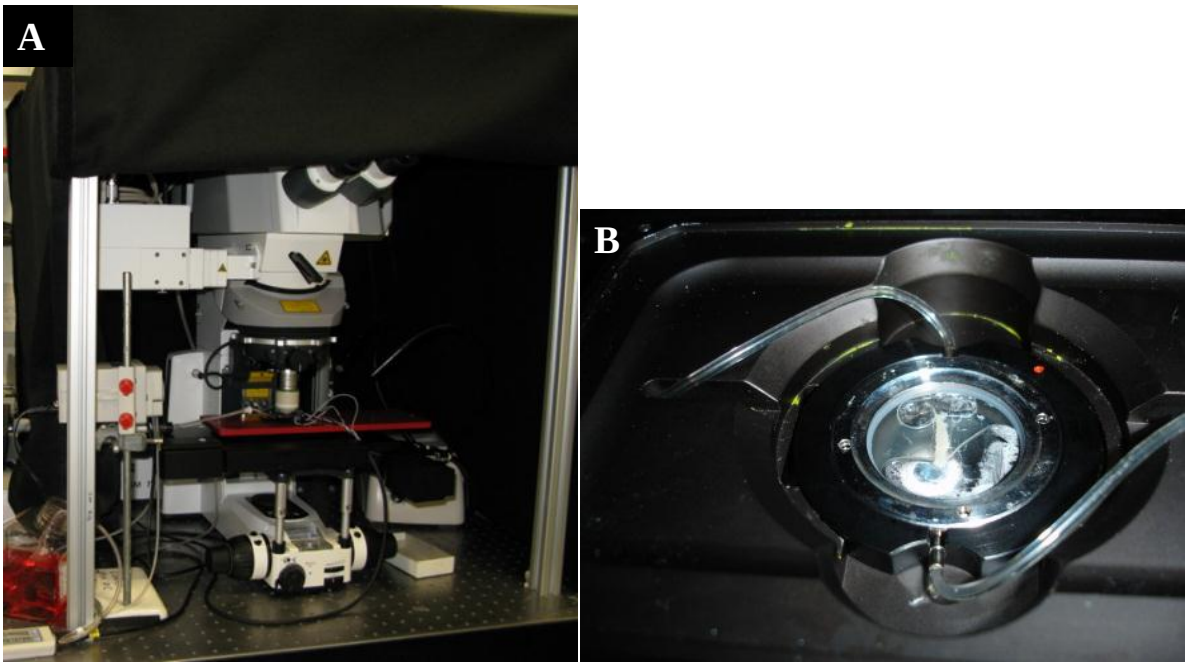

Figure 2.8 Maintenance and superfusion of explants for *ex vivo* imaging
A) Neurobasal A medium bubbled with 95% O_2 and 5% CO_2 with the use of a pump for steady flow rates**.** Black curtains were used in a frame around the multiphoton microscope B) Superfusion chamber and the spinal tissue was attached to the plastic coverslip, using 3M Vetbond tissue adhesive.

2.18 Stabilisation of the spinal cord for imaging with multiphoton microscope

To stabilise the fresh dissected spinal cord at the glass bottom microwell Petri dish, with 14 mm diameter of microwell (MakTek Corporation, PART no.: P35G-1.5-14-C), agarose was used. Low melting agarose melts at 65^{o}C and solidifies at 37^{o}C. A 3% solution of agar (type VII, low melting; Sigma) was made in DMEM in a sterile bijoux with screw-top lid, melted in 65^{o}C water bath, and then transferred to 37^{o}C water bath 5-10 min before required. It usually takes 8 min for the agar to cool to 37^{o}C in the water bath (Thomson et

al 2006). About 2 ml of the liquid agar was used to stabilise 1.5 cm of spinal cord of the mouse and the mould was set on ice to gel.

2.19 Detailed image analysis

For detailed morphological analysis of the axons, oligodendrocytes and myelin sheath formation, images were captured using either an Olympus FV1000 or Zeiss 710 laser scanning confocal microscope. Image processing and movies were made with FV10 ASW (Olympus, Essex, UK) Full Version Viewer software. Complex interactions between structures were analysed from maximum intensity projections in the z dimension and visualised with Volocity (Version 5) and Imaris imaging software (Version 7.1.1) which provided high resolution volume rendering of multichannel 3D data sets. Further image processing was performed using Image J 1.44 and Fiji-win 32 software. Manual tracking using Fiji-win 32 was used to follow the dynamics of cGFP and fGFP cell movements in time-lapse imaging.

2.20 Confocal imaging

Fluorescence is a member of the ubiquitous luminescence family of processes in which susceptible molecules emit light from electronically excited states, created by either a physical as for instance, absorption of light, mechanical-friction, or chemical mechanism. Generation of luminescence through excitation of a molecule by ultraviolet or visible light photons is a phenomenon termed photoluminescence, which is formally divided into two categories, fluorescence and phosphorescence, depending upon the electronic configuration of the excited state and the emission pathway.

Different fluorochromes might need different excitation wavelengths. But fluorochromes that can be excited with the same wavelength can have different emission wavelengths. A fluorescence microscope uses a high powered mercury lamp. This lamp has a large part of the spectrum and is able to excite more different fluorochromes. Both flow cytometer and microscope use filters to select for the specific emission. Excitation and emission wavelength determine the fluorochrome(s) that can be used. For the aforementioned

reasons, it was essential to know the exact emission and excitation spectra of all the fluorophores used (Fig. 2.9 and Table 2.3 below), in order to have the best possible quality of images, adjusting the offset and the laser power.

Emission and excitation spectra of FITC and TRITC fluorophores

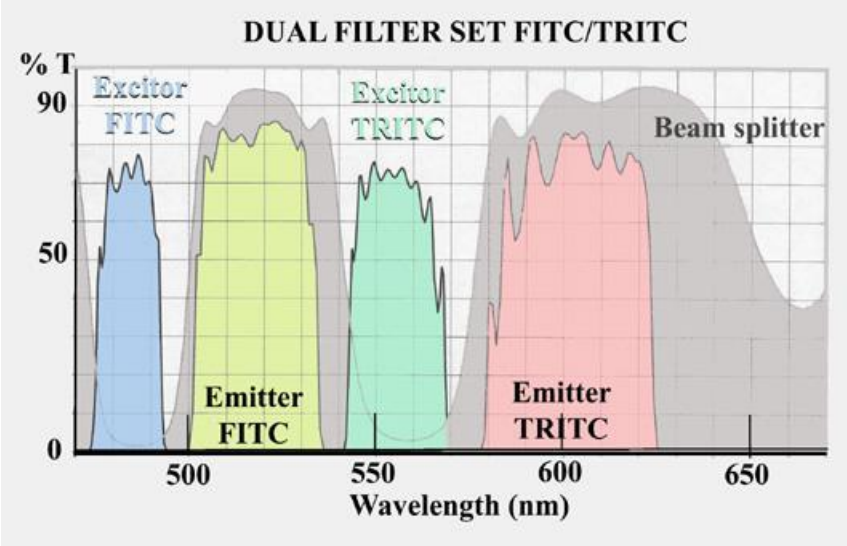

Absorption and fluorescence emission FITC spectra of fluorescein goat anti–mouse IgG antibody

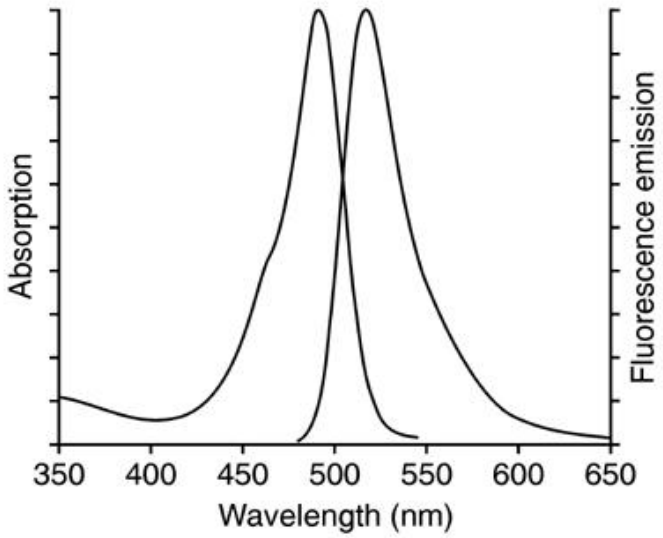

Emission and Excitation spectra of Cascade Blue C-962 (400- 420)

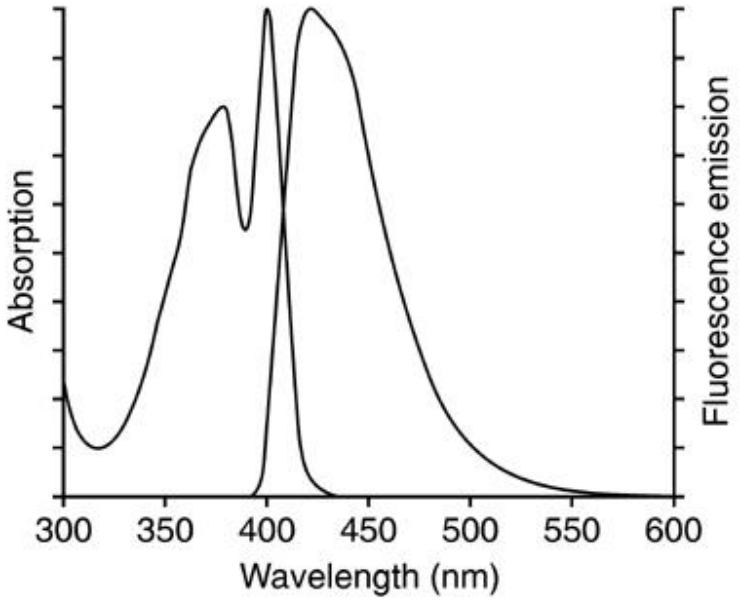

Emission and Excitation spectra of Alexa Fluor (blue) goat anti rat IgG 350

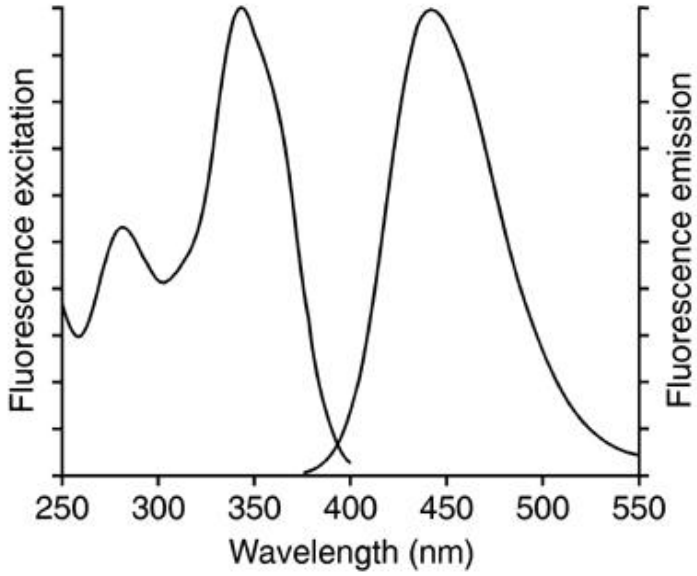

Emission and Excitation spectra of Texas Red

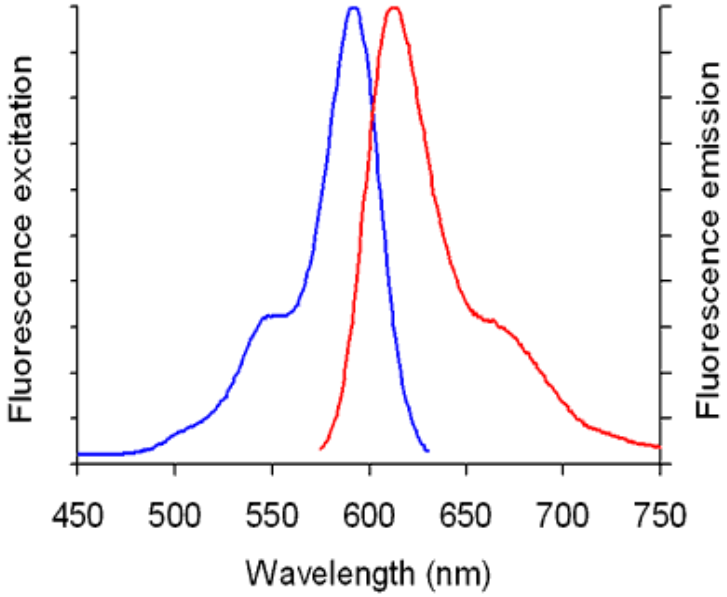

Absorption and fluorescence emission spectra of Alexa Fluor 594 goat anti–rat IgG antibody

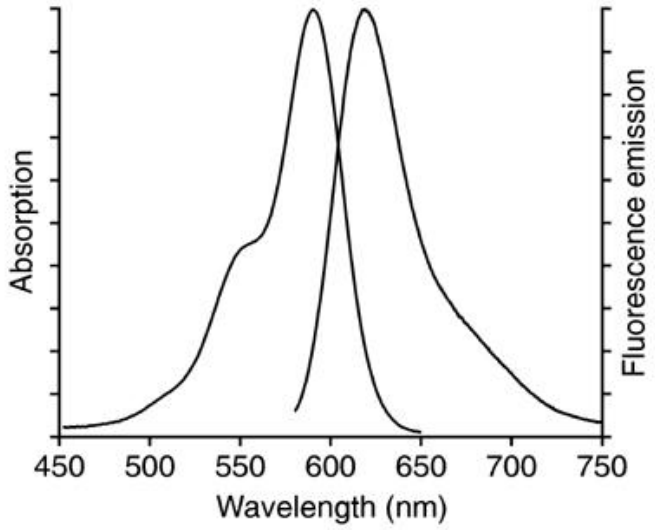

Figure 2.9 Emission and excitation spectra of fluorophores used

The graphs represent the exact emission and excitation weavelength.

Table 2.3 Excitation (ex) and emission (em) of generally used fluorochromes in order of their ex wavelength

Probe	Ex (nm)	Em (nm)	Alternative name
Cascade Blue	375;400	423	
Lucifer yellow	425	528	
NBD	466	539	
R-Phycoerythrin (PE)	480;565	578	
PE-Cy5 conjugates	480;565;650	670	Tri-Color, Quantum Red
PE-Cy7 conjugates	480;565;743	767	
Red 613	480;565	613	PE-Texas Red
PerCP	490	675	Peridinin chlorphyll protein
TrueRed	490,675	695	PerCP-Cy5.5 conjugate
Fluorescein	495	519	FITC
BODIPY-FL	503	512	
Cy3	512;552	565,615	
TRITC	547	572	TRITC
X-Rhodamine	570	576	XRITC
Lissamine Rhodamine B	570	590	
Texas Red	589	615	Sulfonyl chloride
Cy5	625-650	670	

Allophycocyanin (APC)	650	660	
APC-Cy7 conjugates	650;755	767	PharRed
Cy7	743	767	

2.21 Imaging using multiphoton microscopy

Multiphoton microscopy was performed using a LaVision BioTec 2-photon TRIM scope, and a Zeiss 7MP. The LaVision system consisted of a Nikon Eclipse TE2000 inverted stand, Olympus long working distance 20x 0.95 NA water immersion objective and Coherent Chameleon II laser tuned to 830 nm. Fluorescence was detected using non-descanned detectors (NDD, Hamamatsu H6780-01-LV 1 M for < 500 nm detection and H6780-20-LV 1M for > 500 nm detection). A dichroic filter (Chroma 475 DCXR) was used to separate spectrally the second harmonic signal, when present, from the GFP emission of the transplanted cells. Band pass filters (Semrock 435/40 and Chroma 525/50) were used to further filter the emission for the SHG and GFP channels respectively. The Zeiss system consisted of an Axio Imager upright stand, 20x, 1.0 NA water immersion objective, and Chameleon II laser. To keep tissue stationary during *ex vivo* imaging it was glued, dorsal part side up to a plastic cover slip with cyanoacrylate (Vetbond, 3M Health Care Ltd, Leicestershire, UK). The cover slip was cut to fit in a perfusion chamber (Harvard Apparatus ltd, Kent, UK) where it was held in place by grease. The perfusate was equilibrated with oxygen and thermo-stated to 35-37ºC. The chamber was placed on the motorized stage of the upright microscope and fluorescent cells located using epifluorescence with (blue) excitation. The wavelength of the laser was set to either 840 nm (to excite predominantly CFP) or 940 nm (to excite predominantly GFP). Detection channels selected light with wavelength < 485 nm (for CFP) and 500 - 550 nm (for GFP).

2.22 Time-lapse microscopy

The Nikon time-lapse microscope TE2000 is fitted with a Nikon perfect focus system (PFS) to maintain focus over the imaging. The PSF only works with glass bottom dishes. So 35 mm glass bottom microwell Petri dishes, with 14 mm diameter of microwell (MakTek Corporation, MA, USA, PART no.: P35G-1.5-14-C) were used for all the time-lapse experiments. The system has a temperature-controlled 37^{o}C chamber, provided with an oxygen supply and images were acquired using a 40x short distance 0.75 NA air objective. Analysis was performed with MetaMorph (Version 5) imaging software, which compensate for stage shift, vibration or similar small whole field movement that can occur during time-lapse acquisition.

The incubator enclosure is most often constructed of Plexiglas and surrounds the microscope stage, objectives, fluorescence filters, and transmitted light condenser. Temperature is maintained with an external heating unit (usually forced air) and the carbon dioxide concentration is controlled with a sensing unit coupled to a regulator that is fed by a cylinder of pure gas. The development of high-sensitivity charge-coupled device (CCD) video cameras and computer routines for automated image capture and analysis has extended the scope and practicality of high-resolution time-lapse microscopy. In order to reduce room and building low-frequency vibrations, the time-lapse microscope is located on feedback-controlled isolation tables that are gas-filled flexible synthetic polymer vibration isolation pads. A combination of the vibration pads and a heavy sheet of half-inch aluminium or a pre-drilled isolation platform reduces vibrations to an unnoticeable level (Fig. 2.10) (www.microscopyu.com).

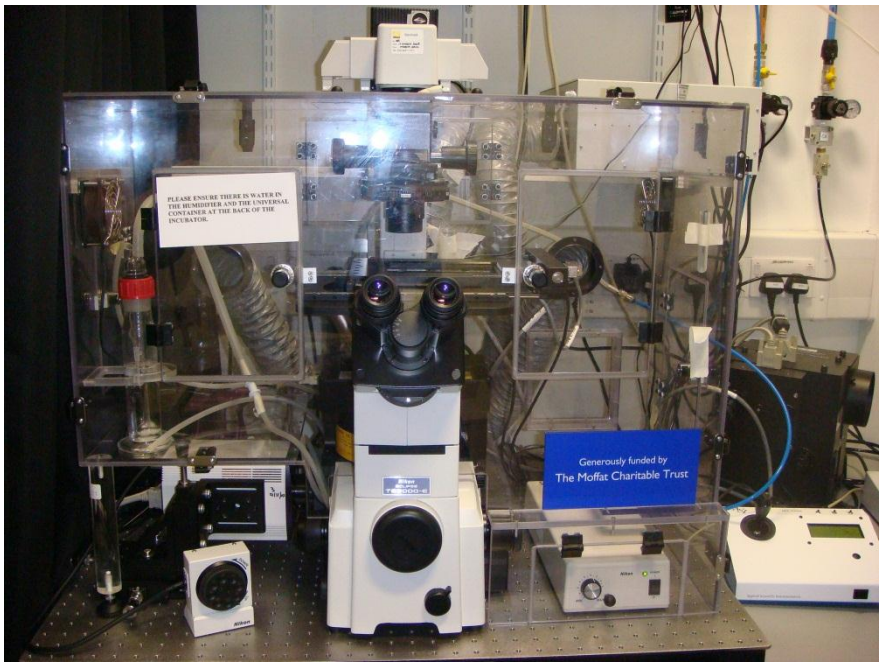

Figure 2.10 Nikon (TE2000) time-lapse inverted microscope.
Plexiglas live cell imaging chamber is illustrated equipped with temperature control system.

2.23 *In vivo* imaging after transplantation of GFP-labelled neurospheres into *shiverer* mice

Animals were kept in conventional animal facilities and all experiments were carried out in compliance with UK Home Office guidelines. To permit live imaging, mice were terminally anaesthetised by injection of 300-400 µl/ 10g body weight of a mix of Hyprorm/Hypnovel/dH_2O at 1:1:8 by volume. After laminectomy a small segment of the spinal cord was exposed where GFP-labelled neurospheres were transplanted and the mouse maintained at 37ºC, using a heated electrical blanket and an infra-red lamp. The mouse was placed dorsally on a V-shaped plastic plinth with a small opening to allow the microscope lens to access the spinal cord.

2.24 Statistics

All data within this thesis were expressed as mean ± SD. All statistical comparisons were performed using paired Student's T-test in Microsoft Excel, in case of significance to determine group differences. The level of significance was set to 5% (also called an alpha level), so any comparison with a p value of less that 0.05 was considered statistically significant, and was marked with one (*), if $p < 0.05$.

Symbol	**Meaning**
ns	P>0.05
*	P<0.05

2.25 Neurosphere media preparation

Stock solutions

30% glucose: 30g of glucose (Sigma G7021) were slowly added to 100ml ddH2O with constant stirring. Filter sterilised through a 0.22um cellulose acetate filter. Stored at 4°C.

7.5% NaHCO3: 7.5g of NaHCO3 (Sigma S-5761) were slowly added to 100ml ddH2O. Filter sterilised and stored at 4°C.

1M HEPES: 23.8g of HEPES (H-4034) were added to approximately 80ml ddH2O. Once dissolved final volume was brought up to 100ml. Filter sterilised and stored at -20°C.

10x DMEM/F12 (Gibco BRL/Invitrogen 52100-021/21700-026): 800ml ddH2O were measured into a sterile 1000ml beaker. 1 pot of DMEM (makes 5L normally) was added and allowed to dissolve. 5 pots of F12 (1L/pot) were then added and allowed to dissolve. Final volume was brought to 1000ml and filter sterilised and aliquoted into 25ml aliquots.

10x Hormone mix:

For 250ml of 1x DMEM/F12:

10x DMEM/F12	25ml
30% Glucose	5ml
7.5% NaHCO3	3.75ml
1M HEPES	1.25ml
ddH2O	187.5ml

To this solution, it was added:

Transferrin: apo-human (Sigma T2252) 250mg straight into the above solution.

Insulin solution (human recombinant) (Sigma I-9278) 6.25ml insulin was added to 19.75ml of ddH2O. Then 25ml were added to 1xDMEM/F12.

Putrescine: (Sigma P-7505) 96.6mg of putrescine were added to 100ml of ddH2O and mixed till dissolved (concentration: 600uM or 9.6ug/ml). 25ml were added to above solution. Final concentration was 60uM.

Selenium: to 1mg Sodium selenite, (Sigma S-9133) 1.93ml ddH2O (3x10-3M) were added, mixed and then 25ul added to solution. The rest were stored at -20°C.

Progesterone: (Sigma P-6149) 1.59ml 95% EtOH was added to 1mg and stored at -20°C. 25ul were added and mixed. Final concentration was 0.00629ug/ml.

Once all ingredients had been added, they were mixed and filter sterilised. 25ml aliquots were made and stored at -20°C.

Neurosphere Media

To make 250ml the following were added in the written order:

ddH2O	185ml
10x DMEM/F12	25ml
10x hormone mix	25ml
30% glucose	5ml
7.5% NaHCO3	3.75ml
1M HEPES	1.25ml
L-Glutamine (Gibco 25030-081 100%)	2.5ml
4% BSA (Sigma A-3059) in HBSS (Sigma H4891)	0.625ml

2.26 Setting up the theatre for surgery

Baby incubator ON

Extractor fan ON (Theatre 1)

Shaver on charge

Isofluorane topped up (key in drawer in Theatre 1)

Steri 340 (hot bead steriliser) ON

Radiator ON

Electric blanket (or heat pad) ON

Anaesthetic:

Extractor tube attached to induction box and to frame or mask

Isofluorine tube to face mask

For cleaning skin:

HYDREX and cotton buds

Surgical tools:

Sterilised tools and glass electrodes including blade handle, fine spring scissors, fine forceps, needle holder, suturing forceps

Suture material 6.0 silk

Blade (small)

Orange needle or dural hook for piercing the dura

General:

Heating Lamp

Operating microscope (check focal plane)

CellTram oil injection system (check if it needs filling with oil)

Sterile blue pad for animal to lie on

Yellow bag for biological waste

70% ethanol and blue roll

Tape for removing hair after shaving and for stabilising tubes

Pipette (p100) and sterile tips to remove excess medium from cell suspension

Vaseline/ocular lubricant to keep eyes moist during surgery

10 ml syringe for sterile saline (from bags hanging above benches) to moisten tissue

1 ml syringe for RIMADYL

2 bijeaux, each with 900 µl of sterile water, labelled A and B

Add 100 µl of RIMADYL to 900 µl of sterile water in A

Add 100 µl of solution A to 900 µl of sterile water in B

Inject 100 µl of solution B per 10g i.e. if mouse is 30 g (approximate weight of young adult, inject 300 µl solution B, subcutaneously)

Small clean cage (no sawdust) with sterile pad, baby food + dry food + water

Record keeping:

Recovery sheets and ops book

For operator:

Gloves, green apron

3. Assessment of the stages of glial-axonal interactions culminating in myelination in mouse mixed spinal cord cell cultures

3.1 Introduction

3.1.1 Background

Myelination is a highly complex process that involves the formation of internodes of myelin separated by nodes of Ranvier. CNS myelin is produced by a specialised subdomain of the oligodendrocyte's plasma membrane, during postnatal development. The oligodendrocytes synthesise large amounts of specific proteins and lipids to generate myelin that wraps and compacts around axons, in response to selective glial-axonal interactions (Sherman & Brophy 2005). In mature compact myelin, the membranes are condensed, whereas the non-compact areas are filled with cytoplasm. The non-compact areas are named after their topological location in the myelin sheath, the periaxonal loop, the abaxonal loop at the outer surface and the lateral paranodal loops. Tight junctions composed of claudin-11/OSP serve as a physical barrier between compact and non-compact myelin (Gow et al 1999, Morita et al 1999).

The mechanism by which a myelin sheath is formed over the axon is not well understood. Undoubtedly, a major challenge for oligodendrocytes, most of which ensheath multiple axonal segments simultaneously, is the temporal and spatial orchestration of myelin synthesis. Additionally, oligodendrocytes are responsible for the trafficking of molecules, for example the integrin/contactin complex, which coordinate signals from ECM and the axonal surface to regulate both oligodendrocyte survival and myelination (Laursen et al 2009). Myelinating oligodendrocytes are able not only to control membrane domain morphogenesis but also the directed growth of the emerging myelin sheath (Baron & Hoekstra 2010). Several myelin proteins such as PLP/DM20, MAG and MOG undergo distinct endocytic sorting and recycling associated with plasma membrane remodelling (Feldmann et al 2011, Winterstein et al 2008).

Chapter 3 - Assessment of the stages of glial-axonal interactions

The importance of glia has become clearer with the development of molecular biology techniques and the generation of more complex cell cultures. The use of *in vitro* models of myelination has contributed to the understanding of how oligodendrocytes mature and ensheath axons. Interestingly, while cultured oligodendrocytes are capable of wrapping inert materials such as carbon (Althaus et al 1984), glass and vicryl microfibers (Howe 2006) and fixed neurons (Rosenberg et al 2008), the extent of wrapping is considerably decreased compared with that seen in living neurons. Tissue culture approaches have been used to study myelination since the mid-1950s (Jarjour et al 2011). Myelination requires a number of sequential steps beginning from the maturation of the oligodendroglial cell lineage (Hardy & Reynolds 1993, Raff et al 1983b) to axonal contact and ensheathment.

The current *in vitro* techniques used to model *in vivo* myelination in the literature are summarised as follows:

1) Dissociated cultures: The spinal cord dissected from the embryonic CNS is enzymatically dissociated, plated on coverslips and allowed to differentiate over a period of approximately 4 weeks at which point oligodendrocytes have myelinated axons. These three-dimensional mixed cell populations of neurons and glia partially recreate CNS myelination and allow visualisation of the cellular interactions using immunocytochemical analysis (Thomson et al 2008). Other models, for example when mixtures of CNS cells are grown as spheroids, known as the spheroid model, all CNS cell types are present forming three-dimensional contacts which form glial-axonal interactions similar to that seen *in vivo* situation (Atterwill 1987). A major feature of both models is the presence of multi-layered myelin. In addition, unlike *in vivo* models it is easier to add pharmacological reagents to these cultures and follow their effect (Jarjour et al 2011).

2) Oligodendrocyte-DRG co-cultures: DRG neurons are maintained in the presence of NGF and a mitotic agent to kill Schwann cells or other contaminating cells. This is followed by the addition of oligodendrocytes or OPCs, prepared independently from the same source. This system allows myelination to be observed after 10-15 days (Chan et al 2004, Huang et al 2011, Wang et al 2007). This technique was the basis for a variety of studies, for example, that axons promote proliferation of embryonic and adult OPCs and that OPCs from adult CNS can differentiate into myelin-forming cells (Wood & Bunge 1986a, Wood & Bunge 1986b). Other studies demonstrated that PDGF and FGF-2 could inhibit myelination, whereas soluble neuregulin increased myelin formation (Wang et al

2007). The major advantage of the oligodendrocyte-DRG co-culture is its flexibility. Oligodendrocytes prepared by different methods (e.g. tissue explants, immunopanning, magnetic or fluorescent activated cell sorting), from different species, CNS regions, tissues of different age can all be used to study myelination of the DRG neurons. However, the most significant disadvantage is that DRG neurons may not be perceived to be true CNS neurons, as their cell bodies are located outside the CNS and they form both CNS and PNS connections (Jarjour et al 2011).

3) Oliogodendrocyte-CNS neuron co-cultures: Oligodendrocytes and CNS neurons are derived from independent sources compared to DRG neuron co-cultures. Rat retinal ganglion cell (RGC) neurons were purified from retinae of P5 animals plated on chamber slides. After 10 days in culture to allow for axon growth, purified OPCs were added to the RGC cultures (Watkins et al 2008). A second approach is the use of explants of E14 rat spinal cord cultured on Matrigel-coated coverslips pre-seeded with OPCs. However, this method has the disadvantage of requiring the use of fluorescently-labelled oligodendrocytes to distinguish them from the oligodendrocytes of the explant.

4) *Ex vivo* slice culture model. This involves slices generated from new-born rodent brain or spinal cord which are cultured on membranes to study neurite outgrowth and myelination (Jarjour et al 2011, Thomson et al 2006). The three-dimensional structure and the cytoarchitecture of the brain or spinal cord are well retained within the slice. However, in organotypic cultures, the tissue fragment is thick and usually requires sectioning (physically or optically) before visual examination under the microscope. Currently, slices are grown on semiporous membranes (e.g. Millipore organotypic inserts), which cause less tissue thinning and allow for simpler maintenance and processing (Zhang et al 2011). Also, direct visualisation of myelinating cells in slice cultures can be achieved if the cultures are prepared from transgenic mice expressing a fluorescent protein under an oligodendrocyte promoter, or lentiviruses which are extremely useful to manipulate cell biology (Harrer et al 2009).

Besides *in vivo* models, the *in vitro* models are widely used to study myelination. To some extent they mimic the CNS environment but they do not model all aspects of *in vivo* myelination effectively.

3.1.2 Aims of the chapter

Previous work from the lab was carried out on rat myelinating cultures. The main aim of this chapter was to first characterise the various stages of oligodendrocytes' differentiation in the mouse cultures, over the time frame of the culture period, and also to use these data as reference points for subsequent time-lapse imaging. Furthermore it has previously been shown that a supporting astrocyte monolayer was necessary for cell survival and myelination in rat but not mouse myelinating cultures (Sorensen et al 2008, Thomson et al 2008). Thus, it was important to determine if this was necessary for optimal myelination as its absence may make the optical properties for imaging improved by not imaging through an astrocyte monolayer.

More specifically the aims of this chapter were to:

1) Validate if a monolayer of astrocytes is necessary to promote myelination in the mouse cultures.

2) Use confocal microscopy to determine if the oligodendroglial-axon unit during initial contact, ensheathment and myelination *in vitro* was affected by genetically tagging oligodendrocytes with fluorescent markers, or by viral infection and if the cultures could be myelinated by exogenously applied neurospheres.

3) Carry out the ultimate aim, of studying myelination from exogenously added fluorescently labelled oligodendrocytes to mixed cultures using time-lapse microscopy.

3.2 Materials and Methods

3.2.1 Myelinating cultures

The myelinating cultures used in these experiments, were compromised of dissociated mouse E13.5 spinal cord cells from wild type mice, which were then plated on PLL-coated coverslips or on PLL-coated glass bottom Petri dishes. The cultures were maitntained for 26-28 days, a period that leads to a measurable level of myelination. For the study of glial-axonal interactions under time-lapse, several modifications were used to produce the culture: i) a mix of GFP-positive and GFP-negative spinal cord cells at a 70:30% ratio from the β-actin GFP mouse: wild type mouse, as a completely GFP-positive culture would be visually "confusing" to follow glial-axonal contact over time. ii) addition of cGFP tagged neurospheres to wild type myelinating cultures or iii) addition of wild type neurospheres previously infected with fGFP to wild type myelinating cultures to label cellular membranes.

For terminology the non myelinated process is called a neurite but once wrapped in a myelin sheath is termed an axon. In addition, in all immunostaining experiments, the term "myelin" is used to define myelin that had apparently wrapped around nerve processes.

3.2.2 Astrocytes derived from neurospheres

To assess if a monolayer of astrocytes was necessary for myelination in mixed mouse spinal cord cultures, neurospheres were generated from striata of *β-actin* (as described in detail, in chapter 2) GFP-expressing transgenic mice or wild type mice or rats. After 7-10 days *in vitro* (DIV), large spheres were triturated, using a Pasteur pipette to produce smaller spheres/cell clusters. The spheres were differentiated into astrocytes by plating onto PLL-coated coverslips, as described in Chapter 2. After 7-10 days, a confluent layer of astrocytes was formed and dissociated embryonic spinal cord cells were plated on top of them, as described by Sørensen (Sorensen et al 2008).

3.2.3 Infection of wild type neurospheres with lentiviruses

Wild type striatum-derived neurospheres were generated from P1 embryos. Briefly, both striata dissected from the brains of wild type mice, were mechanically dissociated and the cell suspension centrifuged at 800 rpm for 5 min. The pellet was resuspended in 20 ml of neurosphere medium. After 7 DIV, the spheres were large enough and confluent for use in culture. They were triturated and placed in a 6-well plate and left to settle for 1 hour in the incubator. Lentivirus carrying the GFP-IRES-dsRed gene with a titer of $2.5x10^7$/ml was added to the wells with a MOI of 50. After 2 days, the medium was collected from the wells by aspiration and the cells spun down at 800 rpm, for 5 min and triturated with 1 ml of fresh neurosphere medium to produce smaller spheres/cell clusters. Six days after the infection, many labelled cells were detected under the fluorescence microscope. Wild type neurospheres infected with lentivirus carrying the GFP-IRES-dsRed gene with a titer of $2.5x10^7$/ml, were infected with the lentivirus carrying the fGFP gene at a titer of $7.5x10^8$ /ml (GFP-tethered to the membrane).

3.2.4 Time-lapse imaging

Real-time imaging parameters were used to follow the dynamic cellular interactions of the fluorescently-labelled glial cells with the axons. Time-lapse images were captured using 40x dry (NA=0.75) and optivar 1x or 1.5x (60x magnification) objectives mounted on a Nikon time-lapse microscope.

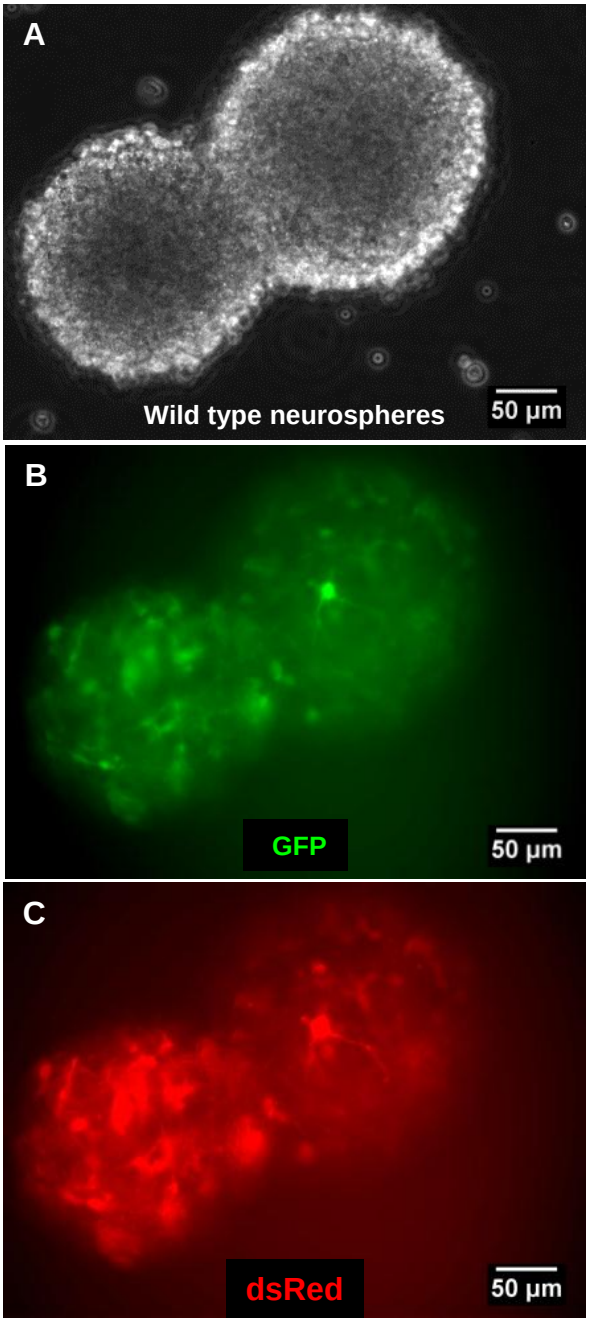

Figure 3.1 Wild type neurospheres infected with lentivirus carrying the GFP-IRES-dsRed gene

A) Bright field view of wild type spheres, appearing dense and healthy. B-C) Many fluorescently-labelled cells (GFP-green/ dsRed-red) seen on the surface and within the spheres with obvious cell processes were visualised 6 days after infection. Representative images from at least 10 separate experiments.

3.3 Results

3.3.1 Characteristics of mouse myelinating cultures after fixation and immunostaining

Previously, it was reported that a supporting astrocyte monolayer was necessary for cell survival and myelination in rat myelinating cultures (Sorensen et al 2008, Thomson et al 2008). As the time-lapse microscope had an inverted stage, the lack of an extra cell monolayer would facilitate clarity of image acquisition. Although addition of a monolayer may be somewhat less efficient for myelination, the optical properties for imaging would be improved by not imaging through an astrocyte monolayer.

It was therefore essential to compare the effect of a mouse or rat astrocyte monolayer on myelination in mouse cultures, compared to a PLL-coated substrate (Fig.3.2A-C). It was found that neurite density was similar on all substrates tested (around 70% of SMI-31-immunoreactivity per field of view) but there was a small but significant increase in myelination in mouse cultures plated on rat or mouse neurosphere-derived astrocytes, compared to cultures plated on PLL alone (Fig.3.2D and E). Means were 29 ±0.7% standard error myelinated fibres on PLL compared to 42 ± 0.9% standard error and 44 ±0.6% standard error on mouse and rat astrocytes respectively, $p < 0.05$. As myelination was relatively high even in the absence of a supporting astrocyte substrate, subsequent studies were carried out on myelinating cultures plated on PLL alone.

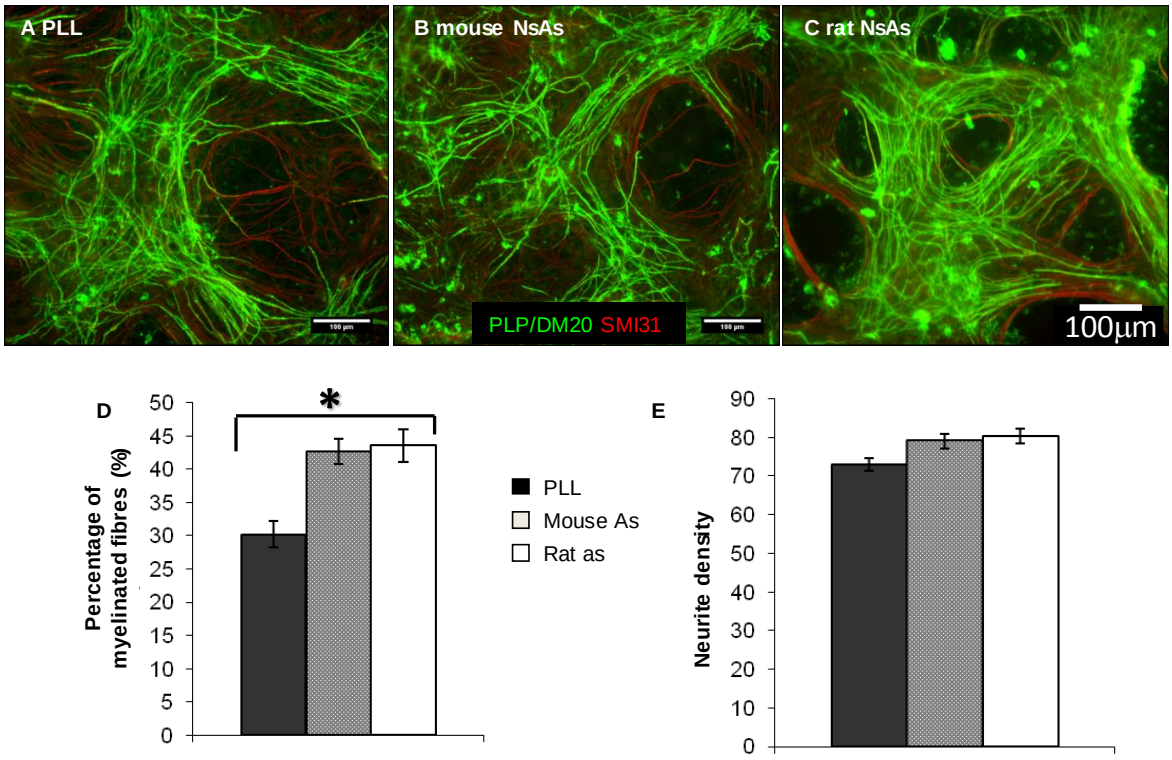

Figure 3.2 Myelination in mouse culture is slightly enhanced when spinal cord cells are plated on an astrocyte monolayer

Images of myelinated fibres in the mouse myelinating cultures plated on PLL (A) compared to monolayers of astrocytes derived from mouse neurospheres (B) or rat neurospheres (C)**.** SMI-31 labels axons (red) and PLP/DM20 labels myelin (green). Graphs show the quantification of myelination (D) and neurite density (E). Myelination was significantly greater on astrocyte monolayers compared to PLL **p*=0.027< 0.05 (t test), n=3.

3.3.2 Assessment of initial contact between oligodendrocytes and neurites in fixed cultures

Initial interactions between oligodendrocytes and neurites, in the mixed population of the myelinating cultures, were examined as static images using immunocytochemistry. At an early stage in culture, the glial cell processes formed multiple contacts with the neurites.

Wild type mouse cultures were immunostained for expression of characteristic marker molecules that are frequently used to define oligodendrocyte differentiation such as the antigen recognised by the O4 antibody (Sommer & Schachner 1981) and PLP/DM20. To investigate the morphology of the processes as they initially contacts the axons, immunostaining was performed between 7-9 DIV. Oligodendrocyte processes surrounding the axon bundles were clearly visualised at the early time points in culture. Oligodendrocytes exhibited striking morphological diversity with respect to the number and length of their processes. The number of initial contact points was highly variable and ranged from 1-8. Over the period of 1 week i*n vitro,* oligodendrocytes labelled with the O4 antibody appeared to make contacts with the nearby neurites (Fig. 3.3A) through single or multiple processes (arrows, Fig. 3.3A). Quite frequently, confocal observations also showed two oligodendrocytes making contact with the same fascicles (asterisks, Fig. 3.3A).

Using the myelinating cultures, cells with a typical oligodendroglial morphology (Fig. 3.3B) were observed contacting axonal bundles. In a magnified view (insert in Fig. 3.3B), bundles of neurofilament-positive fibres were initially seen to be contacted by a thin cytoplasmic process (arrow, Fig. 3.3Bi). A protrusion having a slender, rounded morphology was formed while another process appeared to engulf the axonal bundles (arrows, Fig. 3.3Bii). As the initial interactions progressed, more processes were seen to wrap around the neurites (arrows, Fig. 3.3Biii).

During initial contact, processes extending from the oligodendrocytes are likely to be contacting axonal fascicles. The tips of the oligodendrocyte's processes appeared very flexible as they formed many round protrusions towards and around the targeted neurites. These protrusions were related to the sites of anchoring of the processes possibly in order to help envelop the neurites and attach on the neurite surface. The aforementioned observations demonstrated the early glial cell contact with CNS neurites in culture.

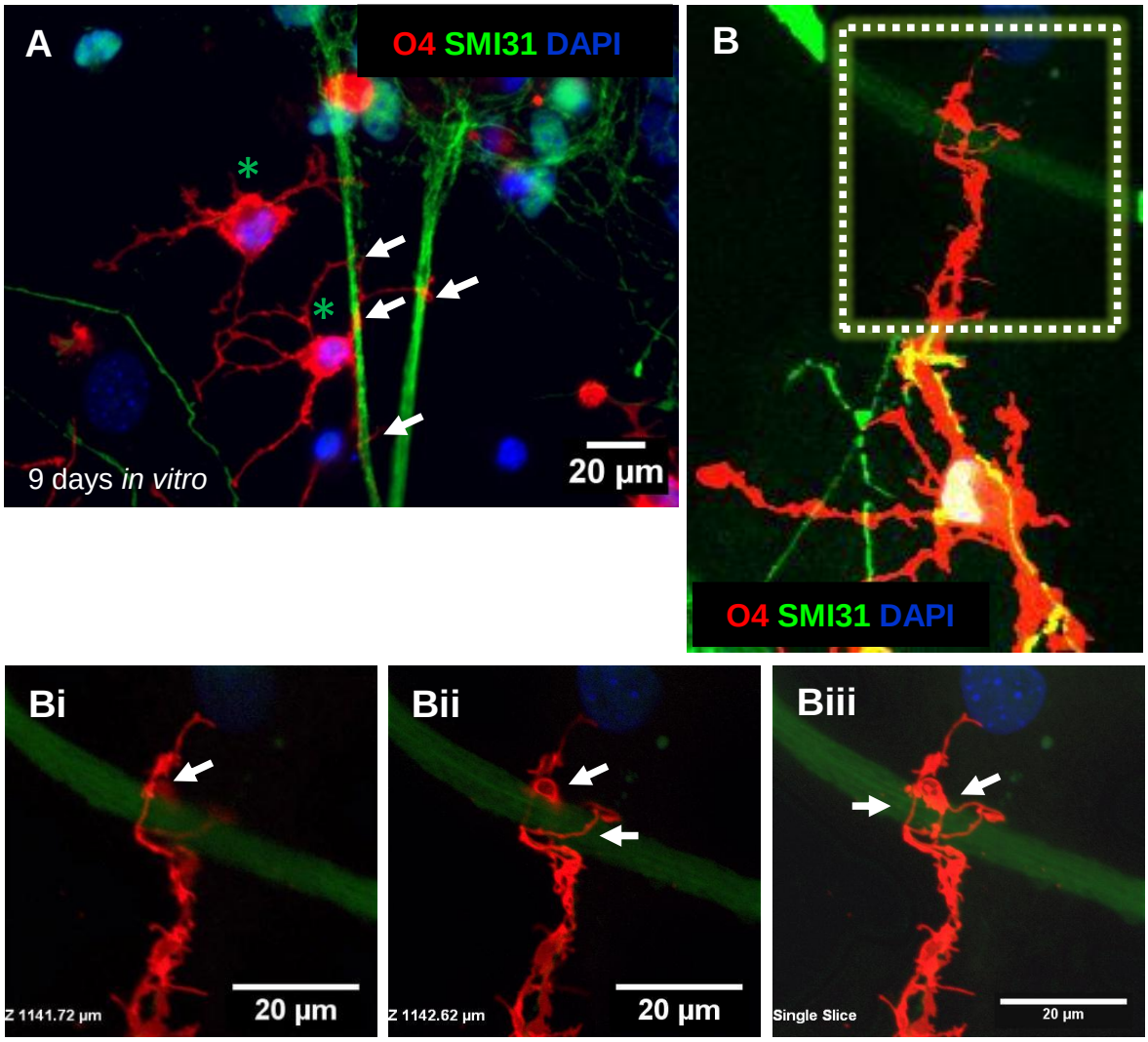

Figure 3.3 Static observations of initial glial-axonal contact using fluorescent microscopy

Wild type mouse cultures were plated on PLL and immunostained after 9 DIV. A) O4-positive cells (asterisks, red) appeared to contact at least two neurites through single or multiple, four or five cell processes (arrows). Bi) In a magnified view, bundles of neurofilament-positive neurites (SMI-31, green) were initially seen to be in contact with an oligodendrocyte by a thin cytoplasmic process (arrow). Bii) A protrusion having a slender, rounded morphology was formed (arrow), while another process was generated that appeared to engulf the axonal bundle (arrow). Biii) A further cell process generated presumably from the same oligodendrocyte engulfed the axonal fascicles. Representative images from at least 4 separate experiments.

3.3.3 The oligodendroglial-axonal unit in fixed cultures

As observed for rat myelinating cultures plated on astrocytes, there was a temporal progression in glial-axonal interactions in the mouse cultures that culminated in the formation of compact myelin sheaths, which has previously been confirmed by electron microscopy (Thomson et al 2008). The myelinating cultures allowed the visualisation of direct interactions between axons and the surrounding glial cells. As the main aim of this thesis was to examine oligodendroglial-axonal interaction using time-lapse in these cultures, it was important to establish the various stages before and during myelination.

After 1 week in culture, initial contact between the oligodendrocyte and nerve process was observed. Individual oligodendrocytes extended many processes (O4, red) and contacted many neurites (SMI-31 green), (Fig. 3.4A). The oligodendrocyte processes appeared to align with neurites, then prior to the formation of a myelin sheath (Fig. 3.4C), the membranous process “filled-out” over the axon from the initial narrow cytoplasmic spiral (Fig. 3.4B and C). Later stages of myelination were defined by an increased intensity of PLP/DM20 (Fig. 3.4D) compared to intermediate stages (Fig. 3.4C).

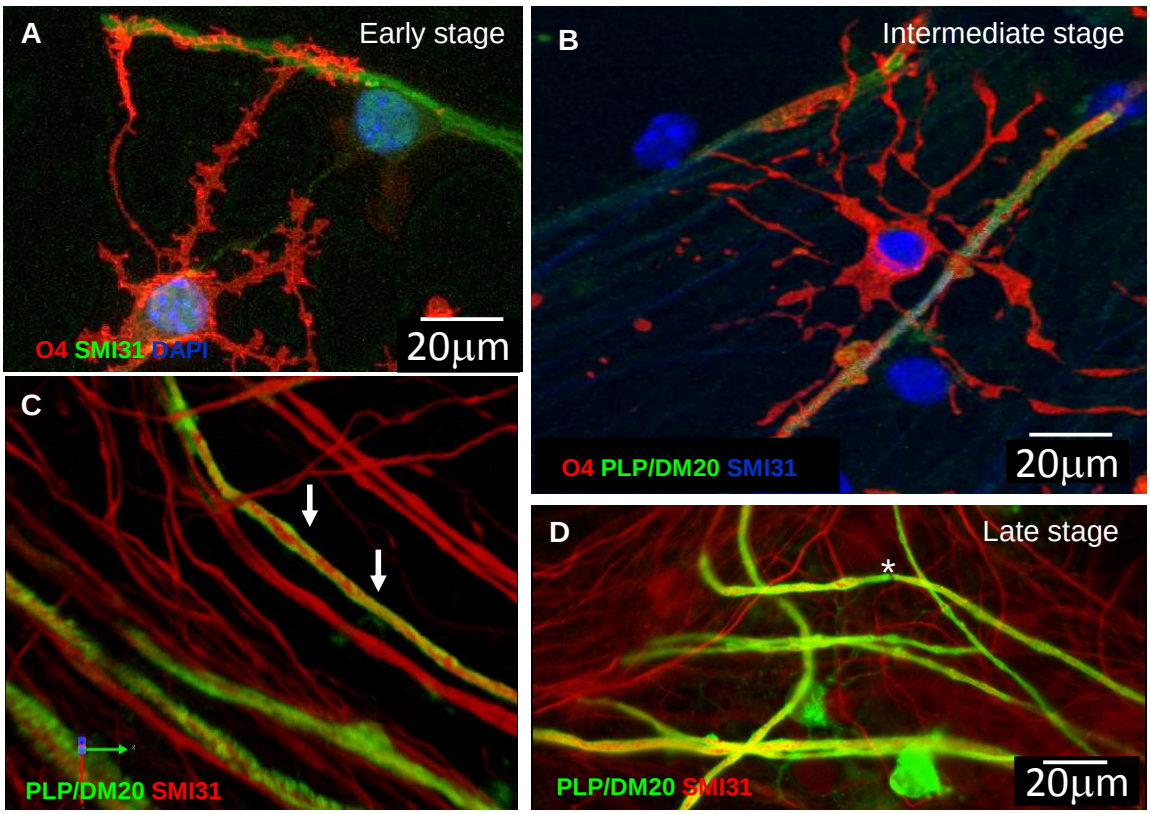

Figure 3.4 Static images of myelination from mouse cultures using differentiation markers and confocal microscopy

A and B) Confocal image showing the initial contact between oligodendrocytes (O4, red) and neurites (SMI-31, green) in a wild type mouse myelinating culture. After 9 DIV, the oligodendrocyte's processes appear to align along neurites. B) Subsequent stages in axon-oligodendrocyte differentiation where PLP/DM20 expression was detected alongside expression of the O4 antibody. The staining suggested that myelin sheaths wrap around segments of the axon at this stage (solid regions of red and green; arrows) around 9 DIV. C) Image of a culture after 28 DIV. The oligodendrocyte's many processes appear to "fill-out" (solid green sheaths) from the initial spirals (arrows) of the membrane visualised by PLP/DM20 (green) around SMI-31 (red) neurites. See supplementary video 3.1. D) Single contiguous myelin sheaths began to appear around 17-18 DIV using anti-PLP/DM20. Representative images from at least 15 separate experiments.

3.3.4 Structural observations of initial and intermediate stages of ensheathment as assessed in fixed cultures

As myelination progresses, the oligodendroglial processes contact the axons with multiple processes. Both *in vitro* and *in vivo*, CNP is the earliest known myelin specific protein to be synthesised by developing oligodendrocytes. MBP, MAG and PLP/DM20 are expressed 2-3 days later, immediately before myelin formation. MBP, MAG and PLP/DM20 appear sequentially and signify a mature oligodendrocyte (Baumann & Pham-Dinh 2001).

To examine intermediate stages of myelination PLP/DM20 and MBP was examined. After 1 week *in vitro*, spirals of cytoplasm-filled oligodendrocyte processes were detected around bundles of axons (Fig. 3.5A). It appeared that the oligodendroglial processes generated at least two loops around the neurites before spreading out in both directions on the same axonal segments (arrows, Fig. 3.5B). Immuocytochemical studies from 9 to 15 DIV, showed oligodendroglial cells relating to a single axon, as well as multi-branched varieties associated with several bundle of neurites (arrows, Fig. 3.5C and D). At this stage, it appeared that the oligodendrocytes had selected the axons they were going to ensheath. This establishment of the aforementioned stable cell-cell interaction was confirmed by the subsequent ensheathment of the neurite with the extension from the oligodendrocyte's membrane (arrowheads, Fig. 3.5D).

Frequently, oligodendrocyte processes appeared to wrap around axons in a cork-screw like pattern (Fig. 3.5E). Moreover, the myelin marker PLP/DM20 was only weakly expressed and appeared as early small spherical-structures (arrowheads, Fig. 3.5E). In some cases the oligodendrocyte's membrane was positive for both (in yellow) the O4 antibody and the PLP/DM20.

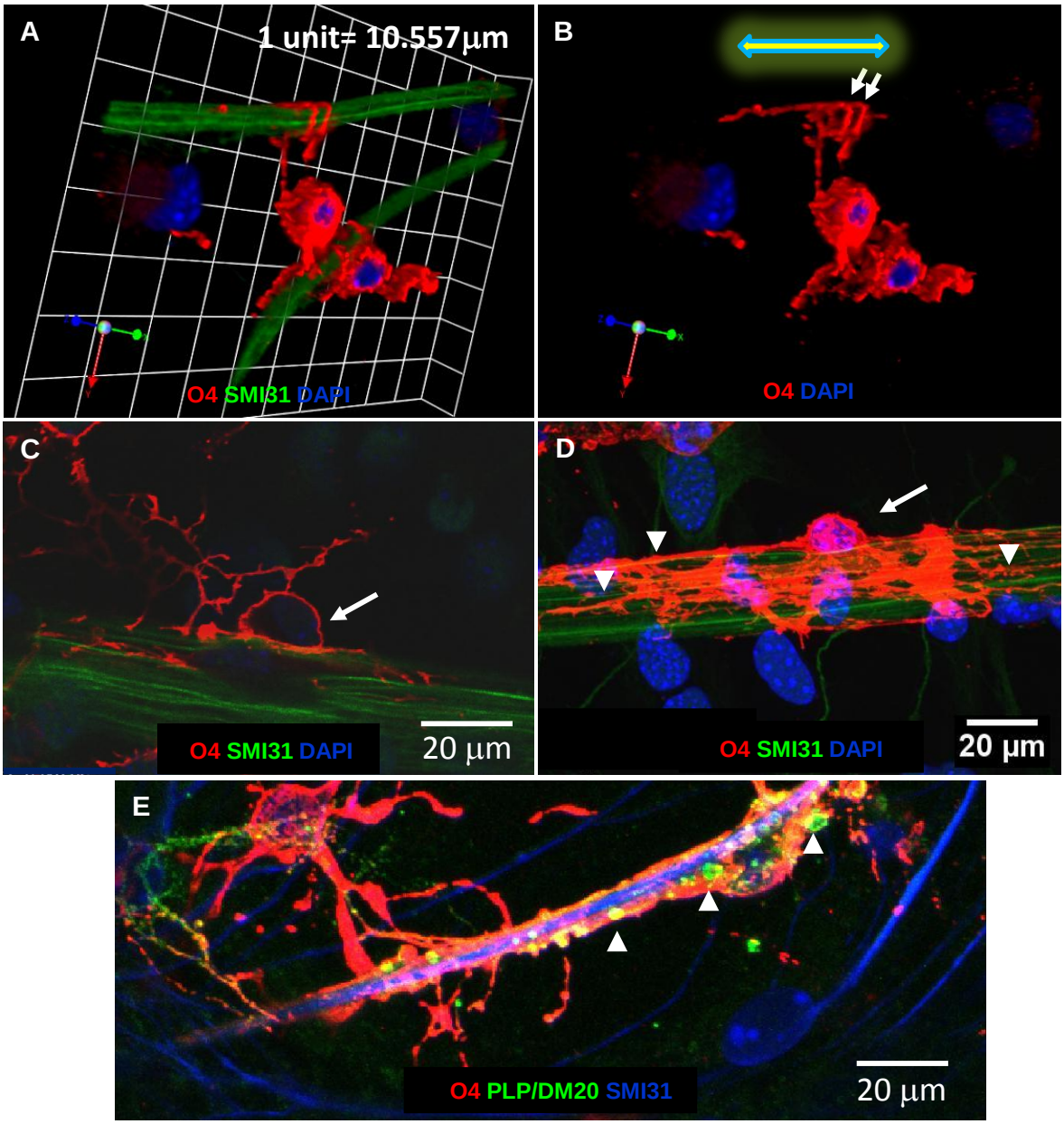

Figure 3.5 *In vitro* observations of initial and intermediate stages of ensheathment

A and B) High magnification confocal images taken using the Olympus FV1000 microscope, revealed cytoplasmic process extending from cells which were positive for O4 (red), appearing to enwrap a bundle of neurites (SMI31-green) in a spiral way in a wild type myelinating culture, after 9 DIV. The oligodendroglial processes appeared to produce two loops around the neurites before spreading out in both directions on the same axonal segments (arrows, B). See supplementary video 3.2. Representative videos from at least 2 separate experiments. C and D) Oligodendrocytes were shown in close association with the neurites, establishing stable cell-cell interaction which was confirmed by the ensheathment of the neurites with the extension of the oligodendrocyte's membrane (arrowheads, D). E)

An oligodendrocyte extending a process forming a sheath around a single axon. Immunostaining revealed colocalisation of sulfatide and PLP/DM20. Spherical PLP/DM20-positive structures probably represent PLP/DM20 within transport vesicles. Representative images from at least 15 separate experiments.

3.3.5 Visualisation of the stages of myelination after the addition of cytoplasmic GFP labelled cells in fixed cultures

cGFP labelled neurospheres were added to wild type myelinating cultures from between day 6-10 to generate a proportion of oligodendrocytes that expressed the *cGFP* reporter gene (Fig. 3.6). The ultimate aim was to assess stages of ensheathment or even myelination of axons by the exogenously added fluorescently tagged oligodendrocytes.

After 2 weeks *in vitro*, a proportion of the cGFP labelled cells had differentiated into cells with typical morphology of oligodendroglial lineage cells (Fig. 3.6A). Such cells stained with the antibody O4 (Fig. 3.6B). These oligodendrocytes extended multiple processes among the spinal cord neurites (blue, Fig. 3.6C). These oligodendrocytes were also characterised by the extension of multiple distinctive smooth tubes typical of myelin sheaths (arrows, Fig. 3.6). Mostly, GFP-positive processes and sheaths were also positive for O4, but in some cases O4-positive fragments were seen that did not co-express GFP (dotted boxes, Fig. 3.6C).

The wild type cultures with exogenous cGFP neurospheres also immunolabelled with the major myelin proteolipid protein PLP/DM20. More importantly, using the myelinating cultures in which axons were widely dispersed spatially, the addition of cGFP-expressing cells enabled glial-axonal relations to be resolved in three-dimensions using confocal microscopy and Volocity Software. After around 3 weeks *in vitro,* the oligodendrocytes appeared to contain both non-ensheathing and ensheathing net-like processes enwrapping the spinal neurites (Fig. 3.7A). From 3D reconstruction images, the expression of PLP/DM20 was detected in between the cGFP “veins” and spirals of cytoplasm (arrows, Fig. 3.7B).

To address if the spirals of cGFP derived from the entire oligodendrocyte membrane or just a thin vein of cytoplasm-filled membrane, cultures were stained with the O4 antibody

together with anti-GFP. At early stages of ensheathment the O4 antibody (membrane marker) and cGFP-positive ribbon-like spirals of cytoplasm were observed to colocalise, extending along and around axons (white arrows, Fig. 3.8A). Unlike cGFP which was confined to this narrow, ribbon-like structure, intense expression of sulfatides (as identified by the O4 antibody) was sometimes observed as sheath-like immunoreactivity along the nerve fibre (asterisks, Fig. 3.8A). A similar pattern was observed for PLP/DM20, the transmembrane protein that is carried by vesicular transport through the biosynthetic pathway to myelin (Colman et al 1982, Trajkovic et al 2006) (asterisks, Fig. 3.8B). PLP/DM20 was also observed in the gaps between the cGFP "spirals", presumably representing deposition in the adjacent plasma membrane (asterisks, Fig. 3.8B). In Fig. 3.8C-D, extension of the myelin like-sheath over an axon was visualised as short cuffs where PLP/DM20 appeared to spread out from the cGFP spirals. Details of the expression of the myelin marker PLP/DM20 which covered a larger area of the axon underneath (SMI-31, blue) in comparison to the GFP expression is depicted in single images (white arrows, Fig. 3.8Di-Dii).

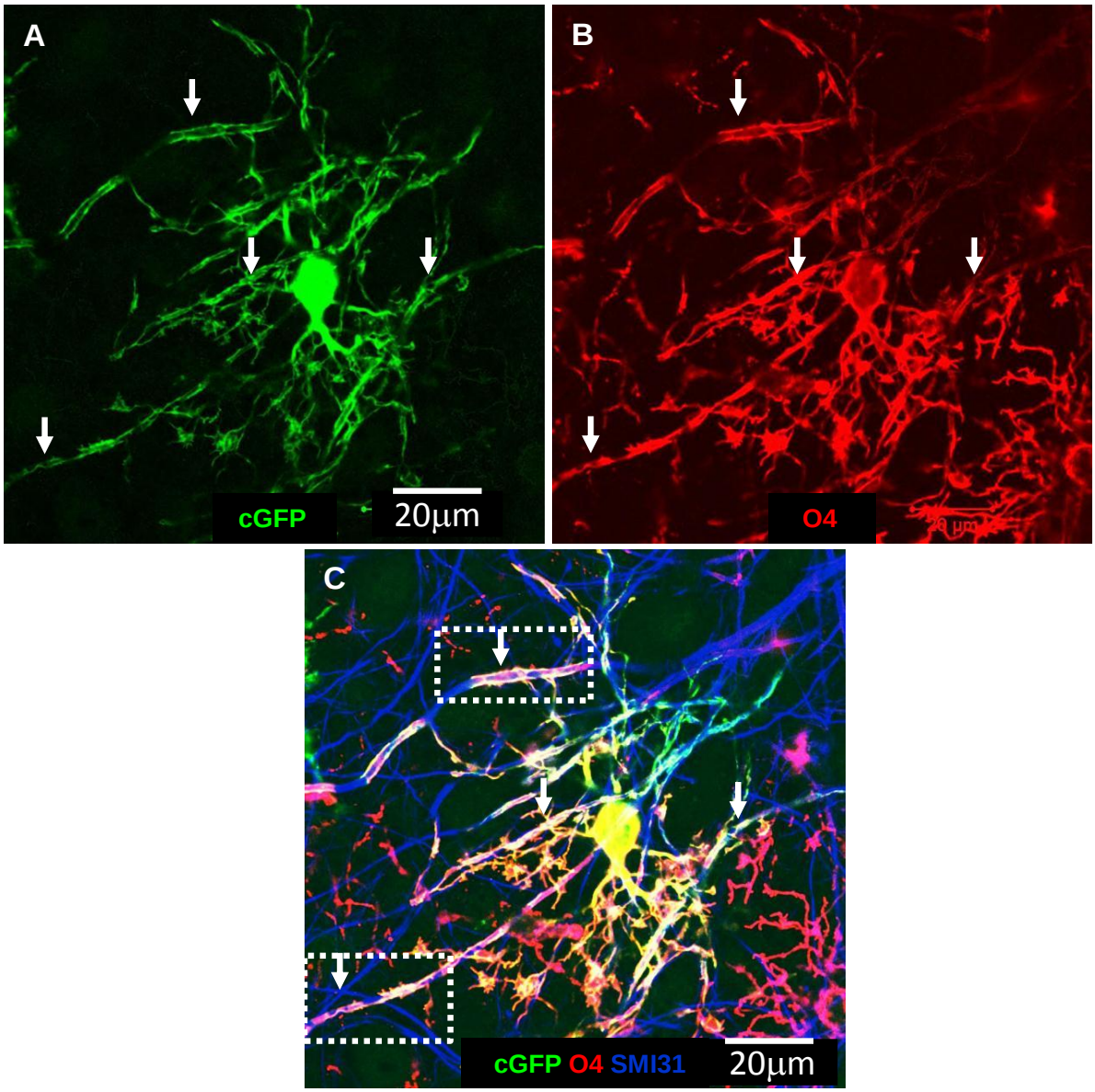

Figure 3.6 cGFP labelled neurospheres differentiated into cells with a typical morphology of an oligodendroglial cell

A-B) Confocal images using a Zeiss 710 microscope depicted oligodendrocytes (O4, red) extending multiple processes among the spinal cord neurites (SMI-31, blue). These myelinating-like oligodendrocytes were also characterised by their extension of multiple distinctive smooth tubes (arrows). C) Most, cGFP-positive processes and tubes also labelled with the O4 antibody (red), but in some cases there were dense fragments positive for O4 which were not GFP-positive (arrows, dotted boxes). Representative images from at least 3 separate experiments.

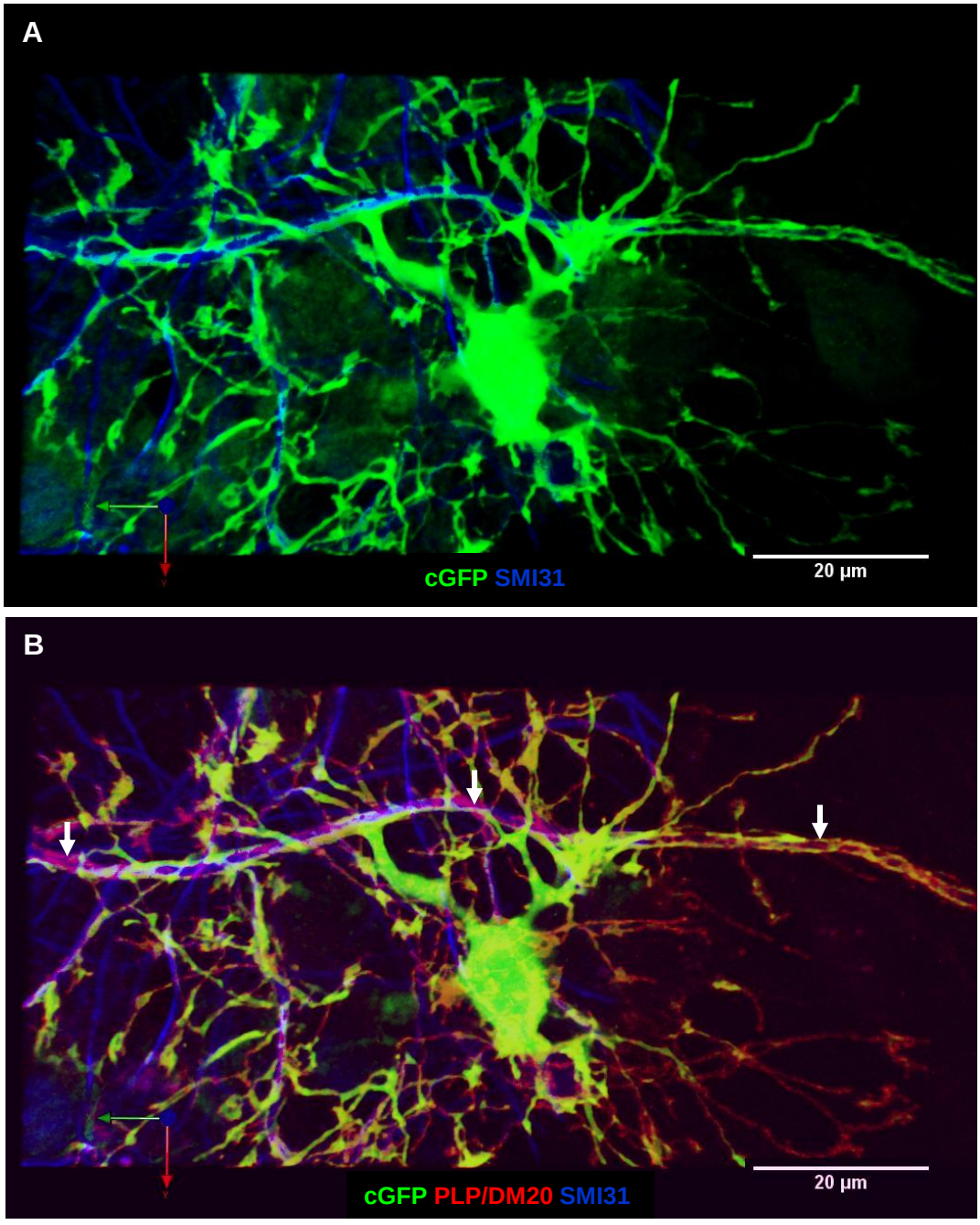

Figure 3.7 3D reconstructed images to examine the morphology of PLP/DM20-positive membrane domains

A and B) Wild type cultures with exogenous cGFP neurospheres (GFP, green) were immunolabelled with the antibody to PLP/DM20 (red) to examine the morphology of the myelin membrane domains. From confocal images and Volocity software, after 3 weeks *in vitro*, the oligodendrocyte appeared to contain both non-ensheathing and ensheathing net-like processes enwrapping the spinal neurites. The expression of PLP/DM20 (red)

immunoreactivity was visible between the cGFP positive "spirals". Representative images from at least 3 separate experiments.

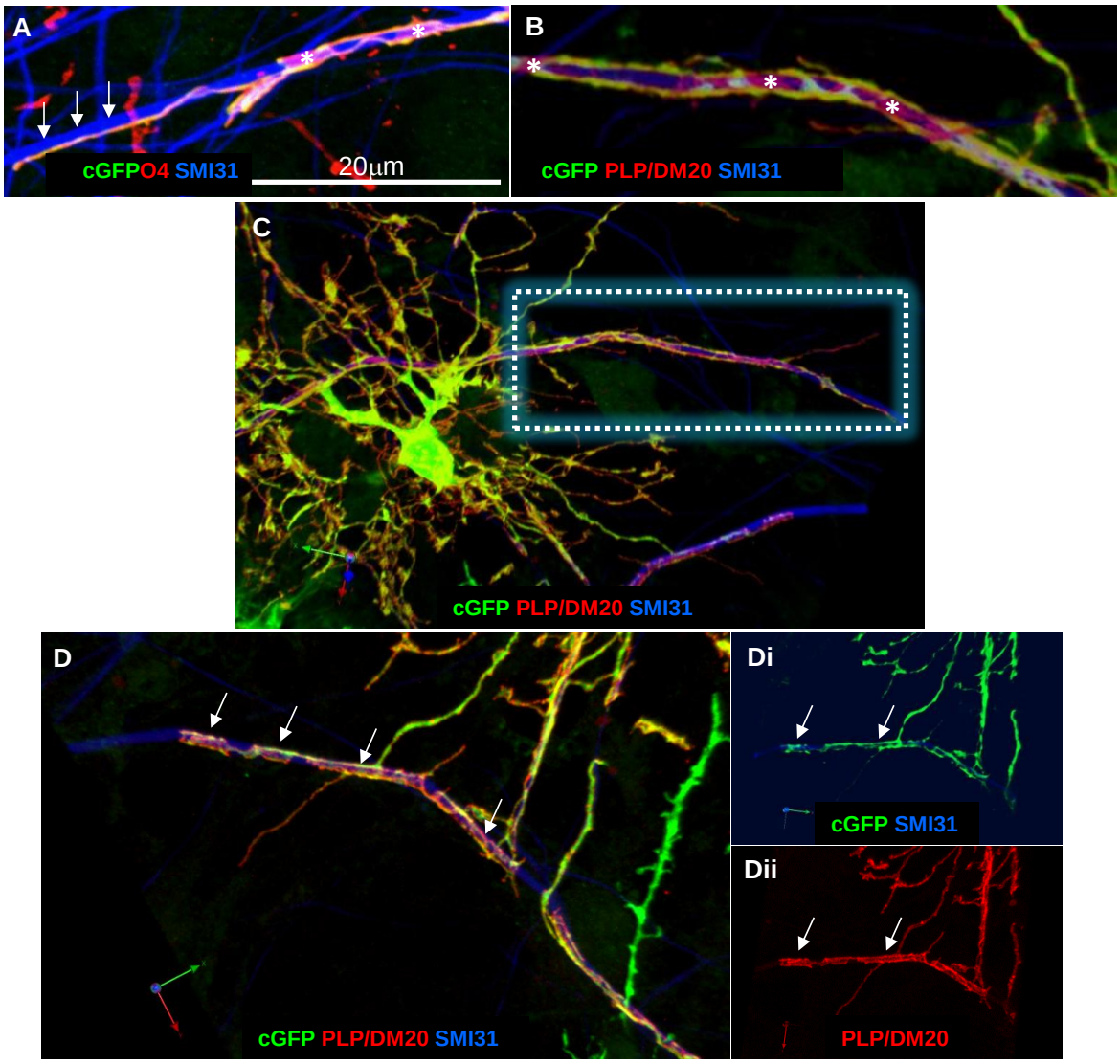

Figure 3.8 cGFP labelled neurospheres generated oligodendrocytes which produce a spiralled cell process around neurites

A) Neurospheres expressing cGFP under the *β-actin* promoter were added on day 6 to myelinating cultures prepared from wild type mouse embryos. Confocal imaging on 21 DIV demonstrates that cell processes initially formed spirals around neurites. Since cGFP (green) was only present in the cytoplasm, O4 antibody (red) which labels myelin membrane was also used to determine whether the membrane and cGFP were contiguous. It was observed that at some point the anti-GFP and O4 antibody (red) immunoreactivity were contiguous (white arrows) over the neurites (SMI-31, blue). B) Staining with anti-

PLP/DM20 (red) and anti-GFP (green) showed that myelin membrane positive for PLP/DM20, but lacking cGFP, extended from the cGFP strands (asterisks). C) Many cytoplasmic cuffs of cGFP (green) labelled with anti-PLP/DM20 (red) were seen along the neurites (dotted box). Di-ii) Single images of the cGFP with neurites SMI-31 (blue) and PLP/DM20 (red) immunoreactivity, where PLP/DM20 was spread in a larger area in places of the cGFP tracks (white arrows). Representative images from at least 3 separate experiments.

3.3.6 Assessment of later stages of ensheathment of the axon with oligodendrocyte processes in fixed cultures

Experiments to analyse the morphological profile of the cGFP-positive oligodendrocytes at later time points *in vitro,* were studied using immunocytochemistry. At these later stages, the gaps between cGFP-positive spirals appeared to fill in with non GFP-postive membrane. The myelin-like membrane expanded and PLP/DM20 was detected in the compartments formed by the net-like processes of the cGFP oligodendrocytes' extensions.

The exogenous oligodendrocyte exhibited a more mature oligodendrocyte phenotype by wrapping multiple processes around the axons in the culture (Fig. 3.9A). Double labelling with anti-GFP and anti-PLP/DM20 demonstrated localisation of both at the edges of the processes (white arrows, Fig. 3.9B). However, PLP/DM20 appeared to be expressed over the axon whereas cGFP expression was more apparent at the periphery of the processes. In some cases cGFP-positive "spirals" from the oligodendrocyte cytoplasm did not colocalise with the myelin marker PLP/DM20 (purple arrowheads, Fig. 3.9B).

3.3.7 Details of myelin assembly assessed in fixed cultures

Since it was technically demanding to follow cytoplasm-filled oligodendroglial processes looping around neurites using time-lapse imaging, fixed myelinating cultures with exogenous added cGFP labelled oligodendrocytes were immunolabelled and visualised using confocal microscopy.

A looping, ribbon-like pattern of cGFP staining was observed frequently and was consistent with corkscrew-like spiralling of the cytoplasm-filled process around the axon, as demonstrated by z-stacks. Even when the presumptive myelin sheath was intensely and solidly stained with PLP/DM20, suggesting at least one wrapping of a myelin sheath had occurred, the spiral pattern of cGFP-positive processes was retained (Fig. 3.10A-C). The spiralling of the cGFP ribbon around the axon (Fig. 3.10D-H) was confirmed in confocal images in which individual z-steps at various depths through the image were made, as illustrated in a schematic (Fig. 3.10I).

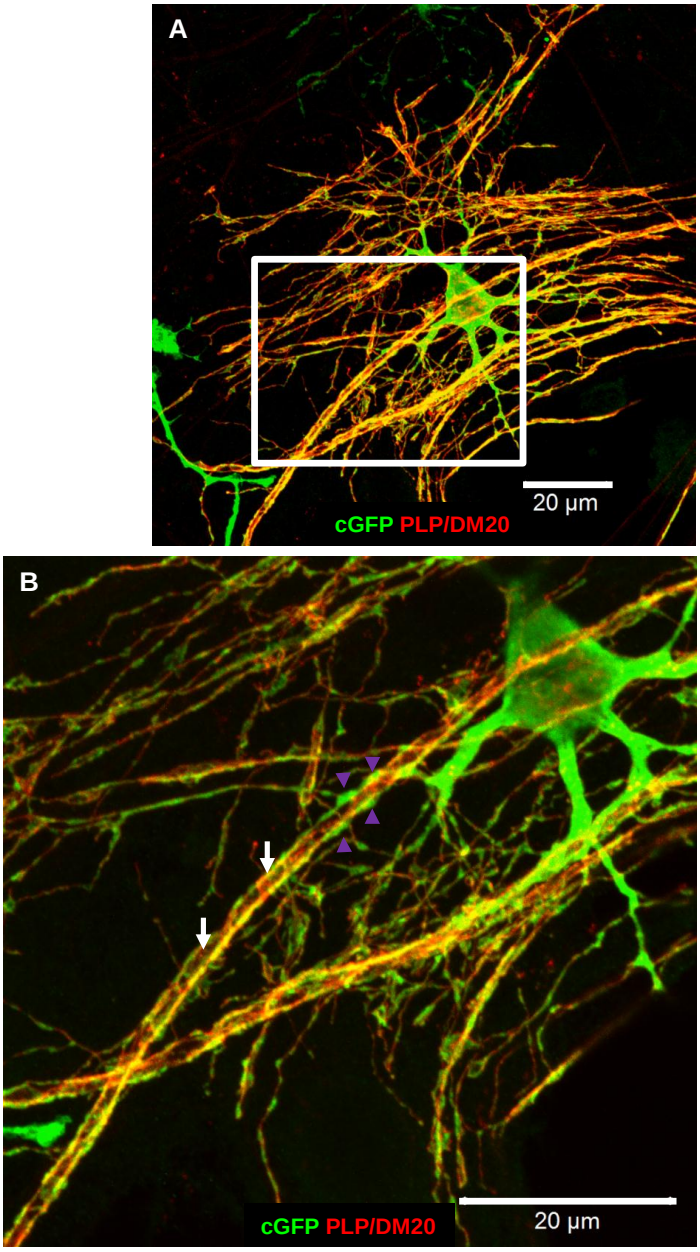

Figure 3.9 Examination of the cGFP-positive oligodendroglial processes at later time points *in vitro*

A) Maximum projection of a Z-stack of confocal images with an interval of 0.8 µm, of exogenous cGFP postive cells (green) which also expressed PLP/DM20 (red) on 27 DIV. B) The gaps between the cyto-positive spirals are filled with the myelin protein PLP/DM20. Double immunostaining of the exogenous cells with GFP and PLP/DM20 demonstrated localisation of dense PLP/DM20 immunoreactivity which occupied more area than the cGFP immunoreactivity (white arrows). However in some cases at the periphery of the processes there was only cGFP expression (purple arrowheads). Representative images from at least 3 separate experiments.

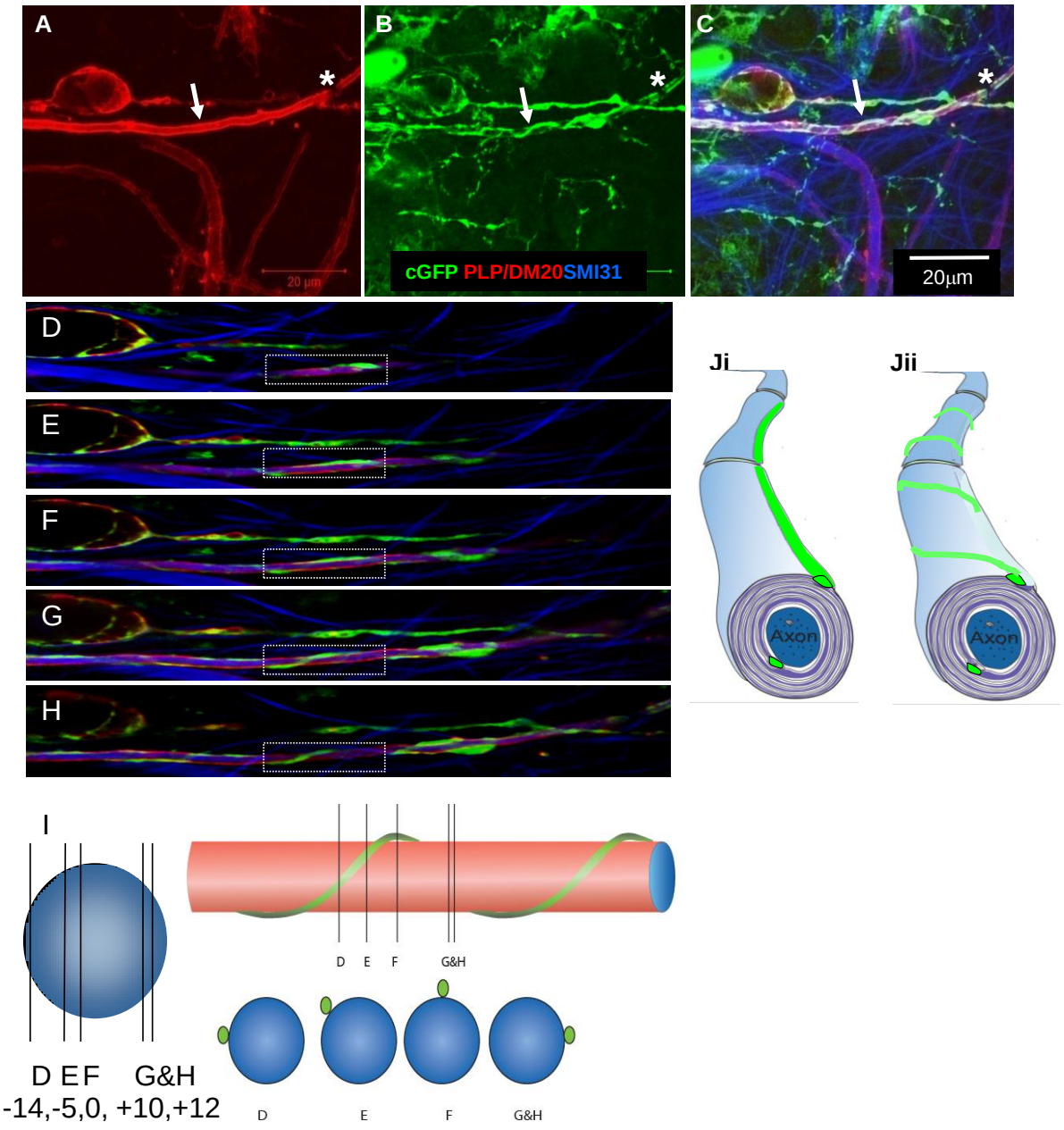

Figure 3.10 Evidence that oligodendrocytes form spiral processes around neurites

A-C) Confocal images with maximum projection of a z-stack, with step interval of 0.06 µm of a culture immunolabelled on 27 DIV using anti-GFP and anti-PLP/DM20. cGFP strands (green) were visualised to spiral around a neurite (SMI-31, blue) on top of intense PLP/DM20 (red) immunoreactivity. Presumptive nodes of Ranvier are indicated by asterisks. D-H) To confirm that the process was contiguous around the neurite, serial confocal images were taken of a z-stack with a step size of 0.24 µm in depth, of a cGFP (green) strand spirally looping around a myelinated axon (PLP/DM20, red). I) The pattern of axonal wrapping is summarised in the adjacent schematic where D-H represent the images in Fig. 3.10. D-H) visualised in cross section and longitudinally. Ji-ii) Illustrates a

schematic of the myelinated fibre and the cGFP immunoreactivity. Ji) Illustrates the typical schematic of a myelinated fibre with the lateral cytoplasmic loop forming a straight line. In these images it appeared that this may not be the case and that it forms a spiral over the axon, at least during wrapping. Representative images from at least 3 separate experiments.

3.3.8 Disposition of Caspr in the node of Ranvier in wild type myelinating cultures with exogenous cGFP-lebelled cells is observed in fixed cultures

The aim of this set of experiments was to investigate the most mature stages in glial-axonal contact and wrapping with the formation of internodes of myelin and nodes of Ranvier. This study was performed using the wild type myelinating cultures in which cGFP-expressing cells were added after 6 DIV.

Frequently, cGFP expression was observed (in relation to the long axis of PLP/DM20-positive sheaths) on either side of a space in immunoreactivity typical of a presumptive node of Ranvier (arrows, Fig. 3.11A, asterisks, Fig. 3.11Bi-iii), presumably representing cGFP in the paranodal loops. The distribution of the cGFP expression on either side of the axon was not the same, possibly reflecting the different differentiation stages of the glial-axonal interaction (Fig. 3.11Bi-iii).

Colocalisation with axonal Caspr confirmed that this cGFP expression occurred at the paranodes (arrows, Fig. 3.12A). Nodes of Ranvier were apparent between the internodes of myelin (MBP) (asterisk, Fig. 3.12A). In some cases Caspr staining resembled that of a loosely coiled spring (arrowheads, Fig. 3.12A), as described previously for unmyelinated axons (Colman et al 1982). Radial lines appeared as coil-like structures when images were reconstructed in 3D (arrows, Fig. 3.12B)

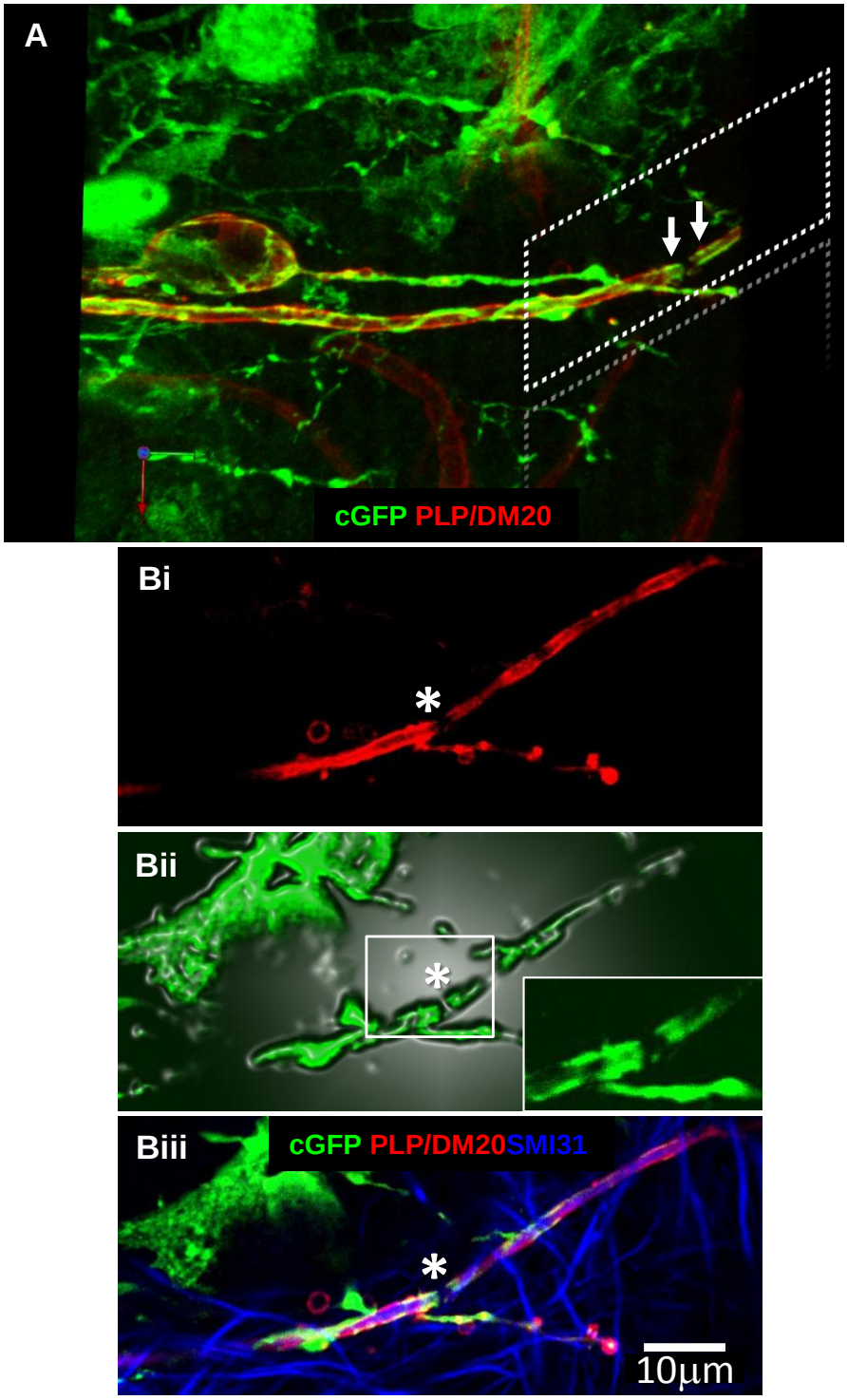

Figure 3.11 Distribution of cGFP expression on either side of a presumptive node of Ranvier

A) Confocal images through a Z-stack with a step size of 0.08 µm revealed asymmetric cGFP (green) expression on either side of a presumptive node of Ranvier, in the myelinating cultures where myelin was expressed using an antibody against PLP/DM20 (red), after 27 DIV. Bi-iii) Optical sections presumably represented cGFP in the paranodal

loops. The distribution of the cGFP expression possibly reflects the different developmental stages of the establishment of the axonal-glial contact on either side of a presumptive node of Ranvier (asterisks). Representative images from at least 3 separate experiments.

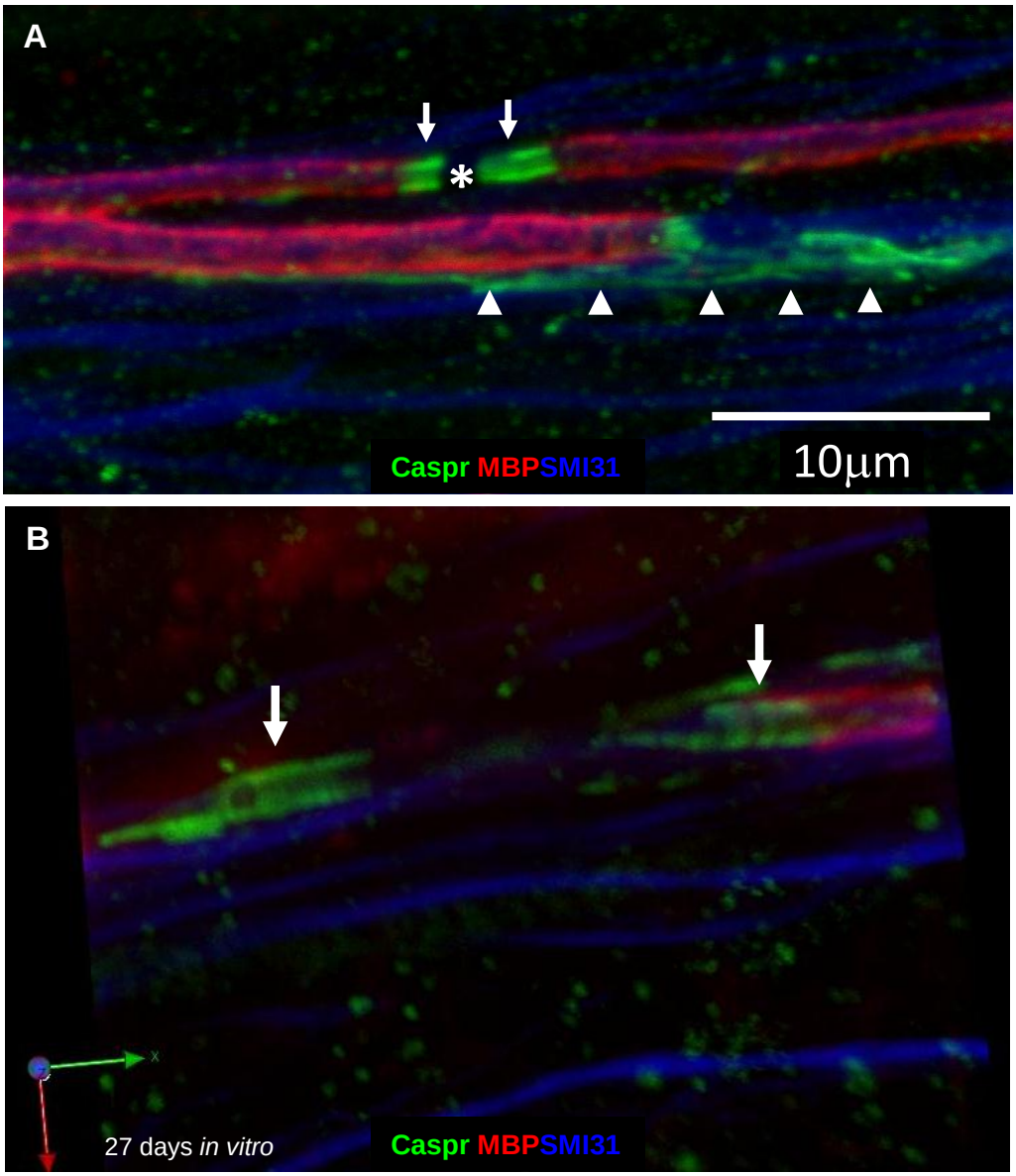

Figure 3.12 Caspr disposition at glial-axonal contact

A) Nodes of Ranvier were apparent between the internodes of myelin as depicted with MBP (red), using an antibody to the nodal protein Caspr (green, asterisk) which is present in paranodes. In some cases Caspr immunostaining resembled that of a loosely coiled spring (arrowheads) as described previously for unmyelinated axons. B) 3D reconstructed

images after confocal imaging illustrate radial lines (arrows) as coil-like structures. Representative images from at least 2 separate experiments.

3.3.9 Time-lapse visualisation of a GFP-positive process along an axonal fascicle

The ultimate aim from the *in vitro* approach in visualising glial-axonal interactions was to follow the process of myelination using time-lapse microscopy. Using a 70:30% ratio of cells, obtained from cGFP mice and wild type mice, in order to have a proportion of cells green, the spinal cord cultures over a series of time points were visualised using time-lapse (Nikon TE2000 with perfect focus and Metamorph software) for periods of between 8 and 18 hours and images were taken every 3 min.

Dual colour time-lapse acquistion was carried out (Fig. 3.13) using Cholera toxin B rhodamine, as well as the cGFP-labelled cells. Ascorbic acid 0.5 µl/1ml was included in the media to promote cell survival. Time-lapse imaging revealed several dynamic processes, involving all cell types. For example, time-lapse imaging showed a GFP-positive process extending down a bundle of axons for a distance of up to 45 µm. Due to the long distance and morphology of the process it is thought this is more likely to be a neurite than a glial cell process.

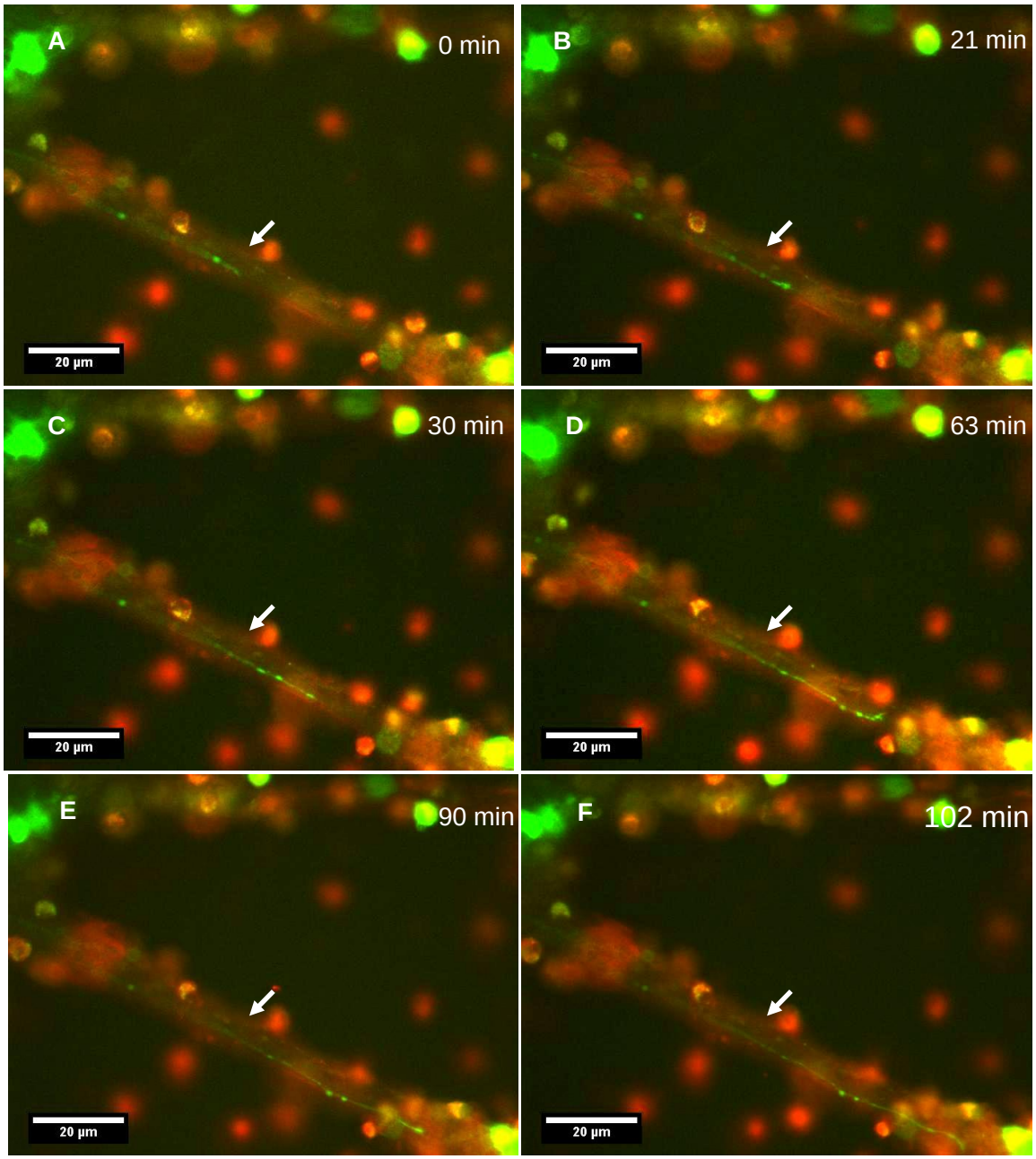

Figure 3.13 Time-lapse visualisation of a GFP-positive process along an axonal fasicle
A mixed CNS culture was generated for direct observation of cellular interactions between axons and surrounding glial cells. Using a 70:30% ratio of cells obtained from wild type and cGFP mice, in order to have a proportion of cells green, the cultures were visualised on 27 DIV, using time-lapse. A GFP-positive glial process or neurite was seen to extend down a bundle of neurites for a distance of up to 45 µm. Time frames obtained with 40x magnification and 3 min time interval. See supplementary video 3.3.

3.3.10 Visualisation of oligodendrocyte-oligodendrocyte interactions using time-lapse

Spinal cord cells were visualised in the mixed myelinating culture after 28 days *in vitro.* Images captured from time-lapse sequence revealed interactions of at least three labelled oligodendrocyte-like cells (arrows, Fig. 3.14A-D). It was observed that process extension and retraction occurred after apparent contacts between neighbouring oligodendrocyte-like cells on the neurite surface. Moreover, the motile processes seemed to extend and retract in an apparently random and repetitive way. Furthermore, the processes of a single cell generally seemed to cross over each other's "territories".

3.3.11 Visualisation of glial-axonal contact *in vitro* using time-lapse imaging

To study glial-axonal interactions using time-lapse, mixed spinal cord cells from cGFP and wild type embryos were used as previously described. The purpose of the study was to visualise cells extending processes along axons and to observe directly cellular interactions between axons and surrounding glial cells.

The results suggested that oligodendrocyte-like cells, constantly formed and reformed numerous processes (Kirby et al 2006) (Fig. 3.15) and interacted not only with neurites but with each other as well. To confirm that the imaged cells were of the oligodendroglial lineage, sister spinal cord cultures were set up on PLL-coated coverslips and by immunocytochemical studies it was determined that many cGFP labelled cells were positive for O4 (Fig. 3.15E) on day 28 *in vitro*, where time-lapse imaging was performed.

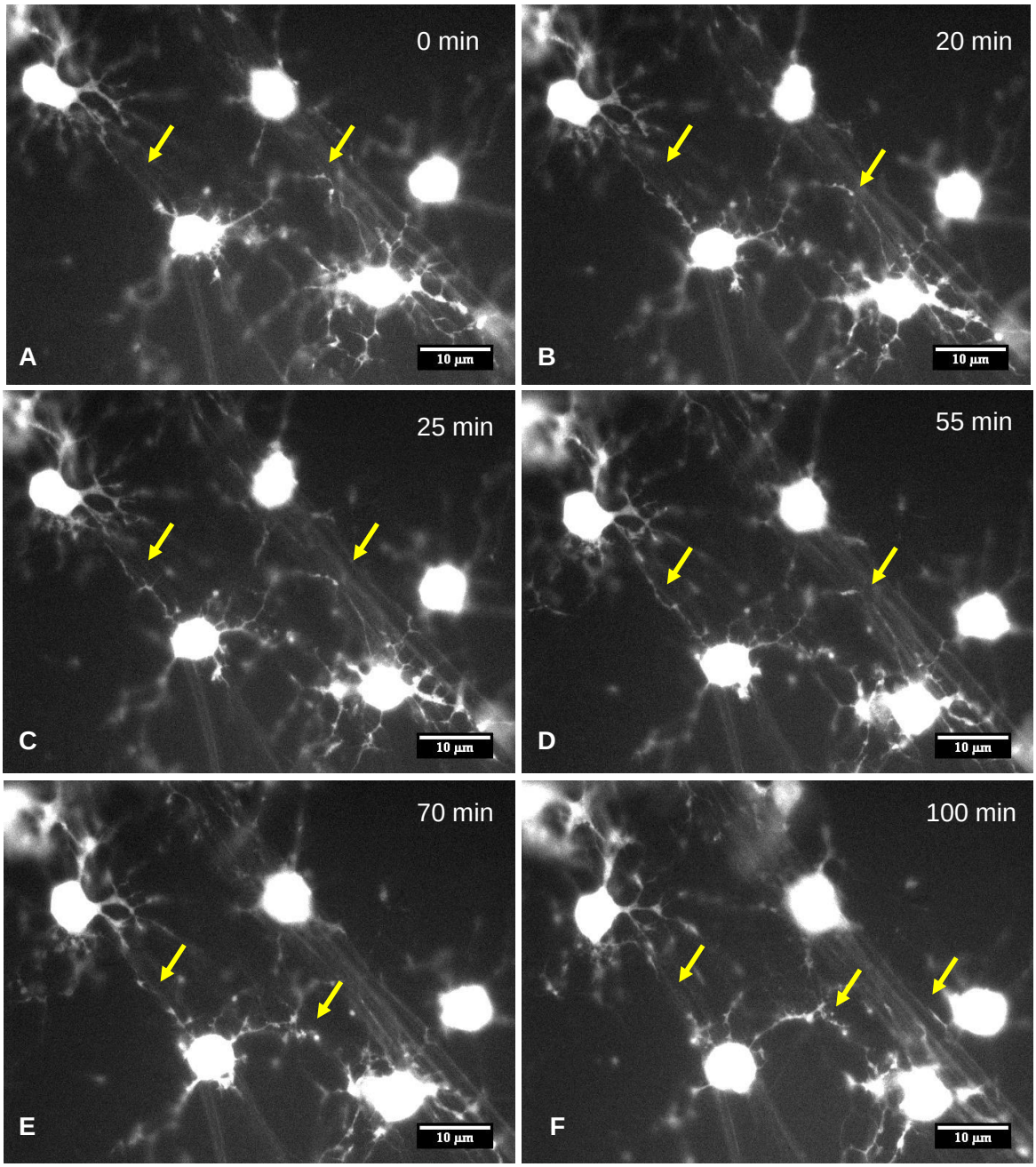

Figure 3.14 Two or more oligodendrocyte-like cells contacting the same neurite bundles or different neurite bundles, appeared to make contact with each other on the same or either side of the axons, remodelling their processes

Spinal cord cells from the mix of cGFP-wild type cells from the mixed myelinating culture were imaged on 28 DIV. Image sequence over a period of 15 hours with 5 min time interval, allowed the close examination of the behaviour of OPC-like cells, before axon wrapping begins. The oligodendrocytes seemed to interact with each other (arrows), prior to myelination of the axons underneath. See supplementary video 3.4. Representative images from at least 2 separate experiments.

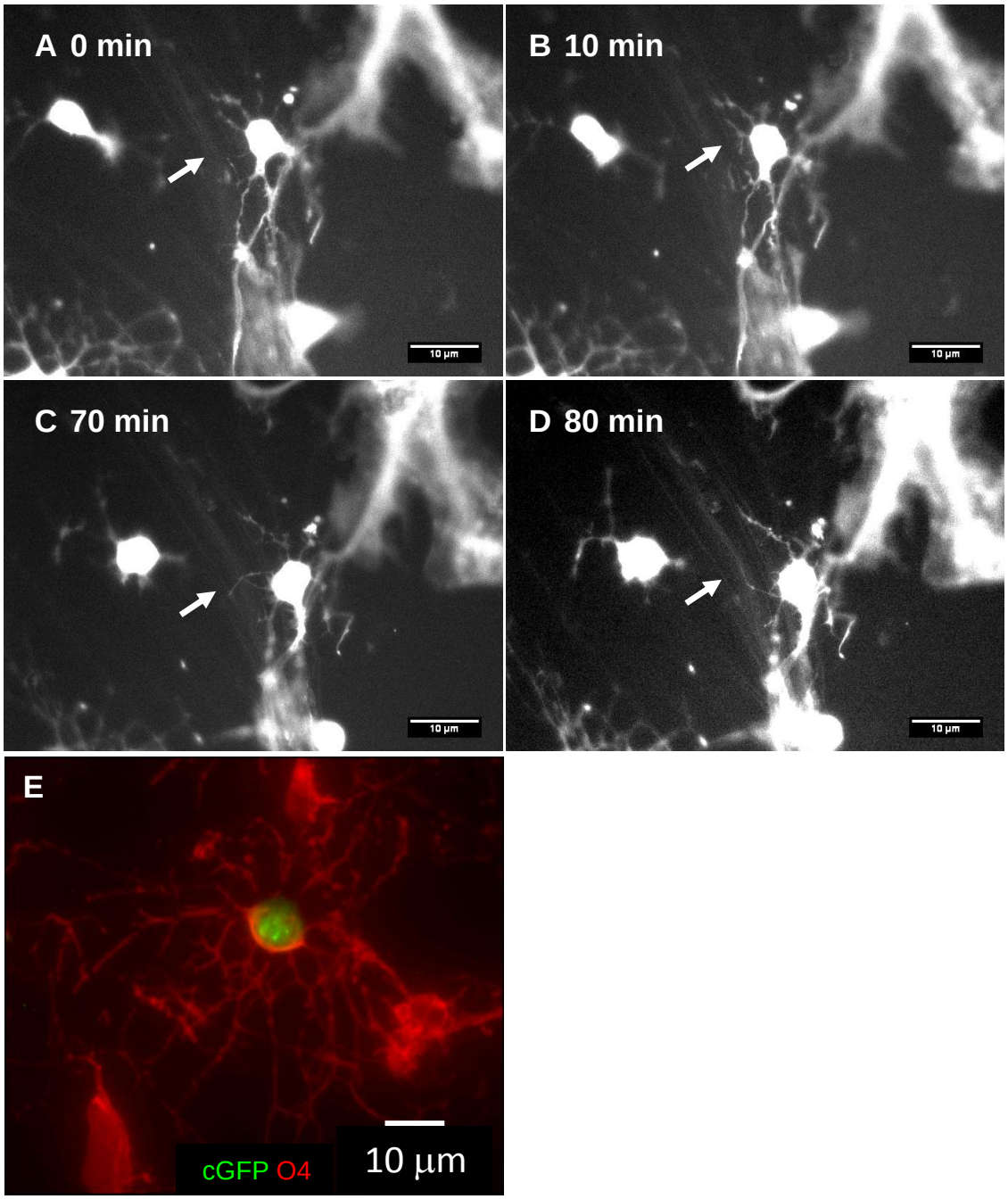

Figure 3.15 Time-lapse imaging of glial-axonal interaction

A-D) Time frames of a myelinating culture captured with high magnification, over a short period of two hours with 5 min time interval, on 28 DIV. An oligodendrocyte-like cell was imaged in close association with a bundle of neurites. During the time-recordings, the oligodendrocyte-like cell seemed to extend processes (arrows) which appeared as if it was either checking the environment or contacting the neurites. E) Immunostaining of a sister myelinating culture on the same day confirmed that cGFP labelled cells were positive for the myelin marker O4. See supplementary video 3.5. Representative images from at least 2 separate experiments.

3.3.12 Elongation of a neurosphere-derived labelled cell

The initial stages of interaction of the fGFP and dsREd GFP neurosphere-derived cells with the axonal surface were followed using time-lapse microscopy. The labelling with the dsRed GFP virus was in some cases very weak; in that case the neurospheres were also infected with fGFP virus. The advantages of these exogenously added cells were that the fGFP allowed the visualisation of the oligodendrocyte membrane even if the myelin sheath became compacted.

Many labelled cells had a leading process projecting towards one direction of the axonal fascicle. In the majority of cells, that leading process was highly dynamic, extending and retracting slowly during the time studied. The leading process (arrow, Fig. 3.16A-D) constantly sent out growth cone-like structures. Direct observation of the exploratory mode of these exogenous cells can reveal the dynamism of cells in the CNS. So far, it is known that process extension by oligodendrocytes is a critical, early step in myelin formation. Immunostaining of sister myelinating cultures showed the presence of MBP, associated with GFP-positive labelled cells (Fig. 3.16E).

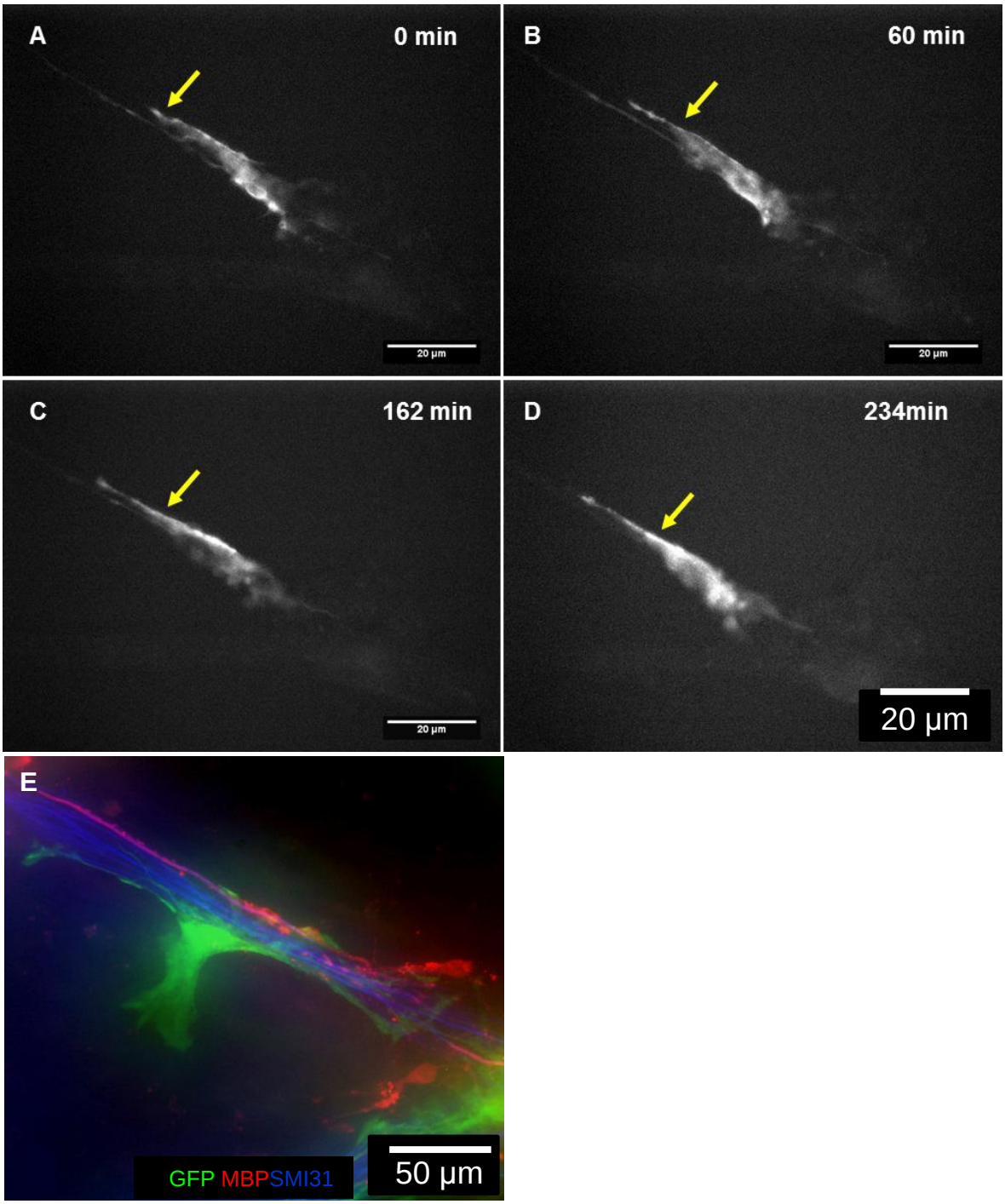

Figure 3.16 Time-lapse imaging of a cell process' elongation

Frames were captured from a 17 hours time-lapse sequence. Times shown in upper right corner, represent time elapsed after the start of imaging. fGFP and dsRed GFP infected neurospheres were added to myelinating cultures prepared from wild type embryos, on 12 DIV. The culture was visualised on 19 DIV, every 3 min. A GFP-positive cell was detected that appeared to made contact with a bundle of neurites beneath it. Continual movement along these neurite bundles were followed over time. The arrow indicates the process

extension which was variable, ranging from <1 µm to >15 µm. The process length changed during the first 160-min of the imaging sequence. Immunostaining of a sister myelinating culture for MBP (red) and for neurites (SMI-31, blue) showed the presence of myelin-like membrane in association with GFP-positive cells (green). See supplementary video 3.6. Representative images from at least 4 separate experiments.

3.4 Discussion

A detailed understanding of the mechanism and regulation of CNS myelination demands a variety of approaches, both *in vitro* and *in vivo.* The *in vitro* study of the already described myelinating system (Sorensen et al 2008) relies on the production of many internodes of myelin and nodes of Ranvier that mimics the CNS and therefore over time provides extensive glial-axonal contacts. However, one question that is not addressed by this method of quantification is how effectively myelination has occurred in terms of thickness and compaction of the myelin sheath. Immunolabelling for axons surrounded by myelin shows only that oligodendrocytes have wrapped axons, but does not distinguish between initial wrapping and mature compact myelin. The gold standard for conclusively demonstrating that myelination is complete and compact at internodes flanked by formed paranodal loops is to use electron microscopy. Using MBP and Caspr distribution as an indirect measure, each oligodendrocyte can be scored according to the extent to which it has myelinated underlying axons. One categorisation scheme is to score oligodendrocytes as ‘‘contacting’’ axons, ‘‘extending’’ processes, ‘‘wrapping,’’ and ‘‘mature’’ (Huang et al 2011). Although this approach has the disadvantages of both being subjective and requiring manual analysis, it is still considerably more rapid and inexpensive than processing an equal number of samples using electron microscopy (Jarjour et al 2011).

Regarding the first aim of this chapter, initial stages of glial-axonal contact from the *in vitro* observations demonstrated that the endogenous oligodendrocytes were able to myelinate axons in mouse cultures, without the need of an astrocyte monolayer. However, there was a small but significant increase in myelination in mouse cultures plated on rat or mouse neurosphere-derived astrocytes, compared to cultures plated on PLL-substrate alone. This suggests that the mice cultures either are i) not as dependent on soluble factors as seen for the rat myelinating cultures (Nash et al 2011b, Sorensen et al 2008) but also ii) more astrocytes are generated from the mouse spinal cord cultures which compensate for lack of the additional astrocyte monolayer. These hypotheses require further studies out with the remit of the thesis aims.

As far as the second aim of this chapter is concerned, neurospheres generated from wild type mice that were genetically labelled either with fluorescent markers or by viral infection, were added exogenously to the wild type myelinating cultures. It was confirmed the cGFP-labelled neurospheres could differentiate in a similar manner as non-

fluorescently labelled neurospheres by co-labelling with the anti-GFP and differentiation specific markers. In any case, the myelinating cultures allowed observations of the different differentiation stages of myelination over time, from initial contact between cells of the oligodendroglial lineage with the neurites to ensheathment and expansion of the myelin-like membrane.

Confocal imaging of the myelinating cultures, after fixation, labelled with cell specific cytoplasmic and/or membrane markers, cGFP, PLP/DM20 or the O4 antibody, allowed the observations of initial spirals of the oligodendrocyte membrane around neurites. At progressively later stages, gaps between spirals appeared to fill in with membrane, evetually forming a solid sheath-like strucute that stainined intensely with PLP/DM20 or MBP. Since cGFP could be localised in the inner and outer loops of the oligodendrocyte and does not reflect all of the membrane, cGFP labelled cells were immunolabelled with the O4 surface myelin marker to determine if the markers colocalised. PLP/DM20 staining appeared to be more intense and uniform while spirals of cGFP were in general much narrower. Taking a series of stacked images of cells labelled with anti-GFP and anti-PLP/DM20 it was possible to follow the cGFP-filled spirals of membrane.

This leads to hypothesis that the outer cytoplasmic loop of the oligodendrocytes over a sheath of PLP/DM20-postive myelin may be visualised as a spiral rather the classical straight line usually represented on a myelinated axon (see Schematic in Fig. 3.10J). However, as non compact myelin comprises the adaxonal layer of internodal myelin, as well as the abaxonal myelin layer it is possible that the cGFP spirals are associated with the aforementioned areas. However, the resolution provided by light microscopy does not easily allow to determine categorically if the process is inside or outside of the MBP stain.

From observations of the cells at later time points in culture, Caspr, a transmembrane nodal protein was located, by immunocytochemistry, at the axonal surface (Pedraza et al 2009) indicating that is recruited to the cell surface at the contact zone between axons and oligodendrocytes. Additionally, it has been suggested that the wave of glial membrane growth is mirrored by the distribution of Caspr (rings), presuming that the oligodendroglial myelinating cell influences the organisation of membrane proteins on the axonal surface (Pedraza et al 2009). This detailed examination of the close physical contact between the oligodendrocytes and the axons in the myelinating culture, suggested similar ribbon-like structures that were characterised earlier in this chapter. The aforementioned observations

lead to the conclusion that Caspr follows the movement of the coiling myelin-like membrane. On the axonal side, the localisation of contactin depends on the interaction with glial neurofascin but also on the association with Caspr (Pedraza et al 2009), contacts that are of major significance for the initiation of myelination. The formation of the paranodes is dependent on glial-axonal interactions. The interaction of glial loops with the axonal membrane is mediated by neurofascin 155 and contactin (Tait et al 2000). Moreover, the attachment of the lateral edges of the glial cells to the axonal membrane creates a diffusion barrier that might help to concentrate the nodal protein complex by restricting its lateral diffusion (Pedraza et al 2001).

The third aim of this chapter was to study myelination using fluorescently labelled oligodendrocytes added to cultures using time-lapse microscopy and a range of cultured cell combinations. Using these transgenic lines and time-lapse microscopy, dynamic developmental processes were captured in real time. From these time-lapse observations using the mixed spinal cord cells and fGPP and dsRedGFP-labelled added neurospheres, early interactions between an oligodendrocyte and neurites were investigated. It appeared that cells with an OPC or early oligodendrocyte morphology contacted the axons several times. The initial stage of contact included the formation of protrusions at the end of the oligodendrocyte processes similar to the observations of lamellipodia by others (Asou et al 1995b). Time-lapse microscopy revealed that these processes extended and retracted continually, persisting for several hours. In addition the oligodendrocytes' processes underwent changes in their length prior to ensheathing the axon, possibly sensing the length of myelin membrane required to enveloping the axon.

Quite frequently, time-lapse imaging showed interactions between neighbouring oligodendroglial cells. Axons can be ensheathed by several different oligodendrocytes which are invariably intermixed, thereby providing for direct contact between oligodendrocyte somata, their processes and their myelinating segments. Thus, the possibilities of both homologous and/or autologous oligodendrocyte-to-oligodendrocyte gap junctions, forming a glial network should be considered (Nagy & Rash 2000) and potentially connected with the time-lapse interactions. Gap junction channels formed by connexins are intercellular conduits that allow diffusional exchange of ions, second messengers, and small molecules (<1 KDa) such as metabolites, cAMP and inositol 1,4,5-trisphosphate (IP_3) (Tress et al 2011). Such an exchange of signals (or intercellular coupling) has been implicated in various cellular mechanisms, including ionic homeostasis,

electrical synchronisation, proliferation and migration (Bruzzone et al 1996, Kumar & Gilula 1996). Oligodendrocytes are known to express Cx47, Cx32 and Cx29 whilst astrocytes express Cx43 and Cx30 (Maglione et al 2010). In addition, abundant astrocytes and their fine-diameter processes are intermingled with oligodendrocytes throughout grey and white matter regions of the CNS, thereby providing for the possibility of heterologous oligodendrocyte-to-astrocyte gap junctions. Generally, astrocytes are coupled to each other (A:A coupling) by Cx43:Cx43 and Cx30:Cx30 homotypic channels and are thought to be coupled to oligodendrocytes (O:A coupling) by heterotypic Cx47:Cx43 and Cx32:Cx30 channels (Altevogt & Paul 2004, Li et al 2004, Nagy et al 2004). The multiple roles of astrocytes can promote the survival of OPCs *in vitro* through the actions of PDGF and leukemia inhibitory factor (LIF). Other astrocyte-derived growth factors that support OPC survival include NT-3, insulin-like growth factor-1 (IGF-I) and ciliary neurotrophic factor CNTF (Gao et al 2006, Talbott et al 2007, Wolswijk & Noble 1992)

Additionally, the interactions observed between neurons and glial cells is important as it controls the development, differentiation and survival of the oligodendrocytes and these are the signals that will match the number of oligodendrocytes to the axonal surface requisite myelination (Barres & Raff 1994, Osterhout et al 2011). Process activity and maturation seem to be influenced by many growth factors such as PDGF, a survival factor for oligodendrocyte precursors (Grinspan & Franceschini 1995), IGF-I which stimulates proliferation of both oligodendrocyte progenitors and pre-oligodendrocytes O4-positive cells, CNTF as co-mitogen with PDGF which also promotes oligodendrocyte *in vivo* (Barres et al 1993), glial growth factor which delays differentiation into mature oligodendrocytes and interleukin-6 which may also act on oligodendrocyte survival (Canoll et al 1999).

It is well known that oligodendrocytes myelinate exclusively axons *in vivo*, although oligodendrocytes are able to form uncompacted myelin or myelin-like structures in the absence of neurons (Wood & Bunge 1986b). The signals indicating which axon should be myelinated remains unclear. Several studies support the idea of a critical diameter for myelination; however individual axons are not myelinated along their entire length at the same time, implying that other factors are involved (Suzuki & Raisman 1994). The Notch pathway which was considered to regulate neuronal development, it was also shown that Notch receptors are present on oligodendrocytes precursors. Jagged 1, a ligand of Notch 1 receptor is developmentally downregulated in axons with a time period that parallels

myelination, indicating that Jagged 1 signals to Notch 1 on the preoligodendrocytes' surface inhibit their differentiation into myelinating oligodendrocytes. It is suggested that downregulation of Jagged1 in axons occurs in response to the onset of myelination (Baumann & Pham-Dinh 2001). The process activity and alignment was possibly influenced by signals perhaps mediated by contact with the axons underneath or even the astrocytes (Fig. 3.17). Several studies have shown that astrocytes induce oligodendrocyte process to align with and adhere to axons, providing a new role for astrocytes in controlling the beginning of myelination. Time-lapse imaging also showed the activity of cytoskeleton dynamics of these cells, which might be required for the appropriate trafficking of glial molecules. For example, cells of the oligodendrocyte lineage express a novel form of MAP, MAP 2c localised in the cell body of pre-oligodendrocytes that may support the initiation of process extension.

To summarise, the data in this chapter validate the mouse cultures for study without an astrocyte monolayer thus allowing optimal imaging. Furthermore it shows that cGFP tagged oligodendrocytes myelinate the cultures in a similar manner as wild type cells.

4. Time-lapse imaging of the dynamics of glial-axonal interactions after the addition of GFP-expressing neurospheres into *shiverer* myelinating cultures

4.1 Introduction

4.1.1 Background

By their very nature, biological systems are dynamic and a proper understanding of the cellular and molecular processes and how to manipulate them is a prerequisite to combat diseases. More specifically the understanding of CNS function and especially the complicated mechanisms related to the essential role of myelin-forming glia, wrapping around axons, has attracted lots of interest. Therefore, research into biological and pathological mechanisms in the CNS requires both *in vivo* and *in vitro* models.

One of the major currant challenges of biomedical research, therefore, is to unravel not just the spatial organisation of these complex system but their spatiotemporal relationships, in real time. The reported myelinating culture method (Sorensen et al 2008, Thomson et al 2008) which recapitulates many of the features of the CNS *in vivo* and time-lapse microscopy are useful tools to study aspects of establishment of glial-axonal contact culminating in myelination. However, each myelinating oligodendrocyte *in vivo* can produce roughly 500 times the area of myelin membrane than an oligodendrocyte in culture (Pfeiffer et al 1993) as reviewed in Jarjour et al., 2011.

Direct visualisation of the initial stages of glial-axonal interactions can be achieved by using fluorescently-labelled cells, by adding for instance cGFP-expressing neurospheres into *shiverer* myelinating cultures, which are characterised by deficiency of myelin and MBP in the CNS. Therefore, the addition of neurospheres transduced with lentiviral constructs containing GFP (membrane bound) into the *shiverer* myelinating cultures, may allow for visualisation of GFP-positive myelin sheaths, which would not be ascribed to endogenous myelination. The exogenous labelled cells would thus offer the opportunity to study the initiation and several stages of myelination into the host MBP-deficient *shiverer*

cultures. Nevertheless, in both cases a myelinating cell process that is continuous with the plasma membrane must be assembled and extended.

After oligodendrocytes have established proper contact with the axonal membrane, they start to extend their membrane by spirally wrapping it around the axon. Because each oligodendrocyte can produce up to 60 myelinated segments on multiple axons, they have to synthesise a tremendous amount of membrane in a relatively short time (Pfeiffer et al 1993).

The discovery that MBP is synthesised in the growing myelin process was a crucial step towards the understanding of how proteins might be delivered to the myelin membrane. MBP mRNA rather than MBP itself is transported and targeted into the oligodendrocyte processes, thereby enabling protein synthesis "on site". This not only prevents premature ectopic expression of MBP, but also a fast and selective insertion of MBP into myelin membranes (Baron & Hoekstra 2010). On the other hand, glial-axonal interactions, attachment of the complex to the axonal cytoskeleton and lateral diffusion barriers within the axonal membrane are possible mechanisms that contribute to the segregation of the plasma membrane (Simons & Trajkovic 2006).

Upon appropriate target interaction, pre-myelinating, oligodendrocyte processes transit from process outgrowth to membrane sheet formation. These critical final and distinct steps of oligodendrocyte maturation are regulated by complex interactions of the oligodendrocyte's processes (protrusions) with their extracellular environment and are considered crucial for efficient myelination. Generally, cells extend four different plasma membrane protrusions at the leading edge including: lamellipodia, filopodia, blebs and invadopodia. Actin cytoskeleton and regulators of actin dynamics are involved in all protrusions. Lamellipodia, thin-sheet like regions at the leading edge of migrating cells, can extend long distances through the extracellular matrix *in vivo*, pulling cells through tissues (Friedl & Gilmour 2009). Filopodia have a role in surveying the cells' surroundings and are especially important for guidance of neuronal growth cones or endothelial cells (Eilken & Adams 2010). Membrane blebbing has been described to drive directional cell migration after stimuli (Charras et al 2008). Invadopodia are protrusions that allow focal degradation of the extracellular matrix. These different kinds of protrusions can co-exist at the leading edge.

From previous studies it was shown that oligodendrocytes displayed many bulbous protrusions scattered over the entire extended membrane surface, following 24 hour exposure to anti-sulfatide affecting myelination (Dyer & Benjamins 1988). The wrapping of the myelin membrane around axons of a diameter of > 0.2 μm (~1μm) and the compaction of the myelin sheath are poorly understood processes that hopefully future studies will shed light on.

4.1.2 Aims of the chapter

Having assessed glial-axonal interactions in static images *in vitro* (Chapter 3), the principle aim of this chapter was to visualise the progression between initial cell contact and myelin formation over time. For this reason *shiverer* myelinating cultures were used, which have almost no endogenous myelination and to which fluorescently-labelled neurospheres were added and differentiation followed using time-lapse microscopy. More specifically, the aims of this Chapter were to:

1) Visualise cGFP- and fGFP-expressing oligodendroglia in *shiverer* myelinating cultures, including initial contact, extensions and elongation of membranous sheaths in association with *shiverer* axons over time.

2) Image myelin sheath-like formation.

3) Confirm by immunohistochemical methods, myelin formation by GFP-expressing wild type cells in *shiverer* cultures that lack MBP.

4.1.3 Materials and Methods

4.1.3.1 Isolation and culture of cGFP and fGFP-expressing neurospheres

Neurospheres were generated from either *β*-actin cGFP-expressing transgenic mice or wild type mice that were then infected with fGFP-lentivirus. In some cases, wild type neurospheres were transduced with lentiviral constructs containing both fGFP (membrane bound) and cGFP-dsRed.

4.1.3.2 Myelinating cultures

The method of generating myelinating cultures is based on previously published work (Sorensen et al 2008, Thomson et al 2008). *shiverer (shi/shi)* female mice were time-mated and embryos were collected on embryonic day 13.5 (E13.5). The spinal cord was dissected and dissociated mechanically and enzymatically to produce a mixed population of neuronal and glial cells, as described in detail, in chapter 2. *Shiverer* myelinating cultures were then treated with neurospheres infected by virus carrying cGFP or fGFP labelling cellular membranes or both.

4.1.3.3 Time-lapse microscopy

Real-time imaging parameters were used to follow the dynamic cellular interactions of the fluorescently-labelled glial cells with the *shiverer* axons. Time-lapse images were captured using 40x dry (NA=0.75) objectives mounted on a Nikon time-lapse microscope TE2000. Therefore, 35 mm glass bottom microwell Petri dishes, with 14 mm diameter of microwell or 6-glass bottom well plates were used for all the time-lapse experiments. In some cases, ascorbic acid was added to cultures to ensure cell viability during time-lapse recordings.

4.2 Results

4.2.1 Visualisation of cGFP-expressing oligodendroglia-like cells in *shiverer* myelinating cultures

To investigate behaviour of OPC-like cells as they move and make contact with *shiverer* axons *in vitro*, cGFP-expressing neurospheres were added in *shiverer* myelinating cultures between 8-15 DIV when neuronal survival and neurite extension has occurred. Time-lapse was initially performed at early time points *in vitro*, within a few days after the addition of the cGFP-positive neurospheres.

Since neurospheres can differentiate into oligodendrocytes, astrocytes and infrequently neurons, the cells visualised were defined on their classical morphology. OPCs generally are bi-tri potential with small cell bodies, astrocytes tend to be flat or stellate with large cytoplasmic area, and neurons have long neurites (Raff et al 1983c). In the cultures, exogenous cGFP oligodendroglia-like cells formed numerous highly branched processes which extended in the direction of movement. Initially, OPC-like cells appeared to make contact with the *shiverer* axons with one or more than two processes (arrows and arrowheads, Fig. 4.1A and B) that became thicker over time (arrow, Fig. 4.1C). Later in the time-lapse sequence, the cell processes seemed to align with the *shiverer* axons (Fig. 4.1D) suggesting that a closer physical contact might be necessary before myelination. Interestingly, time-lapse imaging showed that cGFP added cells' activity was highly dynamic. Additionally, examination of the interactions between neighbouring cells more carefully, revealed extensive overlap at the process terminals of neighbouring cGFP-positive oligodendroglia-like cells (arrowhead, Fig. 4.1F). Overlapping terminals were constantly remodelled during the time-lapse recordings.

Observations from time-lapse imaging over 20 hours with 4 min time interval, allowed the monitoring of the movements of the exogenous cGFP cells and their contacts with *shiverer* axons of the myelinating cultures. In addition, time-lapse imaging showed a synergetic activity of nearby and neighbouring oligodendroglial-like cells, an example of cell-cell interaction, which in combination with the dynamic process activity might be general features of vertebrate glial cells.

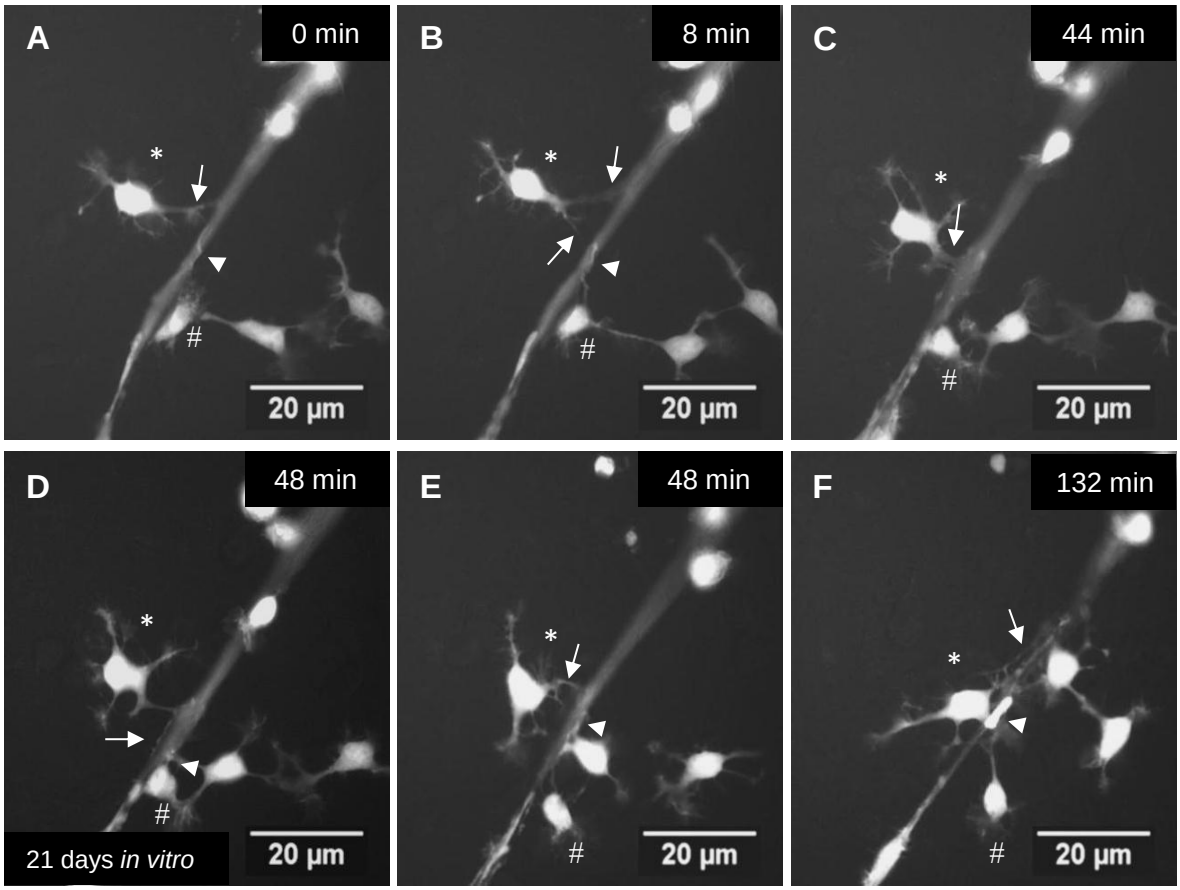

Figure 4.1 Time-lapse imaging of cGFP-positive OPC-like cells added to *shiverer* myelinating cultures

Frames were captured from a 24-h time-lapse sequence with 4 min time interval, on 21 DIV. A-C) Two oligodendroglial-like cells marked by * and # extended processes making contacts with the *shiverer* axons (arrows and arrowheads). D-F). The processes appeared to align with the *shiverer* axons (arrows) as they became thicker over time. Time sequence showed a synergetic activity between the exogenous cGFP-positive cells (arrows and arrowheads). See supplementary video 4.1. Representative video from 50 analysed movies.

4.2.2 *In vitro* time-lapse imaging of OPCs in *shiverer* myelinating cultures

Shiverer myelinating cultures and cGFP labelled neurospheres were imaged after 17 DIV (4 days after neurosphere addition) every 4 min for 24 hours. OPCs actively migrated along the neuritic fascicles. Thin processes emanating from OPC cell bodies appeared to spiral around neurites (Fig. 4.2A-I, illustrates a 4 hour section of the video) and formed occasional small and transient thickenings (asterisk Fig. 4.2E). Process extension was very dynamic and the pattern of association with the neurites changed continually. Manual tracking of the complete video illustrates the pathway of the putative OPCs (asterisks yellow and blue) over time demonstrating their highly motile behaviour (Fig. 4.2J). A sister myelinating culture was immunolabelled for MBP (myelin) and neurites (SMI-31) after 28 days to illustrate and confirm the formation of myelin-like sheaths (Fig. 4.2K).

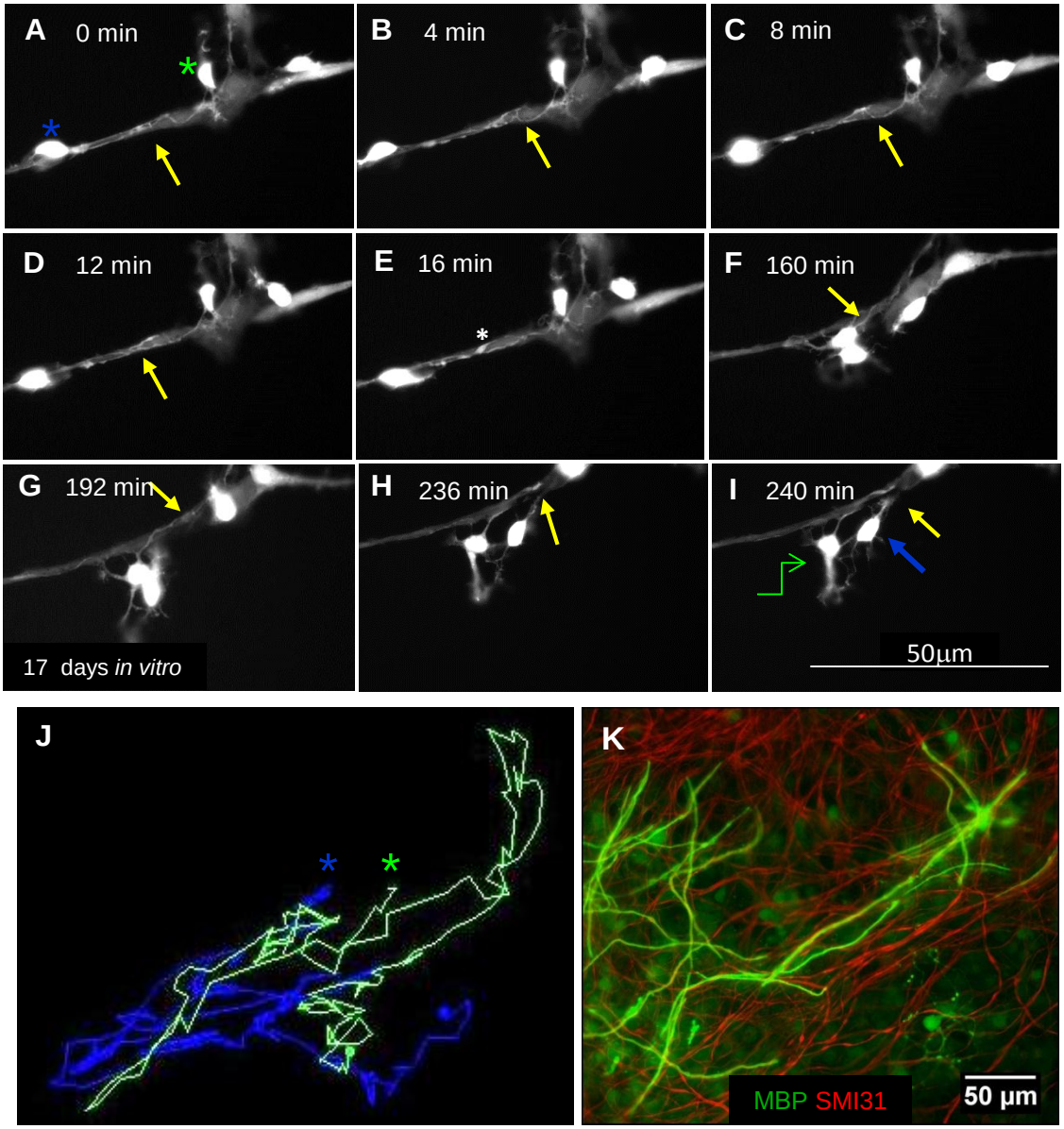

Figure 4.2 *In vitro* time-lapse imaging of cGFP labelled OPC-like cells in *shiverer* myelinating cultures reveal dynamic cellular interactions

Neurospheres expressing cGFP were added to myelinating cultures prepared from *shiverer* embryos on DIV 13 and visualised on DIV 17 over 24 hours in 4 min intervals, using a Nikon TE 2000 time-lapse microscope (40x, 0.75NA short distance working lens) with perfect focus. A-I) Images captured from a time-lapse sequence illustrate cells with morphology typical of OPCs. Spirals of processes appeared over the neurites. Both the cell soma and processes were highly motile, continually moving along the neurites. Processes appeared to move over the nerve bundles (arrows and asterisk). J) Manual tracking of the cell bodies of the entire video illustrates the pathway of the putative OPC-like cells (asterisks green and blue) over time, demonstrating their highly motile behaviour. K) A

sister culture was immunostained for myelin (MBP, green) and neurites/axons (SMI-31, red) on DIV 27, demonstrating that the added cGFP neurospheres myelinated the axons. See supplementary video 4.2. Representative images from at least 2 separate experiments.

4.2.3 Assessment of the close contact between the exogenous cGFP cells with the *shiverer* axons

To examine more closely the morphology and behaviour of the different cell types derived from the exogenous cGFP neurospheres which were added to the *shiverer* myelinating cultures, time-lapse experiments were performed at higher magnification over a longer time period.

In order to capture the earliest possible events after the addition of the cGFP neurospheres to the *shiverer* cultures, time-lapse imaging was performed on 13 DIV. In this set of experiments cGFP neurospheres were added on 6 DIV. One of the most notable features of the exogenous cGFP neurospheres was that they morphologically differentiated quickly, within a few days after addition to the myelinating cultures. As oligodendrocyte-lineage cells developed, they produced fine processes that eventually contacted the *shiverer* axons (Fig. 4.3). These processes contacted underneath the axons at several points (red arrows, Fig. 4.3 A-F). Moreover, this extensive cellular organisation reflects a continual sensing of the axon and may represent a mechanism for axon recognition and contact that might explain early stages in the process of myelination.

In the same plane of view cells that resembled macrophages appeared with a morphology that was characterised by membrane ruffles, continual moving and changing positions (red asterisk, Fig. 4.3). Time-lapse imaging showed that these cells where highly motile moving in all directions, suggesting a possible role in surveying their environment to remove any cellular debris. Moreover, other type of cells appeared in the time sequence bearing transient processes, but without the use of differentiation specific markers it was difficult to identify them.

Time-lapse imaging for these experiments was achieved with 60x magnification. Because of the risk of phototoxicity, the time interval between the time frames was set at 5 min, as high exposure can be detrimental to cell survival over long periods of recording.

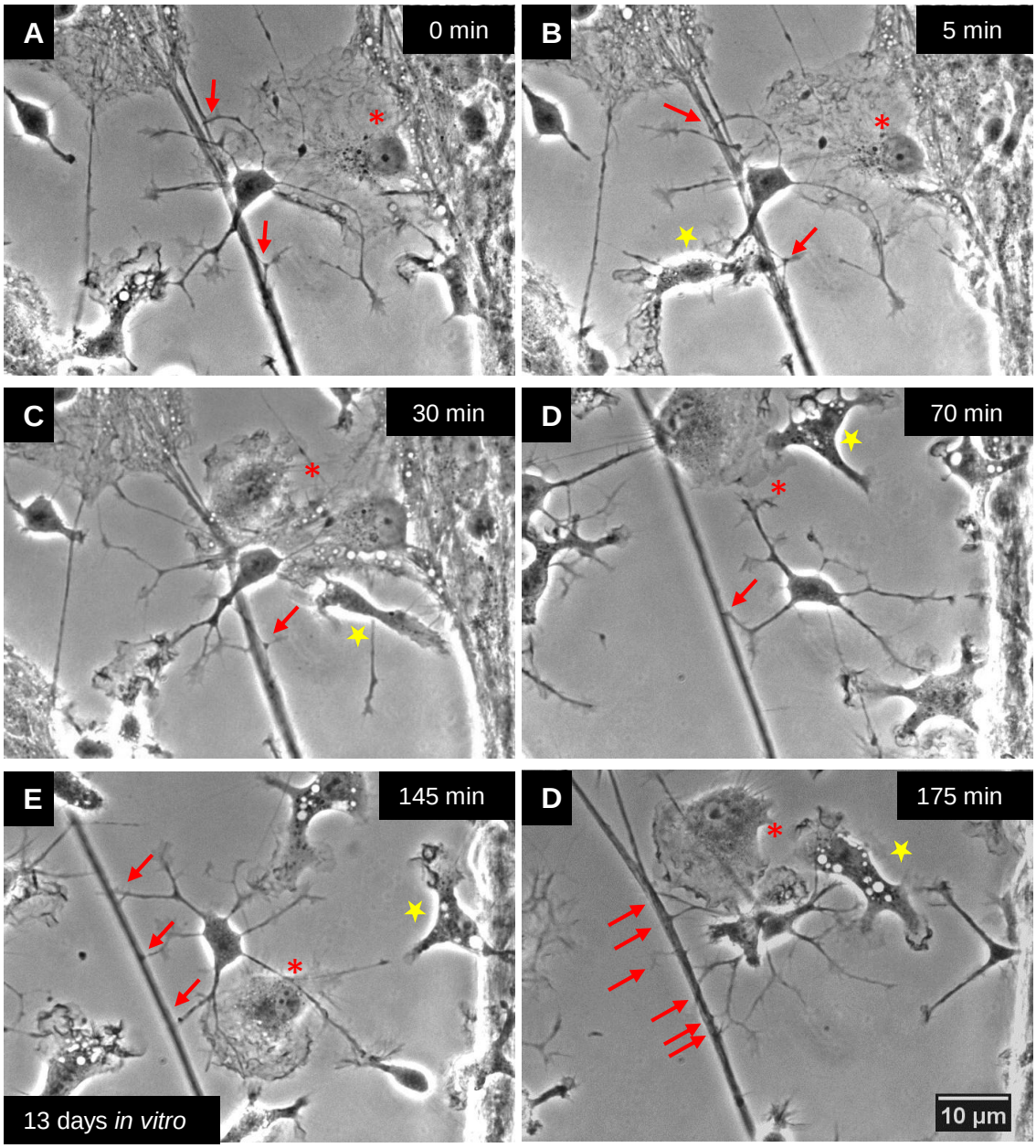

Figure 4.3 Bright field time-lapse imaging of cGFP-positive OPC-like cells in *shiverer* myelinating cultures

cGFP neurospheres were added to the myelinating cultures on 6 DIV. Frames were captured from a 20-h time-lapse sequence with 5 min time interval, on 13 DIV. A-C) An oligodendrocyte-like cell appeared to contact underneath the axon at several points (red arrows). In the same plane of view a cell that resembled a macrophage appeared with a morphology that was characterised by membrane ruffles and continual movement (red asterisk). D-F). At later time points of the time-lapse sequence the oligodendrocyte-like cell made further contacts with the axon. Another unidentified type of cells also appeared bearing transient processes (yellow star). Representative images from 50 analysed videos.

4.2.4 *In vitro* time-lapse of cGFP oligodendrocyte-like cells in *shiverer* cultures

Using time-lapse it was possible to follow the continuous extension and retraction of glial cell processes over time in *shiverer* cultures, after the addition of cGFP neurospheres. Some of the cGFP-labelled cells appeared differentiated with a morphology typical of an oligodendrocyte with multiple processes emanating symmetrically from the cell body (Fig. 4.4A-C and E-G). The pattern of formation of their processes changed constantly over the time course. Long projecting processes that sometimes exceeded 20 μm in length were shown to align with the underneath *shiverer* neurites (arrows, Fig. 4.4A-B and F). There were also dynamic minor processes emanating from the cell body that extended and retracted rapidly within minutes.

Sister *shiverer* myelinating cultures were immunolabelled for MBP (myelin) and SMI-31 (neurites) after 27 DIV to confirm myelination (broken arrow, Fig. 4.4D). The cGFP cells that also expressed the myelin marker MBP were seen to extend small processes connecting the cell body with the myelin-like sheath (thin arrow, Fig. 4.4D). Furthermore, fluorescence microscopy revealed features such as presumptive nodes of Ranvier in *shiverer* myelinating cultures (asterisk, Fig. 4.4D) suggesting that the exogenous cGFP-cells could correctly form myelin-like sheaths in the MBP-deficient *shiverer* cultures.

In the imaged Petri dish, apart from cells with an oligodendrocyte morphology (dotted box, Fig. 4.4 E-G), other cGFP-positive cells with thick and flatten processes appeared in the same time sequence. These cells resembled astrocytes (arrowheads, Fig. 4.4E-G).

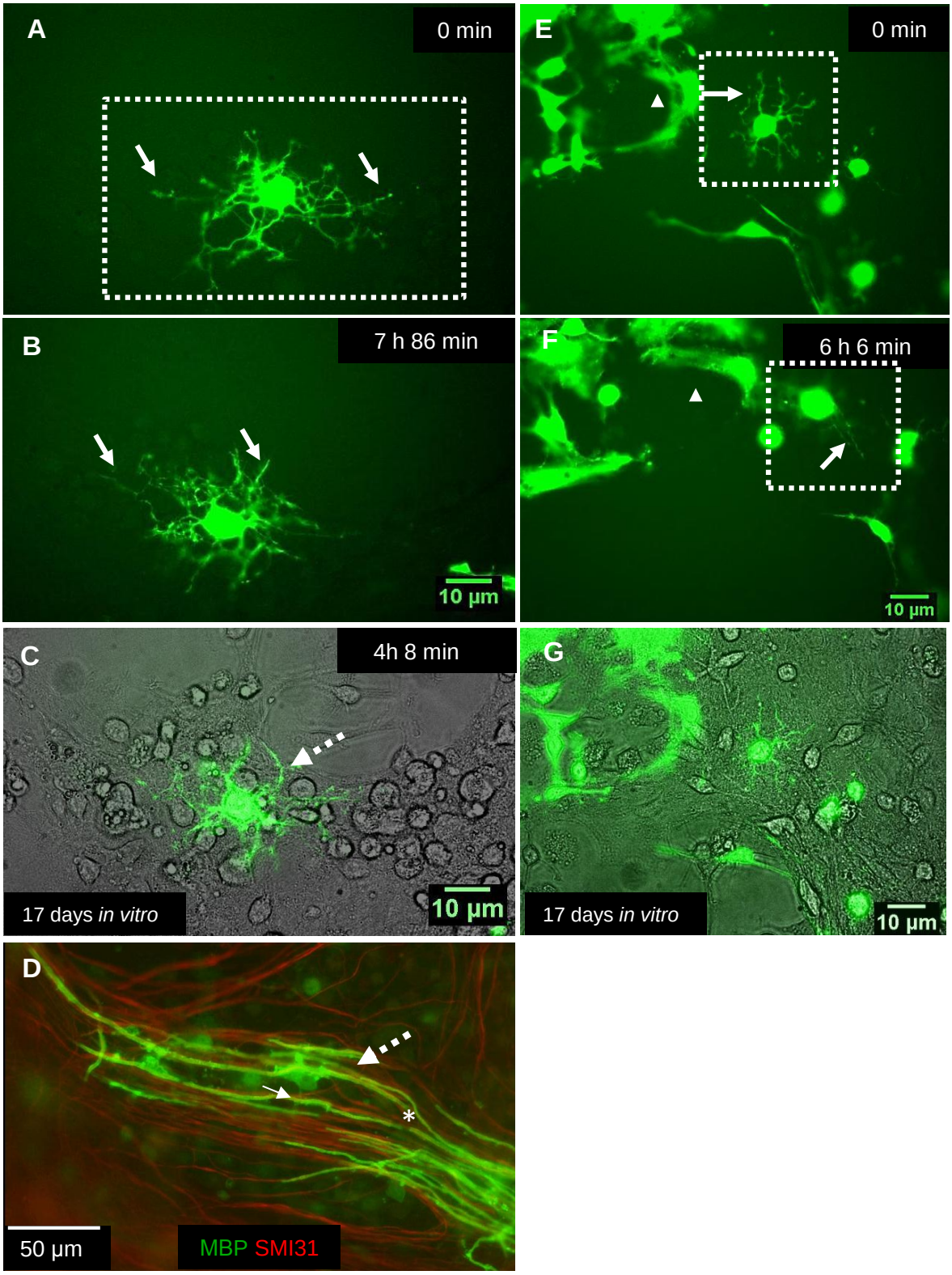

Figure 4.4 Time-lapse imaging of cGFP oligodendrocyte-like cells in *shiverer* myelinating cultures

cGFP-neurospheres differentiated into cells with morphology very similar to that of oligodendrocytes. A-C and E-G) Time-lapse sequence on 17 DIV, over 24 hours with 4 min time interval showed oligodendrocyte-like cells (dotted box) with multiple processes,

emanating symmetrically from the cell body, which constantly changed their pattern. Other cells with flat and thick processes resembling astrocytes could be detected in these cultures (arrowheads). A, B and F) Long processes (arrows) were shown to align with the *shiverer* neurites. C and G) Merged image of bright field and GFP channel showed the association of an oligodendrocyte-like cell with the neurites. D) Immunostaining of sister *shiverer* cultures showed that the cGFP cells (broken arrow) co-expressed the myelin marker MBP (green) and appeared to myelinate the *shiverer* axons (SMI-31, red). A gap between two myelin internodes suggests the formation of the nodes of Ranvier (asterisk). Representative images from 50 analysed movies.

4.2.5 *In vitro* time-lapse of fGFP-expressing cells into *shiverer* myelinating cultures

The next step was to visualise the progression between initial cell contact and myelin formation in the *shiverer* myelinating cultures. For this purpose, wild type neurospheres that had been infected previously with a lentivirus encoding membrane bound fGFP were added to the *shiverer* cultures. In this way it was predicted that processes could be detected that were not seen using labelling with the cytosolic GFP lentivirus.

One of the most distinguished features of oligodendrocytes is their formation of extensive membrane processes. As a consequence, it was essential to investigate the morphology of oligodendrocyte-like cells during and after initial contact and ensheathment in the developing *shiverer* myelinating cultures. fGFP neurospheres were added to the *shiverer* cultures on 8 DIV. By this time point, the dissociated spinal cord cells have established neurite extensions, so it was anticipated that these would be amenable to myelination by fGFP neurospheres as well as sending pro-myelination signals to the oligodendroglial lineage. To follow changes in the oligodendrocyte-like cells during the glial-axonal contact, time-lapse imaging was performed at several time points.

As shown in Fig. 4.5 time-lapse experiments of a culture after 24 DIV showed that oligodendrocyte-like processes extension persisted for several hours from the beginning of the time sequence. In these cultures, membrane protrusions resembling bubbles or membranous flaps were detected. In some cases two processes could be seen, one 5 μm above the other and both extending towards the same axon. After 5 hours the fGFP-

positive membranous flap formed a solid and stable process that continued to interact with the axon below (arrowheads, Fig. 4.5A-C). At later stages of the time sequence, a solid sheath was generated over another axon in the same plane of view (arrowheads, Fig. 4.5D). However, it was not possible to conclude if this is one wrapping of the axon or several.

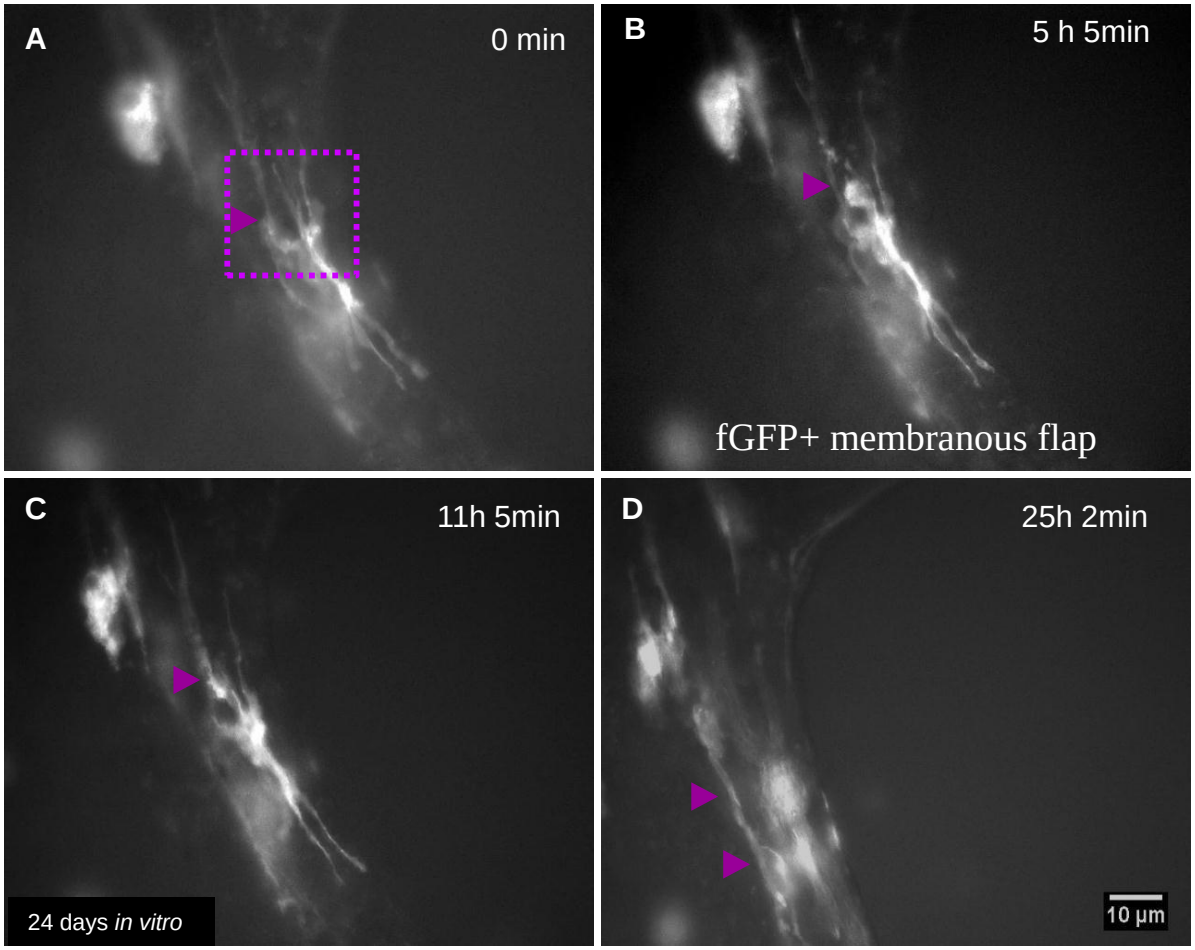

Figure 4.5 Time-lapse of fGFP-positive membranous flap

Time-lapse images were captured over 30 hours of a *shiverer* myelinating culture on 24 DIV, in which fGFP-positive neurospheres had been added on 8 DIV. A) A process is indicated by arrowhead. B-C) A second process was formed from a new branch. D) A thick membranous sheath in the same plane of view is indicated by arrowheads. See supplementary video 4.3. Representative video from 5 separate experiments.

4.2.6 *In vitro* time-lapse imaging of assembly of myelin-like membrane using fGFP-labelled neurospheres

To visualise the oligodendrocyte membrane during myelination, time-lapse imaging was performed on 29 DIV over longer time to identify interactions associated with membrane changes, as myelination proceeds to the ensheathment stage.

fGFP-positive cells formed a large network of branching processes (arrows, Fig. 4.6A) and in some images appeared to wind around neurites (Fig. 4.6Ai). From images taken at low magnification it was impossible to determine the morphology of the labelled cells and to distinguish if the glial processes came from either astrocytes or oligodendrocytes. Immunostaining with anti-MBP confirmed that fGFP-positive neurospheres differentiated into cells of the oligodendroglial lineage (Fig. 4.6B). Immunostaining also revealed large spherical extensions of the fGFP-labelled membrane, resembling the 'bubble' in Fig. 4.7Ai-Aiv, contained MBP. Furthermore, co-immunolabelling neurites with anti-SMI-31 and myelin with anti-MBP, in an alternate *shiverer* myelinating culture around the same time point *in vitro*, showed a membranous lateral expansion of MBP over the myelin segments (arrows, Fig. 4.6C).

Using the fGFP lentivirus allowed for time-lapse imaging to reveal the membrane dynamics of fGFP-positive cell processes. During the time course studied, waves of membrane were occasionally seen that moved along the length of the neuritic processes. The initial membranous wave appeared to twist in relation to the orientation of the axon (arrowheads, Fig. 4.7Ai-Avi) and later extended smoothly along the neurite to form a continuous sheath. A second membranous wave occurred at the same starting point (arrowhead, Fig. 4.7Avii) moving progressively along the neurite until another one formed (arrowhead, Fig. 4.7Aix-x). In the field of view, in less than 3 hours three membrane waves that resembled "bubbles" were generated and seemed to wind around the neurites, suggesting a possible mechanism of membrane deposition during the process of myelination.

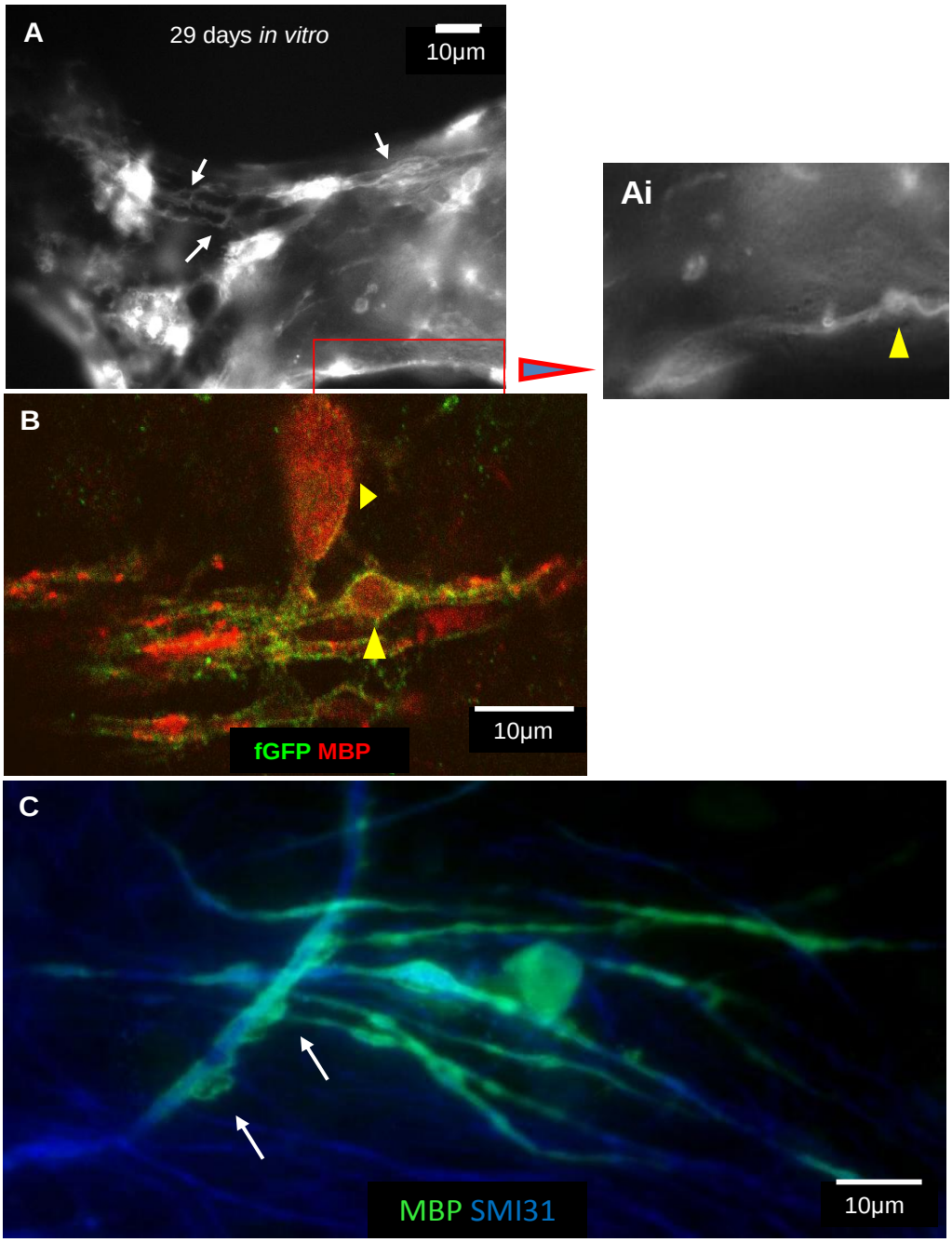

Figure 4.6 Imaging of fGFP-positive membranous features in *shiverer* myelinating cultures

A) Neurospheres expressing fGFP added to *shiverer* myelinating cultures were imaged on 29 DIV forming a large network of branching processes (arrows) Ai) Magnified view of the inset in A illustrating a fGFP-positive process looping around a presumptive neurite and forming a membranous protrusion resembling a flap or 'bubble' (yellow arrowhead). B) The cells from the Petri dish imaged with confocal microscopy were immunostained with anti-GFP and anti-MBP to confirm differentiation of fGFP-labelled neurospheres into oligodendrocytes (yellow arrowheads). C) Immunostaining from another *shiverer*

myelinating culture around the same time point *in vitro*, showed a membranous lateral expansion of MBP-expressing membrane (arrows) over a myelin MBP-positive segment (fGFP, green, SMI-31, blue and MBP, red).

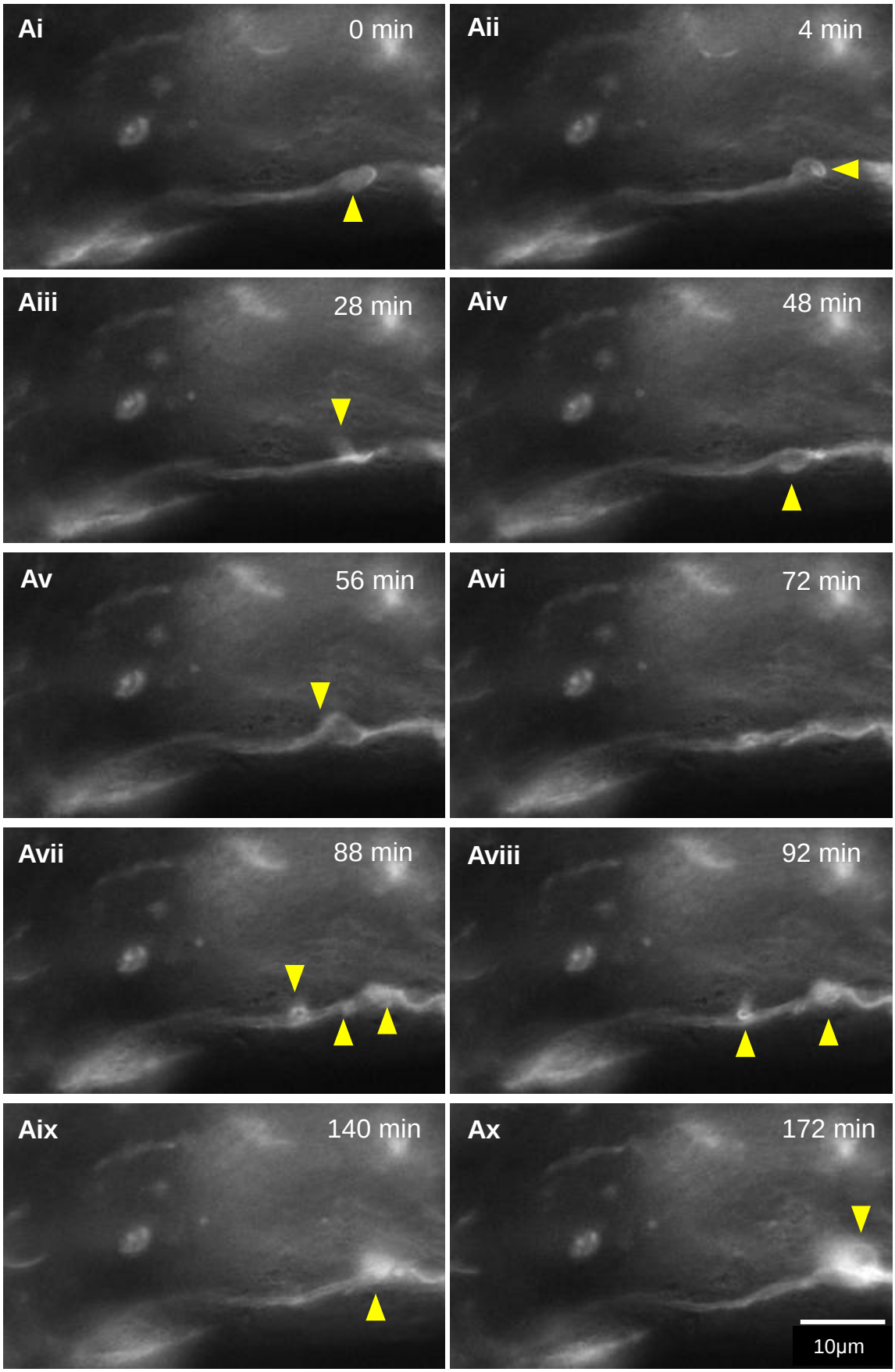

Figure 4.7 Time-lapse imaging of the putative assembly of myelin membrane

Ai-x) Time-lapse imaging of fGFP-expressing neurospheres, which had been added to *shiverer* myelinating cultures, on 29 DIV, over 24 hours with 4 min time interval. During the time sequence, membranous waves (yellow arrowheads) were occasionally generated that moved along the length of the presumptive neuritic processes. These membrane protrusions or "bubbles" were also shown to wind around the neurites as they progresed suggesting a possible mechanism by which membrane is wrapped around the neurite. See supplementary video 4.4. Representative video from 5 separate experiments.

4.2.7 *In vitro* time-lapse imaging of myelin-like sheath formation using fGFP-labelled cells

The next aim using time-lapse was to examine myelin formation in *shiverer* myelinating cultures. From the immunostaining data of myelination in the cultures, axonal ensheathment and myelination peaks between 20-28 DIV.

From time-lapse imaging, fGFP membrane cuffs were observed (arrowheads, Fig. 4.8A), over a presumptive axon. The axon was approximately 70 μm in length. Over the course of the time-lapse acquisition these cuffs appeared to extend and coalesce after approximately 2 hours (Fig. 4.8B and C). At around 13 hours the fGFP-labelled membrane thickened to form a more continuous sheath (Fig. 4.8D). Time-lapse imaging also showed dynamic activity of numerous membranous vesicles merging together leading to the extension of the initial individual membranous fragments. Manual tracking of the pathway of a weakly labelled GFP-positive cell which was possibly associated with the membranous cuffs is illustrated in Fig. 4.8E, suggesting that the oligodendrocyte-like cell was highly motile during this process. The cells appeared to migrate up and down the neurite as the membrane changes occurred.

Time-lapse imaging of *shiverer* cultures 26 DIV, at a time when the exogenous cells have formed many myelinated fibres, illustrated a fGFP-labelled myelin-like sheath extending longitudinally (Fig.4.9Ai-iii). The distance between the point at which the oligodendrocyte process merges with the sheath (white arrow) and the lateral edge of the sheath, increased by approximately 10 μm, i.e. ~1/3 of its initial length, over a period of 128 minutes (see yellow and blue lines). Cultures immunolabelled after time-lapse imaging for MBP, GFP

and SMI-31 provided evidence that these fGFP sheath-like structures are likely to represent myelin or myelin-like sheaths around *shiverer* axons (Fig. 4.9B).

Time-lapse of another position in the same *shiverer* culture showed active interactions between the differentiated oligodendrocyte-like cells with *shiverer* axons. Relatively rapid formation of a membranous sheath was observed that appeared to initiate from two different areas) on the same axonal region (arrows, Fig. 4.10A). Within minutes, a growing sheath was imaged and in less than 60 min increased its size by 10 μm (arrows, Fig. 4.10B-D). fGFP-positive processes appeared to make contacts with the growing sheath suggesting that they might deposit new membrane on top of the axonal surface (arrowheads, Fig. 4.10 C). During the image acquisition, a cell body was imaged close to the membranous sheath, but there was no clear evidence that the sheath was generated from the processes extending from that cell.

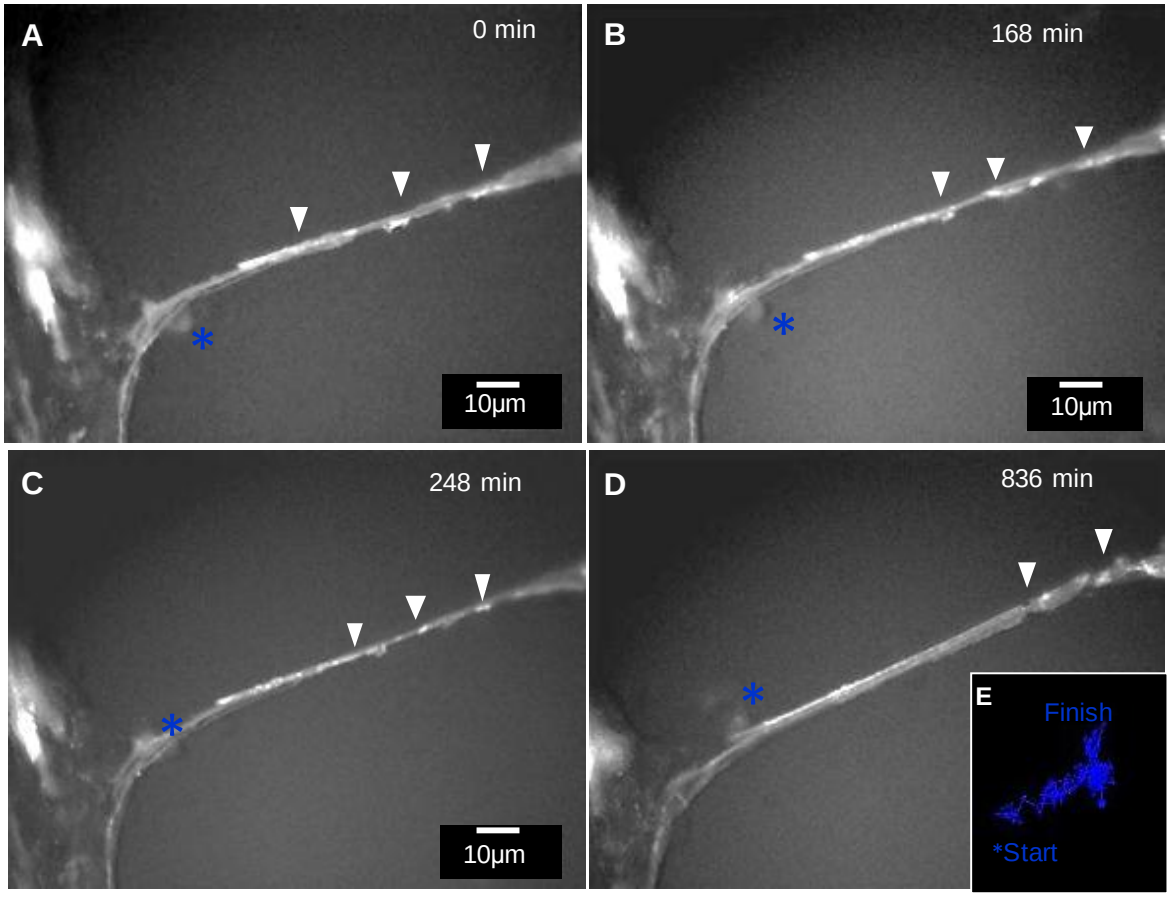

Figure 4.8 Time-lapse imaging of myelin-like sheath formation from exogenous fGFP-positive neurospheres

A-D) Time-lapse sequence of a *shiverer* culture for a period of 30 hours, with 3 min time interval on 24 DIV revealed membrane cuffs (arrowheads) extending and joining up over

an axon (approximately 70 µm in length). After about 13 hours, the fGFP-positive cuffs were observed to form a single, united thick membrane sheath over an axon. E) Manual tracking of the pathway of a weakly GFP-positive cell which was possibly associated with the membranous cuffs illustrates that the cell was very motile. See supplementary video 4.5. Representative video from 5 separate experiments.

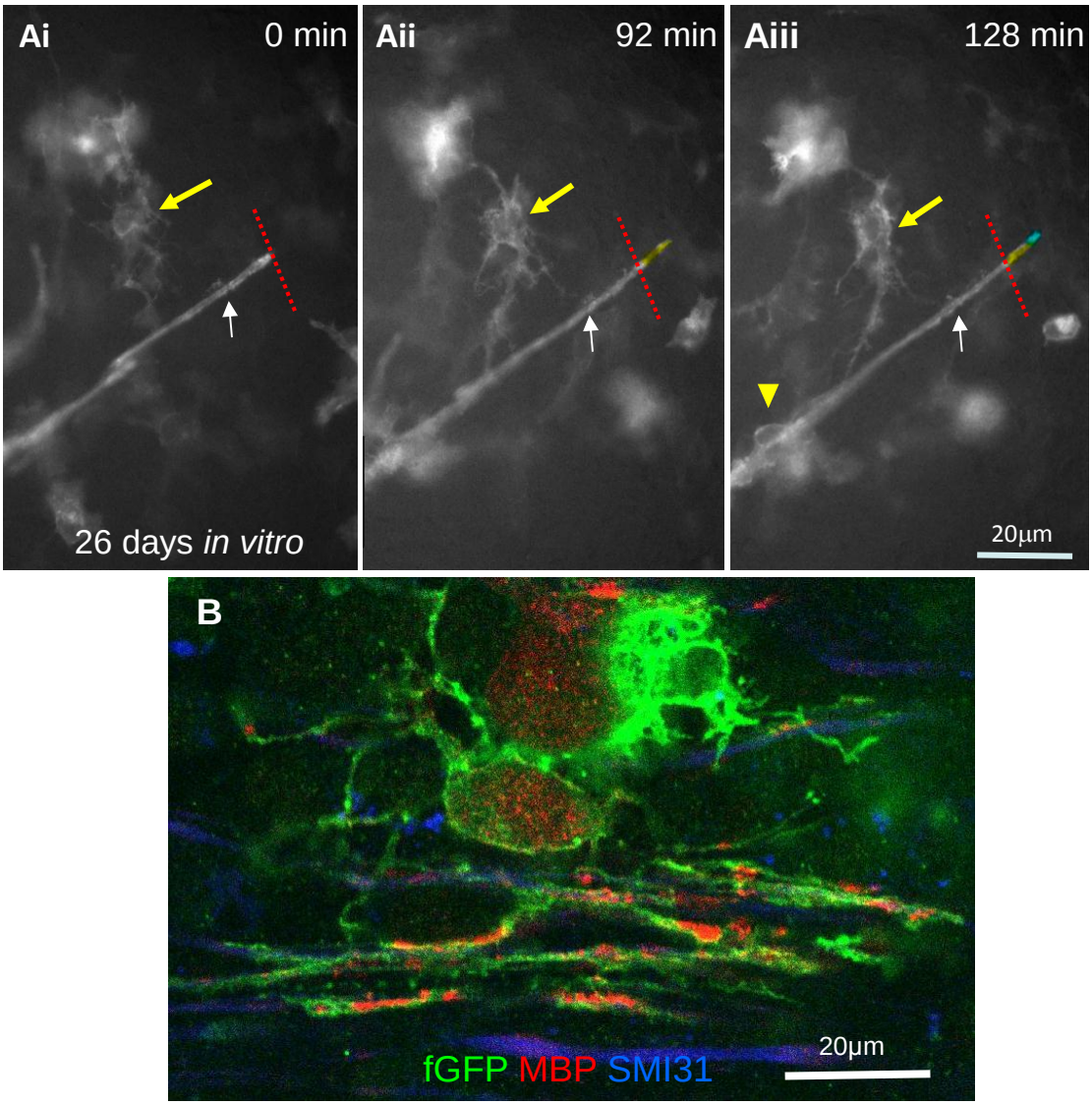

Figure 4.9 Time-lapse imaging of the elongation of a putative fGFP labelled myelin-like sheath

Time-lapse imaging (Nikon TE2000) of fGFP-expressing neurospheres added to *shiverer*, was performed on 26 DIV, for a period of 14 hours with 4 min time interval. **Ai-iii)** A fGFP process increased in length by 10 µm, over the time course. Membranous protrusions were seen (yellow arrowhead) in addition to the cell body of the fGFP labelled oligodendrocyte-like cell (yellow arrow). **B)** MBP staining of cells in the Petri dish using a

Zeiss 710 (x63, 1.4NA) after imaging, confirms that fGFP-expressing cells belong to the oligodendroglial lineage. See supplementary video 4.6. Representative video from 5 separate experiments.

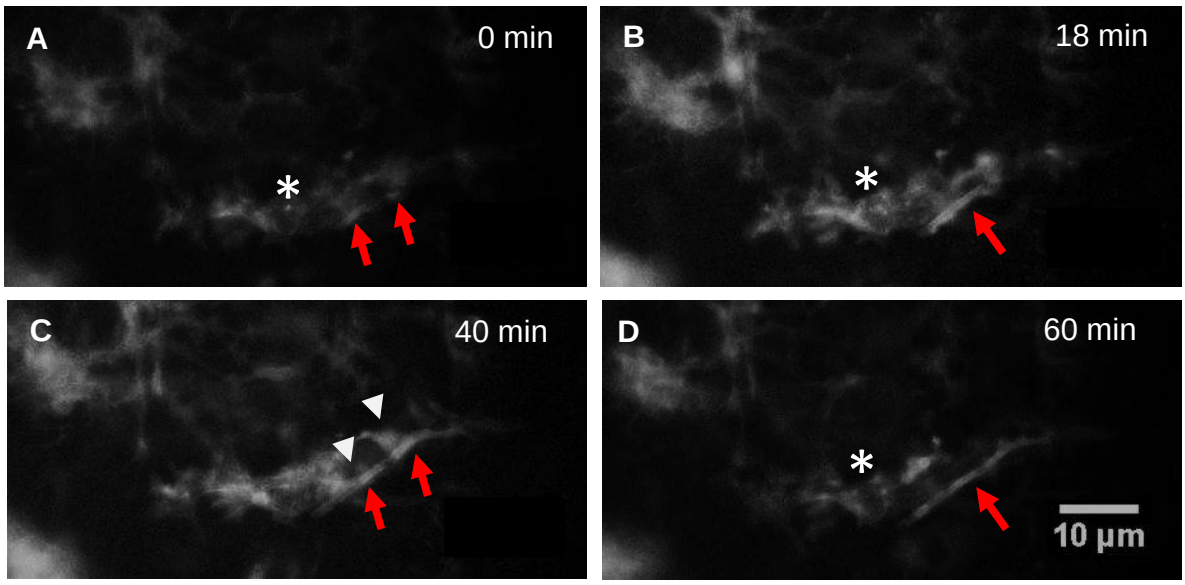

Figure 4.10 Time-lapse imaging of myelin-like sheath extension.
A-D) Time-lapse sequence over 20 hours demonstrated relatively rapid formation of a membranous sheath that appeared to initiate from two different areas (arrows) on the same axonal region. A cell body (asterisk) and fGFP-positive processes appeared to make contacts with the growing sheath suggesting that they might deposit new membrane on top of the axonal surface (arrowheads). See supplementary video 4.7. Representative video from 5 separate experiments.

4.2.8 *In vitro* time-lapse imaging of the membrane changes of fGFP-positive cells

During the active phase of myelination, each oligodendrocyte must produce as much as approximately 5-50x10^3 µm^2 of myelin membrane surface area per day (Pfeiffer et al 1993). fGFP-positive neurospheres were added to s*hiverer* myelinating cultures as described previously and imaged using time-lapse microscopy on 22 DIV. The fGFP-positive neurospheres differentiated into cells which appeared to have huge membranes with a length exceeding 20 µm in perimeter.

Time-lapse recording showed two fGFP-positive cells extending massive membranes which at the periphery were contacting presumptive axons of the culture (Fig. 4.11A and bright field B). Occasionally, intracellular membrane-bound compartments or vesicles that resembled endosomes (arrows and dotted box, Fig. 4.11C and 4.11 Ei-iii) were generated moving towards the leading edges of the cell boundaries producing or fusing new membrane (arrowheads, Fig. 4.11Ci-Civ and D) and (arrow in the first cell *and dotted line in the second cell #, Fig. 4.11E). At the edges of the fGFP-positive cells, membranous protrusions seemed to be constantly generated connecting or joining together at the cell borders. These protrusions resembled membrane flaps or bubbles seen in previous time-lapse recordings (Fig. 4.7).

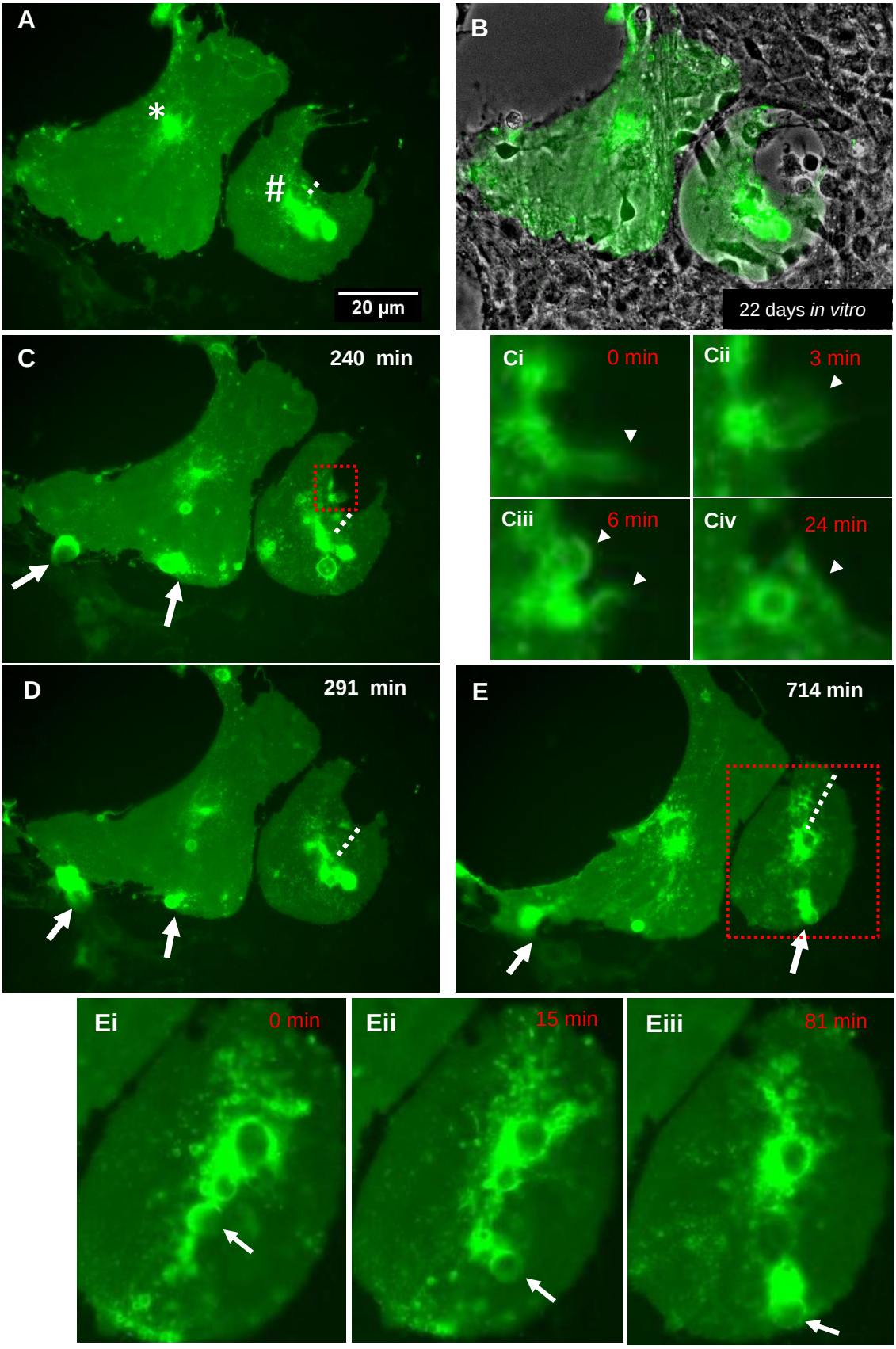

Figure 4.11 Time-lapse imaging of membrane extension of fGFP-positive cells

Two fGFP-positive cells were imaged with extensive membranes which at the periphery were contacting presumptive axons in the culture (Bright field, B). A, C, D and E) Time-lapse sequence of a *shiverer* culture for a period of 21 hours, with 3 min time interval, on 22 DIV, revealed intracellular membrane-bound vesicles that resembled endosomes (arrows and dotted box), generated de novo, moving towards the edges of the cell boundaries producing or fusing new membrane. Ei-iii) Membranous protrusions (arrows) were constantly depositing new membrane. Representative images from 2 separate experiments.

4.2.9 *In vitro* time-lapse imaging of membrane extension over *shiverer* axons

Time sequence over 21 hours revealed axons that had both thick and thin fGFP-positive layers (broken and white arrows, Fig. 4.12A and B). These axons where surrounded by fGFP-positive cells with extensive membranes. At the beginning of the time-lapse sequence within the magnified area (dotted box, Fig. 4.12A) at least two contact points could be seen between the cells and the axons. Over time, the central part of the membrane was seen to move dynamically like a wave towards the axon that eventually reached the axonal surface at several points (red arrows, Fig. 4.12Ci-ii). At later stage of the time-lapse sequence the membrane seemed to contact the axon (Fig. 4.12Cii). Around the same time, a vesicle of about 10 μm was generated from the main membrane which crossed over and started to produce membrane material towards the same axon (Fig. 4.12Civ-v). At the end of the time course, the imaged axon appeared to have a thicker GFP-positive layer than its lower part (Fig. 4.12Cvi), where no visible interactions between membranes of GFP-positive cells with axons were observed.

Moreover, during the time-lapse imaging, numerous round protrusions were imaged to move intracellularly displaying a dynamic activity of the membrane of the fGFP-positive cells, as they seemed to generate more membrane pushing it to the periphery (green arrows, Fig. 4.12Civ-vi).

It is remarkable that no changes on top of the fGFP-positive ensheathed axon (broken arrow, Fig. 4.12A and B) were observed in association with the membrane of the exogenous cells, during the time-lapse recordings (data not shown).

4.2.10 *In vitro* time-lapse imaging of fGFP-positive oligodendrocyte-like cells and its membrane protrusions

Time-lapse microscopy of fGFP-labelled oligodendrocyte-like cells (arrow, Fig. 4.13A and B, bright field) were imaged in close contact with axons of the *shiverer* myelinating cultures. The fGFP-positive processes extend in parallel (broken arrows, Fig. 4.13A) over the axons suggesting some kind of interaction. Membrane changes over the time sequence included spherical protrusions that moved along the axonal surface, changing morphology and size (arrows, Fig. 4.13Ai-vi), which then smoothly receded underneath the axon. Immunostaining of sister cultures 28 DIV confirmed myelin-positive sheaths around *shiverer* axons.

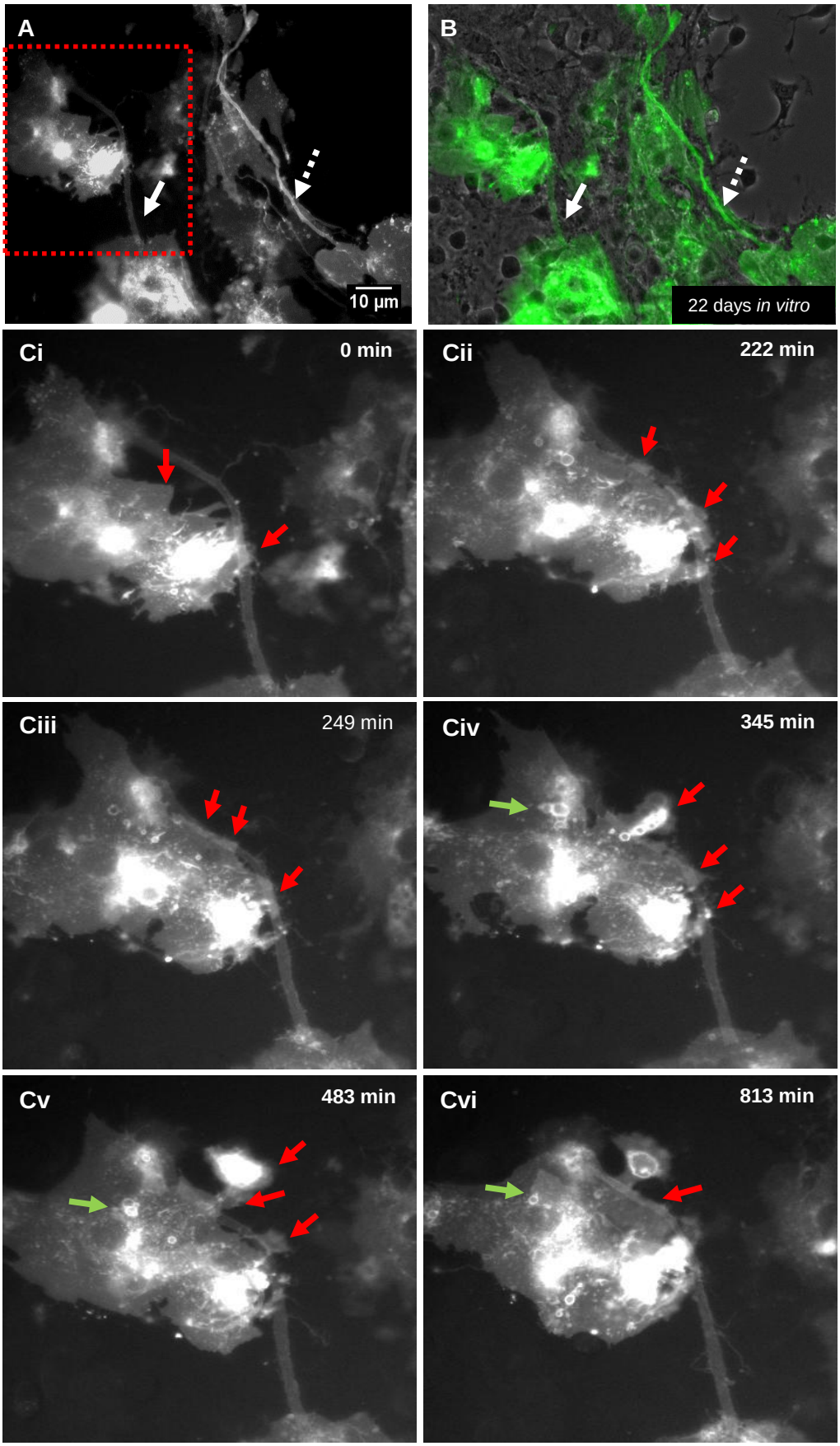

Figure 4.12 Time-lapse imaging of membrane extension

fGFP neurospheres were added in *shiverer* cultures and time-lapse imaging was performed on 22 DIV for 21 hours with 3 min time interval. A and B bright field view) Both thick (broken arrow) and thin (white arrow) fGFP-positive ensheathed axons were detected surrounded by fGFP-positive cells with extensive membranes. Ci-vi) Time sequence of a magnified area showed the membrane of a fGFP-positive cell moving dynamically like a wave towards a thin fGFP-positive *shivere* axon (red arrows). During the recordings, numerous intracellular, round structures (green arrows) were imaged displaying a dynamic activity of the membrane of the fGFP-positive cells. See supplementary video 4.8. Representative video from 2 separate experiments.

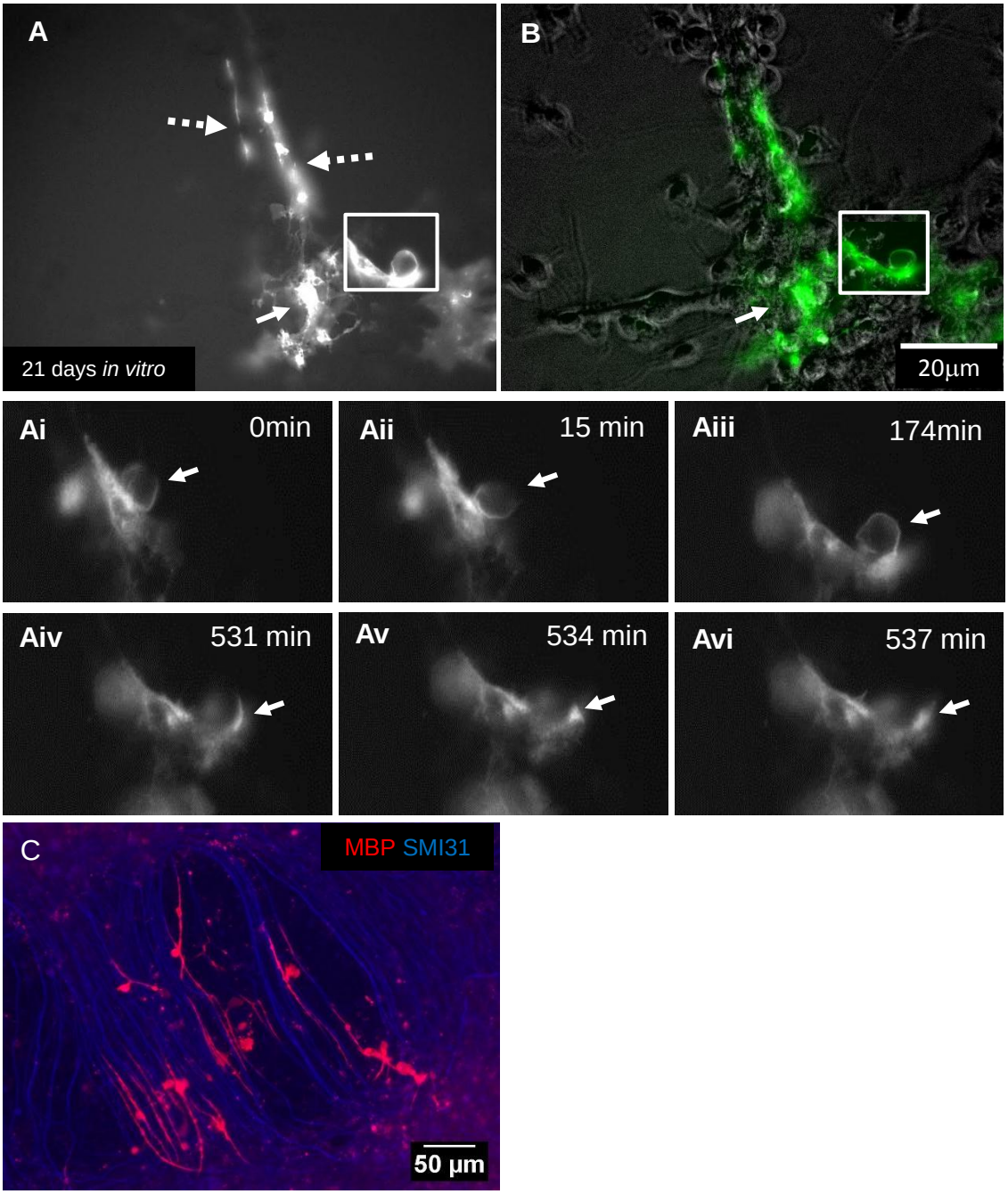

Figure 4.13 Time-lapse imaging of membrane protrusions of fGFP-positive cells in *shiverer* cultures

Time-lapse imaging was performed on 21 DIV for a period of 24 hours with 3 min time-interval. A and B) fGFP-labelled neurospheres appeared to have been differentiated into oligodendrocyte-like cells (arrow) with prosesses aligned with the *shiverer* axons (broken arrows). Ai-vi) Time-lapse sequence of the magnified area (box) revealed the generation of membrane protrusions (arrows) which changed shape and appeared to be eventually deposited on the axonal surface. C) Immunolabeling for myelin (MBP, red) and neurites (SMI-31, blue) of a sister culture on 28 DIV, confirmed that the added fGFPcells gave rise

to oligodendrocytes capable of myelination. See supplementary video 4.9. Representative video from 10 separate experiments.

4.2.11 *In vitro* time-lapse imaging of fGFP and cGFP-dsRed-positive oligodendroglial-like cells

To examine both cytoplasmic and membrane-bound processes, wild type neurospheres were transduced with lentiviral constructs expressing both fGFP and cGFP-dsRed.

The cultures generally survived well, as the double-labelled neurospheres infected with the two separate lentiviruses did not appear toxic. The double-labelled neurospheres differentiated into cells that resembled oligodendrocytes, with many fine membrane processes emanating from the cell body. Time-lapse sequence showed that the exogenous labelled cells made contacts with the axons that persisted for more than 20 hours (Fig. 4.14A-E). During the time-lapse sequence, the added cells extended processes that in some cases formed membranous protrusions (broken arrow, Fig. 4.14D). The processes also appeared to either embrace the axons (arrows, Fig. 4.14A-D) or align with them (arrow, Fig. 4.14E). However, it was not possible to clearly distinguish the cGFP-dsRed (mcherry channel) from the fGFP (GFP channel) processes of the double labelled cells.

Immunostaining studies of sister cultures at a late time point illustrated the presence of MBP with a sheath-like morphology suggesting that the double labelled cells had successfully formed myelin (Fig. 4.14F). The axonal density appeared sufficient with many axons covering 50% of the field of view. More importantly, the myelin appeared to have formed correctly, as nodes of Ranvier were visible on either side of the myelin internodes suggesting that the neurospheres infected with the lentiviruses were able to efficiently myelinate the host axons (arrowheads, Fig. 4.14F).

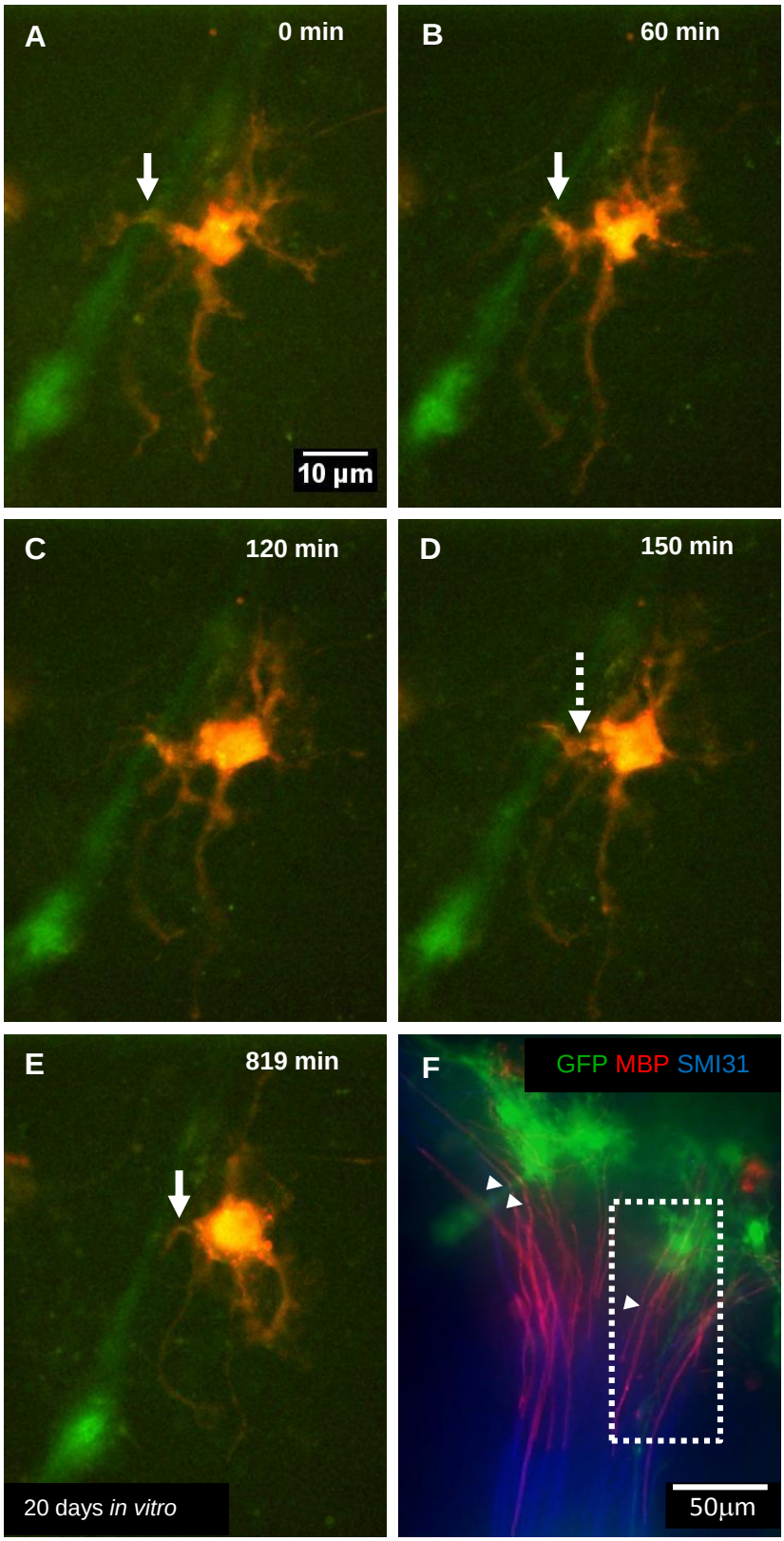

Figure 4.14 Time-lapse imaging of fGFP and cGFP-dsRed-positive oligodendroglial-like cells

A-E) Time-lapse sequence showed that the exogenous double labelled cells made contacts with the axons that persisted for more than 20 hours. Time-lapse imaging was performed

on 20 DIV for 21 hours with 3 min time interval. During the time-lapse sequence, the added cells extended processes that in some cases formed membranous protrusions (broken arrow, D). The processes also appeared to either embrace the axons (arrows, A-D) or align with them (arrow, E). F) Immunostaining of a sister culture on 28 DIV with anti-GFP and anti-MBP confirmed co-expression of MBP and GFP suggesting that MBP is ascribed to the exogenous neurospheres.

4.3 Discussion

Fundamental biological studies on glial-axonal interactions that culminate in myelin biosynthesis require appropriate *in vitro* models and advanced imaging techniques with the use of fluorescence labelled glial cells or axons. Neonatal and adult myelin-deficient *shiverer* mice have been used extensively as hosts for testing cell engraftment, migration, and myelination due to their lack of myelination in certain areas (Iturria-Medina et al 2011). Electron microscopy studies (Remahl & Hildebrand 1990) and time-lapse imaging GFP-labelled oligodendrocytes *in vivo* (Kirby et al 2006) and *in vitro* (Watkins et al 2008) have helped to elucidate the mechanisms of glial-axonal interaction during the initial stages of myelination. Nonetheless, the processes of axonal ensheathment and myelin compaction are still not fully understood.

The studies presented in this thesis of time-lapse imaging of *shiverer* mixed CNS myelinating cultures, to which exogenous GFP-labelled cells were added, offered the opportunity to follow myelination over time. One of the most prominent features of the exogenous cells was that they differentiated quickly within a few days after their addition to the myelinating cultures. Due to the lack of cell type specific markers, it was not easy to identify them or their processes with certainty, as either belonging to oligodendrocytes or astrocytes during time-lapse imaging. Nevertheless, in some cases the exogenous differentiated cells morphologically resembled cells of the oligodendroglial lineage, bearing multiple fine processes emanating symmetrically from the cell body.

It is demonstrated that oligodendrocyte-axonal interactions are very dynamic events with continuous retraction and extension of oligodendroglial processes. Time-lapse imaging of cGFP in oligodendroglia, to examine the early stages of myelination *in vitro,* provided data showing thin processes emanating from OPC cell bodies that appeared to spiral around neurites. These observations would be supportive of the second model of myelination where a narrow oligodendrocyte cell process spirals around the axon (Bauer et al 2009). Furthermore OPC-like process extension and retraction persisted for several hours suggesting that OPC-like cells possibly adjusted their positions until the cells began to wrap the host axons (Kirby et al 2006). A caveat to cGFP as a marker for myelination is that once myelin has become compacted then the cytoplasm cannot be visualised (Rivers et al 2008).

However, the use of fGFP labelled neurospheres added to the myelinating cultures allowed the visualisation of processes despite the loss of cytoplasm during the formation of compact myelin. Morphological differences in the fGFP-positive cells revealed less sharp imaging of cell processes and appeared rather nebulous compared to the cGFP labelled cells, impeding the selection of the cells that looked like oligodendroglia for imaging. Time-lapse imaging revealed details about the changes in the membrane-tethered fGFP-positive processes. During the time-lapse recordings, membranous waves were occasionally generated that moved along the length of the presumptive *shiverer* neurites. The initial membranous protrusions were progressively twisted and later were smoothly eliminated along the neurites, suggesting a possible mechanism of membrane deposition at later time points of the process of myelination.

Rho GTPases are well known to regulate actin dynamics and cell polarity and motility through their effects on the cytoskeleton, membrane trafficking and cell adhesion (Jaffe & Hall 2005, Pollard & Borisy 2003). Most Rho GTPases act on membranes and affect the movement of these membranes by changing the membrane-associated actin cytoskeleton (Aspenstrom et al 2004). Rac1 and Cdc42 have long been known to induce plasma membrane protrusions known as lamellipodia and filopodia by stimulating actin polymerisation. Lamellipodia are broad sheet-like protrusions containing a network of branching actin filaments, where Cdc42 and Rac are both active at the leading edge of cells and inhibition of each reduces lamellipodium extension (Kurokawa et al 2004). Their target, WAVE proteins are localised at the front of lamellipodia. Several Rho GTPases, including RhoA, RhoB, RhoD and Cdc42 affect specific steps of vesicle trafficking between intracellular compartments, exocytosis or Golgi-to-endoplasmic reticulum transport as with plasma membrane protrusion (Egea et al 2006). Cdc42 may define a distinct phase of actin filament-dependent transport, possibly acting together with myosin motors, whereas N-WASP proteins act indirectly by stimulating delivery of proteins and membrane lipids required for membrane extension to the leading edge [reviewed in (Ridley 2006)]. Myelination is an ideal place for Rho GTPases regulation, as it is the result of fine orchestration of many stimuli from at least two cell types. Recent work has revealed that Rho GTPases are required for Schwann cells to sort, ensheath, and myelinate axons (Feltri et al 2008). Melendez-Vasquez et al. (2004) have also suggested that ‘‘polarised actomyosin-generated forces’’ are involved in inner mesaxon movement around an axon.

Process extension by oligodendrocytes to ensheath axons and the extension and retraction of processes of OPCs for motility, involves continual remodelling of the cytoskeleton. During myelination, there is a reorganisation of the cytoskeleton of oligodendrocytes that possibly interact with the growing myelin membrane. An isoform of neurofascin (FNIII) is specifically expressed by oligodendrocytes at the onset of myelinogenesis and decreases rapidly when the oligodendrocytes have contacted their targeted axons (Collinson et al 1998). This suggests that glial cell adhesion molecules may play a role in axonal recognition and possibly mediate signals influencing the axonal contact through link with the actin cytoskeleton. Kim et al. (2006) have reported that one of these key proteins, WAVE 1, is essential for oligodendrocytes morphogenesis and normal CNS myelination. It has also been shown that N-WASP regulates process extension by OPCs and oligodendrocytes and is essential for axonal ensheathment. In OPCs and oligodendrocytes, F-actin, WAVE 1, contactin, Cdc42 and Rac proteins are present at process tips as well as in cell bodies and in some cases along processes. More specifically, F-actin and N-WASP are also detected at the tips of narrower more filopodia-like processes necessary for actin polymerisation-driven protrusion. In segments of optic nerve, wiskostatin that specifically inhibits N-WASP and therefore dramatically blocks process extension by OPCs, reduced the number of axons in initial contact with an ensheathing oligodendrocyte process, whereas the number of axons that were already myelinated was unchanged. These finding suggest that N-WASP has a role in initial ensheathment of axons by oligodendrocytes (Bacon et al 2007). More importantly, N-WASP, WAVE 1, Cdc42, and Rac proteins are present in myelin sheath preparations, which are free of axonal and oligodendrocyte's cell body contamination (Bacon et al 2007).

The phenomenon of round membrane protrusions, active in the tips, was observed quite frequently in the fGFP-labelled cells to generate more membrane pushing it to the periphery. This is possibly an important mechanism for the cells to sense the local microenvironment and subsequently to respond to signals that implicate a complex of series of recognition, adhesion and cell-cell interaction (Schnadelbach et al 2001). For example, integrins link the extracellular environments of most cells with intracellular signalling molecules and the cytoskeleton and have been shown to regulate the activities of GTPases involved in the control of cell morphology (Hall 1998). More specifically, suggested interactions of oligodendrocyte-derived integrin with axon-derived laminin are likely to contribute to myelination (Piaton et al 2010). Additionally, studies have shown

that β1 integrin may contribute to the glial sensing of axon size that requires myelination, with loss of β1 integrin causing a delay in the myelination of small diameter axons (Camara et al 2009). Furthermore, a correlation between WAVE 1 function in oligodendrocytes and MMP expression might be anticipated, since oligodendrocytes and OPCs have to extend processes over the ECM of the CNS, an event perhaps facilitated by secretion of MMPs at process tips (Suetsugu et al 2003).

From studies it has been suggested, that filopodia as well as lamellipodia are essential for OPC process extension. Indeed, it has been suggested that cells first generate filopodia that push out the membrane in spikes, allowing a lamellipodium to fill in around the filopods and form a thicker protrusion (Machesky 2002). A prerequisite for progression of the inner mesaxon around the axon and the expansion of the whole developing multi-lamellar myelin sheath is that the lipid phase of all membranes is in a fluid, liquid-crystalline state as earlier results have revealed [reviewed by (Crang & Rumsby 1977a, Crang & Rumsby 1977b). A fluid lipid phase will allow for membrane deformability and plasticity and for the necessary slippage and expansion of the myelin membrane as the inner mesaxon moves under accumulating lamellae. A fluid lipid phase will also facilitate delivery of lipid and of intrinsic proteins to the expanding sheath by membrane flow along the oligodendrocyte plasma membrane. From time-lapse recordings, fGFP membrane cuffs were observed over presumptive axons, as well as membranous fragments that during the time-lapse acquisition appeared to extend and join together as they thickened to form a more continuous sheath, data possibly depicting how the membranous myelin sheath might extend and develop from the plasma membrane of the oligodendrocyte.

Both cGFP and fGFP-labelled neurospheres were capable to differentiate into cells of the oligodendroglial lineage as they myelinated the MBP-deficient axons in the *shiverer* myelinating cultures. This was confirmed by classical immunocytochemistry studies which are a useful technique to investigate cells types at the local environment in which the observed interactions took place.

5. Multiphoton imaging of transplanted cGFP neurospheres into the fixed spinal cord of *shiverer* mice

5.1 Introduction

5.1.1 Background

In recent years , the advent of two-photon microscopy (Denk et al 1990) and the generation of transgenic animals, which express fluorescent proteins driven by tissue-specific promoters (Feng et al 2000, Tsien 1998), have allowed the direct observations of cells and their interactions under both physiological and pathological conditions *ex vivo* and *in vivo* (Kerschensteiner et al 2005, Svoboda & Yasuda 2006). Thereby, it became possible to image neuronal and glial subsets in living transgenic mice and/or in *ex vivo* tissue expressing multiple spectral variants of GFP.

In terms of imaging, the evolution in bioluminescence imaging of intact tissues using multiphoton microscopy confers several advantages related to penetration depth, resolution, contrast, speed and tissue damage compared to conventional confocal microscopy. Specimens as diverse as lymphatic organs, kidney, heart, skin and brain can be examined in detail at depths of up to one millimetre, while leaving the tissue intact [Reviewed in (Helmchen & Denk 2005)]. Conversely, limited work has been performed on imaging the living spinal cord. The maximum achievable imaging depth is proportional to the scattering mean-free-path and depends on available laser power, two-photon advantage and collection efficiency (Oheim et al 2001). The achievable imaging depth also strongly depends on other tissue properties such as microvasculature organisation, cell body arrangement, collagen or myelin content, which will more or less degrade the laser focus and limit signal generation deep inside the tissue. These approaches have had a considerable impact on neuroscience and have allowed studies on visualisation of interactions in real time, between labelled axons and glial cells *in vivo* (Nikic et al 2011) or in living spinal tissue. In many areas of biological microscopy, rather than being limited to

analysis of sections only a few microns thick, it is possible to observe tissue features *in situ* throughout a greater volume of the tissue (Centonze & White 1998).

To image glial-axonal interactions *ex vivo* and *in vivo*, it is vital that individual, fluorescently labelled cells can be discerned. Therefore it is desirable to have a system in which only a small portion of cells are labelled. One method that might be expected to produce such a situation is cell transplantation of labelled cells into a non-labelled host.

One such host are mice harbouring myelin mutations. The myelin mutants are a heterogeneous collection of animals, some of whose mutations make them models of human leukodystrophies. However, the most commonly used myelin mutant in transplant experiments is the *shiverer* mouse, but it is not a model of human disease (Duncan et al 2011). The first transplants in the *shiverer* mice or myelin deficient (md) rats (a rat myelin mutant where areas of demyelination occur) (Duncan et al 2011) were performed to test whether cells could myelinate host axons on transplantation. These experiments showed that the transplanted cells produced focal areas of myelination in the brain of *shiverer* mouse with some migration of cells from the site of implantation (Gumpel et al 1989). From these early reports, numerous other studies have confirmed the ability of CNS grafts to generate large, yet predominately focal areas of myelin in *shiverer* mice (MBP-positive) and a similar phenotype has been shown after transplantation in the the md rat (PLP-positive).

Edgar et al (2004) previously showed that neurospheres transplanted into *shiverer* mice, differentiated into oligodendrocytes and formed compact myelin around *shiverer* axons. This method allows transplanted cells to divide and migrate, integrate and myelinate the host axons before the demise of the mouse. The generalised absence of myelin in the *shiverer* mouse makes the analysis of transplant-induced myelination straightforward. First, there is significantly more myelin than in controls and the myelin is MBP-positive (Lachapelle et al 1983, Windrem et al 2008). Further confirmation that this myelin is not endogenous can be seen on electron microscope, in which the myelin has a major dense line and a thicker sheath when compared to the thin myelin sheaths of the host (Windrem et al 2008). Once cells of interest are labelled, various preparations and procedures can be used to study structural and functional dynamics. The question of stability of myelin, made by transplanted cells, is important but from studies, grafts and the myelinated tracts have

been noted to survive for as long as 120 days, limited by the shortened lifespan of the mouse.

The processes of OPC genesis and differentiation from multipotent neural precursors are relatively well characterised (Rowitch 2004). However, molecular mechanisms governing oligodendrocyte myelinogenesis are poorly understood. This presents a particular challenge for myelin repair in demyelinating diseases, in which OPCs are present in a quiescent state within lesions but are not recruited sufficiently to the regenerative process and fail to form myelinating oligodendrocytes (Chang et al 2002).

5.1.2 Aims of the chapter

The ultimate aim of this thesis was to visualise by time-lapse imaging the process of myelination. Before this could be achieved, a number of steps were taken in the development of the protocol. In this Chapter, excised, fixed mouse spinal cord, transplanted with cGFP expressing cells, was used to establish the basic methods.

Specifically the aims of this Chapter were to:

1. Establish the protocol for injecting GFP expressing neurospheres into *shiverer* mouse, and determine the optimal time points for imaging after cell transplantation.

2. Establish a protocol for imaging the spinal cord using multiphoton microscopy, in excised spinal cord in the first instance.

3. Confirm by immunohistochemical methods, the identity of the transplanted cells.

5.1.3 Materials and Methods

5.1.3.1 Transplantation of neurospheres into *shiverer* mice

Neurospheres from new-born (P1) *β-actin* GFP mice were dissociated into a single suspension and resuspended at a concentration of 50.000 cells/μl in L-15 solution. Neonatal *shiverer* mice 19-21 days of age were recipients of neurosphere transplantation, as described in detail, in Chapter 2.

At various time points 3, 7, 8, 12, 14, 15 days and 4 weeks post-transplantation, animals were euthanised with CO_2 and perfused transcardially with saline followed by 4% paraformaldehyde. The spinal cords were dissected out and placed in 0.1 M glycine in PBS to reduce auto fluorescence.

5.1.3.2 Multiphoton microscopy of the spinal excised spinal cord

All imaging was performed on a Nikon Eclipse TE2000-U inverted microscope with an Olympus long working distance 20x 0.95 NA water immersion lens. The excitation source used for image acquisition was a Ti:Sapphire femto-second pulsed laser (Cameleon, Coherent UK), lasing at 80 MHz and tuned to a wavelength of 830 nm. A dichroic filter (Chroma 475 DCXR) was used to separate spectrally the second harmonic signal, when present, from the GFP emission of the transplanted cells. Band pass filters (Semrock 435/40 and Chroma 525/50) were used to further filter the emission for the SHG and GFP channels respectively.

5.1.3.3 Tissue processing and immunohistochemistry

After multiphoton imaging, the fixed spinal cords were cryo-protected and frozen, then serial cryostat sections (10 μm) were cut and mounted onto APES-coated slides. To verify the identity of the transplanted cell type and to study cell morphology and differentiation,

immunohistochemistry was performed, as described in Chapter 2. Sections were stained with antibodies to GFP for cGFP-positive transplanted cells, MBP for mature oligodendrocytes, GFAP for astrocytes, PDGF-αR for immature oligodendrocytes, Olig 2 and O4 for cells of the oligodendroglial lineage.

5.2 Results

5.2.1 Multipotential ability of striatum-derived neurospheres to generate glial cells

While optimising the *in vivo* imaging techniques, the multipotentiality of striatum-derived neurospheres was confirmed, by determining their capacity to express oligodendroglial and astroglial markers *in vitro*. Striatum-derived neurospheres were shown as free-floating aggregates consisting of spheres of various sizes (Fig. 5.1A).

To confirm the differentiation potential and viability of cGFP-positive neurospheres, neurospheres were harvested from the same flask used for an *in vivo* transplantation and cultured on PLL-coated coverslips in differentiation medium, used to prepare the myelinating cultures, as described in Chapter 2, for 3 days. Immunocytochemistry using an antibody to GFAP showed that the majority of these cells acquired morphological and antigenic properties of astrocytes (Fig. 5.1B). However, a proportion of the cultured neurospheres showed a propensity for oligodendrocytic differentiation as they were immunoreactive for the oligodendrocyte marker O4 (Fig. 5.1C).

These results confirmed that neurospheres generated in the lab are multipotent and had the ability to differentiate into both oligodendrocytes and astrocytes. Overall, the results highlighted the flexibility of the cGFP-expressing neurospheres and their capacity to generate glial cells if provided with the appropriate environment. As a consequence, striatum-derived neurospheres were considered to be good candidates for cell transplantation into *shiverer*.

Chapter 5 - Multiphoton imaging of transplanted cGFP neurospheres into the fixed spinal cord of *shiverer* mice

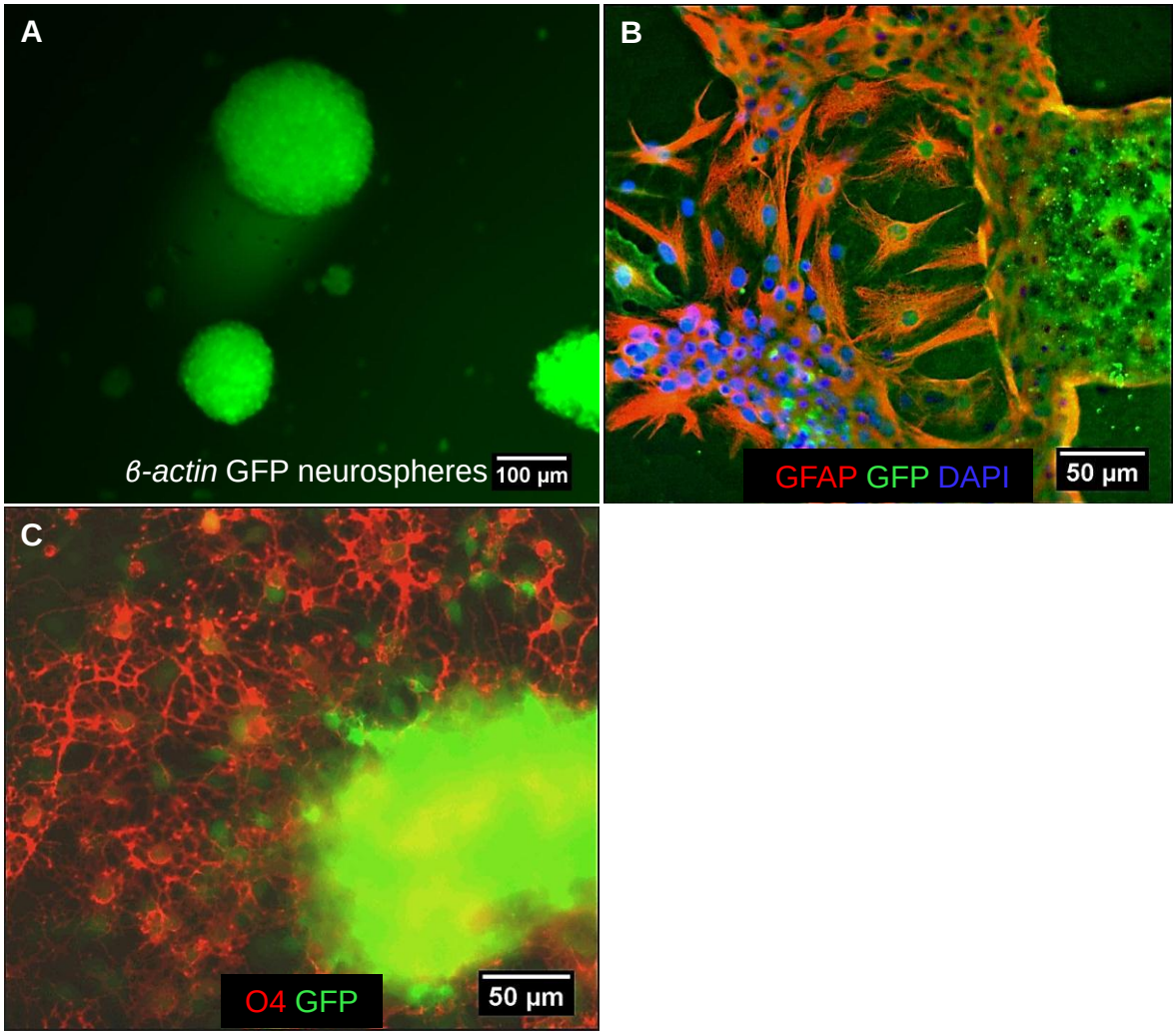

Figure 5.1 Neurospheres differentiated into glial cells when cultured in differentiation medium *in vitro*

A) cGFP-positive neurospheres, maintained 12 days in neurosphere medium *in vitro,* were observed as free-floating aggregates consisting of either large or smaller spheres. It appeared that every cell within the sphere was GFP-positive. Upon withdrawal of growth factors and culture in differentiation medium, on PLL-coated coverslips for 3 days, the majority of neurospheres acquired antigenic properties of astrocytes, as shown with antibody to GFAP (red) (B) or oligodendrocytes as illustrated with the oligodendroglial marker O4 (red) (C). In B and C, the endogenous GFP signal is enhanced with an antibody to GFP. Representative images from at least 2 separate experiments.

5.2.2 Transplantation of cGFP neurospheres into the non-labelled hypomyelinated tracks of *shiverer* mouse

The technical challenges of cell transplantation into neonatal mice had to be overcome. One of the crucial steps in the process of transplantation was to perform laminectomy without causing damage to nearby blood vessels or bruising on the surface of the spinal cord that could lead to ischemia and tissue injury. It was important to use a sharp glass electrode precisely placed into the dorsal columns, immediately adjacent to the midline vein, and to avoid causing injury to axons of motor neurons in the ventral columns (Fig. 5.2A-C). During surgery, normal body temperature and respiration rate had to be maintained and the duration of the surgery had to be kept to a minimum, in order to minimise the risk of death.

To investigate engraftment and differentiation of the cGFP-labelled neurospheres in the mouse spinal cord following transplantation, animals were sacrificed and perfused at various time points; 3 days, 7-8 days, 12-15 days and 4 weeks after the transplantation. After perfusion fixation, spinal cords were dissected out and examined using the epifluorescence microscope and low magnification lens, 4x. Over 80% of all spinal cord transplantations were successful. Green cells were observed in the dorsal columns at all-time points post-transplantation (Fig. 5.3). They were often found in long narrow strips, particularly at longer time points, suggesting that the transplanted cells had migrated for a short distance along the dorsal columns. At early time points, even with low power magnification, multi-process bearing cells could be distinguished.

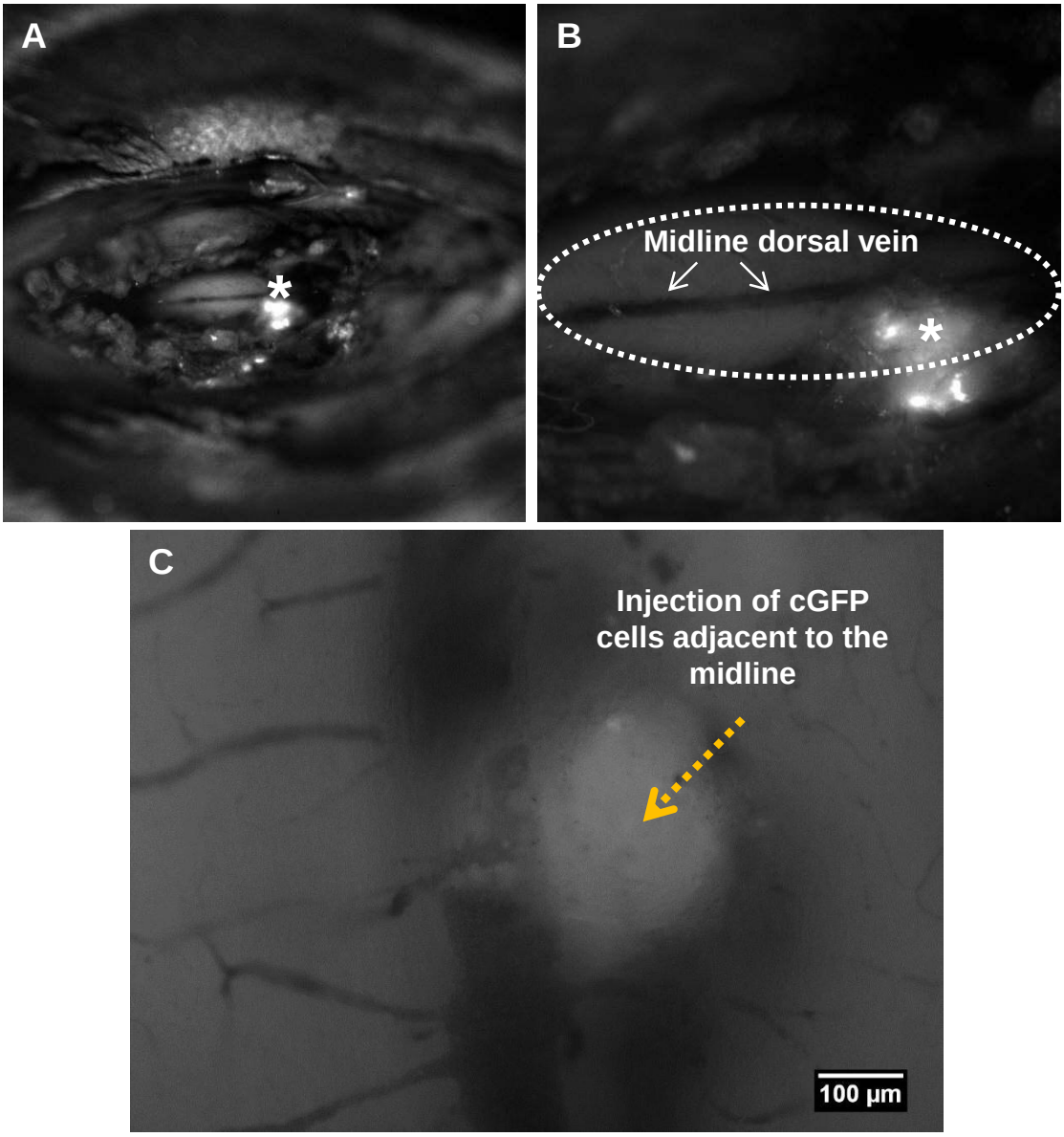

Figure 5.2 Detection of cGFP-expressing cells at the point of transplantation using the OV100 microscope

A) Low power image of cGFP-labelled neurospheres transplanted into the spinal cord of a *shiverer* mouse and visualised using the OV100 to detect the point of transplantation (asterisk). B) Dotted lines outline the spinal cord. The injection was made into the dorsal columns, immediately adjacent to the midline to avoid the midline dorsal vein (white arrows). C) Low power 10x image illustrates the transplantation point (orange, broken arrow). Vessels appear black.

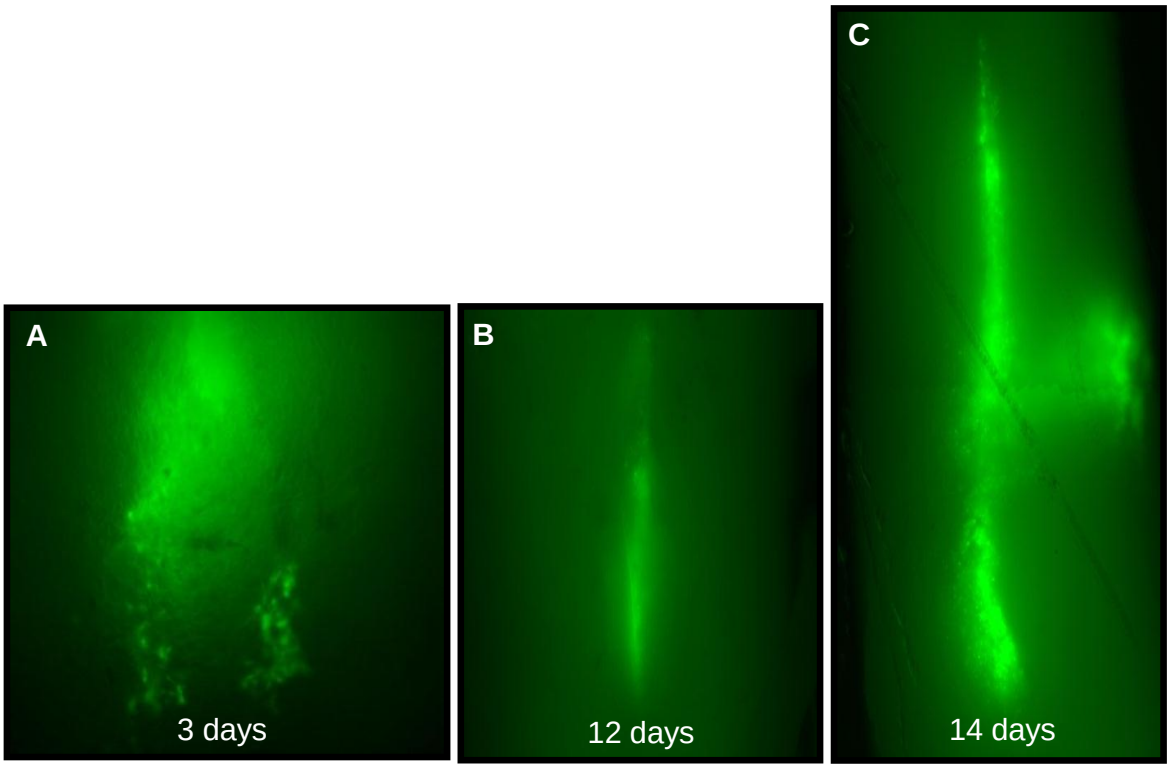

Figure 5.3 Transplanted cGFP-positive cells populated the spinal cord dorsal columns Micrographs of spinal cords of *shiverer* mice transplanted with cGFP-positive neurospheres 3 days (A), 12 days (B), or 14 days (C) previously. Images were obtained with a conventional, wide field epifluorescence microscope. Cells were often found in long narrow strips, particularly at later time points demonstrating their propensity to populate the dorsal columns. Low power images obtained using 4x magnification objective. Representative images from at least 30 separate experiments.

5.2.3 Imaging of a fixed spinal cord 3, 7 and 14 days post-transplantation of cGFP neurospheres using multiphoton microscopy

To gain familiarity with multiphoton microscopy and begin to develop a protocol for imaging mouse spinal cord, while minimising the use of live experimental animals, fixed spinal cord was used that could be imaged on multiple occasions.

After confirming that transplant cells were present using a standard wide-filed epifluorescence microscope, the spinal cords were placed in a glass-bottom–micro well Petri dish. During the initial experiments, agar was used to stabilise the cord in the Petri dish. Subsequently, stable images were achieved without stabilisation.

Z-stacks were obtained through a maximum depth of 130 μm. Multiphoton microscopy of spinal cord, dissected 3 days post-transplantation demonstrated that cGFP-expressing cells formed a single aggregate, in which cell density decreased towards the periphery. A single z-step from an image stack is shown in (Fig. 5.4A). In the centre of the aggregate, individual cells were difficult to discern, but both thick (thick arrow) and thin cell processes (thin arrow) were visible. Towards the periphery of the aggregate, where cell density was lower, individual cells with multiple cell processes could be discerned (broken arrow). Collagen and intermediate filaments generated the second harmonic signal (blue).

With increasing time post-transplantation, cGFP-expressing cells appeared to form a dense network of morphologically differentiated cells (Fig. 5.4 B) with multiple processes (white arrow). The glycine treatment was considered to have been effective in reducing auto-fluorescence because the background fluorescence was low (Fig. 5.4 A and B).

Chapter 5 - Multiphoton imaging of transplanted cGFP neurospheres into the fixed spinal cord of *shiverer* mice

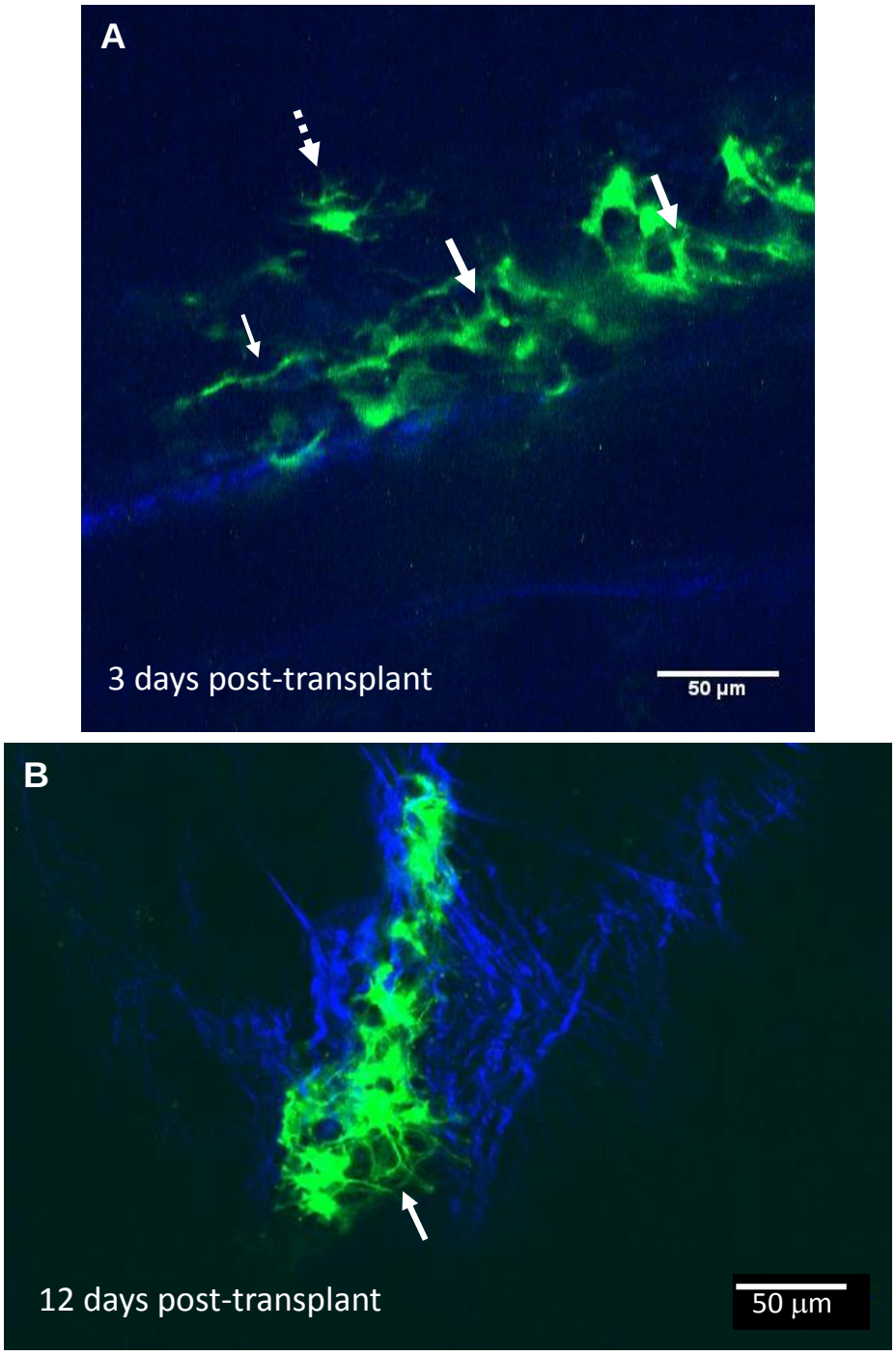

Figure 5.4 Transplanted cGFP-positive neurospheres survived and acquired a differentiated morphology

A) A single z-step from an image stack, illustrating the complex morphology of the cGFP-transplanted cells in the *shiverer* spinal cord parenchyma, 3 days post-transplantation. cGFP cells were usually found as aggregates, with cell density decreasing towards the periphery. In the centre of the aggregate, the morphology of individual cells could not be

discerned, but both thick (thick arrow) and thin cell processes (thin arrow) were present. Towards the periphery of the aggregate, individual cells with multiple fine processes could be discerned (broken arrow). B) A single z-step of 0.5 μm through a Z- stack of 60.5 μm in depth, from a spinal cord 12 days post-transplantation. cGFP-expressing cells were present as a dense network of cells. Cells appeared to have acquired a more advanced differentiation, having a more complex morphology than at 3 days post-transplantation (white arrow). It is assumed that collagen and intermediate filaments generated the second harmonic signal (blue). See supplementary videos 5.1 and 5.2. Representative videos from at least 10 separate experiments.

5.2.4 The complex morphology of cGFP-positive cells can be discerned using multiphoton microscopy of fixed spinal cord

Next, multiphoton imaging of littermates, transplanted with the same population of neurospheres, was undertaken at 3, 7, 14 and 15 days post-transplantation, in order to provide comparable descriptions of cell morphology post-transplantation.

Three days post-transplantation, the transplant-derived cells were no longer simple, spherical structures (as observed *in vitro*, pre-transplantation). The transplanted cells had extended processes but still retained a relatively simple morphology, characterised by few processes emanating from a central cell body (Fig. 5.5A). Seven days post-transplantation, cells or cell processes appeared more complex in morphology than at 3 days. Some had multiple long, narrow processes emanating in all directions from a central cell body (white arrow, Fig. 5.5B). Other appeared to have a simpler morphology, with fewer but thicker processes (broken arrow, Fig. 5.5B). Fourteen and fifteen days post-transplantation, cGFP-expressing transplanted cells appeared similar to cells visualised at 7 days post-transplantation. The marked morphological complexity of the transplanted cells supported the hypothesis that the neurospheres were capable of surviving and differentiating *in vivo* (Fig. 5.5C and D).

In conclusion, using multiphoton microscopy of fixed spinal cord it was possible to visualise transplanted cells up to 500-800 μm from the surface of the excised spinal cord,

and extract visual information about their morphology. Fine processes could also be discerned. These processes were most likely narrower than the resolution limit of the microscope, but appeared approximately 1 μm thick when imaged. That suggested that the technique would be useful for visualising glial-axonal interactions during myelination.

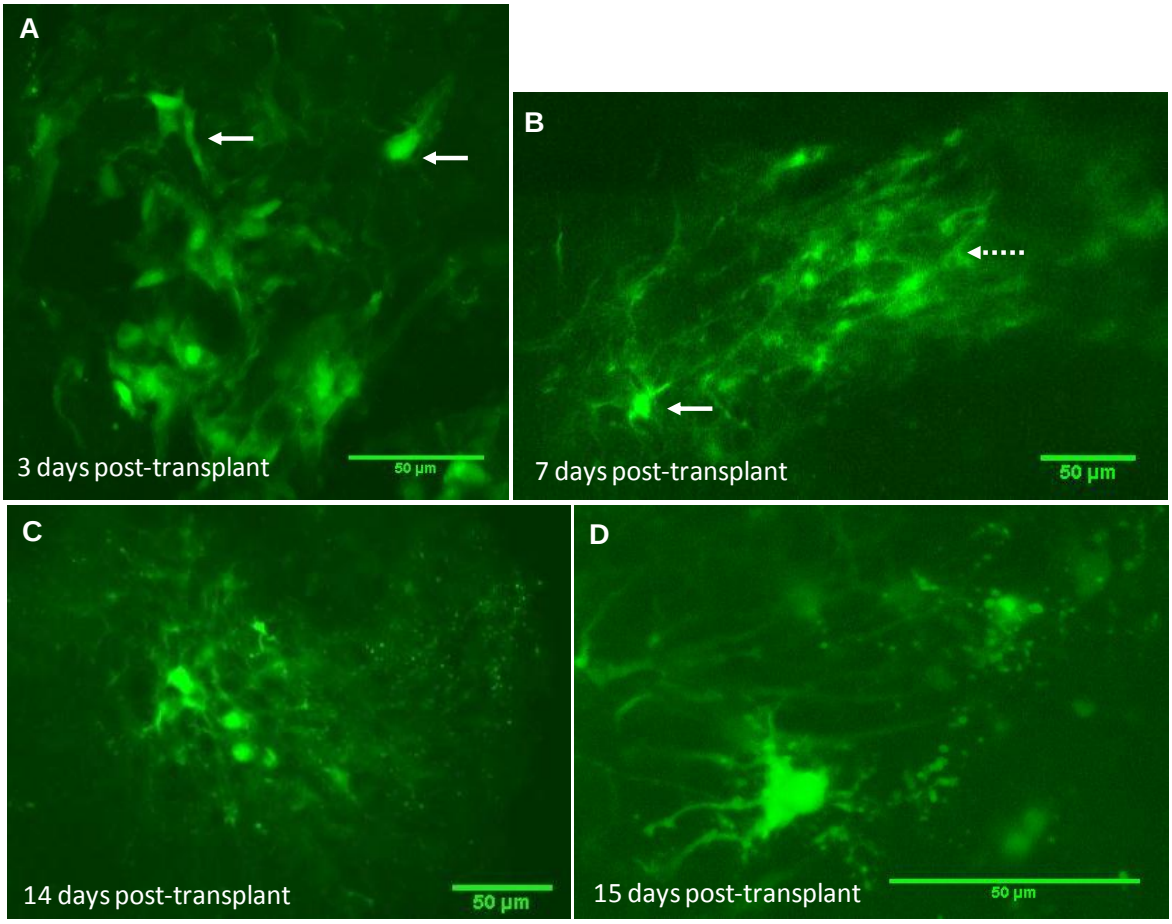

Figure 5.5 Morphological comparison of the differentiation of cGFP transplanted cells at increasing times post-transplantation

A) Average Z-projection over 20 µm, with 0.5 µm step-size, of a *shiverer* spinal cord 3 days post-transplantation. Most of the transplanted cells had acquired a relatively simple morphology (white arrows) characterised by only a few processes emanating from a central cell body. B) Average Z-projection over 10 µm, with 2 µm step-size from a spinal cord 7 days post-transplantation showing cells that appeared more complex than at 3 days. Some had multiple long, narrow processes emanating in all directions from a central cell body (white arrow). Other appeared to have a simpler morphology, with fewer but thicker processes (broken arrow). C-D) Fourteen and fifteen days post-transplantation, cGFP-expressing transplanted cells appeared similar to the cells visualised at 7 days post-transplantation from average Z-projection over 35 µm, with 0.5 µm step-size. Representative images from at least 30 separate experiments.

5.2.5 cGFP neurospheres survived, integrated and differentiated into glial cells in the white matter of the *shiverer* mouse spinal cord

To confirm the identity of cells in the imaged cords and to correlate cell morphology with cell type, imaged cords were frozen and serial, longitudinal sections were cut on a cryostat at 10 μm thickness and collected on APES-coated slides, then immunostained with cell type specific markers.

Confocal microscopy of tissue sections immunostained with a panel of markers was used to identify the transplanted cells at 3 days, 7 days and 14 days post-transplantation. At 7 days post-transplantation a proportion of cGFP-positive cells were positive for PDGF-αR, a marker for immature oligodendrocytes (Fig. 5.6A-C). In contrast, at 14 days post-transplantation and later, very few cGFP-positive cells were PDGFRa-positive. However, transplanted cells did not all differentiate at the same rate, or to the same extent. For example, at later points, immature oligodendrocytes could be observed in spinal cords where nearby transplant-derived cells were producing myelin-like sheaths (Fig. 5.9C).

Many transplanted cells colocalised with markers of the oligodendroglial lineage and a high percentage of cGFP-positive cells double stained for the oligodendrocyte transcriptional factor Olig 2, which is expressed in oligodendrocytes at all developmental stages (Fig. 5.6D-G) (Ligon et al 2006). In addition, many cGFP-positive cells also expressed MBP, indicating that at 14 days post-transplantation some of the transplanted cells had differentiated into myelinating oligodendrocytes (white arrows, Fig. 5.6F). MBP-positive oligodendroglia will be described in more detail in section 5.2.6.

At all time-points post-transplantation, it was observed that, at the injection site, many neurosphere-derived cells had differentiated into astrocytes, as identified by immunostaining using an antibody to GFAP (Fig. 5.7A-C). This dense network of astrocytic processes spread from the injection site up to 0.5 mm in the rostral and caudal directions (Fig.5.7 D-F).

Notably, the central area (dotted box, Fig. 5.8A) of the injection site had a remarkably higher density of GFAP-positive cells than at its perimeter (Fig. 5.8A-C). cGFP-expressing

astrocytes delineated the site where the transplanted cells had integrated, from the adjacent white matter. A few microns from the transplantation point, the transplanted cells throughout the putative white matter, had morphology resembling that of oligodendrocytes with many fine processes (Fig. 5.8D-F).

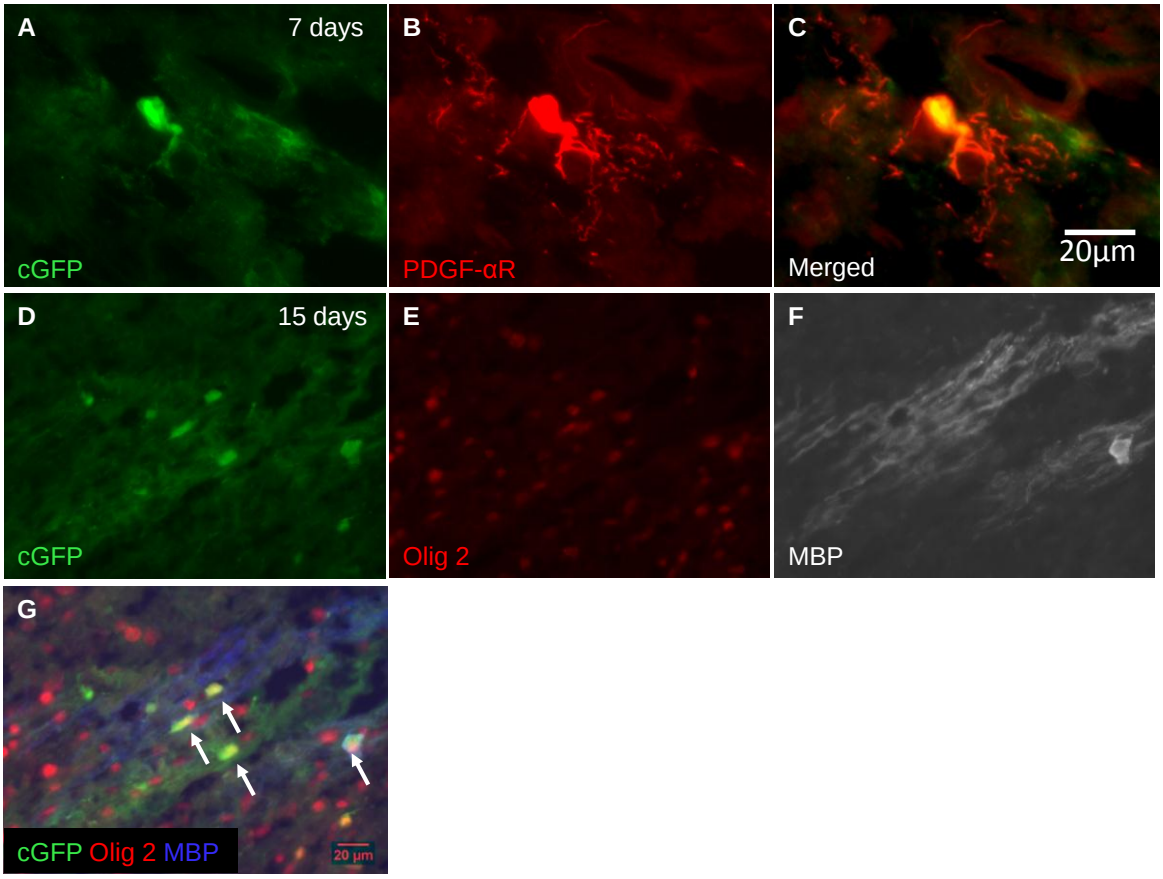

Figure 5.6 cGFP-positive transplanted cells expressed markers of the oligodendroglial lineage 7 and 14 days post-transplantation

A-C) cGFP-labelled cells (A, green) colocalised with PDGF-αR, (B, red) a marker for immature oligodendrocytes, at 7 days post-transplantation. D, E, and G) At 14 days post-transplantation, a proportion of the cGFP-positive transplanted cells (arrows) were double labelled with Olig 2. F-G) At 15 days post-transplantation, the engrafted cells expressed MBP and produced myelin sheath-like structures. Representative images from at least 15 separate experiments.

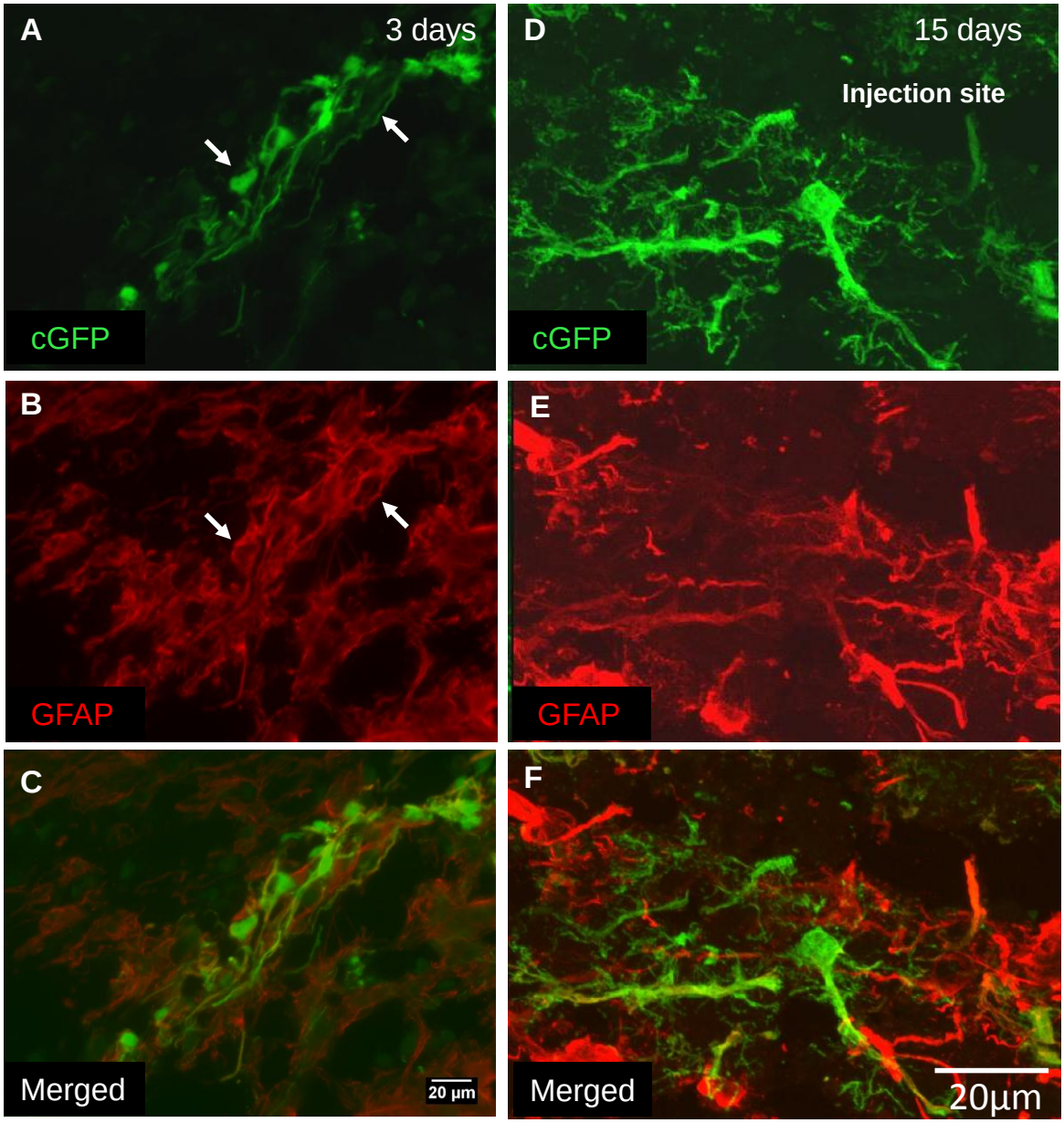

Figure 5.7 cGFP-positive transplanted cells near the transplantation site differentiated into astrocytes

A-C) 3 days post-transplantation many transplanted cells had differentiated into astrocytes, as indicated by colocalisation with the antibody to GFAP. D-F) High magnification confocal images, using the confocal Olympus FV1000 microscope, revealed the morphological details of the cGFP-positive astroglial cells, which extended from the injection site, for up to 0.5 mm, 15 days post-transplantation. Representative images from at least 15 separate experiments.

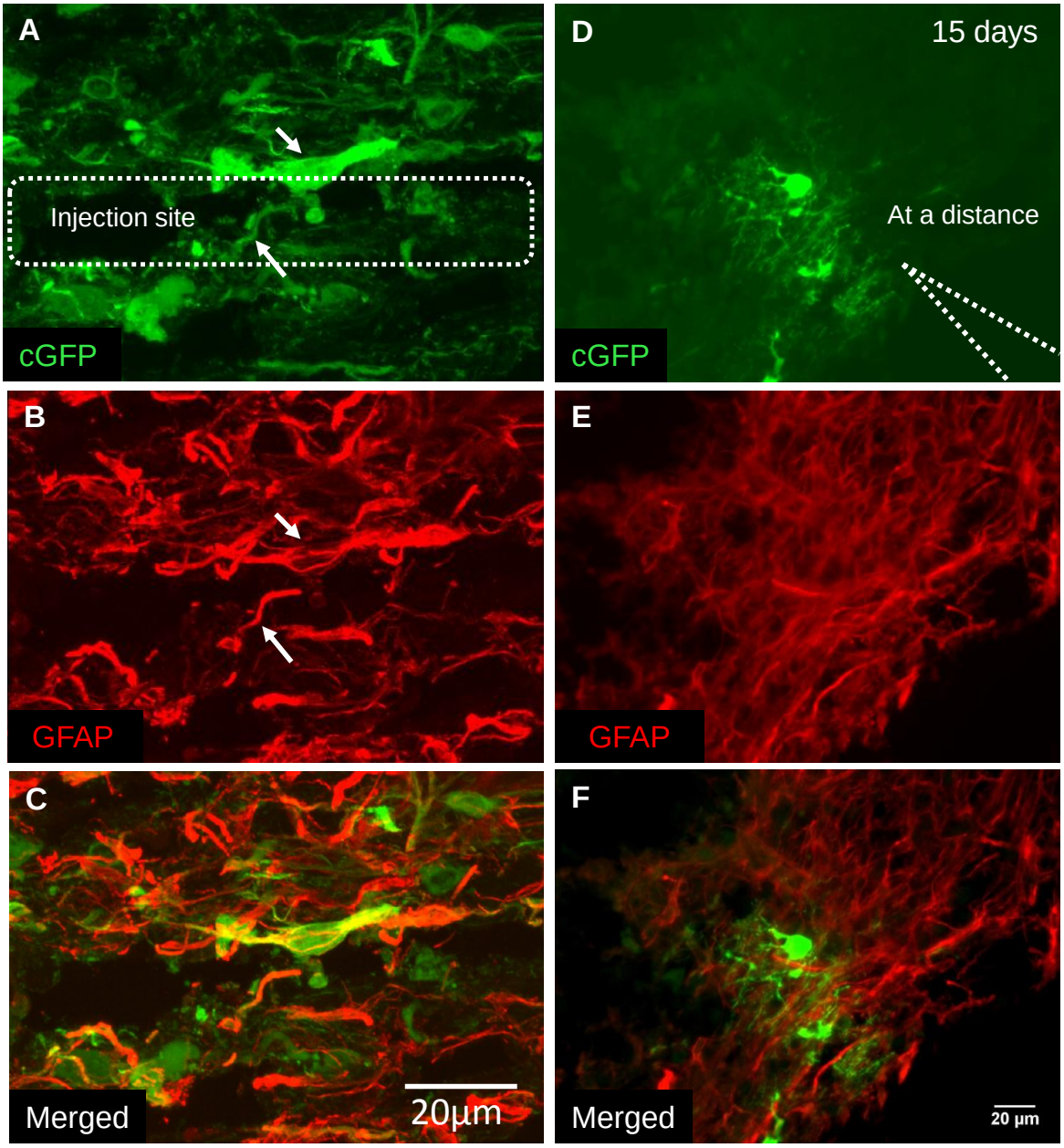

Figure 5.8 Expression of the GFAP marker in relation to the injection site

Images were obtained from spinal cord of a *shiverer* mouse, sacrificed 15 days post-transplantation. A-C) At the transplantation point (dotted box), cGFP-expressing transplanted cells had long processes (white arrows) and differentiated into astrocytes as indicated by colocalisation with the GFAP marker. D-F) A few microns from the transplantation point, the transplanted cells had morphology resembling that of oligodendrocytes with many fine processes. Representative images from at least 15 separate experiments.

5.2.6 Myelin-like sheaths were produced by cGFP transplanted cells in the spinal cord of *shiverer* mice

As described previously, the ultimate aim of the thesis is to visualise oligodendroglial-axonal interactions *in vivo*, during the process of myelination. Therefore it was essential to determine if the transplanted cells would express late markers of the oligodendroglial lineage. More specifically, it was important to investigate if the transplanted cGFP cells co-expressed MBP, as *shiverer* mice are MBP-deficient.

MBP immunostaining showed that transplanted cells were capable of producing large numbers of myelin-like sheaths in the *shiverer* spinal cord (Fig. 5.9A and B). In tissue sections, cGFP-positive cells with numerous fine processes emanating symmetrically from a central cell body co-labelled with the MBP marker. However, in the same section multi-branched cGFP-positive cells were not immunoreactive for MBP (Fig. 5.9 C). Early stages of MBP deposition were characterised by cGFP-positive cells producing MBP-positive fragments spread in a disorganised, dispersed way (Fig. 5.9 D). However, the morphology of the cGFP-positive cells did not allow differentiation between immature, pre-myelinating cells and more mature cells with myelin-like sheaths.

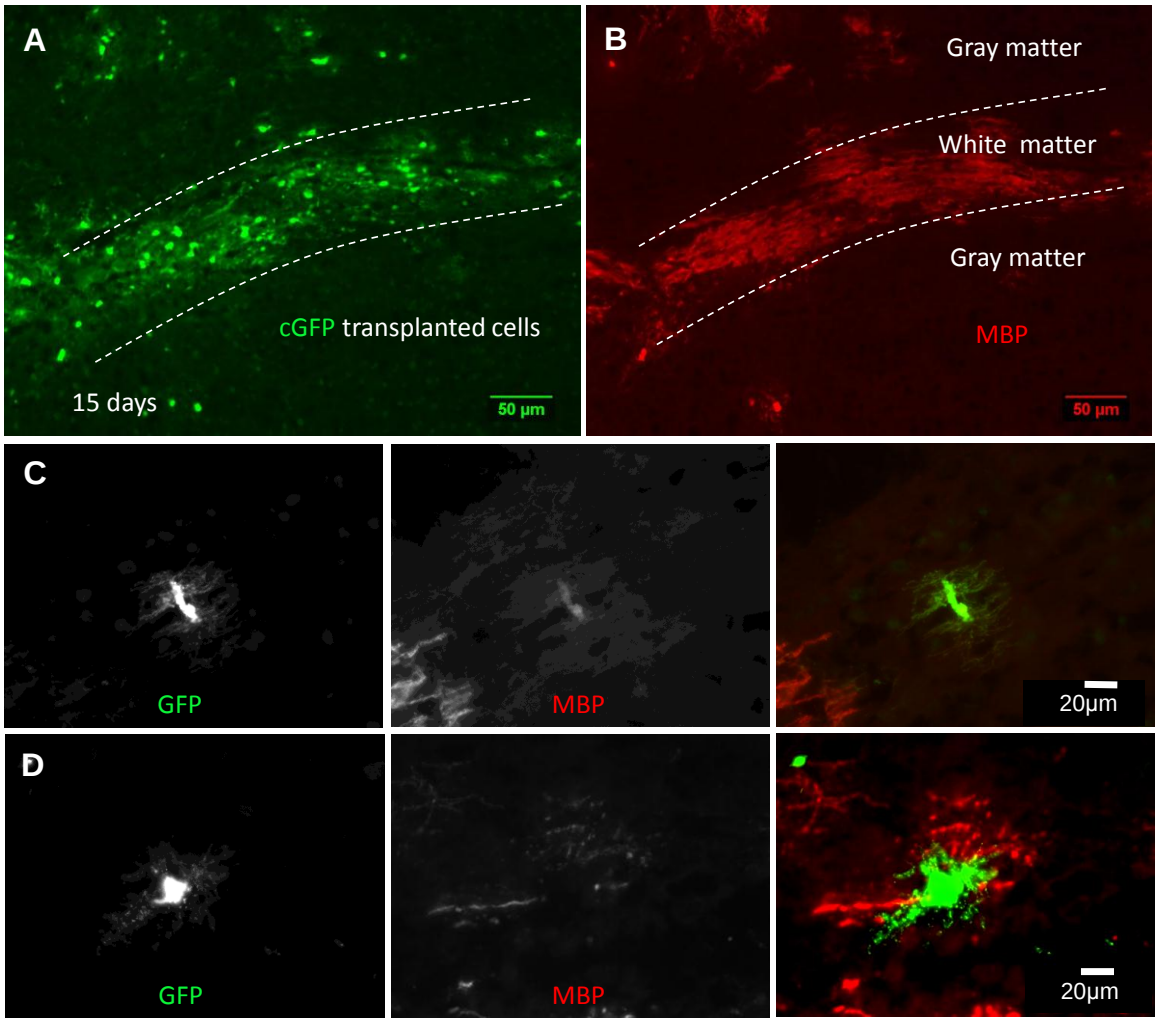

Figure 5.9 Immunohistochemistry of transplanted neurospheres showed that cGFP - positive cells differentiate into oligodendroglia

Low magnification images of a dorso-ventral section of *shiverer* spinal cord, 15 days post-transplantation stained with antibodies to GFP (A) and MBP (B). Transplanted cells were located in both grey and white matter (dorsal columns are delineated by the dotted lines) and produced MBP-positive myelin-like sheaths. C) A presumptive pre-myelinating cell with multiple fine cGFP-positive processes emanated from a central cell body. The soma is lightly stained with MBP, confirming the identity of the cell as that of the oligodendroglial lineage. MBP-positive myelin-like sheaths, belonging to a second cell are seen in the bottom left hand corner of the image. D) An early myelinating cell in which short MBP-positive profiles were present at the periphery of the cGFP-positive soma. Representative images from at least 15 separate experiments.

5.2.7 Time-course analysis of the myelination capacity of the transplanted cells 3, 8, 14 and 28 days post-transplantation

To determine the optimal time point for the *ex vivo* studies described in Chapter 6, a time course analysis of the differentiation status of myelinating oligodendrocytes was performed. Three days post-transplantation, very few MBP-positive cells could be observed. Furthermore those cells that were positive for MBP were very lightly stained. Morphologically, the cells appeared to be multi-process bearing, with processes emanating directly from the cell body. Myelin-like sheaths were not present at this stage (Fig. 5.10A-C).

At 7-8, 14 and 28 days post-transplantation MBP-positive cells were observed more frequently than at 3 days post-transplantation. MBP strongly stained myelin-like sheaths, but was no longer visible or was only faintly visible in the cGFP-positive cell body. At all-time points, cGFP-positive cell bodies with symmetrical, multiple fine processes, which were not MBP-positive, were observed. These cells resembled the faintly MBP-positive cells described above, suggesting that they were immature oligodendrocytes which had not yet begun to express MBP and indicating that differentiation of the transplanted cells is not synchronous (Fig. 5.10B-D). In any case, the oligodendrogenic potential of the cGFP neurospheres was demonstrated on these transplantations into *shiverer* mice.

In summary, cGFP-positive cells with thick processes were identified as astrocytes, while cells with numerous fine processes extended in a symmetrical way, were identified as oligodendrocytes that in some cases, formed myelin-like sheaths, as they expressed MBP. The immunohistochemical studies provided an insight about the morphology of the different types of glial cells that could help to interpret the observations of the cGFP transplanted cells visualised with the multiphoton microscope.

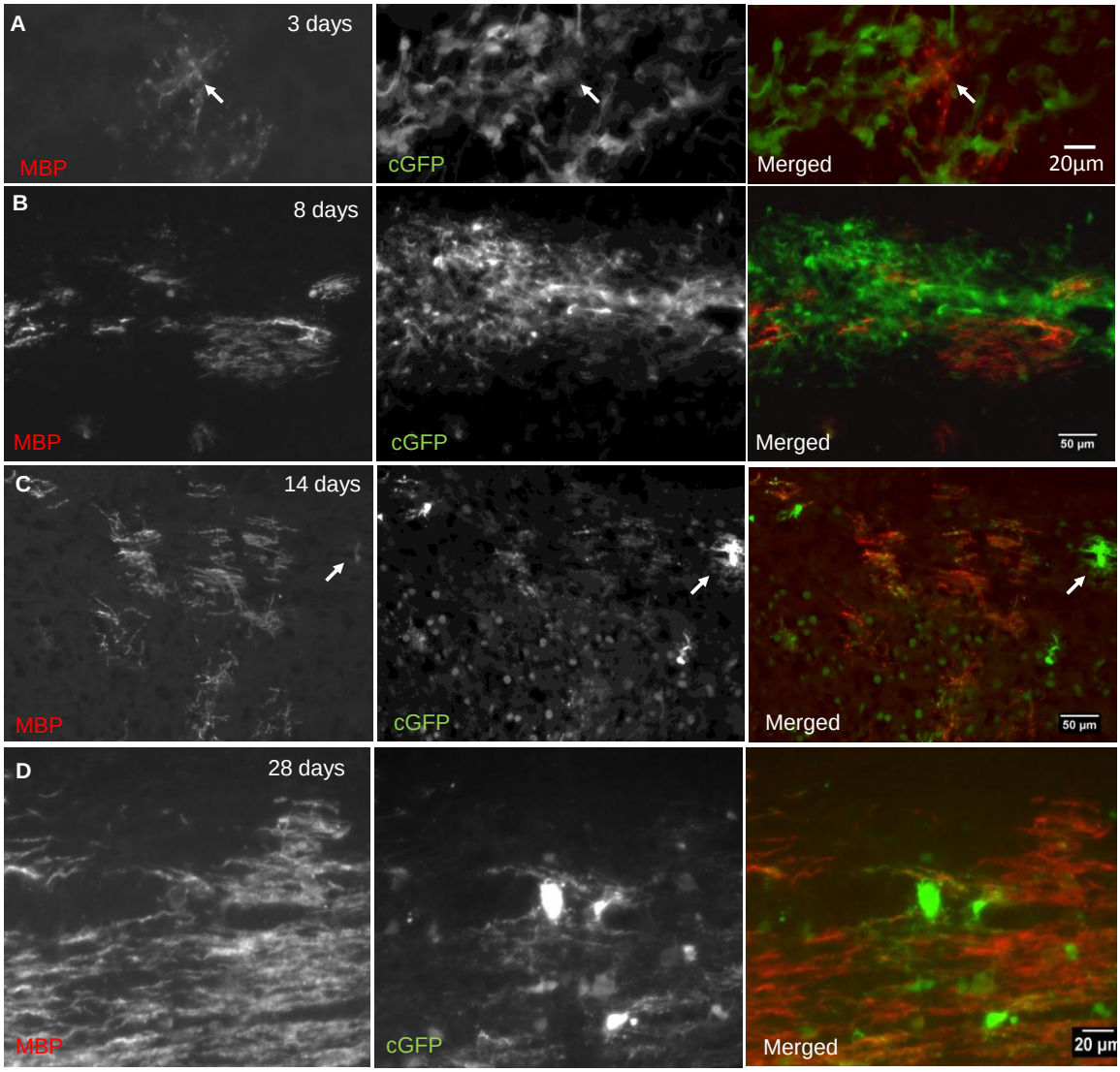

Figure 5.10 Immunohistochemistry of transplanted cGFP cells showed different stages in MBP expression

A) 3 days after the transplantation, light MBP-positive fragments started to appear without visible MBP-positive cell bodies. B-C) 8 and 14 after the transplantation, MBP-positive structures were observed. In the same field of view, a cGFP cell [white arrow, (C)] was imaged having multiple symmetrical, fine processes but not expressing MBP yet. D) At late stages, 28 days post-transplantation, thick myelin-like sheaths were imaged. Representative images from at least 15 separate experiments.

5.2.8 Distribution of the cGFP transplanted neurospheres into the spinal tissue of *shiverer* mouse

Generally, although the cGFP neurospheres were transplanted in the dorsal areas of the white matter of the spinal cord of *shiverer* mice, cells were observed along the grey-white matter interface (Fig. 5.11A and B). Using Image J and a special macro (generated in the lab) that created homocentric circles, allocated from the epicentre of the injection area, the distance of oligodendroglial cells, astrocytes and other non-identified cells from the transplantation site was measured, based on immunohistochemical studies. The transplanted cells were found at a distance of up to 600 μm from the injection site (Fig. 5.12A). In many cases cGFP-positive cells were double labelled with an antibody to MBP and extended myelin-like sheaths. These cells were found close to and at a distance from the needle track (Fig. 5.12B and C). Close to the injection site, a similar proportion of transplant cells had differentiated into MBP-positive cells or GFAP-positive cells, while a minority of cGFP-positive cells could be detected that did not express GFAP or MBP. At a distance from the injection site, the majority of transplant cells were positive for MBP (Fig. 5.12D).

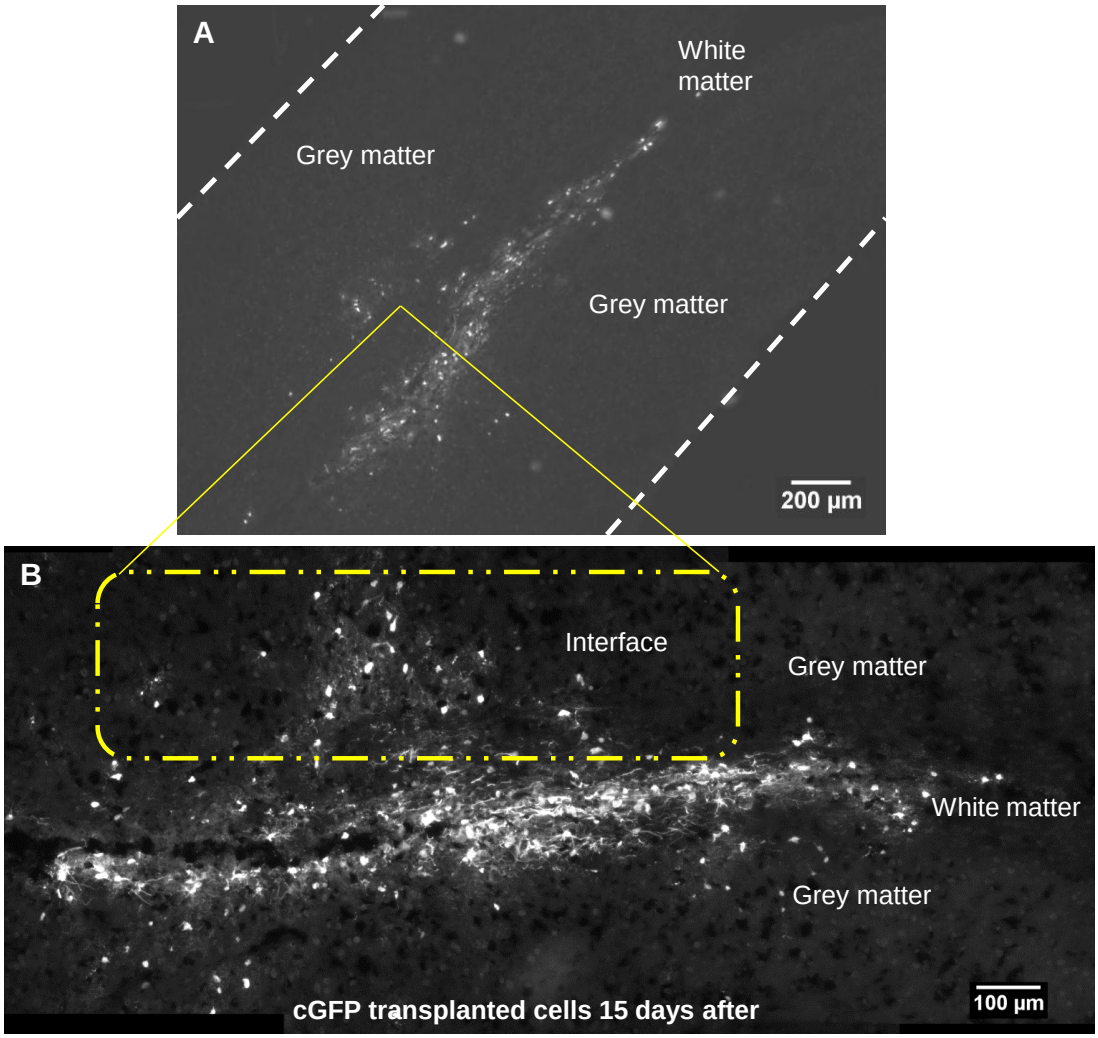

Figure 5.11 Distribution of cGFP-positive transplanted cells in the *shiverer* spinal tissue 15 days post-transplantation

A) Low magnification view of the spinal cord of a *shiverer* mouse that received injection of cGFP-expressing neurospheres into the dorsal columns. B) Magnified view of the area outlined by the yellow box, showed a preferential spreading of the cells along the grey-white matter interface. Representative images from at least 4 separate experiments.

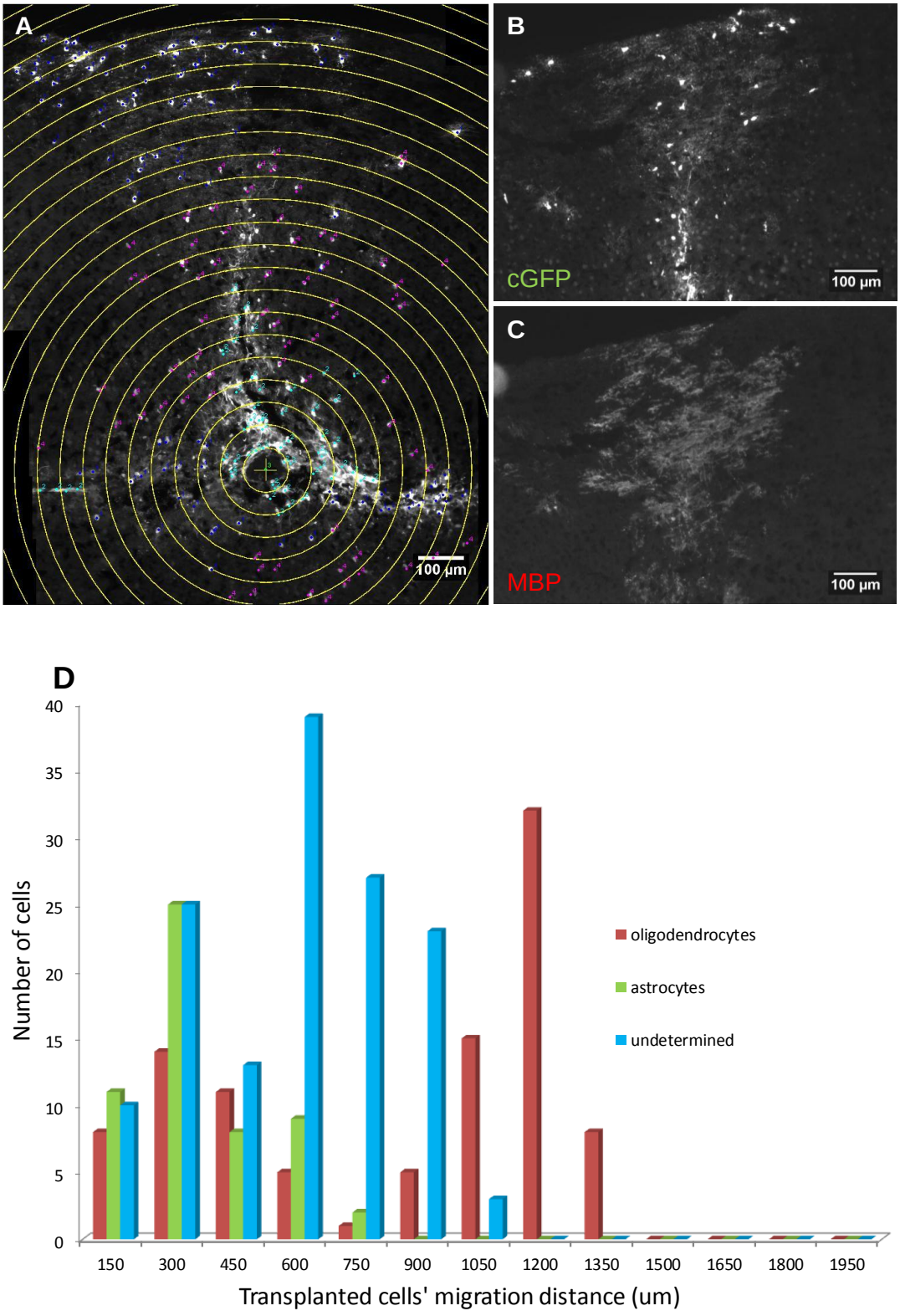

Figure 5.12 cGFP-expressing cells' topography 15 days post-transplantation

A) Using Image J and a macro that created homocentric circles from the injection site (epicentre), the distance of the various cell types was measured in relation to the epicentre.

B-C) Some of the cGFP-positive transplanted cells, which colocalised with the MBP marker, were found at a distance of 600 μm from the needle track. D) Graph shows the percentage of all cGFP-positive cells constituting oligodendrocytes, astrocytes or undetermined cells, according to their relative location from the needle track (n=2).

5.2.9 Examination of tissue sections of imaged spinal cord

In transverse sections of transplanted cord, green cells could be observed throughout the dorsal columns (Fig. 5.13). Fewer cells were evident in the grey matter, suggesting that in this case, the majority of transplanted cells remain within the aberrant white matter, associated with axons (Fig. 5.14).

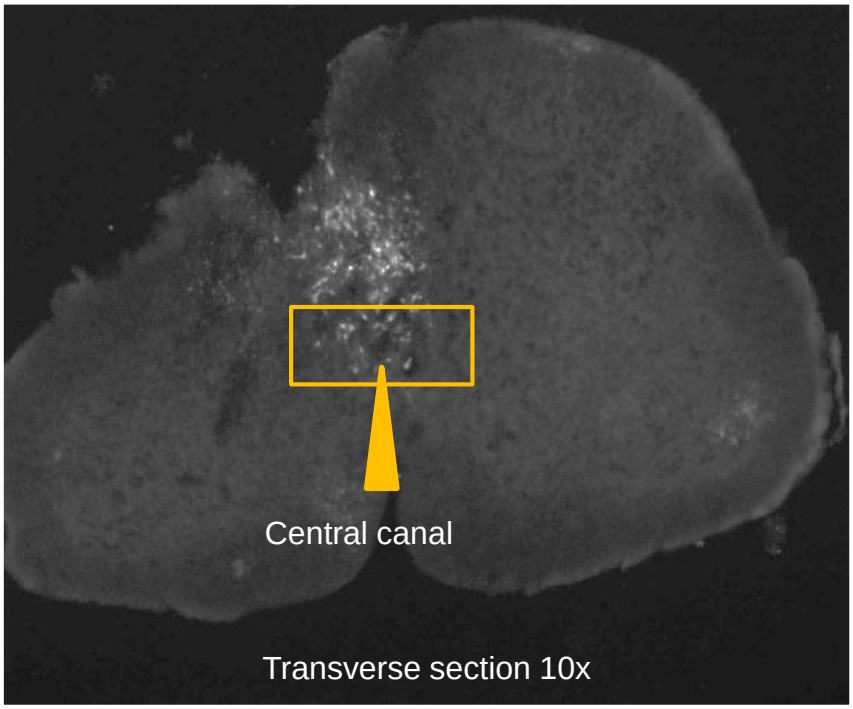

Figure 5.13 Transplanted cells were found throughout the dorsal columns of the transplant recipient

Low magnification view of a 10 μm thick transverse section of the thoraco-lumbar region, of a *shiverer* mouse spinal cord, transplanted 3 days previously with 5 μl of cGFP-expressing neurospheres. The images showed cells deep within the dorsal columns and reaching close to the central canal (within the orange box). Part of the section was missing,

probably as a consequence of tissue injury at the time of injection. Representative image from at least 4 separate experiments.

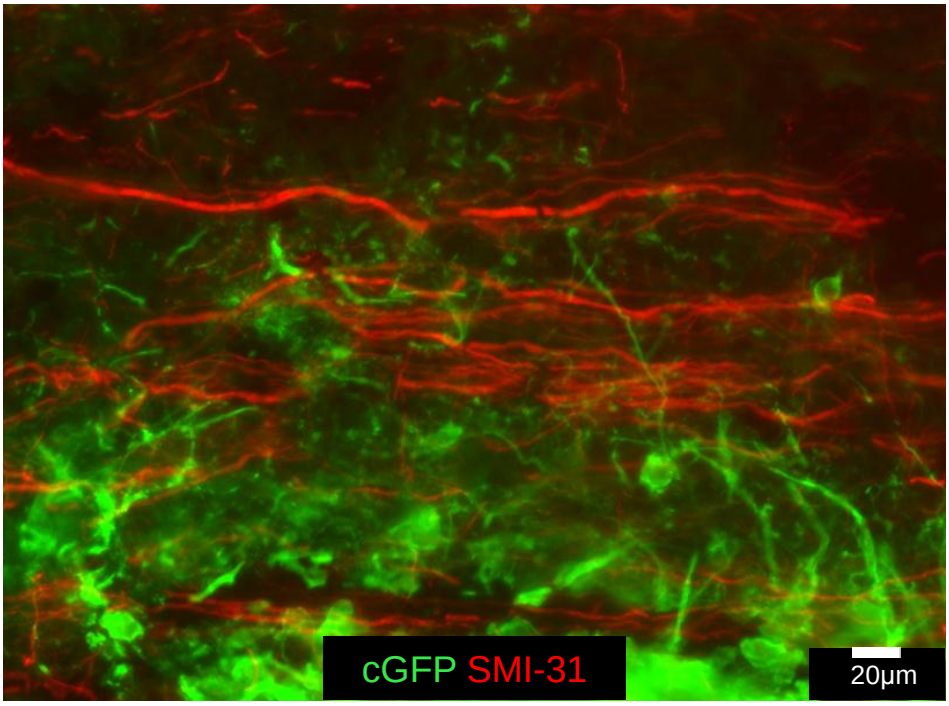

Figure 5.14 Transplanted cells associated with axons throughout the white matter of the transplant recipient.

7 days post-transplantation the cGFP-expressing cells (GFP, green) were imaged extending processes associated with the intact axons (SMI-31, red) of the white matter. Representative image from at 15 separate experiments.

5.3 Discussion

The work presented in this chapter focused on establishing techniques for two-photon imaging using multiphoton microscopy that would allow the direct, stable and repetitive imaging of GFP transplanted cells and axons in the living spinal cord of *shiverer* mice during the developmental process of myelination, in future studies. For this purpose, initially a protocol for two-photon imaging of mouse spinal cord was established using fixed spinal cord containing transplanted cGFP-expressing cells. Fixed spinal cord provided an ideal system with which to establish the technique. In terms of minimising animal use, by also avoiding any stress and operative techniques to the animal, the fixed cord could be imaged multiple times. Furthermore, long-term imaging did not require any special preparation for the maintenance of the excised spinal cord. Therefore a single cord could be imaged for long periods and on multiple occasions. This proved to be extremely useful in terms of gaining familiarity with the technically demanding operation of the multiphoton microscope. The main strength of multiphoton microscopy and other nonlinear microscopy techniques undoubtedly is the ability to maintain resolution and contrast within scattering tissue. However, there were several technical problems found in imaging using multiphoton microscopy that had to be overcome, as for example second-harmonic signals which had a large impact in the understanding of structural features of the spinal tissue, as this signal came up frequently and was difficult to interpret.

In regard to cell transplantation, *shiverer* mouse is an ideal recipient that has been extensively used to study myelination. Although other myelin mutants exist which are used to test the myelinating capacity of exogenous cells, most notably the *shiverer* mouse provides great opportunity to study oligodendrocyte-axonal interactions without the confusion of endogenous glial cells. The function of MBPs is still not well understood, but it is thought that they play an important role in myelin sheath formation, particularly in tightening the myelin lamellar structure. In addition to the general reduction in the amount of CNS myelin, *shiverer* mutant mice have a specific ultrastructural defect in CNS myelin. Electron microscopy clearly revealed that ensheathment, although thin and abnormal in form, is widespread in *shiverer* CNS (Rosenbluth 1980). Thus, a thin layer of oligodendrocyte cytoplasm remains in sheaths. Undoubtedly, *shiverer* and GFP-

transplanted neurospheres is a useful method to investigate early glial-axonal interactions *in vivo.*

The selection of the most appropriate cell for transplantation was crucial for these studies. Practically, all stages of the developmental lineage of the oligodendrocytes have been transplanted into the myelin mutants (Ben-Hur & Goldman 2008, Duncan 2005, Duncan et al 2008). Although OPCs and oligodendrocytes can be derived from dissociated cell preparations from the freshly isolated CNS, it is now more common to culture the cells as free-floating preparations, either as neural stem cell neurospheres (Reynolds & Weiss 1992) or OPC oligospheres (Avellana-Adalid et al 1996, Zhang et al 1998a, Zhang et al 1998b). The former can give rise to both astrocytes and oligodendrocytes. However, few oligodendrocytes are derived from these cells *in vitro*, but when transplanted into a dysmyelinated background, they can generate large numbers of myelinating oligodendrocytes (Mothe et al 2008, Mothe & Tator 2008). In this chapter, cGFP neurospheres were used for all transplantations into *shiverer* mice. As a first step, it was demonstrated that neurospheres when cultured in differentiation medium *in vitro*, produced both oligodendrocytes and astrocytes. This was not unexpected, however it was important to establish the viability and differentiation potential of the cells before transplanting them into living animals.

Since the visualisation of oligodendrocyte-axon interaction, was the aim of the study, mice expressing GFP in oligodendrocytes specifically, would have been the ideal source from which to generate neurospheres. However, these were not available. Moreover, attempts to purify culture and expand primary mouse oligodendrocyte precursors in the presence of growth factors, such as FGF and PDGF-α in sufficiently large numbers for transplantation, had not succeeded (from attempts in the lab). Therefore, it was inevitable that a proportion of neurospheres would give rise to astrocytes, when transplanted into *shiverer* spinal cord. Indeed to some extent, particularly at early time point, immediately after transplantation, the environment at the site of injection-induced injury, possibly influenced the fate of the transplanted cells towards the formation of a glial scar, in which astrocytes usually have a central role.

Astrocytes *per se* were not considered detrimental, as astrocytes can be beneficial for myelination. It has been shown that astrocytes release cytokines, as for instance LIF that

promote myelination by mature oligodendrocytes (Ishibashi et al 2006). CNTF secreted by astrocytes has also been shown to be an important survival factor for oligodendrocytes. (Albrecht et al 2007). However, since transplanted cGFP-expressing neurospheres gave rise to both astrocytes and oligodendroglia, it became essential that the two cell types could be distinguished based on morphology. Therefore, immunohistochemical and morphological comparisons were made.

After the injection of neurospheres, GFAP immunoreactivity was most intense at the needle track. It is possible that the neurospheres injected at this traumatic site differentiate into astrocytes and therefore it is possible to speculate they might interact with the environment by secreting neurotrophic factors and cytokines. Immunohistochemical studies provided evidence that the transplanted neurospheres survived and successfully formed MBP-positive cells as early as 3 days post-transplantation and by 7 days post-transplantation. Clearly, differentiation takes place rapidly *in vivo*, as the local micro- and macro- environment of the host *shiverer* spinal tissue consisting of axons lacking compact myelin, influences oligodendrocyte differentiation. Additionally, MBP-positive cells were present both at the injection site and locations distant from it. This area, being less populated by transplanted cells, facilitated the visualisation of dispersed cGFP transplanted cells that resembled oligodendrocytes, using multiphoton microscopy. Several previous studies have also shown that endogenous or transplanted neural progenitors migrated towards areas of brain damage although the mechanisms underlying this directed migration have not been generally elucidated. Specifically, transplanted GFP-positive OPCs derived from oligospheres, into the brain at P0 to P1 and into the dorsal column of the thoracolumbar spinal cord of *shiverer* mice (Kondo et al 2005) were found to have extensively migrated throughout the brain, associated with MBP-positive myelin patches, and across the entire spinal cord at the site of injection (Duncan et al 2011). Examinations of the brains of *shiverer* mice, into which human fetal glial precursors were transplanted, showed remarkable dispersion of GFP-positive cells that increased with time (Windrem et al 2008).

Most importantly, a necessary step in this chapter was to correlate morphology of cGFP-positive cells with cell type. Immunohistochemical studies gave an insight into the morphology of the two different types of glial cells and even of cells at different developmental stages of the oligodendroglial lineage. cGFP cells with thick processes were

identified by their GFAP-positivity as astrocytes. By contrast, cells with multiple fine processes emanating symmetrically from a central cell body were identified as members of the oligodendroglial lineage, based on staining with an antibody to MBP. Nevertheless, the morphology of the cGFP-positive cells did not allow distinction between immature, pre-myelinating cells and more mature cells. This was due to the fact that cGFP, by its nature, is located in the cell cytoplasm, and not in compact myelin. The localisation of cGFP in the non-compact myelin sheath was described in more detail, in Chapter 1. However, from the immunocytochemical studies it was evaluated that the exogenous cells around 3 days post-transplantation, were just started to produce MBP, whilst some days later, on day 7 onwards post-transplantation, the presence of MBP-positive patches defined the optimal period where the oligodendrocytes interact actively and dynamically with axons to produce myelin-sheaths. To conclude, these results provided the base for *ex vivo* imaging and also information about the optimal time, post-transplantation for visualising the transplanted cells into the living spinal cord using two-photon microscopy in order to achieve direct visual confirmation of axonal contact and interaction. The ability to label entire cell populations in living animals, has allowed two-photon imaging of neural and glial network activity with cellular resolution (Helmchen & Denk 2005).

6. *Ex vivo* studies of the dynamics of the glial-axonal interactions in the CNS

6.1 Introduction

6.1.1 Background

Many fields of biology have benefited from the advances in light fluorescence microscopy, which is used to visualise and monitor cellular behaviour in tissues. In this study, *ex vivo* time-lapse multiphoton microscopy and genetic manipulations in mouse models were combined to reveal information about the glial-axonal interactions through which axons become myelinated. Myelination is multifocal and individual axons are serially ensheathed by both myelinating and pro-myelinating oligodendrocytes (Butt et al 1997). Also, axonal permissivity to myelination involves both targeting of axonally transported molecules to the axonal surface, fine regulation of protein kinases and phosphatases that control cytoskeleton structure and targeting of transported organelles. Only few axonal surface molecules (including laminin 2, L1 and PSA-NCAM) involved in the wrapping process have been identified [reviewed in (Piaton et al 2010)].

Once again GFP labelling of cells has advanced our knowledge of cell-cell interactions *in vivo*. One useful variant of GFP is CFP which was used to mark a subset of neurons in the *thy1*-CFP mice (Feng et al 2000), resulting in CFP labeling of tract axons within the dorsal columns. *Thy1* levels in neurons increase markedly during early postnatal life and *thy1*-derived transgenes have been reported to exhibit corresponding developmental regulation (Caroni 1997, Feng et al 2000).

Kerschensteiner group (Misgeld et al 2007) provided a protocol that described for the first time, imaging of single fluorescently labelled axons in the spinal cord of living mice. This approach allowed direct observation of axons which could be traced over long distances in the spinal cord *in vivo*. This provided a means to assess the success of imaging and promoting therapies *in vivo*.

In this chapter, aspects such as glia attachment to axons, cell alignment in *ex vivo* conditions and extension of processes following successful transplantation of either cGFP

or fGFP-labelled neurospheres into the spinal cord of *shiverer* mice were investigated in detail. For all the *ex vivo* experiments of this study, it was vital to ensure a good supply of energy and oxygen during imaging. This was important as mature oligodendrocytes support membranes up to 100-times the weight of their cell body. As a consequence, oligodendrocytes have the greatest metabolic activity of any other cell in the CNS on a per volume basis, with cell respiration rates at least double that of neurons (Connor & Menzies 1996). This high metabolic rate requires oligodendrocytes to consume large amounts of ATP and oxygen (McTigue & Tripathi 2008).

Time-lapse multiphoton microscopy was extremely useful in comparison with conventional tracing techniques and post-mortem analysis. Without knowledge of the dynamic behaviour of the transplanted cells and direct observations of individual axons, the intertwined process of glial-axonal interactions that lead to myelination might be hard to untangle. With time-lapse imaging in real time, it was possible to document the morphology of the GFP transplanted cells and their positions in relation to the CFP-positive axons over periods of time with high spatial (sub-micron) and temporal (minutes or seconds) resolution.

Moreover, the fact that only a few of the transplanted cells differentiated into oligodendrocytes (confirmed with immunohistochemical studies in Chapter 5), potentially facilitated the ability to follow and image live isolated cGFP or membrane bound fGFP-positive cells resembling oligodendrocytes and establishing contact with the axonal membrane. Furthermore the detailed live imaging of glial-axonal interactions in an *ex vivo* and *in vivo* situation closely resembling the three dimensional cytoarchitecture of the CNS, provided a useful experimental system for the evaluation of such dynamic behaviours and allowed us to shed light on the mechanism of myelination.

6.1.2 Aims of the chapter

The main aim of this chapter was to visualise in real time, *ex vivo* and *in vivo*, the dynamics of the GFP-labelled cells after transplantation into *shiverer* mice and to image any interactions between these cells and the *shiverer* axons, using multiphoton microscopy. For this purpose, the methodology described in the previous Chapter, was used (with modification).

Specifically the aims of this Chapter were to:

1. Establish a protocol for *ex vivo* imaging of spinal cord harbouring GFP-expressing cells.

2. Visualise axons in the dorsal columns of the spinal cord of *Thy1*-CFP mouse. Establish also parameters for simultaneously visualising CFP and GFP.

3. Visualise *ex vivo* GFP-labelled cells after transplantation into the white matter of *Thy1*-CFP**shi/shiv* mice and follow glial-axonal interactions, performing time-lapse.

4. Visualise cGFP-transplanted cells *in vivo*.

6.1.3 Materials and Methods

6.1.3.1 Transplantation of two different types of GFP-labelled neurospheres into *shiverer* mice

Neurospheres from new-born (P1) wild type mice were dissociated into a single suspension and resuspended in L15 solution. To generate fGFP-positive spheres fGFP-lentivirus was added to a flask of dense small neurospheres. Neonatal *shi/shi* or *Thy1*-CFP**shi/shiv* mice 19-21 days of age were recipients of either cGFP or fGFP (membrane bound) neurospheres, as described in detail, in Chapter 2.

6.1.3.2 Maintenance of the explant spinal cords for *ex vivo* imaging

At various time points 3, 7, 9 and 10-14 days post-transplantation, mice were sacrificed and the spinal cords were dissected out. The dissection dish was placed on a container filled with ice and covered with aluminium foil. The dissection medium however was not ice-cold, as lowering the temperature below 10^{o}C, could lead to temperature shock. The protocol that was followed for the *ex vivo* imaging experiments was based on studies by Kerschensteiner and colleagues (Kerschensteiner et al 2008), as described in Chapter 2. Briefly, it was essential to ensure sufficient O_2 and nutrient supply in order to keep the excised spinal cord viable during 5 hours of imaging. Several different physiological solutions, including F12, CO_2 independent medium and neurobasal A medium were used. It was important to bubble the solution with carbon dioxide if required to attain a physiological pH. The temperature of the explant was maintained at 35-37^{o}C.

6.1.3.3 Multiphoton imaging of the explant spinal cord

Time-lapse and Z-stacks were performed using either a Nikon Eclipse TE2000-U inverted microscope with an Olympus long working distance 20x 0.95 NA water immersion lens or an upright Zeiss 7MP laser-scanning multiphoton microscope, providing high resolution.

Band pass filters (Semrock 435/40 or 470/40 and Chroma 525/50) were used to filter the emission for the CFP and GFP channels respectively, as described in detail, in Chapter 2. Post-acquisition images and movies were adjusted for brightness, contrast and background noise, using Image J and Fiji. 3D reconstruction images and videos were created using Imaris and Volocity software.

6.1.3.4 *In vivo* imaging of the cGFP-transplanted cells in *shiverer* mice

Mice were terminally anaesthetized by injection of 300-400 μl/ 10 g^{-1} body weight of a mix of Hyprorm/Hypnovel/dH_2O, at 1:1:8 by volume. After laminectomy, a small segment of the spinal cord was exposed, where cGFP-labelled neurospheres had been transplanted and the mouse maintained at 37ºC, using a heated electrical blanket and an infra-red lamp. The mouse was placed dorsally on a V-shaped metallic plinth with a small opening to allow the microscope lens to access the spinal cord.

6.2 Results

6.2.1 *Ex vivo* imaging of cGFP neurospheres after transplantation into *shiverer* mice

Having gained familiarity with the morphology of the cGFP-transplanted cells, using fixed cords, especially at later time points, where the cells appeared morphologically differentiated, the next step was to visualise these cells in living tissue. Spinal cords were dissected out at various time points post-transplantation from freshly euthanised *shiverer* mice that had been transplanted with cGFP-neurospheres previously. Initial experiments were carried out using F-12 medium and images were obtained from the inverted TRIM LaVision two-photon microscope. An approximately 15 mm longitudinal portion of the *ex vivo* spinal cords encompassing the transplant site, were placed in a 35 mm Petri dish with a 14 mm glass microwell (MatTek) and transferred to the imaging stage of the microscope, as described in Methods and Materials. The *ex vivo* spinal cords were maintained at room temperature for up to 3 hours. The main problems impeding successful *ex vivo* imaging of the explants, such as hypoxia, inadequate supply of energy, inadequate buffering of the samples for too long, resulting in absence of cellular dynamics or abnormal morphology had to be overcome.

Prior to time-course experiments, it was necessary to investigate whether it was possible to visualise the transplanted cells *ex vivo*, as it was a race against time due to the risk of degradation of the tissue and proteolysis by enzymes (proteases). An overview scanning of the transplanted site was required before selecting and zooming in the particular area of interest. Initial experiments were carried out using freshly excised spinal cords at late time points post-transplantation. At that stage and especially for a few hours after dissection of the spinal cords, the cGFP-expressing cells appeared with differentiated morphology that could further analysed, based on the morphology of the processes of the transplanted cells. Therefore, some cGFP-expressing cells were depicted to have numerous, fine, short processes emanating symmetrically from the cell body (white arrow, Fig. 6.1). On the other hand, there were cGFP cells with longer, thick processes that bore branches at the periphery (broken arrow, Fig. 6.1).

According to standard laser-scanning microscopy procedures, during image acquisition, laser power, detector gain and offset levels were set as to minimise background noise and partly saturate cell bodies so that fine cell processes could be visible and sharp.

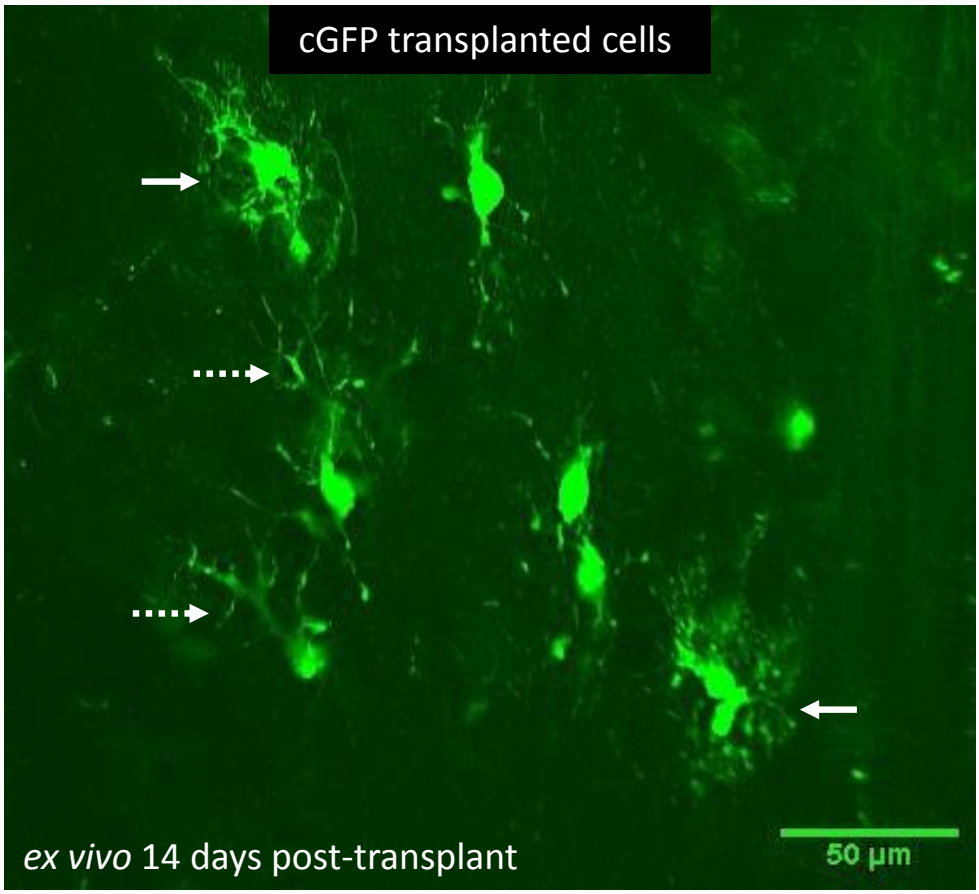

Figure 6.1 *ex vivo* imaging of a spinal cord 14 days post-transplantation illustrated cGFP differentiated cells bearing complex morphology

An average Z-stack illustrated the complex morphology of cGFP-expressing cells, visualised *ex vivo*, 14 days post-transplantation. Some cGFP cells were visualised bearing many fine, short processes emanating in a symmetrical way from the cell body (solid arrow). In the same plane of view there were cGFP-expressing cells with long, thick and branched processes (dotted arrow). Representative image from at least 8 separate experiments.

6.2.2 *Ex vivo* time-lapse of cGFP-expressing cells revealed their dynamic behaviour

Initial *ex vivo* experiments over short periods

Visualisation of cGFP-expressing cells in spinal cords transplanted 12 or 14 days previously, demonstrated that the processes of the exogenous cells were motile. Isolated cells with clear and visible processes were a privileged target for imaging. Although, clarification of the identity of the visualised cells was difficult, cGFP-expressing cells with multiple processes emanating for the cell body could be distinguished to some extent from cells with thick asymmetrical processes. Additionally, cGFP-expressing cells bearing fine processes were usually found as single cells or in association with another one of similar morphology, in the plane of view. On the contrary, cGFP transplanted cells with thick processes appeared to be part of a dense cellular network.

Time-lapse imaging over a short period revealed changes in the pattern of cGFP localisation over time in both cell types (Fig. 6.2A-C and D-F). Since cGFP is free to diffuse in the cell cytoplasm, these changes most likely represented changes in cellular morphology that was accompanied by the translocation of cytoplasm into the newly formed cellular space. In both cases, new processes were formed rapidly.

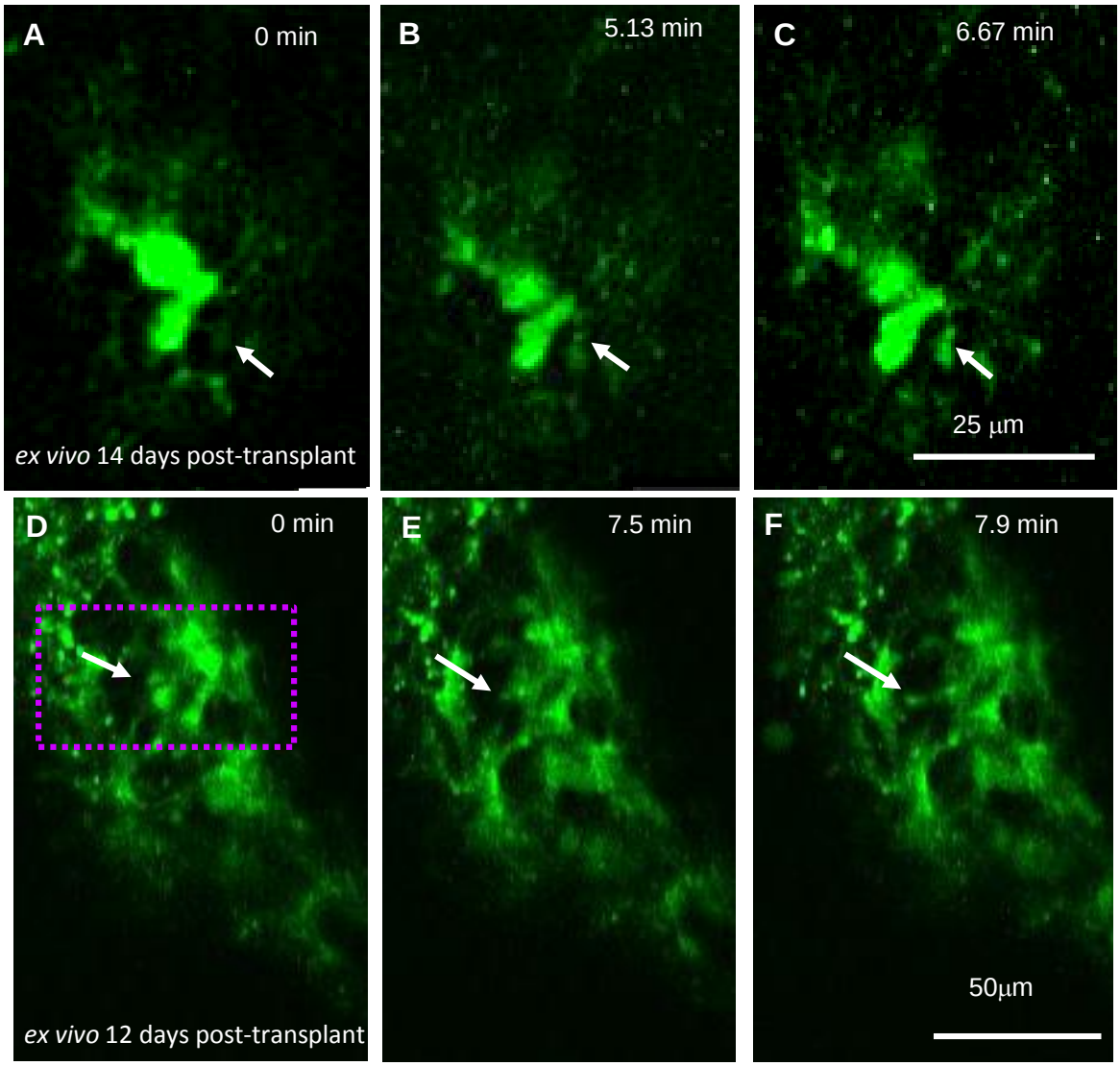

Figure 6.2 Time-lapse of ex vivo spinal cords revealed that exogenous cells were motile

A-C) *ex vivo* time-lapse imaging of a spinal cord from *shiverer* mouse, 14 days after transplantation of cGFP-expressing neurospheres. cGFP within a cell process can be seen to increase in intensity, as it progressively extends out (arrow) over 6 min. D-E) *ex vivo* time-lapse of a spinal cord 12 days post-transplantation illustrates a process extending from a cGFP labelled cell around the graft, over a period of less than 8 min. See supplementary videos 6.1 & 6.2. Representative videos from at least 2 separate experiments.

6.2.3 *Ex vivo* time-lapse of cGFP transplanted cells showed changes in distribution and intensity of the GFP signal

To study directly the dynamic changes of the cytoplasm of the cGFP-expressing cells, time-lapse imaging was performed for longer time periods. The longer time course revealed information about the transplanted cells when compared to conventional analysis of fixed material. Z-stack images from *ex vivo* spinal cords, 14 days post-transplantation, revealed that cGFP-expressing cells were highly branched, extending multiple processes (some > 50 μm long) that radiated from the soma and had many thin, finger-like protrusions which extended from the primary branches (white arrow, Fig. 6.3A). In the same plane there were cGFP cells with long ramified extensions.

Ex vivo time-lapse imaging was performed over a cycle of 30 min with 3 seconds time interval and through Z-stacks, composed of 8-18 optical sections, from 3 to 6 μm apart, spanning up to 60 μm in the axial (z) dimension, while still providing adequate representation and reconstruction of the cells. It should be reported that there was no drift in the field of view, using the TRIM Lavision multiphoton microscope. During 20 min of time-lapse observations, there were changes in distribution of the cytoplasmic signal and intensity signal, possibly indicating diffusion of the cytoplasm of the cGFP transplanted cells bearing numerous fine processes (white arrow, Fig. 6.3A and B). Fluorescence intensity versus time plot confirmed that there was a decrease, approximately 35% of the normalised intensity of the cell body of the highly branched cGFP transplanted cells (Fig. 6.3C) suggesting that the activity of the cells had as a result transit of cGFP expression to the periphery for presumptive extension or growth of the processes.

On the other hand, the overall morphology of the other type of cGFP-expressing cells with the long extensions did not change at all over the long-term time course (broken arrow, Fig. 6.3A and B). Additionally, there was no difference in the intensity levels.

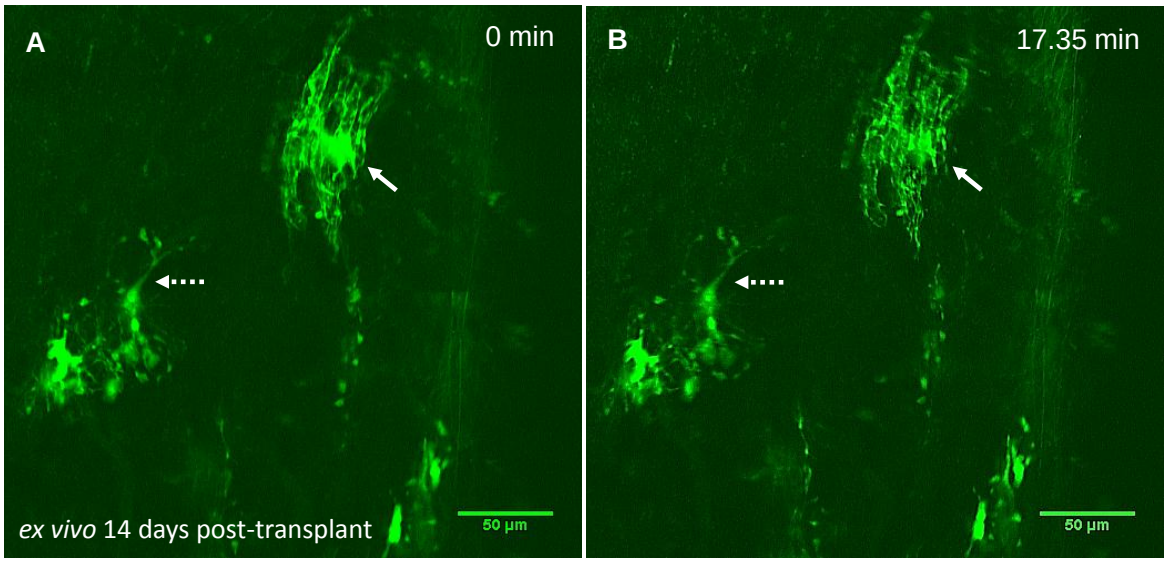

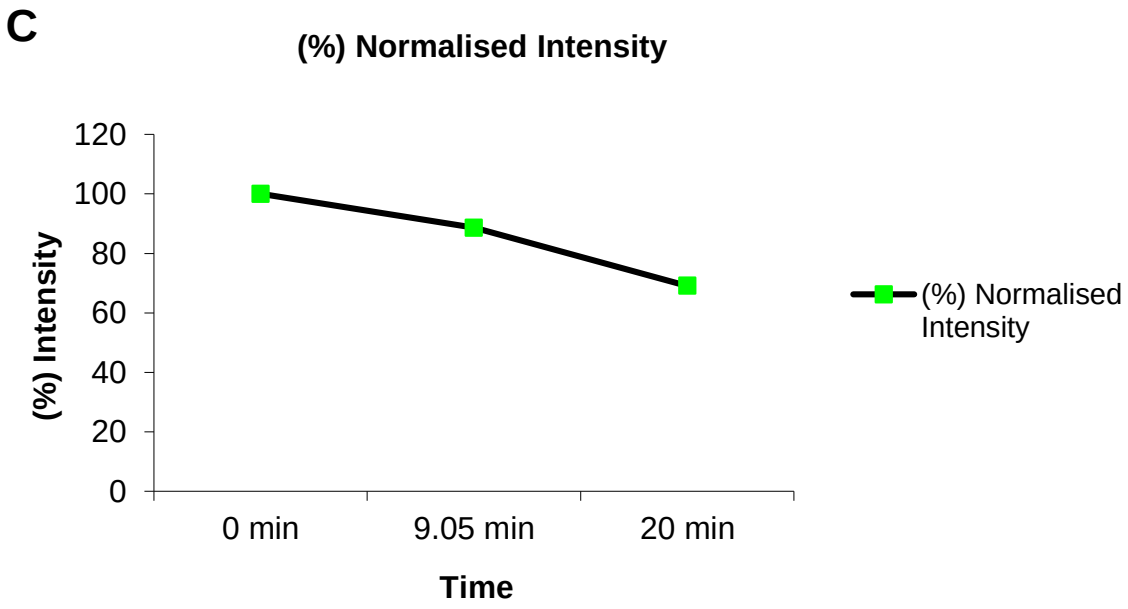

Figure 6.3 Longer term time-lapse of an *ex vivo shiverer* spinal cord showed changes in the intensity signal of the cGFP-expressing cells

A-B**)** Time-lapse over 20 min with 3 sec time-interval, 14 days post-transplantation into a *shiverer* spinal cord showed dynamic morphological changes in the distribution of the cytoplasm of the cGFP-transplanted cells bearing many fine processes (solid arrows). The morphology of the cGFP cells that had long but not so branchy processes did not change during the time-lapse (broken arrows). C) Fluorescence intensity vs. time plot confirmed that there was a decrease, approximately 35% of the normalised intensity of the cell body of the highly branched cGFP transplanted cells.

6.2.4 *Ex vivo* imaging of cGFP-labelled cells resembling oligodendrocytes using two-photon microscopy

Technical improvements for better *ex vivo* imaging

Taking a step further in visualisation of the dynamic behaviour of the transplanted cGFP-expressing cells, several parameters were taken into consideration that ensured better maintenance of the explant spinal tissue. The *ex vivo* cord was maintained at 35-37^{o}C using a heating stage, in Neurobasal A medium minus phenol red that had been bubbled with 95% O_2 and 5% CO_2 for at least 15 min before imaging. Furthermore, during imaging the explant was superfused with pre-warmed O_2-bubbled medium. Generally, the tissue was kept well oxygenated after careful dissection and steady flow rates and room temperature created conditions as close to physiological as possible, minimising the drift during recording.

Ex vivo imaging was performed using the upright Zeiss 7MP laser scanning-multiphoton microscope. A tile scan of the whole area of transplantation revealed many cGFP-expressing cells bearing long processes forming a dense network at the centre and the periphery of the injection site (Fig. 6.4A). The long tails and the morphology of the processes of the cGFP-transplanted cells across the spinal tissue appeared typical of astrocytes. At a distance from the main transplantation area, individual cells with clear symmetric processes were observed at the bottom of the engraftment region (purple box, Fig. 6.4A). Real time imaging over a Z-stack, brought to light fine processes of individual cells that resembled oligodendrocytes (Fig. 6.4B). Time course experiments showed oligodendrocyte-like cells which were depicted to be in close association with nearby cells of similar morphology, both of them extending several processes (Fig. 6.4C).

However, there was a lot of drifting during the acquisition of the time-lapse, possibly due to the flow rate of the medium in the superfusion chamber which inhibited steady recordings of the processes' movements and the interactions between the oligodendrocyte-like cells. More importantly, the *ex vivo* imaging approach offered the opportunity to study in detail the structure of the cGFP transplanted cells and provided a perspective into the spatial organisation of the transplanted cells throughout the spinal tissue.

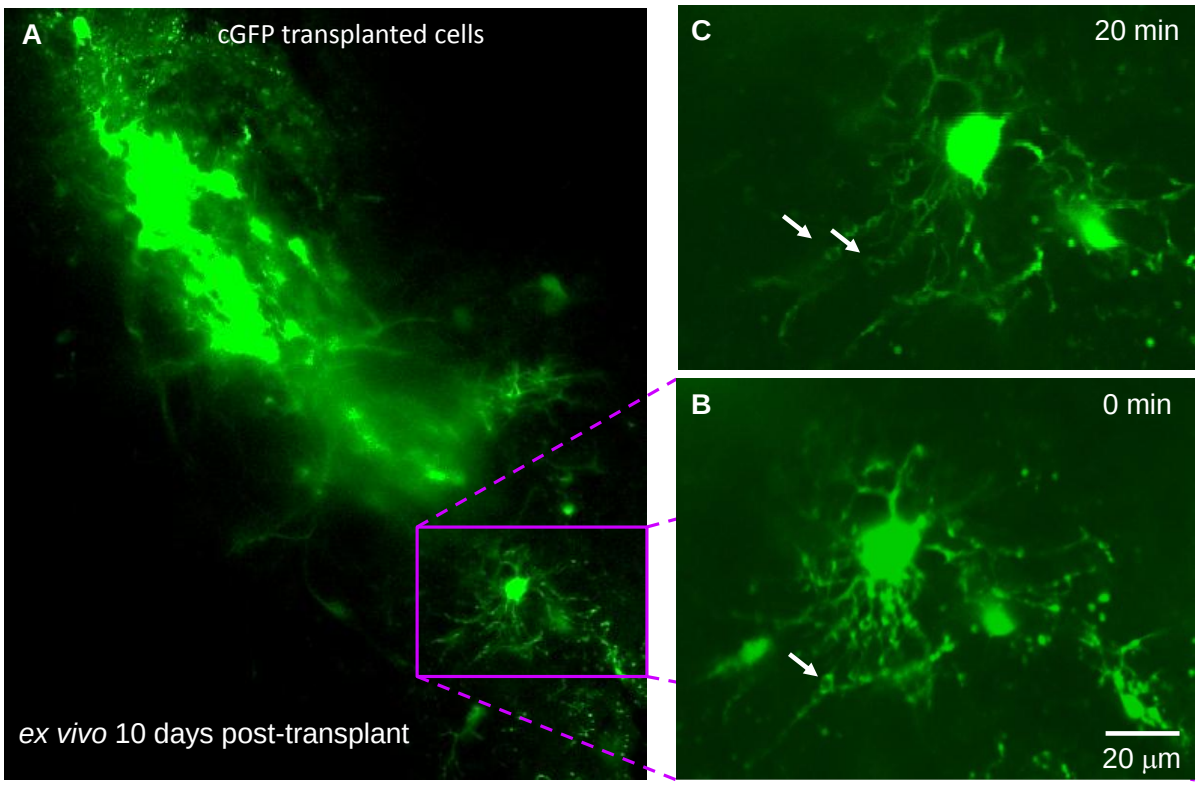

Figure 6.4 *ex vivo* imaging of cells resembling oligodendrocytes 10 days post-transplantation into a *shi/shi* spinal cord

A) Tile scan using multiphoton microscopy of the transplanted area showed a dense cellular network comprised of cells having long processes at the centre and the periphery of the injection site, typical of astrocytes. At a distance and at the bottom of the engraftment area, individual cells (outlined with a purple box), with clear symmetric, fine processes were detected resembling oligodendrocytes. B-C) Time-lapse imaging over 30 min with a time interval of 3 min through a Z-stack with 0.50 μm step size, showed helical coil extensions (arrows) of the processes of the differentiated oligodendrocyte-like cell which appeared to be in close association with another nearby cell. See supplementary video 6.3. Representative images from at least 2 separate experiments.

6.2.5 *Ex vivo* time-lapse of fGFP-transplanted cells into *shiverer* spinal cord

To delve into the understanding of how the membranous cell processes of the transplanted cells develop, expand and potentially transform to myelin sheaths, fGFP-labelled neurospheres were transplanted into the white matter of *shiverer* spinal cord, as described in detail, in Chapter 2.

The main aim of this set of experiments was to examine the morphology of the transplanted cells, expressing GFP which is tethered to the membrane by farnesylation, thus allowing visualisation of the membrane sheath in order to observe any change of their plasma membrane that could extend and develop to myelin membrane. Three-dimensional time-lapse multiphoton imaging was performed in the maintained *ex vivo* spinal tissue at progressively later stages post-transplantation, through Z-stacks of sections that were collected at 3 min intervals. Such volume imaging provided a means for observing the 3D structure and movements of live cells within the tissue volume.

Ex vivo imaging showed distinct differences in the morphology of the fGFP-tagged cells in comparison to the cGFP-expressing cells. fGFP-tagged cells were imaged in a dense network with flat processes and with rather diffused branches (Fig. 6.5A). Time-lapse analysis through a maximum projection in z-volume, revealed fGFP-positive extensions filling gaps and sustaining growth of pre-existing branches (white arrow, Fig. 6.5B). Additionally, fGFP-tagged cells were shown to generate new protrusions over time, during the image aquisition (white arrow, Fig. 6.5C). Regardless of when the new extensions happened in ralation to the time of recording, fGFP cells generated protrusions rapidly, occuring in seconds.

Once again, it was hard to distinguish whether these processes belonged to astrocytes or oligodendrocytes. However, these results showed that fGFP neurospheres survived after the transplantation into the *shiverer* spinal cord and that the lentivirus was not toxic. Furthermore, fGFP-tagged cells demonstrated a dynamic behaviour characterised by changes in the morphology and length of pre-existing processes and rapid formation of new processes, over long-term time-lapse imaging.

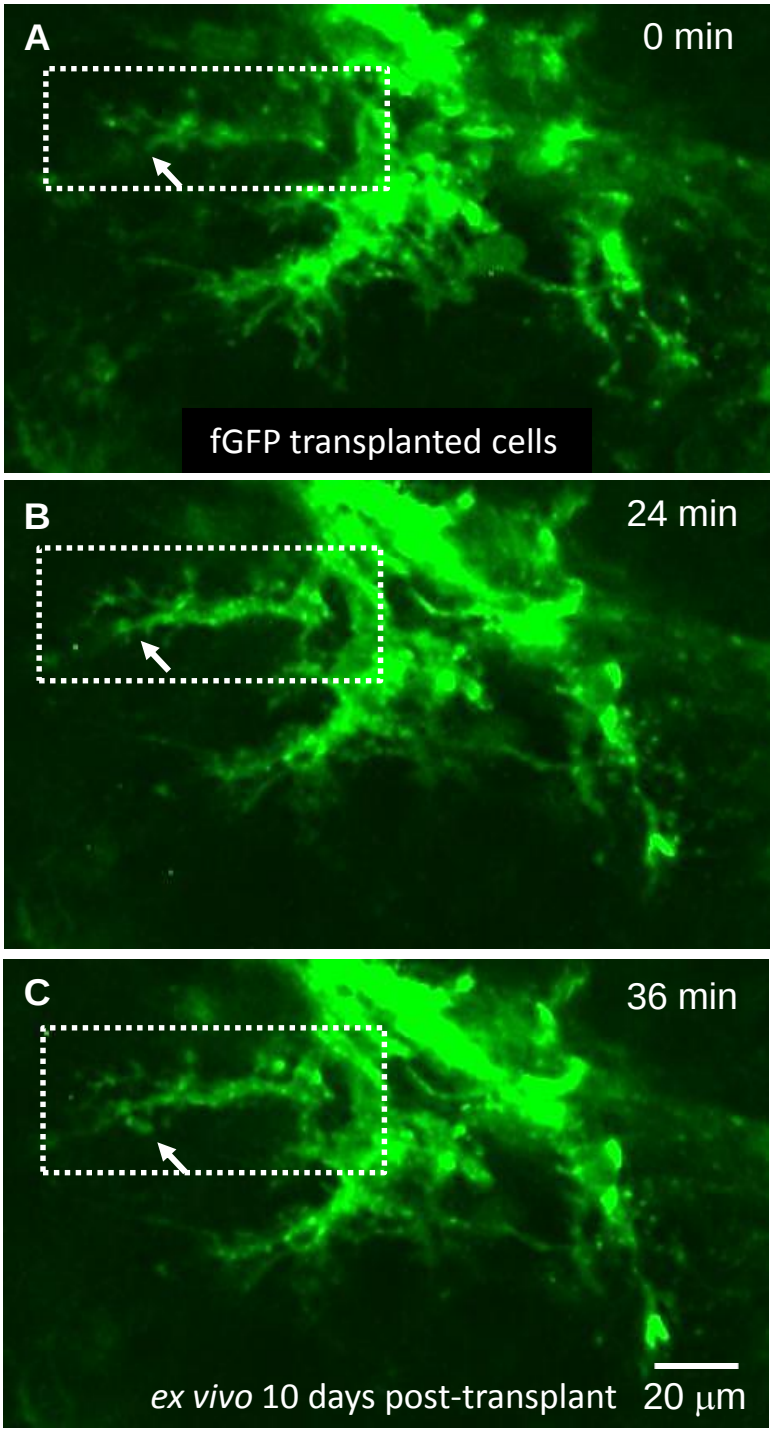

Figure 6.5 *ex vivo* time-lapse of fGFP-tagged cells after transplantation into *shiverer* spinal cord

A) fGFP-tagged cells survived and imaged in a dense network with rather flatter branches than cGFP processes, 10 days post-transplantation. B) Time-lapse over 60 min with 3 min time interval through a maximum projection of 10 optical sections, collected at 1 µm z-step interval, revealed fGFP-extensions filling gaps and sustaining growth of pre-existing branches (dotted box, white arrow). C) fGFP-tagged cells were highly dynamic and rapidly

generated new protrusions over time (white arrow), during recording. Representative images from at least 2 separate experiments.

6.2.6 Next step: Visualisation of axons in the dorsal columns of the spinal cord of *Thy1*-CFP mouse

One of the most essential steps towards *ex vivo* imaging of glial-axonal interactions was to visualise CFP-positive axons. This technique was based on two components. Firstly, a computer-controlled multiphoton microscope with at least two detectors for use of special filters and secondly, transgenic mouse lines in which only a small percentage of axons in the dorsal part of the spinal cord are labelled, that is to say, *thy-1* CFP mice. The sparse labelling allows the tracing of individual axons in the dorsal columns, a region in the spinal cord that can be optically accessible after laminectomy. Without such sparse labelling, resolving and tracing individual axons in the dense white matter would be challenging.

Thy-1 CFP mice were euthanised with CO_2 and the spinal cord was dissected out starting from C1-3 cervical to T12 thoracic part and placed in the appropriate medium, as described previously. The freshly excised spinal cord was then transferred to the imaging heating stage ($37^{c}C$) of the inverted TRIM Lavision multiphoton microscope. Appropriate band pass filters were used to detect the CFP signal as well as low-power objectives which allowed large overview images to be taken that were tiled to produce large-scale reconstructions, covering several millimetres of axonal length. Z-stack images over 30 μm, showed most axons running parallel to the surface, so deep-tissue penetration was not required at this stage (Fig. 6.6). Following previously published protocols (Misgeld et al 2007) sensory axons in the white matter of the dorsal column were traced over long distances (up to several millimetres) in the *ex vivo* spinal cord.

It was also possible to resolve sub-cellular details as for instance, neuronal bodies and presumptive nodes of Ranvier (Fig. 6.7). Multiple short-exposure frames were obtained and averaged to reduce the background noise. The noise though obscured morphological details to some extent. Additionally, multiphoton imaging with a resolution below 1 μm was promising for the subsequent series of experiments to simultaneously visualise CFP-

positive axons and GFP-transplanted cells *ex vivo*, using multiphoton microscopy in order to image glial-axonal interactions.

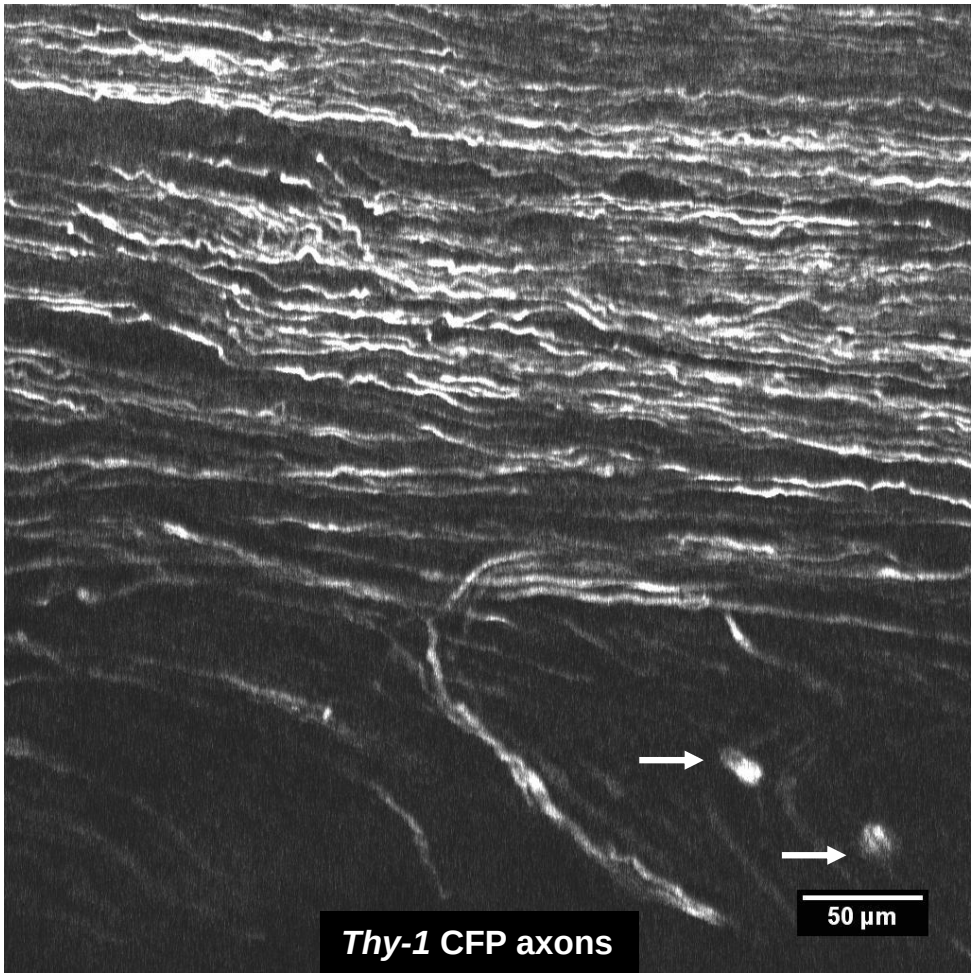

Figure 6.6 e*x vivo* imaging of axons in the dorsal columns of the spinal cord of a *Thy-1* CFP-mouse using multiphoton microscopy

Z-stack images over 30 µm, with 1.875 µm step interval showed most axons in the dorsal column running parallel to the surface. Band pass filter 470/40 was used to detect the CFP signal which was excited with λ= 870 nm. Two neuronal bodies are indicated by the white arrows. Representative images from at least 5 separate experiments.

6.2.7 Establishing parameters for simultaneous visualisation of CFP and cGFP

After successful imaging of individual CFP axons, the main aim was still to visualise simultaneously the cGFP-labelled cells that had previously transplanted into the spinal cord of *Thy1*-CFP**shi/shiv* mice, with the CFP-positive axons.

Even without the "optimal" filter sets, it was possible to visualise both CFP and GFP fluorophores. However, there was a worry that CFP fluorophore "bleeds" through the optical filters used for GFP, thus producing colocalisation artefacts. The amount of "bleed-through" depend on the optical filters and dichroic of the multiphoton microscope. In general, exciting multiple fluorophores simultaneously cannot evaluate the risk of colocalisation artefacts. For these reasons, a quick assessment was accomplished by exciting only one fluorophore at a time, while monitoring emission settings of the other fluorophore. Ideally, the "wrong" fluorophore channels should appear dark, as no signal means no cross-talk. Additionally, in many experiments, second harmonic signal was present that had also to be distinguished from the CFP signal coming from the CFP-positive axons. As a consequence, short and long pass dichroic filters were carefully chosen for each experiment. For absolute rigor, a control sample, a slide of Convallaria was used for the appropriate combination and selection of filters and dichroic, where the best chosen excitation wavelength of CFP would result in emission of CFP that would not picked up from the detector of the GFP channel.

Meanwhile, fluorescence lifetime imaging (FLIM) was performed using multiphoton microscopy to confirm that the GFP signal was real, in those experiments where cGFP cells had been transplanted to *Thy1*-CFP**shi/shiv* mice. Hence, the undesirable effects of cross-talk were further analysed (Fig. 6.7A and B). The fluorescence lifetime is the time a fluorophore remains in its excited state after excitation and it is typically in the order of a few nanoseconds. The sample was excited at 840 nm using 100 fs laser pulses.

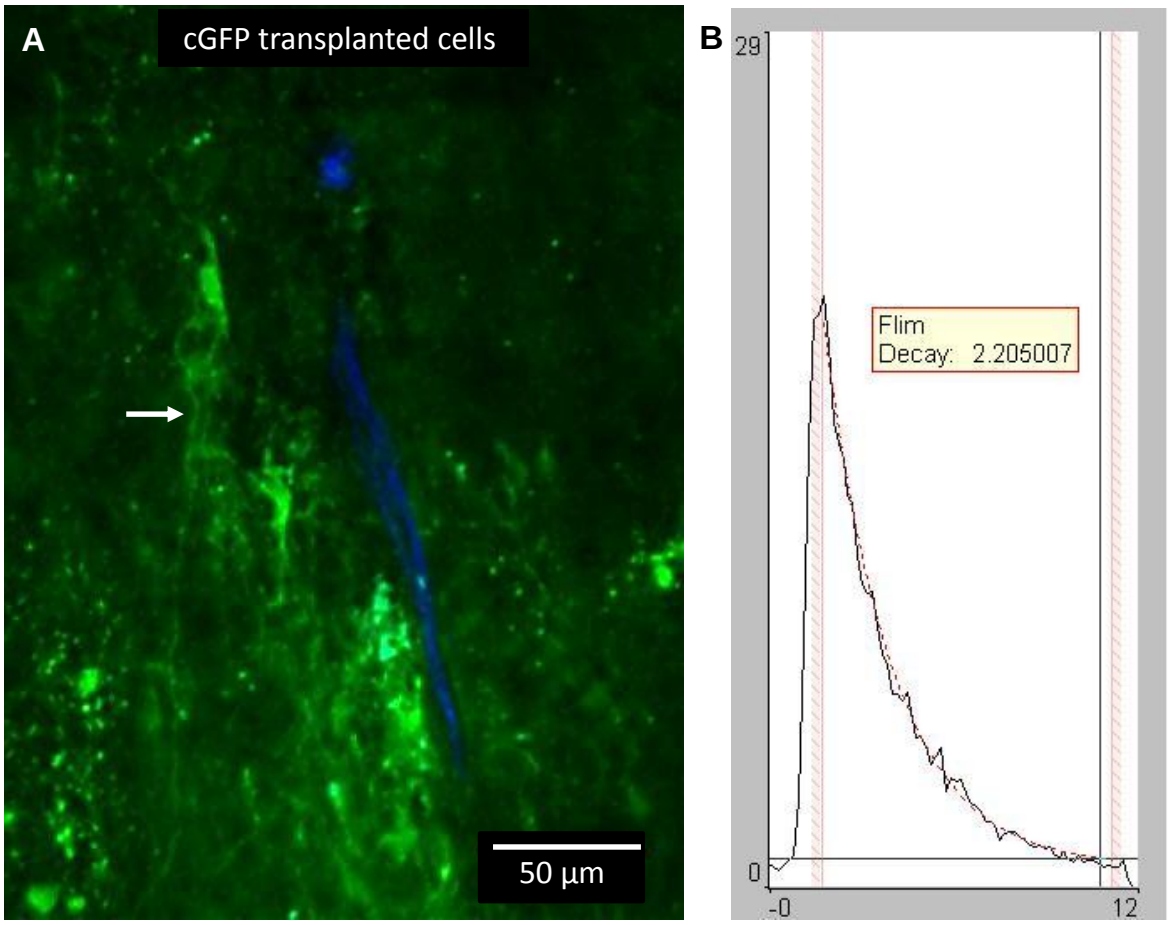

Figure 6.7 Simultaneous imaging of CFP-positive axons and cGFP-labelled cells

A) Average projection of a Z-stack of 70 µm in depth with 0.5 um step size through a tissue of spinal cord of a *shiverer* mouse, 14 days post-transplantation, showed differentiated transplanted cells with long processes (white arrow). B) Flim decay curve of the green signal showed that the detection was generated from the GFP fluorophore. Representative images from at least 5 separate experiments.

6.2.8 *Ex vivo* imaging of GFP-labelled cells after transplantation into the white matter of *Thy1*-CFP**shi/shiv* mice

Having confirmed that cGFP neurospheres can survive and successfully differentiate into oligodendrocytes and produce MBP-positive myelin-like sheaths in the *shiverer* spinal cord (Chapter 5), cGFP-expressing or fGFP-labelled neurospheres were next transplanted into a *shiverer* mouse expressing CFP under the *Thy-1* promoter in order to simultaneously visualise the *ex vivo* transplanted cells and axons. GFP and CFP were excited simultaneously at 860 nm.

The morphology of cGFP and fGFP-labelled cells was compared after transplantation. Imaging of *ex vivo* cord 7 and 8 days post-transplantation, revealed both types of GFP labelled cells extending processes associated with the CFP-positive axons. cGFP cells showed a different morphology in their association with the CFP-positive axons when compared to fGFP transplanted cells and could be seen to extend processes which made contacts with an axon at several points (arrows, Fig. 6.8A). On the other hand, fGFP-labelled cells, which were imaged approximately at the same time post-transplantation, appeared to align with the CFP-labelled axons with thicker processes (Fig. 6.8B). This reflects the differential localisation of the GFP in the cytoplasm or membrane.

Using the cGFP tagged cells it is impossible to visualise compacted membrane. For this reason subsequent experiments were carried out with GFP tethered to the membrane by farnesylation, thus allowing visualisation of the membrane sheath. In the first case, it would be inaccurate to assume that thin processes indicated an immature stage of glial-axonal contact.

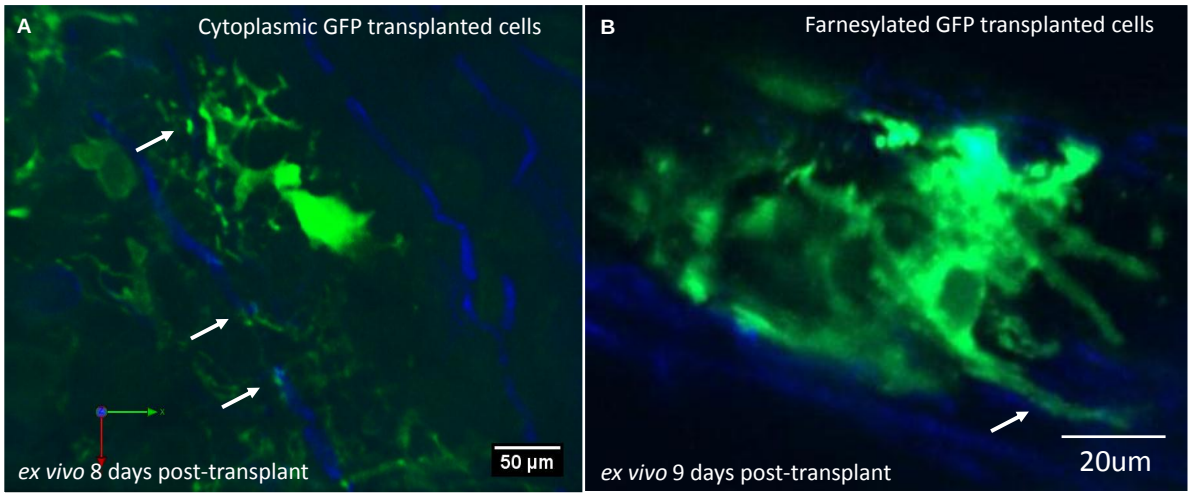

Figure 6.8 *ex vivo* imaging of spinal cords from Thy1-CFPshi/shiv* mice transplanted with cGFP and fGFP-labelled cells respectively**

A) Eight days post-transplantation cGFP-positive cells were seen to extend processes making contacts with the axons at several points (white arrows). B) Nine days post-transplantation fGFP-labelled cells were imaged to align with the CFP-labelled axons extending thick dense processes (white arrow). See supplementary videos 6.4 & 6.5. Representative images from at least 15 separate experiments.

6.2.9 *Ex vivo* time-lapse of glial-axonal interactions between cGFP-labelled cells and CFP-positive axons

6.2.9.1 Dynamic changes of the cGFP-processes

To examine the ability of the cGFP transplanted cells to make contact in real time with the CFP-positive axons, time-lapse was performed using the upright Zeiss 7MP multiphoton microscope, after transplantation of cGFP-labelled cells into the white matter of *Thy1*-CFP**shi/shiv* mice. The *ex vivo* spinal tissue was superfused in a close chamber with pre-warmed O_2-bubbled medium. To eliminate the possibility of drift, steady flow rates were applied and Z-stacks through 10-20 µm in depth were taken during the time course imaging.

Fifteen days after transplantation into *Thy1-CFP*shiv/shiv* mice, cGFP-labelled cells were visualised *ex vivo,* extending processes associated with several CFP-rendered axons in the

field of view. cGFP processes were imaged to align with the CFP-positive axons (red box, Fig. 6.9A). Real time observations showed dynamic changes in the cGFP processes and the area of CFP axons that they occupied. Over a time course of 20 min, cGFP-labelled cells imaged to contact the CFP axons at many points in an almost spiral way (red arrows, Fig. 6.9Bi), which later started to fill and cover larger areas of the axons (red arrow, Fig. 6.9Bii and Biii).

6.2.9.2 cGFP-transplanted cells rapidly remodelled their fine processes

Ex vivo imaging, showed that cGFP cells were densely associated with the CFP-axons (Fig. 6.10A). Time-lapse sequence 15 days post-transplantation showed that cGFP cell process activity was highly dynamic. OPC-like cells bearing many fine processes retracted (Fig. 6.10B-C) and extended branches (Fig. 6.10D-E) within 2-4 min. The cGFP-processes retracted after having made initial contact with the CFP-positive axons. Therefore, process retraction and alteration occurred after apparent contacts between axons and cGFP-labelled glial cells.

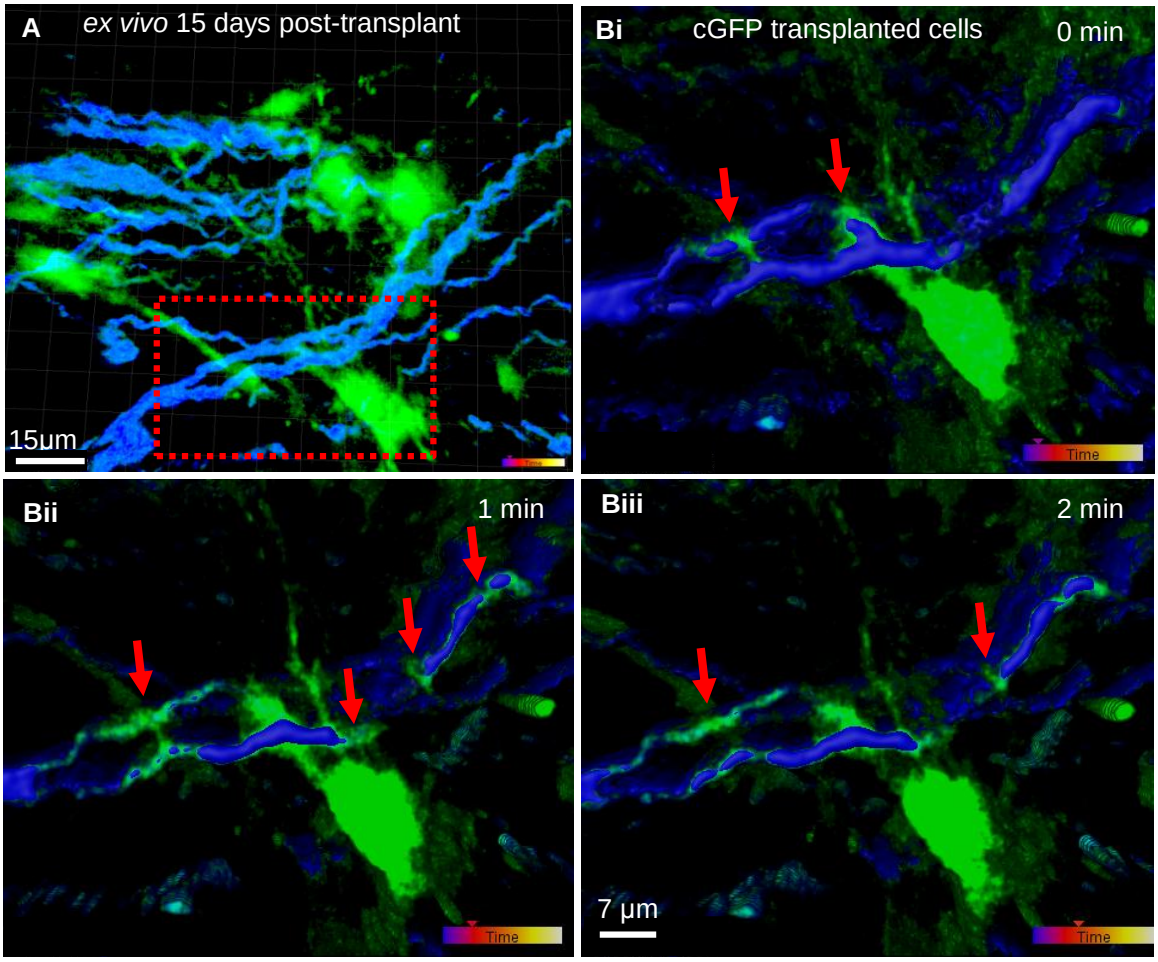

Figure 6.9 *ex vivo* imaging of glial-axonal interactions 15 days post-transplantation into a *Thy1*-CFPshi/shiv* mouse**

A) cGFP-expressing neurospheres were transplanted into a *shiverer* mouse expressing CFP under the *Thy1* promoter, *Thy1*-CFP**shi/shiv*. Z-stacks at 1 µm intervals were acquired using multiphoton microscopy of an *ex vivo* spinal cord at day 15 after transplantation and presented as a volume projection, over a time course of 20 min. cGFP positive processes extending from a cell body were seen to align with the CFP-positive axons. Z interval size was 1 µm. GFP and CFP were excited simultaneously at 860 nm. Bi-iii) Smoothed illustration after applying blend configuration in Imaris imaging software, showed colocalisation of cGFP-positive process with the CFP-positive axons over time. It can be seen that the GFP-positive cell process appears to extend over areas overlying axons. See supplementary video 6.6.

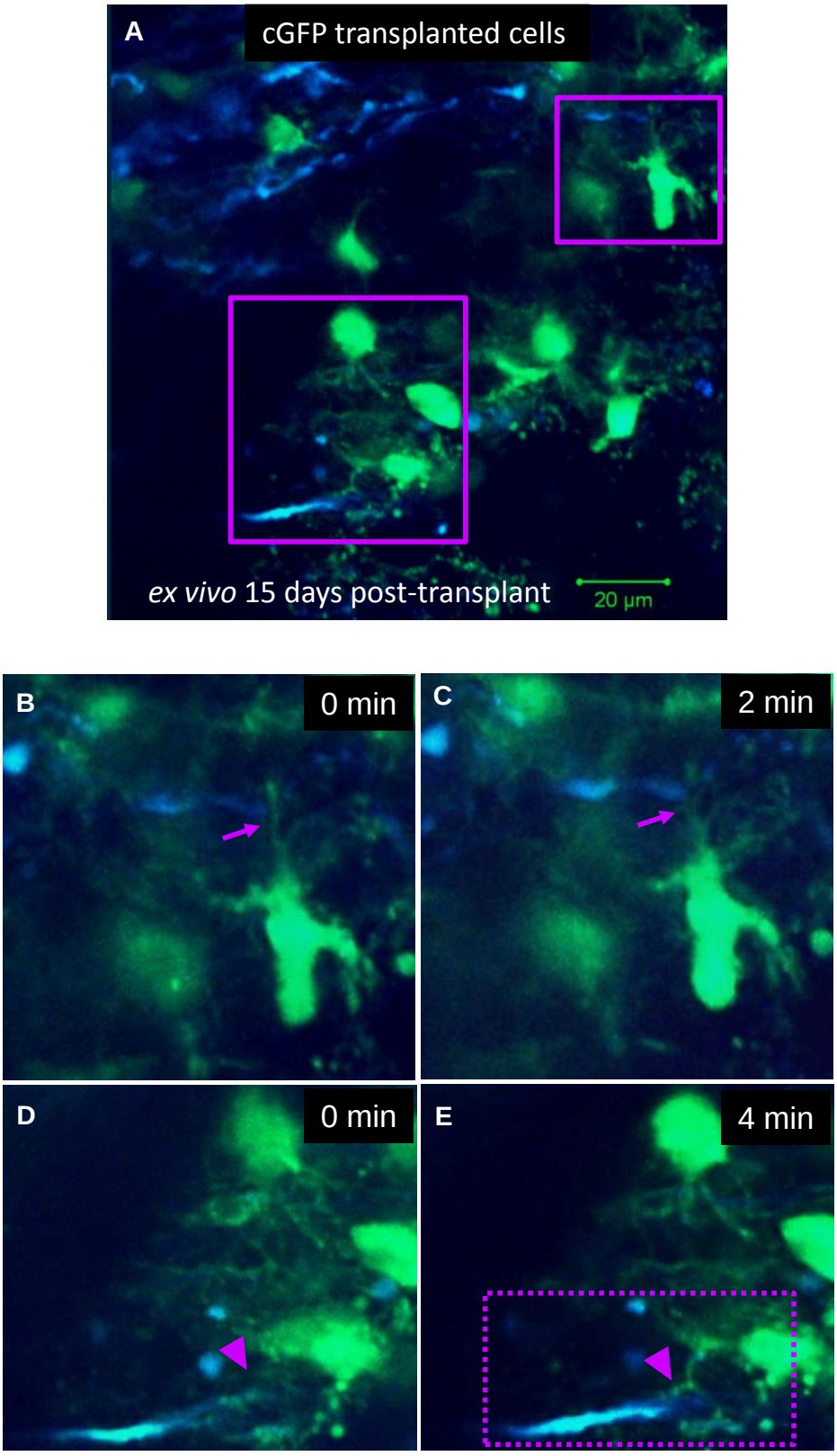

Figure 6.10 cGFP-labelled cells' processes were highly motile

A) cGFP-transplanted cells were constantly associated with the CFP-axons, 15 days post-transplantation into *Thy1*-CFP**shi/shiv* mouse. B-C) At 0 min in the time-lapse sequence, over a maximum projection with 1 µm step interval, a cGFP-positive cell extended a

process (purple arrow). This process withdrew back after 2 min. D-E) a cGFP-positive process (purple arrowhead, dotted box) extended rapidly within 4 min. Representative images from at least 3 separate experiments.

6.2.10 *Ex vivo* time-lapse of fGFP-labelled cells after transplantation into the spinal cord of *Thy1*-CFP**shi/shiv* mice

In order to follow glial-axonal interactions in real time, after transplantation of membrane-tethered GFP-labelled cells into *Thy1*-CFP**shi/shiv* mice, time-lapse imaging was performed over short periods. The technical challenges of identifying the transplantation point, since both CFP-positive axons and fGFP-transplanted cells appeared green under epifluorescence microscopy and the drift because of the superfusion process using the upright Zeiss 7MP multiphoton microscope, raised difficulties for the image acquisition. However, with high magnification multiphoton microscopy, it was possible to examine the association of membranous plasma processes of cells resembling oligodendrocytes and extract information about the early events before the wrapping of axons begins.

Analysis of the *ex vivo* cord 8 days post-transplantation of fGFP cells revealed the extension of flattened membranous processes around the CFP-positive axons (Fig. 6.11A). *ex vivo* imaging through a z-volume, demonstrated fGFP-labelled cells extending many branches and forming occasional membrane protrusions (Fig. 6.11B and C). In the *ex vivo* cord, fGFP-labelled cell processes appeared thicker compared to the cell processes of the cGFP labelled cells (Fig. 6.11D) and many fGFP-positive membrane protrusions were observed which were similar to those detected in the *in vitro* cultures.

6.2.11 *In vivo* imaging of the dynamics of cGFP-transplanted cells after transplantation into the spinal cord of *shiverer* nice

The ultimate aim to visualise the transplanted cells *in vivo* was possible despite the limitations and specific problems interfered with the steady image acquisition, in real time. These limitations were correlated with the anaesthesia, laminectomy without causing bleeding and problems such as heart beat and breathing, access of the *in vivo* spinal tissue and particularly of the transplantation area to the lens and survival of the mice during imaging. During the whole experiment, the mice were kept warm at 37^{o}C, with the aid of an infra-red lamp and a heated electrical blanket.

To assess the behaviour of the cGFP transplanted cells, *in vivo,* laminectomy was performed carefully and the mice were placed dorsally in a custom made V-shaped metallic plinth with adjustable legs and a small opening to allow the microscope lens to access the spinal cord. Special adjustable hooks stabilised the thoracic part of the spine, keeping the skin and muscles away from the opened segment of imaging. Repetitive administration of anaesthetic drugs every 2 hours, kept the heart beat and breathing relatively low to facilitate the acquisition of images during time-lapse. The mice survived excellent even after 5 hours of imaging.

In vivo time-lapse nine days post-transplantation, showed cGFP-labelled cells with long processes that resembled astrocytes (Fig. 6.12). During the whole period of imaging, the heart beat did not allow to record any changes or movements of either the cGFP processes or of the cell body.

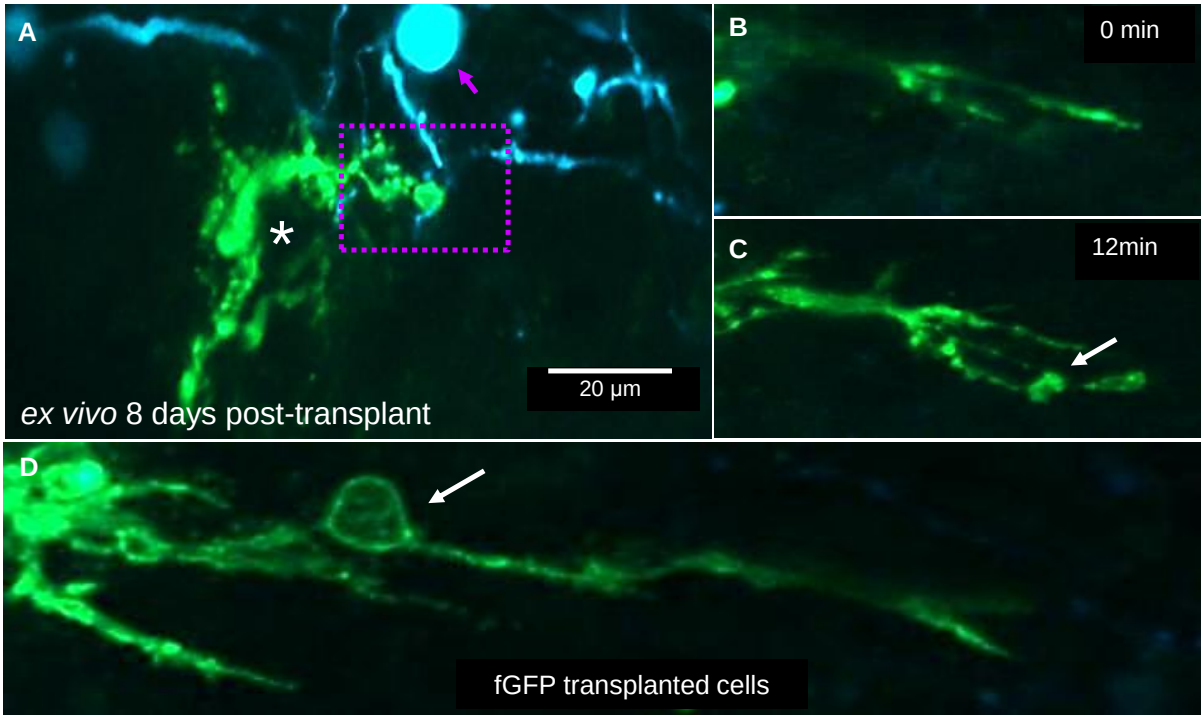

Figure 6.11 *ex vivo* imaging of fGFP-labelled cells and CFP-positive axons 8 days post-transplantation

A) fGFP-transplanted cells (asterisk) were imaged to extend flatten processes, making contact with the CFP-positive axons (dotted box), 8 days post-transplantation into *Thy1*-CFP**shi/shiv* mouse. In the same field of view, a neuronal body (purple arrow) was also imaged. B) fGFP processes were generally thick and formed "bubbles"(white arrow). C-D) Time-lapse imaging over a Z-stack, with 1 µm step size, showed fGFP-positive thick branches to be generated and to be extended with the formation of new "blebs" (white arrow). See supplementary video 6.7. Representative images from at least 2 separate experiments.

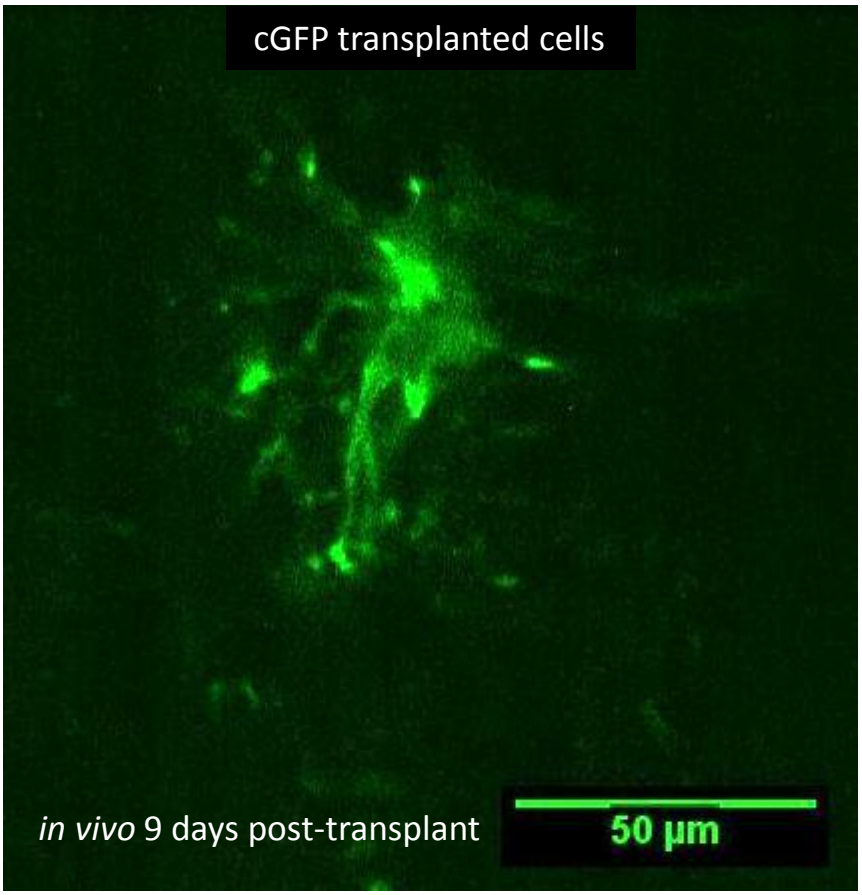

Figure 6.12 *in* vivo imaging of cGFP-labelled cells 9 days post-transplantation

In vivo time-lapse nine days post-transplantation, showed cGFP-labelled cells with long processes that resembled astrocytes. See supplementary video 6.8.

6.3 Discussion

To study the function of individual glial cells that are embedded in a complex neural network is difficult in living mice. However, direct observation of cells and their behaviours *in vivo*, have lately offered unique insight in the understanding of the nervous system function. Imaging the living brain has revealed unexpected details of the dynamics and the functional properties of neuronal, astrocytic and microglial structures under conditions following stimulation or injury (Davalos et al 2005, Grutzendler et al 2002, Nimmerjahn et al 2005). However, limited work has been performed on imaging the living spinal cord due to the close proximity of the animal's heart and lungs to the spinal column, resulting in artefacts generated by the heartbeat and breathing movements which significantly impede the acquisition of steady images from the spinal cord of anesthetised mice (Davalos et al 2008). As a result, imaging studies have been predominately performed on *ex vivo* spinal tissue (Kawakami et al 2005). Nevertheless, *in vivo* 2P-LSM was applied to simultaneously record central axons of projection neurons and microglia in the spinal cord (Dibaj et al 2010a, Dibaj et al 2010b). Moreover recently, *in vivo* imaging revealed distinct inflammatory activity of CNS microglia versus PNS macrophages in a mouse model for ALS (Dibaj et al 2011).

In this chapter, the main focus of experiments was to establish a protocol for *ex vivo* imaging of GFP-labelled cells after transplantation into the spinal cord of *shi/shi* mice initially and later of *Thy1*-CFP**shi/shiv* mice. The main aim was to assess and study the glial-axonal interactions in real time that could provide information about the initial contact before myelination happens in the CNS. In order to achieve this, it was necessary first to establish parameters to visualise axons in the dorsal columns of the spinal cord of *Thy1*-CFP mouse. Using multiphoton microscopy it was possible not only to image individual sparse labelled axons in the dorsal columns, but also neuronal bodies with a resolution approximately 1 μm. That was promising for the subsequent series of experiments to simultaneously visualise CFP-positive axons and GFP-transplanted cells *ex vivo.* That therefore underlined the basis to assess the interactions on axonal surfaces that comprised a moveable, macromolecular scaffold of glial cells.

Having extensively imaged fixed spinal cords after transplantation of cGFP cells into *shiverer* mice (Chapter 5), the next step was to image *ex vivo* the living spinal tissue using time-lapse. In order to achieve this, it was necessary first to establish parameters for

simultaneous visualisation of GFP-transplanted cells and CFP-positive axons. Challenges as the cross-talk of CFP and GFP, the signal form the second harmonic that generated from the connective tissue, such as collagen which was detected in the CFP channel, had to be overcome. With control samples and performing FLIM it was feasible to distinguish the real GFP signal and subsequently the GFP-positive cells with their processes from the CFP-positive neuronal bodies and axons, using multiphoton microscopy.

One of the most fundamental approaches of this research was to image the different expression of GFP in the transplanted cells. cGFP-labelled cells showed a different pattern in terms of morphology than fGFP cells. It was crucial to elucidate the spatial and temporal expression of the two above, in order to understand the process of myelination, where the biosynthetic mechanism of myelin membrane follows the extension of the plasma membrane of the myelinating oligodendrocyte. Myelin sheaths compose of mixed compacted and non-compacted segments. Therefore, using cGFP it was not possible to visualise compacted membrane. That was the main reason for using fGFP-labelled cells. So it is postulated that the constraint of proteins to the axonal surface, is accomplished in part by discriminative membrane-embedded filters and diffusion barriers, which serve to organise proteins after vesicular transport to oligodendrocyte plasma membrane (Pedraza et al 2001).

Ex vivo observation using the cGFP-labelled neurospheres for transplantation, revealed cells with clear distinct morphology (Fig. 6.14). There were cells with multiple fine processes emanating from the cell body and resembled oligodendrocytes when compared to those cells from immunohistochemical studies. On the other hand, cells with long asymmetrical processes were also imaged. In any case, although the morphology could refer to either oligodendrocytes or cells with long processes such as astrocytes, there was no clear evidence about the identity of the imaged cells. Time-lapse imaging after transplantation of cGFP cells, over short or longer time periods, through a maximum projection in Z, showed changes in the intensity of the GFP signal, possibly suggesting changes in the distribution of the cGFP cytoplasm. Furthermore, time sequence obtained from *ex vivo* spinal tissues, revealed changes in the area of the axon the cGFP-processes occupied.

Ex vivo observations after transplantation of fGFP cells into the spinal cord of *shiverer* mice, showed a rather different array of the membrane bound GFP expression. The fGFP

transplanted cells appeared with thicker and flatter processes than cGFP cells. Time-lapse imaging showed fGFP-positive extensions to fill spaces and fGFP cells to extend new branches in a longer time than cGFP. Moreover, fGFP cells seemed to form membranous protrusions, possibly carrying storage membrane to use for outgrowth and extension. Current concepts of lipid rafts, which propose the existence of micro-domains in membranes, might help to explain how proteins and lipids are delivered to the growing membrane (Munro 2003).

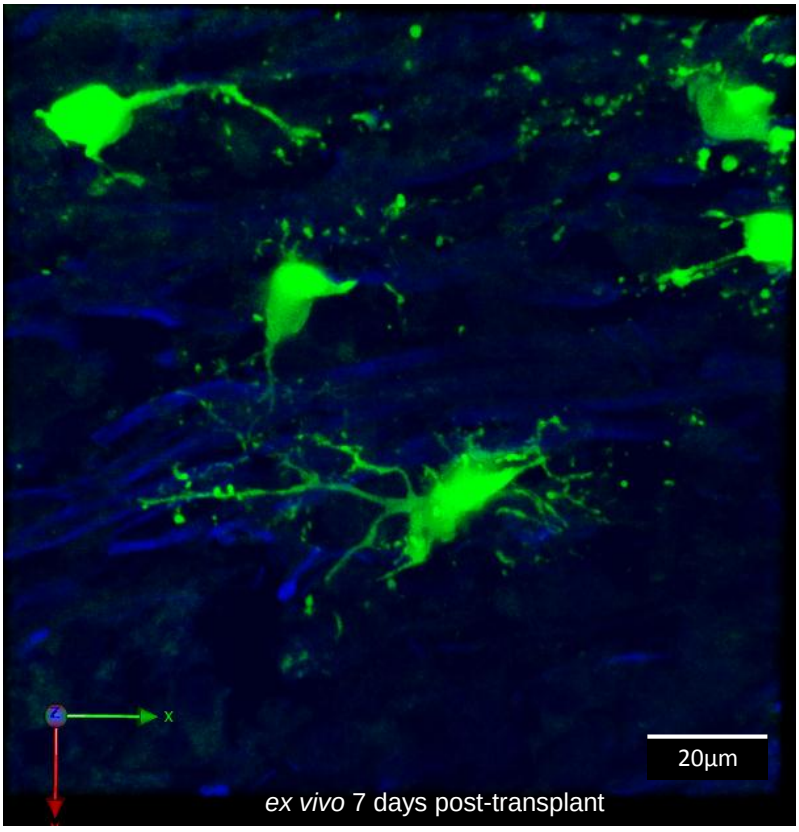

Figure 6.14 *Ex vivo* imaging of cGFP-labelled cells and CFP-positive axons 7 days post-transplantation

3D reconstruction of cGFP-transplanted cells that resembled oligodendrocytes were imaged to extend processes, making apparent contact with the CFP-positive axons. Representative image from at least 3 separate experiments.

From the *ex vivo* explants studies, image analysis provided evidence that glial transplanted cells established close physical contact with extensions or retractions of processes with the host axons. From other studies it was suggested that it is likely that the first axonal contacts

made by oligodendrocytes are through multiple filopodia, which overlap and extend along the axons for short distances to transform into the initial ensheathing processes. Hardy and Friedrich (1996) termed these “initiator processes” and suggested that multiple lamellae expanded circumferentially and simultaneously along the length of the axon, consistent with serial section EM analyses of axonal ensheathment (Remahl & Hildebrand 1990). Oligodendrocytes initially supported a few ensheathing processes and countless non-ensheathing processes or filopodia, which may or may not form axonal contacts later. These transitional oligodendrocytes developed into myelin-forming oligodendrocytes after a phase of considerable remodelling, during which the non-ensheathing processes were lost and only those forming axonal sheaths were retained to establish the definitive number of sheaths supported by the unit (Butt et al 1997).

Generally, the association between myelin-forming glia and the axons that they ensheath is a remarkable example of cell-cell interaction, not least because the paranodal axo-glial junction is by far the largest intercellular adhesion complex found in vertebrate biology. These processes are the result of a fascinating combination of mutual intercellular signalling and cell autonomous mechanisms (Sherman & Brophy 2005). However in this study, that association which included alignment of the GFP cells with the CFP-positive axons could not give much information that could efficiently explain the early pattern of myelin synthesis.

Last but not least, the *in vivo* studies although they were a substantial step towards the development of this project, overall did not provide enough data for the analysis of the dynamics of the transplanted cells into the spinal tissue. The spatial and temporal resolutions of these studies were limited. One could only deduce dynamic events associated with glial-axonal contact by comparing static images. Fundamental questions therefore remained unanswered, including how the oligodendrocytes extend their membrane and wrap the axons.

7. Discussion

Myelination is fundamentally a problem of topography: how is a single myelin strand as it has been observered in this thesis, transformed into a compact myelin sheath? In this study, the dynamic behaviour of oligodendroglia-like cells was demonstrated as they engage with axons in order to generate myelin-like sheaths, using time-lapse imaging of cells *in vitro* and *ex vivo*. Using cells expressing cGFP or fGFP it was possible to visualise cytoplasmic or membranous-aspects of oligodendroglia. Taken together the results suggested that oligodendrocyte processes engage with axons by wrapping, like the threads of a screw, around axons, before extending longitudinally (in relation to the length of the axon) to generate myelin internodes.

The discovery of neural stem cells in the adult mammalian brain (Reynolds & Weiss 1992) has allowed for the generation of oligodedrocytes and astrocytes in culture and also implicated their therapeutic application in CNS diseases (Sugaya 2005). Stem and progenitor cells from a wide range of sources, including murine, primate and human fetal or adult tissues have been used for myelination and remyelination studies (Cummings et al 2005, Keirstead et al 2005, Nistor et al 2005, Sasaki et al 2006). In this thesis, mouse striatum-derived neurospheres were extensively used to study myelination after transplantation into *shiverer* mice for the study of glial-axonal interactions that culminate in myelin compaction in the CNS.

The process of myelination is very complex and the visualisation of the way in which glial cells ensheath an axon is technically demanding, due in part to the complexity and dynamic nature of the process. However, advances in microscopic technology have allowed more detailed visualisation of this process. Although molecular studies have provided information about signalling molecules that regulate the various stages of myelination (Colman et al 1982, Laursen et al 2009), less is known about the dynamic changes in cell morphology that occur over time. It has been reported that an individual oligodendrocyte can generate up to 60 separate myelin sheaths (Pfeiffer et al 1993, Remahl & Hildebrand 1990), each from a single cell process spirally wrapping an axonal segment (Bunge et al 1962, Matthews & Duncan 1971, Uzman 1964). This fact precludes the possibility that the cell body could rotate around the axon in order to deposit myelin. Rather, formation of the spiralled myelin sheath must happen at the level of the cells' processes. Several theories

have been put forward. For example, the “carpet crawler” model, in which a sheet-like cell process embraces an axon and then the leading edge completes one turn synchronously around the entire internodal length, before moving under the growing sheet to form a second wrap (Bunge et al 1962, Hirano & Dembitzer 1967, Sobottka et al 2011). However, electron microscopy studies have shown that, at differenct locations along the length of a single developing internode, the number of wraps of membrane varies (Bunge et al 1961, Knobler et al 1976, Luse 1956, Remahl & Hildebrand 1990, Webster 1971, Werner & Jahn 2010). Thus, it is unlikely that myelination occurs through the synchronous wrapping of the leading edge of a single sheet-like process around the axon. For the same reason, the possibility that the sheath grows from the outer loop and rotates around the axon as a rigid cylinder constantly thickening radially and elongating at both ends, has also been dismissed (Hirano & Dembitzer 1967).

There have been various methods proposed to study myelination. Recently, a new method was described to model CNS myelination *in vitro*. According to this, exogenous rat oligodendrocytes precursor cells were added to DRG neurons that had grown for 7 days on highly restrictive micro-patterned substrates (10 μm Matrigel lines separated by 110 μm non-adhesive PLL-g-PEG strips). Co-cultures were fixed and stained after a further 7 days. Under these conditions, OPCs lose their bipolar morphology, acquire the characteristic multiple-process geometry of mature oligodendrocytes and express late differentiation markers: RIP and MBP. From observations, these cells were capable of engaging and enwrapping multiple axons from two or more different Matrigel lines and by scanning electron microscopy a substantial amount of plasma membrane appeared to wrap around the neurites in a similar way as it was described in this thesis. A major advantage of this system is that the microcontact printing (μCP) is done on top of glass coverslips; therefore, it can readily be adapted to glass-bottom cell-culture dishes which, in conjunction with inverted microscopy, permit live-cell imaging. In this context, the limited number of axons and myelinating cells in each Matrigel line would facilitate the characterisation of morphological and biomechanical events that occur both during axonal ensheathment and myelin compaction (Liazoghli et al 2012).

In vitro and *ex vivo* observations

Confocal imaging of myelinating culture system described in this thesis, after fixation, labelled with cell specific cytoplasmic and/or membrane markers, cGFP, PLP/DM20 or the

O4 antibody, allowed the observation of initial spirals of the oligodendrocyte membrane around neurites. At progressively later stages, gaps between spirals appeared to fill in with membrane, evetually forming a solid sheath-like structure that stained intensely with PLP/DM20 or MBP. Since cGFP could be localised in the inner and outer loops of the oligodendrocyte and does not reflect all of the membrane, cGFP labelled cells were labelled with the O4 surface myelin marker to determine if the markers colocalised. In Fig. 3.8 anti-GFP and the O4 antibody labelled cytoplasm-filled processes along the length of the axon, forming a network of cGFP spirals, which were not always localised with-PLP/DM20. PLP/DM20 staining appeared to be more uniform, while spirals of cGFP were in general much narrower (see also Fig. 3.8D). Taking a series of stacked images of cells labelled with anti-GFP and anti-PLP/DM20 and of confocal images after transplantation of cGFP cells into the *shiverer* MBP-deficient spinal cord, it was possible to follow the cGFP-filled spirals of membrane. This lead to hypothesis that an adaxonal or abaxonal cytoplasmic loop of the oligodendrocyte was being visualised as a spiral rather than the classical straight line that is usually depicted on the myelinated axon (see Schematic in Fig. 3.10J and Fig. 7.1).

To determine if more information could be obtained on the initial interaction of oligodendrocytes and axons, time-lapse imaging of *shiverer* myelinating cultures was performed, in which cGFP-labelled neurospheres were added. Cells that were morphologically similar to OPCs could be seen to continually extend and retract processess, forming a motile network of processes over the nerve bundles as well as rapidly moving along nerve fascicles. This suggest that the cytoplasmic spirals visualised using immunocytochemistry, were initially formed by OPC-like cells moving rapidly over the surface of nerve fibres, throwing out processes and forming many membranous protusions. Nonetheless, within the time frame in which imaging was carried out, it was not possible to distinguish between what may be transient explorations of axons by glial processes and what appear to be permanent or semi-permanent structures.

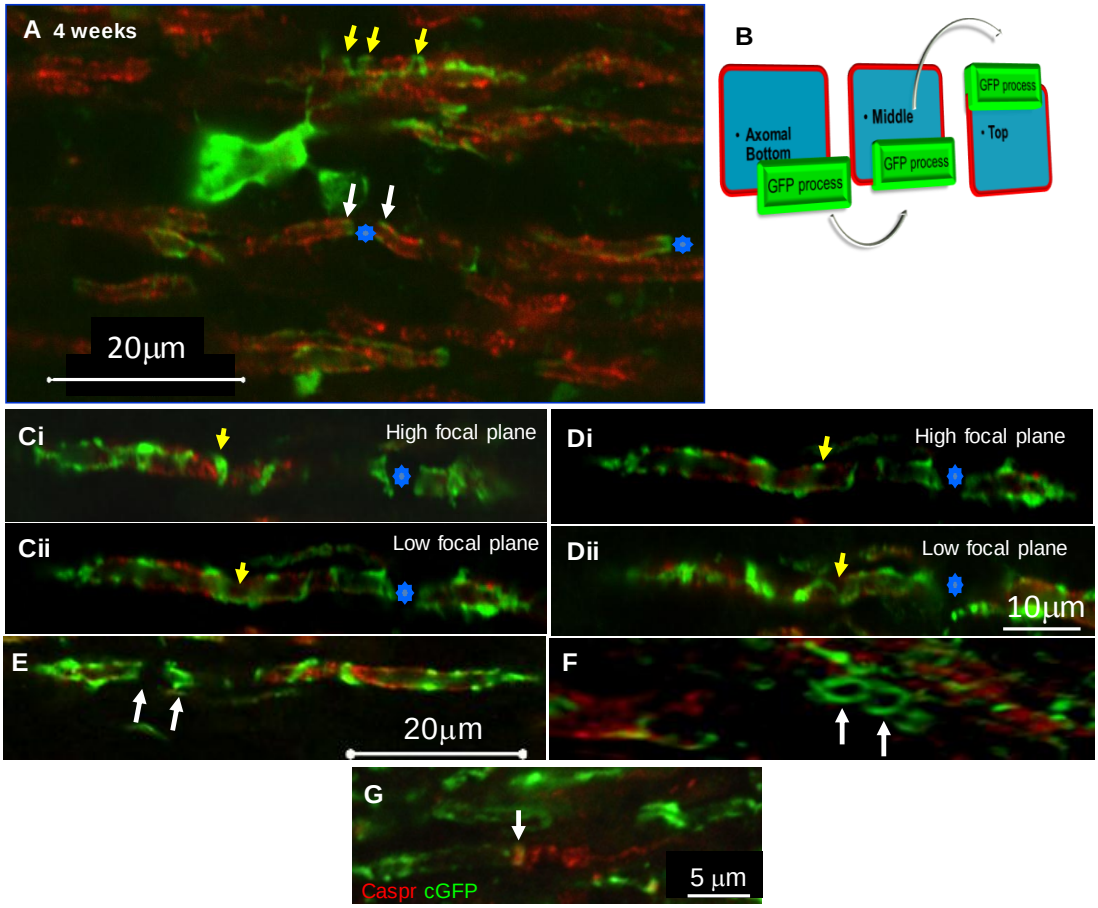

Figure 7.1 Confocal images of transplanted cGFP-expressing cells in the shiverer spinal cord

Four weeks after transplantation of cGFP-expressing neurospheres, fixed sections of the *shiverer* spinal cord were immunolabelled for MBP (red) and GFP (green). A) A cGFP labelled cell appears to extend spirals of cytoplasm around an MBP-positive myelin-like sheath (yellow arrows). Below the cell body, cGFP is seen at the lateral edges (in relation to the long axis of the sheaths, white arrows) of adjacent sheaths and probably represents the cytoplasm filled paranodal loops on either side of the node of Ranvier (asterisks). B) Schematic of visualisation of the sections in C and D. Ci-ii and Di-ii) Spiral of GFP cytoplasm was followed by focussing up and down through the plane of view where they crossed up, traversed the axonal surface, then crossed down again representing the looping as shown in the schematic in B. E-G) 3D reconstruction of cGFP structures (E), illustrates cGFP either side of a space typical of a node of Ranvier (white arrows). F) is a tilted perspective of E) and shows the cGFP form complete rings (white arrows representing the same position in E), consistent with the morphology of paranodal loops. I) Asymmetric Caspr-positive structures in association with cGFP, at either side of a heminode. On the

left, Caspr forms a single vertical line and colocalises with cGFP from the myelinating cell. On the right, Caspr appears like a loose coil, consistent with its pattern of expression in non-myelinated axons. All images were acquired using an Olympus FV1000 confocal microscope (x60, 1.35NA). Representative images from at least 10 separate experiments.

Time-lapse imaging of fGFP neurospheres added to *shiverer* myelinating cultures, demonstrated dynamic changes in the oligodendrocyte membrane over time. Two distinct processes were visualised; i) In the first example of glial-axonal interactions, the glial process wrapped an axon with a myelin-like sheath. The changes were very dynamic and bubbles or protrusions of membrane were observed moving along neurites. When cultures were immunolabelled with differentiation markers at the end of the experiments, MBP-positive GFP-positive membrane extrusions could be detected, suggesting they contained cytoplasmic MBP. It is possible that these protrusions were generated by actomyosin based contractility which pushed the plasma membrane forward before it moved over the axon as a sheath (Ridley 2011). ii) The fGFP myelin like-sheath expanded radially over an axon in cuffs and in some cultures an apparent myelin sheath extended longitudinally (in relation to the length of the axon) over time (Fig. 4.7 and 4.8). It has been suggested that myelin sheath extension (Sherman & Brophy 2005) could occur (i) through synchronous lateral growth of consecutive layers of the mature sheath or (ii) through longitudinal extension of consecutive sheaths as they slip over each other in the spring-like model or (iii) through the addition of consecutive, increasingly wide membrane sheets from the outer loop. The idea that the sheath grows from the external loop has largely been ruled out (Knobler et al 1976), therefore it seems most likely that extension occurs through growth of the sheath or its developing layers (whether it is one or more layers thick radially) at its lateral edge i.e. at the paranodal loops.

However, the energetics of CNS white matter are poorly understood. While the long-term energetic benefit of myelin in terms of action potential cost reduction is well described (Hartline & Colman 2007), little is known about how this compares to the initial energetic investment for building myelin or to the cost of maintaining the myelinating oligodendrocytes (Harris & Attwell 2012). But once myelinated, most of the volume of the axon is spatially remote from the extracellular space, prompting the suggestion that myelinated axons must receive metabolic support from the ensheathing glial cells (Nave

2010a). Myelin comprises a diverse set of lipids (Chrast et al 2011) and considering that only 25% of the myelin is protein (Jahn et al 2009), therefore the total ATP cost to synthesise the myelin is 3.30 x 10^{23} ATP molecules/g of myelin, ignoring though the energetic cost of wrapping the oligodendrocyte process around the axon (Harris & Attwell 2012) .

Electron microscopy studies of the CNS of rats during ensheathment and initial myelination showed cuffs of glial cytoplasm (Remahl & Hilderbrand 1990) which could represent the cytoplasmic cuffs seen in cultures and in fixed spinal cord after transplantation. It is demonstrated using a series of confocal imaging, that a spiral of GFP-cytoplasm appeared to be detected on top of a highly immunoreactive MBP-positive myelin-like sheath, in a ribbon–like structure (Fig. 3.8 and 7.1) and may resemble the model of Hirano and Dembitzer (Hirano & Dembitzer 1967), in which they propose that myelin formation can occur from isolated cytoplasmic islands which slip over each other to form myelin internodes. Thus, it has been suggested that a structure around the axon which is shaped like the coil of a spring ("serpent" model) is formed by a narrow oligodendroglial process that, once wrapping is complete, extends longitudinally (in relation to the axon) so that consecutive coils of the 'spring' slip over the one below [combination of hypotheses by (Hirano & Dembitzer 1967, Remahl & Hildebrand 1990) and reviewed in (Bauer et al 2009)]. By this mechanism, different numbers of wraps could occur at different internodal locales, in line with the electon microscopy data (Hirano & Dembitzer 1967). It has also been suggested that each myelin sheath is formed as many abutting glial processes flatten and fuse together. In this manner the myelin sheath is formed in a similar manner to a patchwork quilt of plasma membrane from many different processes (Bunge et al 1961, Luse 1956). Recently, a liquid croissant model of myelination was proposed which can explain some of the features observed in this study. In this model the authors take in to account the uneven contours of the developing myelin sheath but also suggest that the myelin sheath is thicker at the middle of the myelin internode than at the edges (Sobottka et al 2011). This latter feature was not oberved in the experiments of this thesis.

The use of *shiverer* myelinating cultures was very useful to characterise and manipulate CNS myelination *in vitro*. This method offered the possibility to explore the initial contact and intermediate stages of myelination between the oligodendrocytes and the axons and to identify certain features of this interaction. This involved spiral wrapping of the oligodendrocyte processes around the axons, thickenings of the oligodendrocyte

membrane, cytoplasmic cuffs, longitudinally extension that followed lateral expansion of the plasma membrane. Additionally, the study of the kinetics of the myelin-like membrane, extended during the initial and intermediate stages of the glial-axonal interactions, suggested the generation of protrusions and blebs that may explain partially how the new membrane is deposited to ensheath around the axons. The observations of this thesis, originated from at least 400 analysed time-lapse movies, from which approximately 75-100 were interpretative, gave an insight about the characteristic points of the glial-axonal interactions and established certain stages of the mechanism of oligodendrocyte ensheathment and myelination.

More specifically, the data reported in this study suggest myelination involves a series of dynamic interactions that begins with the initial contact of an OPC process that moves along neurites forming spirals of cytoplasm-filled membrane from which myelin membrane "fills-out", supporting the "serpent" model (Bauer et al 2009, Sobottka et al 2011). Further, real time imaging suggests this membrane sheath forms cuffs which thicken, join up and then extend along the axon. Live imaging experiments of this process should help to define events in oligodendroglial-axonal interactions and ensheathment and confirms results reported in the literature using electron microscopy. Thus, these data suggest that myelination involves a combination of previously proposed mechanisms but the "serpent" model mainly predominates with aspects of the "patchwork quilt" model, thereby termed the "ofiomosaic model" (=όφις+μωσαϊκό , Greek, meaning «snake» in its ancient Greek form and «mosaic») (Fig. 7.2). However, this model does not describe the mechanism of myelination per ce, as there is no solid proof whether the transplanted or exogenously added cells in culture are proper OPCs, ensheathing oligodendrocytes or mature myelin-forming oligodendrocytes, when interacting with the *shiverer* axons in real time imaging. Therefore, a method of purifying mouse OPCs and fluorescently labelled them before transplanting them to the *shiverer* spinal cord is essential for future experiments. Also, a number or molecules such as F3/contactin, Caspr/contactin which form a complex that is targeted to the paranodal junctions (Rios et al 2000) during myelination, synaptophysin, and transient expression of neurofascin by oligodendrocytes at the onset of myelination (Collinson et al 1998) should be investigated using the myelinating culture system, providing evidence of axonal recognition and myelin sheath formation.

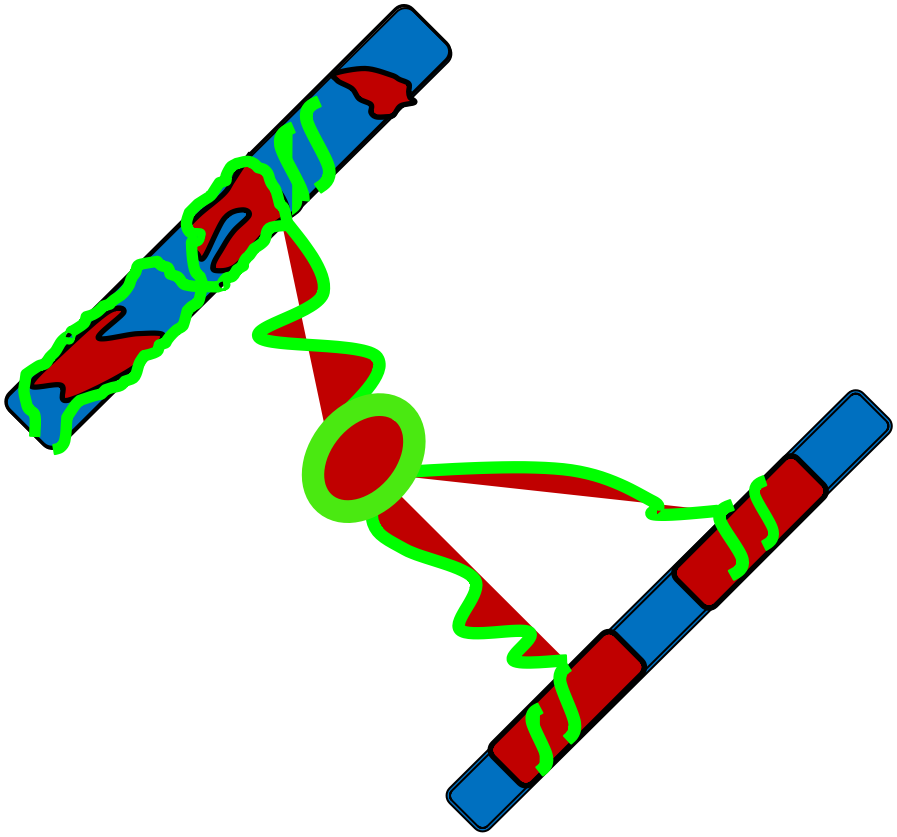

Figure 7.2 Schematic of initiate and intermediate stages of ensheathment

Initial contact of an oligodendrocyte process that moves along neurites (blue), forming spirals (green) of cytoplasm-filled membrane from which myelin membrane (red) “fills-out” from the ensheathing cuffs, described as the "ofiomosaic model".

Future work

Future work should include techniques to determine the mechanism of cytoplasm extension, using novel mutant mice. In addition, the right methodology should be developed to visualise cellular dynamics in the living mouse. More specifically, the following aims could shed light on the current observations towards the understanding of myelin ensheathment and the mechanism of myelination.

Aim 1: How do novel myelin gene mutations affect the dynamic early stages of glial-axonal interaction?

The integrity of the glial-axonal unit requires continual bidirectional signalling between the oligodendrocyte and the axon. Initial recognition and adhesion results in wrapping of the glial process around the axon (ensheathment) followed by the laying down of the multilamellar sheath. Cell adhesion molecules expressed by both axons and glial cells are known to play a crucial role in the establishment of glial-axonal contact and subsequent signalling to the oligodendrocyte, driving the process of myelination (Doyle & Colman 1993, Notterpek & Rome 1994). The myelinating glial cell triggers an axonal reaction, culminating in an increased phosphorylation of neurofilaments and regulation of the axonal diameter (de Waegh et al 1992, Hsieh et al 1994). Mature oligodendrocytes progressively associate GPI-anchored proteins, including the adhesion molecules NCAM 120 and F3 in the plasma membrane rafts. The microdomains in rafts include Fyn kinases, which are correlated with early stages of myelination. In the rafts, Fyn kinases are tightly associated with NCAM 120 and F3. Since the knowledge about the signals exchanged between axons and oligodendrocytes during myelination is incomplete, a role for oligodendroglial Fyn kinase (a nonreceptor tyrosine kinase of the Src family) could be investigated using the myelinating culture system. For this reason, specific mutant mice could be used to generate oligodendrocytes eg. from the *shiverer* mice (mutation in *MBP*) and/or Fyn-/-mice. It will be addressed whether oligodendrocytes generated from neurospheres from these mutant mice can still exhibit the dynamic changes (active protrusions and the event of blebs) seen for wild type cells. Neurospheres generated from the Fyn knockout mice could be infected with lentivirus containing fGFP and added to *shiverer* myelinating cultures to visualise cells during the initial stages of ensheathment and to investigate therefore if they form spirals, using time-lapse imaging.

Aim 2: Identification of the mechanism of wave formation and membrane rafts in the myelinating cultures

Moreover, since NCAM and Fyn has been reported in growth cones of neurons (Beggs et al 1997) the mechanism of Fyn kinase activation and signal transmission across the plasma membrane remains an open question. GPI-anchored proteins expressed by oligodendrocytes which are associated with the major myelin lipids galactocerebroside, sulfatide and cholesterol in membrane domains, colocalise with Fyn kinases, being most active at the beginning of myelination (Kramer et al 1999). For this purpose, Fyn-RFP mice could be used to visualise Fyn in the oligodendrocytes during myelination *in vitro*. The hypothesis is that during the initial stages of myelination the clustering of GPI-anchored proteins with cytoplasmic membrane-associated Fyn kinases, aggregate individual small rafts into larger domains, leading to a focal concentration of kinase activity at the cytoplasmic face of the membrane, suggesting a role of Fyn signalling during the initial phase of myelination. Moreover, inhibiting Fyn by adding specific inhibitors could prevent process outgrowth (Osterhout et al 1999) by Fyn-RFP oligodendrocytes added exogenously in the *shiverer* myelinating cultures. All these studies will focus on the formation of Fyn-RFP-positive rafts which will be assessed using time-lapse imaging and static images using confocal microscopy.

Aim 3: Can wave formation be visualised in live imaging of a mouse?

Using *ex vivo* tissue it has been demonstrated that it is possible to visualise changes in glial-axonal interactions in intact tissue. Initial studies visualising the dynamic glial-axonal interactions in the intact animal was promising and images of GFP-labelled oligodendrocytes were possible in a very similar manner to the *ex vivo* tissue. However, the identification of the GFP-transplated cells was extremely difficult and therefore following and imaging in real time oligodendrocyte-like cells was rather subjective. For this reason, mouse purified OPCs should be used transfected with fGFP lentivirus and then transplanted into the *shiverer* spinal cord.

Moreover, technical issues in data acquisition due to the mouse moving when breathing and heartbeat should overcome. It is necessary to modify the protocol as follows: lesion at T13 which decreases disturbances from breathing. In these cases, Thy1-CFP**shi/shiv* mice which previously received a graft of fGFP-labelled OPCs, 10 days previously, will be deeply anaesthetised with Ketamine-Xylasine mixture (100 mg/kg; 10 mg/kg) and the

spinal cord reopened to reveal the injection site. Animals will be kept freely breathing and warm at 36°C during imaging. Images will be taken as z-stack over time. In this manner the aim is to capture the membrane waves/protrusions in the intact mouse. In the first instance, a live mouse could be imaged and after imaging, the animal will be fixed (perfusion) to examine the viewed area from sections immunostained with classical oligodendroglial and neuronal markers (NG2, O4, PLP, MBP, SMI-31). Then, time-lapse movies will be generated with 1 to 1.5 min intervals between 3D stacks.

The long-term aim is to perform repetitive imaging of the same mouse. For these experiments after the initial imaging, the spinal cord surface will be protected by a thick layer of agarose and the skin sutured. It has been reported that this protocol can be repeated up to 6 times on the same mouse over a 4-month period, at various times (Dray et al 2009). However, if this procedure is not successful a novel innovative method will be used, in which imaging will be carried out via the naturally accessible intervertebral space (Kim et al 2010). In this method, the intervertebral connective tissue is thinned by dissection, sealed above with 2% low melting agarose and a cover glass placed over the area for visualisation. The ultimate aim is to follow oligodendrocyte processes extending and contacting axons in the CNS. Since previous results on *ex vivo* tissue suggest that images can be captured 10 days post-transplantation, imaging will occur on day 7 and 10 and 14.

List of References

Agrawal D, Hawk R, Avila RL, Inouye H, Kirschner DA. 2009. Internodal myelination during development quantitated using X-ray diffraction. *J Struct Biol* 168: 521-6

Albrecht PJ, Enterline JC, Cromer J, Levison SW. 2007. CNTF-activated astrocytes release a soluble trophic activity for oligodendrocyte progenitors. *Neurochem Res* 32: 263-71

Allamargot C, Pouplard-Barthelaix A, Fressinaud C. 2001. A single intracerebral microinjection of platelet-derived growth factor (PDGF) accelerates the rate of remyelination in vivo. *Brain research* 918: 28-39

Almeida RG, Czopka T, Ffrench-Constant C, Lyons DA. 2011. Individual axons regulate the myelinating potential of single oligodendrocytes in vivo. *Development* 138: 4443-50

Altevogt BM, Paul DL. 2004. Four classes of intercellular channels between glial cells in the CNS. *J Neurosci* 24: 4313-23

Althaus HH, Montz H, Neuhoff V, Schwartz P. 1984. Isolation and cultivation of mature oligodendroglial cells. *Naturwissenschaften* 71: 309-15

Asou H, Hamada K, Miyazaki T, Sakota T, Hayashi K, et al. 1995a. CNS myelinogenesis in vitro: time course and pattern of rat oligodendrocyte development. *J Neurosci Res* 40: 519-34

Asou H, Hamada K, Sakota T. 1995b. Visualization of a single myelination process of an oligodendrocyte in culture by video microscopy. *Cell structure and function* 20: 59-70

Asou H, Hamada K, Uyemura K, Sakota T, Hayashi K. 1994. How do oligodendrocytes ensheath and myelinate nerve fibers? *Brain Res Bull* 35: 359-65

Aspenstrom P, Fransson A, Saras J. 2004. Rho GTPases have diverse effects on the organization of the actin filament system. *Biochem J* 377: 327-37

Atterwill CK. 1987. Brain reaggregate cultures in neurotoxicological investigations: adaptational and neuroregenerative processes following lesions. *Molecular toxicology* 1: 489-502

Avellana-Adalid V, Nait-Oumesmar B, Lachapelle F, Baron-Van Evercooren A. 1996. Expansion of rat oligodendrocyte progenitors into proliferative "oligospheres" that retain differentiation potential. *J Neurosci Res* 45: 558-70

References

Back SA, Riddle A, McClure MM. 2007. Maturation-dependent vulnerability of perinatal white matter in premature birth. *Stroke; a journal of cerebral circulation* 38: 724-30

Bacon C, Lakics V, Machesky L, Rumsby M. 2007. N-WASP regulates extension of filopodia and processes by oligodendrocyte progenitors, oligodendrocytes, and Schwann cells-implications for axon ensheathment at myelination. *Glia* 55: 844-58

Bansal R, Stefansson K, Pfeiffer SE. 1992. Proligodendroblast antigen (POA), a developmental antigen expressed by A007/O4-positive oligodendrocyte progenitors prior to the appearance of sulfatide and galactocerebroside. *J Neurochem* 58: 2221-9

Barbarese E, Brumwell C, Kwon S, Cui H, Carson JH. 1999. RNA on the road to myelin. *J Neurocytol* 28: 263-70

Baron W, Hoekstra D. 2010. On the biogenesis of myelin membranes: sorting, trafficking and cell polarity. *FEBS letters* 584: 1760-70

Barres BA, Lazar MA, Raff MC. 1994. A novel role for thyroid hormone, glucocorticoids and retinoic acid in timing oligodendrocyte development. *Development* 120: 1097-108

Barres BA, Raff MC. 1994. Control of oligodendrocyte number in the developing rat optic nerve. *Neuron* 12: 935-42

Barres BA, Schmid R, Sendnter M, Raff MC. 1993. Multiple extracellular signals are required for long-term oligodendrocyte survival. *Development* 118: 283-95

Barros CS, Nguyen T, Spencer KS, Nishiyama A, Colognato H, Muller U. 2009. Beta1 integrins are required for normal CNS myelination and promote AKT-dependent myelin outgrowth. *Development* 136: 2717-24

Bauer NG, Richter-Landsberg C, Ffrench-Constant C. 2009. Role of the oligodendroglial cytoskeleton in differentiation and myelination. *Glia* 57: 1691-705

Baumann N, Pham-Dinh D. 2001. Biology of oligodendrocyte and myelin in the mammalian central nervous system. *Physiological reviews* 81: 871-927

Beggs HE, Baragona SC, Hemperly JJ, Maness PF. 1997. NCAM140 interacts with the focal adhesion kinase p125(fak) and the SRC-related tyrosine kinase p59(fyn). *J Biol Chem* 272: 8310-9

Ben-Hur T, Goldman SA. 2008. Prospects of cell therapy for disorders of myelin. *Ann N Y Acad Sci* 1142: 218-49

References

Ben-Hur T, Rogister B, Murray K, Rougon G, Dubois-Dalcq M. 1998. Growth and fate of PSA-NCAM+ precursors of the postnatal brain. *J Neurosci* 18: 5777-88

Bibollet-Bahena O, Almazan G. 2009. IGF-1-stimulated protein synthesis in oligodendrocyte progenitors requires PI3K/mTOR/Akt and MEK/ERK pathways. *J Neurochem* 109: 1440-51

Bignami A, Dahl D. 1974. Astrocyte-specific protein and radial glia in the cerebral cortex of newborn rat. *Nature* 252: 55-6

Bird TD, Farrell DF, Sumi SM. 1978. Brain lipid composition of the shiverer mouse: (genetic defect in myelin development). *J Neurochem* 31: 387-91

Bretscher MS. 1984. Endocytosis: relation to capping and cell locomotion. *Science* 224: 681-6

Brinkmann BG, Agarwal A, Sereda MW, Garratt AN, Muller T, et al. 2008. Neuregulin-1/ErbB signaling serves distinct functions in myelination of the peripheral and central nervous system. *Neuron* 59: 581-95

Bruzzone R, White TW, Paul DL. 1996. Connections with connexins: the molecular basis of direct intercellular signaling. *Eur J Biochem* 238: 1-27

Bunge MB, Bunge RP, Pappas GD. 1962. Electron microscopic demonstration of connections between glia and myelin sheaths in the developing mammalian central nervous system. *J Cell Biol* 12: 448-53

Bunge MB, Bunge RP, Ris H. 1961. Ultrastructural study of remyelination in an experimental lesion in adult cat spinal cord. *J Biophys Biochem Cytol* 10: 67-94

Bunge RP, Bunge MB, Bates M. 1989. Movements of the Schwann cell nucleus implicate progression of the inner (axon-related) Schwann cell process during myelination. *J Cell Biol* 109: 273-84

Buser AM, Erne B, Werner HB, Nave KA, Schaeren-Wiemers N. 2009. The septin cytoskeleton in myelinating glia. *Mol Cell Neurosci* 40: 156-66

Butler MG, Dasouki MJ, Zhou XP, Talebizadeh Z, Brown M, et al. 2005. Subset of individuals with autism spectrum disorders and extreme macrocephaly associated with germline PTEN tumour suppressor gene mutations. *J Med Genet* 42: 318-21

Butt AM, Ibrahim M, Berry M. 1997. The relationship between developing oligodendrocyte units and maturing axons during myelinogenesis in the anterior medullary velum of neonatal rats. *J Neurocytol* 26: 327-38

Butt AM, Ibrahim M, Berry M. 1998. Axon-myelin sheath relations of oligodendrocyte unit phenotypes in the adult rat anterior medullary velum. *J Neurocytol* 27: 259-69

References

Callizot N, Combes M, Steinschneider R, Poindron P. 2011. A new long term in vitro model of myelination. *Experimental cell research* 317: 2374-83

Calver AR, Hall AC, Yu WP, Walsh FS, Heath JK, et al. 1998. Oligodendrocyte population dynamics and the role of PDGF in vivo. *Neuron* 20: 869-82

Camara J, Wang Z, Nunes-Fonseca C, Friedman HC, Grove M, et al. 2009. Integrin-mediated axoglial interactions initiate myelination in the central nervous system. *J Cell Biol* 185: 699-712

Campagnoni AT, Macklin WB. 1988. Cellular and molecular aspects of myelin protein gene expression. *Mol Neurobiol* 2: 41-89

Canoll PD, Kraemer R, Teng KK, Marchionni MA, Salzer JL. 1999. GGF/neuregulin induces a phenotypic reversion of oligodendrocytes. *Mol Cell Neurosci* 13: 79-94

Caroni P. 1997. Overexpression of growth-associated proteins in the neurons of adult transgenic mice. *J Neurosci Methods* 71: 3-9

Carson MJ, Behringer RR, Brinster RL, McMorris FA. 1993. Insulin-like growth factor I increases brain growth and central nervous system myelination in transgenic mice. *Neuron* 10: 729-40

Centonze VE, White JG. 1998. Multiphoton excitation provides optical sections from deeper within scattering specimens than confocal imaging. *Biophys J* 75: 2015-24

Chalfie M, Tu Y, Euskirchen G, Ward WW, Prasher DC. 1994. Green fluorescent protein as a marker for gene expression. *Science* 263: 802-5

Chan A, Decard BF, Franke C, Grummel V, Zhou D, et al. 2010. Serum antibodies to conformational and linear epitopes of myelin oligodendrocyte glycoprotein are not elevated in the preclinical phase of multiple sclerosis. *Mult Scler* 16: 1189-92

Chan JR, Watkins TA, Cosgaya JM, Zhang C, Chen L, et al. 2004. NGF controls axonal receptivity to myelination by Schwann cells or oligodendrocytes. *Neuron* 43: 183-91

Chang A, Tourtellotte WW, Rudick R, Trapp BD. 2002. Premyelinating oligodendrocytes in chronic lesions of multiple sclerosis. *N Engl J Med* 346: 165-73

Charest PG, Firtel RA. 2007. Big roles for small GTPases in the control of directed cell movement. *Biochem J* 401: 377-90

Charras GT, Coughlin M, Mitchison TJ, Mahadevan L. 2008. Life and times of a cellular bleb. *Biophys J* 94: 1836-53

Chernoff GF. 1981. Shiverer: an autosomal recessive mutant mouse with myelin deficiency. *The Journal of heredity* 72: 128

References

Chrast R, Saher G, Nave KA, Verheijen MH. 2011. Lipid metabolism in myelinating glial cells: lessons from human inherited disorders and mouse models. *J Lipid Res* 52: 419-34

Collinson JM, Marshall D, Gillespie CS, Brophy PJ. 1998. Transient expression of neurofascin by oligodendrocytes at the onset of myelinogenesis: implications for mechanisms of axon-glial interaction. *Glia* 23: 11-23

Colman DR, Kreibich G, Frey AB, Sabatini DD. 1982. Synthesis and incorporation of myelin polypeptides into CNS myelin. *J Cell Biol* 95: 598-608

Compston A, Coles A. 2002. Multiple sclerosis. *Lancet* 359: 1221-31

Connor JR, Menzies SL. 1996. Relationship of iron to oligodendrocytes and myelination. *Glia* 17: 83-93

Crang AJ, Rumsby MG. 1977a. The labelling of lipid and protein components in isolated central-nervous-system myelin with dansyl chloride. *Biochem Soc Trans* 5: 110-2

Crang AJ, Rumsby MG. 1977b. Molecular organization of lipid and protein in the myelin sheath [proceedings]. *Biochem Soc Trans* 5: 1431-4

Cummings BJ, Uchida N, Tamaki SJ, Salazar DL, Hooshmand M, et al. 2005. Human neural stem cells differentiate and promote locomotor recovery in spinal cord-injured mice. *Proc Natl Acad Sci U S A* 102: 14069-74

Czopka T, Lyons DA. 2011. Dissecting mechanisms of myelinated axon formation using zebrafish. *Methods Cell Biol* 105: 25-62

Daskalakis NP, Claessens SE, Laboyrie JJ, Enthoven L, Oitzl MS, et al. 2011. The newborn rat's stress system readily habituates to repeated and prolonged maternal separation, while continuing to respond to stressors in context dependent fashion. *Horm Behav* 60: 165-76

Davalos D, Grutzendler J, Yang G, Kim JV, Zuo Y, et al. 2005. ATP mediates rapid microglial response to local brain injury in vivo. *Nat Neurosci* 8: 752-8

Davalos D, Lee JK, Smith WB, Brinkman B, Ellisman MH, et al. 2008. Stable in vivo imaging of densely populated glia, axons and blood vessels in the mouse spinal cord using two-photon microscopy. *J Neurosci Methods* 169: 1-7

de Vries H, Hoekstra D. 2000. On the biogenesis of the myelin sheath: cognate polarized trafficking pathways in oligodendrocytes. *Glycoconj J* 17: 181-90

de Waegh SM, Lee VM, Brady ST. 1992. Local modulation of neurofilament phosphorylation, axonal caliber, and slow axonal transport by myelinating Schwann cells. *Cell* 68: 451-63

References

Denk W, Strickler JH, Webb WW. 1990. Two-photon laser scanning fluorescence microscopy. *Science* 248: 73-6

Dibaj P, Nadrigny F, Steffens H, Scheller A, Hirrlinger J, et al. 2010a. NO mediates microglial response to acute spinal cord injury under ATP control in vivo. *Glia* 58: 1133-44

Dibaj P, Steffens H, Nadrigny F, Neusch C, Kirchhoff F, Schomburg ED. 2010b. Long-lasting post-mortem activity of spinal microglia in situ in mice. *J Neurosci Res* 88: 2431-40

Dibaj P, Steffens H, Zschuntzsch J, Nadrigny F, Schomburg ED, et al. 2011. In Vivo imaging reveals distinct inflammatory activity of CNS microglia versus PNS macrophages in a mouse model for ALS. *PLoS One* 6: e17910

Doetsch F, Garcia-Verdugo JM, Alvarez-Buylla A. 1997. Cellular composition and three-dimensional organization of the subventricular germinal zone in the adult mammalian brain. *J Neurosci* 17: 5046-61

Doyle JP, Colman DR. 1993. Glial-neuron interactions and the regulation of myelin formation. *Curr Opin Cell Biol* 5: 779-85

Dray C, Rougon G, Debarbieux F. 2009. Quantitative analysis by in vivo imaging of the dynamics of vascular and axonal networks in injured mouse spinal cord. *Proc Natl Acad Sci U S A* 106: 9459-64

Dugas JC, Cuellar TL, Scholze A, Ason B, Ibrahim A, et al. 2010. Dicer1 and miR-219 Are required for normal oligodendrocyte differentiation and myelination. *Neuron* 65: 597-611

Duncan ID. 2005. Oligodendrocytes and stem cell transplantation: their potential in the treatment of leukoencephalopathies. *J Inherit Metab Dis* 28: 357-68

Duncan ID, Goldman S, Macklin WB, Rao M, Weiner LP, Reingold SC. 2008. Stem cell therapy in multiple sclerosis: promise and controversy. *Mult Scler* 14: 541-6

Duncan ID, Kondo Y, Zhang SC. 2011. The myelin mutants as models to study myelin repair in the leukodystrophies. *Neurotherapeutics* 8: 607-24

Dyer CA, Benjamins JA. 1988. Antibody to galactocerebroside alters organization of oligodendroglial membrane sheets in culture. *J Neurosci* 8: 4307-18

Dziewulska D, Jamrozik Z, Podlecka A, Rafalowska J. 1999. Do astrocytes participate in rat spinal cord myelination? *Folia Neuropathol* 37: 81-6

Eckhardt M. 2008. The role and metabolism of sulfatide in the nervous system. *Mol Neurobiol* 37: 93-103

References

Edgar JM, Garbern J. 2004. The myelinated axon is dependent on the myelinating cell for support and maintenance: molecules involved. *J Neurosci Res* 76: 593-8

Edgar JM, McLaughlin M, Werner HB, McCulloch MC, Barrie JA, et al. 2009. Early ultrastructural defects of axons and axon-glia junctions in mice lacking expression of Cnp1. *Glia* 57: 1815-24

Edgar JM, McLaughlin M, Yool D, Zhang SC, Fowler JH, et al. 2004. Oligodendroglial modulation of fast axonal transport in a mouse model of hereditary spastic paraplegia. *J Cell Biol* 166: 121-31

Edgar JM, Nave KA. 2009. The role of CNS glia in preserving axon function. *Curr Opin Neurobiol* 19: 498-504

Egea G, Lazaro-Dieguez F, Vilella M. 2006. Actin dynamics at the Golgi complex in mammalian cells. *Curr Opin Cell Biol* 18: 168-78

Eilken HM, Adams RH. 2010. Dynamics of endothelial cell behavior in sprouting angiogenesis. *Curr Opin Cell Biol* 22: 617-25

Eng LF, Vanderhaeghen JJ, Bignami A, Gerstl B. 1971. An acidic protein isolated from fibrous astrocytes. *Brain Res* 28: 351-4

Feldmann A, Amphornrat J, Schonherr M, Winterstein C, Mobius W, et al. 2011. Transport of the major myelin proteolipid protein is directed by VAMP3 and VAMP7. *J Neurosci* 31: 5659-72

Feltri ML, Suter U, Relvas JB. 2008. The function of RhoGTPases in axon ensheathment and myelination. *Glia* 56: 1508-17

Feng G, Mellor RH, Bernstein M, Keller-Peck C, Nguyen QT, et al. 2000. Imaging neuronal subsets in transgenic mice expressing multiple spectral variants of GFP. *Neuron* 28: 41-51

Fox MA, Afshari FS, Alexander JK, Colello RJ, Fuss B. 2006. Growth conelike sensorimotor structures are characteristic features of postmigratory, premyelinating oligodendrocytes. *Glia* 53: 563-6

Fraher JP, Kaar GF, Bristol DC, Rossiter JP. 1988. Development of ventral spinal motoneurone fibres: a correlative study of the growth and maturation of central and peripheral segments of large and small fibre classes. *Progress in neurobiology* 31: 199-239

Francis DD, Champagne FA, Liu D, Meaney MJ. 1999. Maternal care, gene expression, and the development of individual differences in stress reactivity. *Ann N Y Acad Sci* 896: 66-84

References

Frank M, Schaeren-Wiemers N, Schneider R, Schwab ME. 1999. Developmental expression pattern of the myelin proteolipid MAL indicates different functions of MAL for immature Schwann cells and in a late step of CNS myelinogenesis. *J Neurochem* 73: 587-97

Franklin RJ, Ffrench-Constant C. 2008. Remyelination in the CNS: from biology to therapy. *Nat Rev Neurosci* 9: 839-55

Franklin RJ, Hinks GL. 1999. Understanding CNS remyelination: clues from developmental and regeneration biology. *J Neurosci Res* 58: 207-13

Friedl P, Gilmour D. 2009. Collective cell migration in morphogenesis, regeneration and cancer. *Nat Rev Mol Cell Biol* 10: 445-57

Frost EE, Zhou Z, Krasnesky K, Armstrong RC. 2009. Initiation of oligodendrocyte progenitor cell migration by a PDGF-A activated extracellular regulated kinase (ERK) signaling pathway. *Neurochem Res* 34: 169-81

Fuss B, Mallon B, Phan T, Ohlemeyer C, Kirchhoff F, et al. 2000. Purification and analysis of in vivo-differentiated oligodendrocytes expressing the green fluorescent protein. *Dev Biol* 218: 259-74

Gao L, Macklin W, Gerson J, Miller RH. 2006. Intrinsic and extrinsic inhibition of oligodendrocyte development by rat retina. *Dev Biol* 290: 277-86

Goebbels S, Oltrogge JH, Kemper R, Heilmann I, Bormuth I, et al. 2010. Elevated phosphatidylinositol 3,4,5-trisphosphate in glia triggers cell-autonomous membrane wrapping and myelination. *J Neurosci* 30: 8953-64

Golan N, Adamsky K, Kartvelishvily E, Brockschnieder D, Mobius W, et al. 2008. Identification of Tmem10/Opalin as an oligodendrocyte enriched gene using expression profiling combined with genetic cell ablation. *Glia* 56: 1176-86

Goldman D, Hankin M, Li Z, Dai X, Ding J. 2001. Transgenic zebrafish for studying nervous system development and regeneration. *Transgenic Res* 10: 21-33

Gow A, Southwood CM, Li JS, Pariali M, Riordan GP, et al. 1999. CNS myelin and sertoli cell tight junction strands are absent in Osp/claudin-11 null mice. *Cell* 99: 649-59

Grinspan JB, Edell E, Carpio DF, Beesley JS, Lavy L, et al. 2000. Stage-specific effects of bone morphogenetic proteins on the oligodendrocyte lineage. *Journal of neurobiology* 43: 1-17

Grinspan JB, Franceschini B. 1995. Platelet-derived growth factor is a survival factor for PSA-NCAM+ oligodendrocyte pre-progenitor cells. *J Neurosci Res* 41: 540-51

References

Grinspan JB, Stern JL, Pustilnik SM, Pleasure D. 1990. Cerebral white matter contains PDGF-responsive precursors to O2A cells. *J Neurosci* 10: 1866-73

Gruenenfelder FI, Thomson G, Penderis J, Edgar JM. 2011. Axon-glial interaction in the CNS: what we have learned from mouse models of Pelizaeus-Merzbacher disease. *J Anat* 219: 33-43

Grutzendler J, Kasthuri N, Gan WB. 2002. Long-term dendritic spine stability in the adult cortex. *Nature* 420: 812-6

Gumpel M, Gout O, Lubetzki C, Gansmuller A, Baumann N. 1989. Myelination and remyelination in the central nervous system by transplanted oligodendrocytes using the shiverer model. Discussion on the remyelinating cell population in adult mammals. *Dev Neurosci* 11: 132-9

Hadjantonakis AK, Dickinson ME, Fraser SE, Papaioannou VE. 2003. Technicolour transgenics: imaging tools for functional genomics in the mouse. *Nat Rev Genet* 4: 613-25

Hall A. 1998. Rho GTPases and the actin cytoskeleton. *Science* 279: 509-14

Harauz G, Ladizhansky V, Boggs JM. 2009. Structural polymorphism and multifunctionality of myelin basic protein. *Biochemistry* 48: 8094-104

Hardy R, Reynolds R. 1991. Proliferation and differentiation potential of rat forebrain oligodendroglial progenitors both in vitro and in vivo. *Development* 111: 1061-80

Hardy R, Reynolds R. 1993. Neuron-oligodendroglial interactions during central nervous system development. *J Neurosci Res* 36: 121-6

Hardy RJ, Friedrich VL, Jr. 1996. Progressive remodeling of the oligodendrocyte process arbor during myelinogenesis. *Dev Neurosci* 18: 243-54

Harrer MD, von Budingen HC, Stoppini L, Alliod C, Pouly S, et al. 2009. Live imaging of remyelination after antibody-mediated demyelination in an ex-vivo model for immune mediated CNS damage. *Experimental neurology* 216: 431-8

Harris JJ, Attwell D. 2012. The energetics of CNS white matter. *J Neurosci* 32: 356-71

Hartline DK, Colman DR. 2007. Rapid conduction and the evolution of giant axons and myelinated fibers. *Curr Biol* 17: R29-35

Hartman BK, Agrawal HC, Agrawal D, Kalmbach S. 1982. Development and maturation of central nervous system myelin: comparison of immunohistochemical localization of proteolipid protein and basic protein in myelin and oligodendrocytes. *Proc Natl Acad Sci U S A* 79: 4217-20

References

Hauser SL, Oksenberg JR. 2006. The neurobiology of multiple sclerosis: genes, inflammation, and neurodegeneration. *Neuron* 52: 61-76

Helmchen F, Denk W. 2005. Deep tissue two-photon microscopy. *Nat Methods* 2: 932-40

Herman GE, Butter E, Enrile B, Pastore M, Prior TW, Sommer A. 2007. Increasing knowledge of PTEN germline mutations: Two additional patients with autism and macrocephaly. *Am J Med Genet A* 143: 589-93

Hildebrand C, Waxman SG. 1984. Postnatal differentiation of rat optic nerve fibers: electron microscopic observations on the development of nodes of Ranvier and axoglial relations. *The Journal of comparative neurology* 224: 25-37

Hirano A, Dembitzer HM. 1967. A structural analysis of the myelin sheath in the central nervous system. *J Cell Biol* 34: 555-67

Hochstim C, Deneen B, Lukaszewicz A, Zhou Q, Anderson DJ. 2008. Identification of positionally distinct astrocyte subtypes whose identities are specified by a homeodomain code. *Cell* 133: 510-22

Howe CL. 2006. Coated glass and vicryl microfibers as artificial axons. *Cells Tissues Organs* 183: 180-94

Hsieh ST, Kidd GJ, Crawford TO, Xu Z, Lin WM, et al. 1994. Regional modulation of neurofilament organization by myelination in normal axons. *J Neurosci* 14: 6392-401

Huang JK, Jarjour AA, Nait Oumesmar B, Kerninon C, Williams A, et al. 2011. Retinoid X receptor gamma signaling accelerates CNS remyelination. *Nat Neurosci* 14: 45-53

Huttner WB, Zimmerberg J. 2001. Implications of lipid microdomains for membrane curvature, budding and fission. *Curr Opin Cell Biol* 13: 478-84

Ikonen E, Jansen M. 2008. Cellular sterol trafficking and metabolism: spotlight on structure. *Curr Opin Cell Biol* 20: 371-7

Ishibashi T, Dakin KA, Stevens B, Lee PR, Kozlov SV, et al. 2006. Astrocytes promote myelination in response to electrical impulses. *Neuron* 49: 823-32

Iturria-Medina Y, Perez Fernandez A, Valdes Hernandez P, Garcia Penton L, Canales-Rodriguez EJ, et al. 2011. Automated discrimination of brain pathological state attending to complex structural brain network properties: the shiverer mutant mouse case. *PLoS One* 6: e19071

Jaffe AB, Hall A. 2005. Rho GTPases: biochemistry and biology. *Annu Rev Cell Dev Biol* 21: 247-69

References

Jahn O, Tenzer S, Werner HB. 2009. Myelin proteomics: molecular anatomy of an insulating sheath. *Mol Neurobiol* 40: 55-72

Jahn R, Scheller RH. 2006. SNAREs--engines for membrane fusion. *Nat Rev Mol Cell Biol* 7: 631-43

Jarjour AA, Zhang H, Bauer N, Ffrench-Constant C, Williams A. 2011. In vitro modeling of central nervous system myelination and remyelination. *Glia*

Jean I, Allamargot C, Barthelaix-Pouplard A, Fressinaud C. 2002. Axonal lesions and PDGF-enhanced remyelination in the rat corpus callosum after lysolecithin demyelination. *Neuroreport* 13: 627-31

Jensen AM, Raff MC. 1997. Continuous observation of multipotential retinal progenitor cells in clonal density culture. *Dev Biol* 188: 267-79

Jessen KR. 2004. Glial cells. *The international journal of biochemistry & cell biology* 36: 1861-7

Jessen KR, Mirsky R. 2005. The origin and development of glial cells in peripheral nerves. *Nat Rev Neurosci* 6: 671-82

Kachar B, Behar T, Dubois-Dalcq M. 1986. Cell shape and motility of oligodendrocytes cultured without neurons. *Cell and tissue research* 244: 27-38

Kawakami N, Nagerl UV, Odoardi F, Bonhoeffer T, Wekerle H, Flugel A. 2005. Live imaging of effector cell trafficking and autoantigen recognition within the unfolding autoimmune encephalomyelitis lesion. *J Exp Med* 201: 1805-14

Keirstead HS, Nistor G, Bernal G, Totoiu M, Cloutier F, et al. 2005. Human embryonic stem cell-derived oligodendrocyte progenitor cell transplants remyelinate and restore locomotion after spinal cord injury. *J Neurosci* 25: 4694-705

Kerschensteiner M, Reuter MS, Lichtman JW, Misgeld T. 2008. Ex vivo imaging of motor axon dynamics in murine triangularis sterni explants. *Nat Protoc* 3: 1645-53

Kerschensteiner M, Schwab ME, Lichtman JW, Misgeld T. 2005. In vivo imaging of axonal degeneration and regeneration in the injured spinal cord. *Nat Med* 11: 572-7

Kessaris N, Fogarty M, Iannarelli P, Grist M, Wegner M, Richardson WD. 2006. Competing waves of oligodendrocytes in the forebrain and postnatal elimination of an embryonic lineage. *Nat Neurosci* 9: 173-9

Kettenmann H, Verkhratsky A. 2008. Neuroglia: the 150 years after. *Trends in neurosciences* 31: 653-9

Kettenmann H, Verkhratsky A. 2011. [Neuroglia - living nerve glue]. *Fortschritte der Neurologie-Psychiatrie* 79: 588-97

References

Kidd GJ, Hauer PE, Trapp BD. 1990. Axons modulate myelin protein messenger RNA levels during central nervous system myelination in vivo. *J Neurosci Res* 26: 409-18

Kim HJ, DiBernardo AB, Sloane JA, Rasband MN, Solomon D, et al. 2006. WAVE1 is required for oligodendrocyte morphogenesis and normal CNS myelination. *J Neurosci* 26: 5849-59

Kim JV, Jiang N, Tadokoro CE, Liu L, Ransohoff RM, et al. 2010. Two-photon laser scanning microscopy imaging of intact spinal cord and cerebral cortex reveals requirement for CXCR6 and neuroinflammation in immune cell infiltration of cortical injury sites. *J Immunol Methods* 352: 89-100

Kim SU. 1972. Formation of synapses and myelin sheaths in cultures of dissociated chick embryonic spinal cord. *Experimental cell research* 73: 528-30

Kirby BB, Takada N, Latimer AJ, Shin J, Carney TJ, et al. 2006. In vivo time-lapse imaging shows dynamic oligodendrocyte progenitor behavior during zebrafish development. *Nat Neurosci* 9: 1506-11

Knapp PE, Skoff RP, Redstone DW. 1986. Oligodendroglial cell death in jimpy mice: an explanation for the myelin deficit. *J Neurosci* 6: 2813-22

Knobler RL, Stempak JG, Laurencin M. 1974. Oligodendroglial ensheathment of axons during myelination in the developing rat central nervous system. A serial section electron microscopical sttudy. *Journal of ultrastructure research* 49: 34-49

Knobler RL, Stempak JG, Laurencin M. 1976. Nonuniformity of the oligodendroglial ensheathment of axons during myelination in the developing rat central nervous system. A serial section electron microscopical study. *Journal of ultrastructure research* 55: 417-32

Kolsch V, Charest PG, Firtel RA. 2008. The regulation of cell motility and chemotaxis by phospholipid signaling. *J Cell Sci* 121: 551-9

Komaki H, Sasaki M, Yamamoto T, Iai M, Takashima S. 1999. Connatal Pelizaeus-Merzbacher disease associated with the jimpy(msd) mice mutation. *Pediatr Neurol* 20: 309-11

Kondo Y, Wenger DA, Gallo V, Duncan ID. 2005. Galactocerebrosidase-deficient oligodendrocytes maintain stable central myelin by exogenous replacement of the missing enzyme in mice. *Proc Natl Acad Sci U S A* 102: 18670-5

Kramer-Albers EM, Gehrig-Burger K, Thiele C, Trotter J, Nave KA. 2006. Perturbed interactions of mutant proteolipid protein/DM20 with cholesterol and lipid rafts in

References

oligodendroglia: implications for dysmyelination in spastic paraplegia. *J Neurosci* 26: 11743-52

Kramer EM, Klein C, Koch T, Boytinck M, Trotter J. 1999. Compartmentation of Fyn kinase with glycosylphosphatidylinositol-anchored molecules in oligodendrocytes facilitates kinase activation during myelination. *J Biol Chem* 274: 29042-9

Kramer EM, Schardt A, Nave KA. 2001. Membrane traffic in myelinating oligodendrocytes. *Microsc Res Tech* 52: 656-71

Kronquist KE, Crandall BF, Macklin WB, Campagnoni AT. 1987. Expression of myelin proteins in the developing human spinal cord: cloning and sequencing of human proteolipid protein cDNA. *J Neurosci Res* 18: 395-401

Kumar NM, Gilula NB. 1996. The gap junction communication channel. *Cell* 84: 381-8

Kurokawa K, Itoh RE, Yoshizaki H, Nakamura YO, Matsuda M. 2004. Coactivation of Rac1 and Cdc42 at lamellipodia and membrane ruffles induced by epidermal growth factor. *Mol Biol Cell* 15: 1003-10

Lachapelle F, Gumpel M, Baulac M, Jacque C, Duc P, Baumann N. 1983. Transplantation of CNS fragments into the brain of shiverer mutant mice: extensive myelination by implanted oligodendrocytes. I. Immunohistochemical studies. *Dev Neurosci* 6: 325-34

Ladd CO, Owens MJ, Nemeroff CB. 1996. Persistent changes in corticotropin-releasing factor neuronal systems induced by maternal deprivation. *Endocrinology* 137: 1212-8

Lappe-Siefke C, Goebbels S, Gravel M, Nicksch E, Lee J, et al. 2003. Disruption of Cnp1 uncouples oligodendroglial functions in axonal support and myelination. *Nat Genet* 33: 366-74

Lassmann H. 2005. Multiple sclerosis pathology: evolution of pathogenetic concepts. *Brain Pathol* 15: 217-22

Laursen LS, Chan CW, ffrench-Constant C. 2009. An integrin-contactin complex regulates CNS myelination by differential Fyn phosphorylation. *J Neurosci* 29: 9174-85

LeVine SM, Wong D, Macklin WB. 1990. Developmental expression of proteolipid protein and DM20 mRNAs and proteins in the rat brain. *Dev Neurosci* 12: 235-50

Levison SW, Goldman JE. 1993. Both oligodendrocytes and astrocytes develop from progenitors in the subventricular zone of postnatal rat forebrain. *Neuron* 10: 201-12

Li F, Pincet F, Perez E, Eng WS, Melia TJ, et al. 2007a. Energetics and dynamics of SNAREpin folding across lipid bilayers. *Nat Struct Mol Biol* 14: 890-6

References

Li H, Lu Y, Smith HK, Richardson WD. 2007b. Olig1 and Sox10 interact synergistically to drive myelin basic protein transcription in oligodendrocytes. *J Neurosci* 27: 14375-82

Li X, Ionescu AV, Lynn BD, Lu S, Kamasawa N, et al. 2004. Connexin47, connexin29 and connexin32 co-expression in oligodendrocytes and Cx47 association with zonula occludens-1 (ZO-1) in mouse brain. *Neuroscience* 126: 611-30

Liazoghli D, Roth AD, Thostrup P, Colman DR. 2012. Substrate Micropatterning as a New in Vitro Cell Culture System to Study Myelination. *ACS Chem Neurosci* 3: 90-95

Liberto CM, Albrecht PJ, Herx LM, Yong VW, Levison SW. 2004. Pro-regenerative properties of cytokine-activated astrocytes. *J Neurochem* 89: 1092-100

Ligon KL, Fancy SP, Franklin RJ, Rowitch DH. 2006. Olig gene function in CNS development and disease. *Glia* 54: 1-10

Louis SA, Reynolds BA. 2005. Generation and differentiation of neurospheres from murine embryonic day 14 central nervous system tissue. *Methods Mol Biol* 290: 265-80

Lubetzki C, Demerens C, Anglade P, Villarroya H, Frankfurter A, et al. 1993. Even in culture, oligodendrocytes myelinate solely axons. *Proc Natl Acad Sci U S A* 90: 6820-4

Luse SA. 1956. Formation of myelin in the central nervous system of mice and rats, as studied with the electron microscope. *J Biophys Biochem Cytol* 2: 777-84

Machesky LM. 2002. Sharks' teeth and dunes. *Nature* 417: 494-7

Maglione M, Tress O, Haas B, Karram K, Trotter J, et al. 2010. Oligodendrocytes in mouse corpus callosum are coupled via gap junction channels formed by connexin47 and connexin32. *Glia* 58: 1104-17

Marmur R, Mabie PC, Gokhan S, Song Q, Kessler JA, Mehler MF. 1998. Isolation and developmental characterization of cerebral cortical multipotent progenitors. *Dev Biol* 204: 577-91

Matthews MA, Duncan D. 1971. A quantitative study of morphological changes accompanying the initiation and progress of myelin production in the dorsal funiculus of the rat spinal cord. *The Journal of comparative neurology* 142: 1-22

McCarthy KD, de Vellis J. 1980. Preparation of separate astroglial and oligodendroglial cell cultures from rat cerebral tissue. *J Cell Biol* 85: 890-902

McTigue DM, Tripathi RB. 2008. The life, death, and replacement of oligodendrocytes in the adult CNS. *J Neurochem* 107: 1-19

References

Michailov GV, Sereda MW, Brinkmann BG, Fischer TM, Haug B, et al. 2004. Axonal neuregulin-1 regulates myelin sheath thickness. *Science* 304: 700-3

Milner RJ, Lai C, Nave KA, Lenoir D, Ogata J, Sutcliffe JG. 1985. Nucleotide sequences of two mRNAs for rat brain myelin proteolipid protein. *Cell* 42: 931-9

Miron VE, Zehntner SP, Kuhlmann T, Ludwin SK, Owens T, et al. 2009. Statin therapy inhibits remyelination in the central nervous system. *Am J Pathol* 174: 1880-90

Misgeld T, Nikic I, Kerschensteiner M. 2007. In vivo imaging of single axons in the mouse spinal cord. *Nat Protoc* 2: 263-8

Miyamoto Y, Yamauchi J, Tanoue A. 2008. Cdk5 phosphorylation of WAVE2 regulates oligodendrocyte precursor cell migration through nonreceptor tyrosine kinase Fyn. *J Neurosci* 28: 8326-37

Moffett JR, Ross B, Arun P, Madhavarao CN, Namboodiri AM. 2007. N-Acetylaspartate in the CNS: from neurodiagnostics to neurobiology. *Prog Neurobiol* 81: 89-131

Molineaux SM, Engh H, de Ferra F, Hudson L, Lazzarini RA. 1986. Recombination within the myelin basic protein gene created the dysmyelinating shiverer mouse mutation. *Proc Natl Acad Sci U S A* 83: 7542-6

Moore CS, Milner R, Nishiyama A, Frausto RF, Serwanski DR, et al. 2011. Astrocytic tissue inhibitor of metalloproteinase-1 (TIMP-1) promotes oligodendrocyte differentiation and enhances CNS myelination. *J Neurosci* 31: 6247-54

Morell P, Jurevics H. 1996. Origin of cholesterol in myelin. *Neurochem Res* 21: 463-70

Morita K, Sasaki H, Fujimoto K, Furuse M, Tsukita S. 1999. Claudin-11/OSP-based tight junctions of myelin sheaths in brain and Sertoli cells in testis. *J Cell Biol* 145: 579-88

Mothe AJ, Kulbatski I, Parr A, Mohareb M, Tator CH. 2008. Adult spinal cord stem/progenitor cells transplanted as neurospheres preferentially differentiate into oligodendrocytes in the adult rat spinal cord. *Cell Transplant* 17: 735-51

Mothe AJ, Tator CH. 2008. Transplanted neural stem/progenitor cells generate myelinating oligodendrocytes and Schwann cells in spinal cord demyelination and dysmyelination. *Exp Neurol* 213: 176-90

Munro S. 2003. Lipid rafts: elusive or illusive? *Cell* 115: 377-88

Nagy JI, Dudek FE, Rash JE. 2004. Update on connexins and gap junctions in neurons and glia in the mammalian nervous system. *Brain Res Brain Res Rev* 47: 191-215

Nagy JI, Rash JE. 2000. Connexins and gap junctions of astrocytes and oligodendrocytes in the CNS. *Brain Res Brain Res Rev* 32: 29-44

References

Nair A, Frederick TJ, Miller SD. 2008. Astrocytes in multiple sclerosis: a product of their environment. *Cell Mol Life Sci* 65: 2702-20

Nash B, Ioannidou K, Barnett SC. 2011a. Astrocyte phenotypes and their relationship to myelination. *J Anat* 219: 44-52

Nash B, Thomson CE, Linington C, Arthur AT, McClure JD, et al. 2011b. Functional duality of astrocytes in myelination. *J Neurosci* 31: 13028-38

Nave KA. 2010a. Myelination and support of axonal integrity by glia. *Nature* 468: 244-52

Nave KA. 2010b. Myelination and the trophic support of long axons. *Nat Rev Neurosci* 11: 275-83

Nave KA, Lai C, Bloom FE, Milner RJ. 1987. Splice site selection in the proteolipid protein (PLP) gene transcript and primary structure of the DM-20 protein of central nervous system myelin. *Proc Natl Acad Sci U S A* 84: 5665-9

Nave KA, Salzer JL. 2006. Axonal regulation of myelination by neuregulin 1. *Curr Opin Neurobiol* 16: 492-500

Nave KA, Trapp BD. 2008. Axon-glial signaling and the glial support of axon function. *Annu Rev Neurosci* 31: 535-61

Nguyen T, Mehta NR, Conant K, Kim KJ, Jones M, et al. 2009. Axonal protective effects of the myelin-associated glycoprotein. *J Neurosci* 29: 630-7

Nikic I, Merkler D, Sorbara C, Brinkoetter M, Kreutzfeldt M, et al. 2011. A reversible form of axon damage in experimental autoimmune encephalomyelitis and multiple sclerosis. *Nat Med* 17: 495-9

Nimmerjahn A, Kirchhoff F, Helmchen F. 2005. Resting microglial cells are highly dynamic surveillants of brain parenchyma in vivo. *Science* 308: 1314-8

Nistor GI, Totoiu MO, Haque N, Carpenter MK, Keirstead HS. 2005. Human embryonic stem cells differentiate into oligodendrocytes in high purity and myelinate after spinal cord transplantation. *Glia* 49: 385-96

Norton WT, Poduslo SE. 1973. Myelination in rat brain: method of myelin isolation. *J Neurochem* 21: 749-57

Notterpek LM, Rome LH. 1994. Functional evidence for the role of axolemma in CNS myelination. *Neuron* 13: 473-85

Ogata T, Iijima S, Hoshikawa S, Miura T, Yamamoto S, et al. 2004. Opposing extracellular signal-regulated kinase and Akt pathways control Schwann cell myelination. *J Neurosci* 24: 6724-32

References

Ogawa T, Mikuni M, Kuroda Y, Muneoka K, Mori KJ, Takahashi K. 1994. Periodic maternal deprivation alters stress response in adult offspring: potentiates the negative feedback regulation of restraint stress-induced adrenocortical response and reduces the frequencies of open field-induced behaviors. *Pharmacol Biochem Behav* 49: 961-7

Ogawa T, Suzuki M, Matoh K, Sasaki K. 2004. Three-dimensional electron microscopic studies of the transitional oligodendrocyte associated with the initial stage of myelination in developing rat hippocampal fimbria. *Brain Res Dev Brain Res* 148: 207-12

Oheim M, Beaurepaire E, Chaigneau E, Mertz J, Charpak S. 2001. Two-photon microscopy in brain tissue: parameters influencing the imaging depth. *J Neurosci Methods* 111: 29-37

Okabe M, Ikawa M, Kominami K, Nakanishi T, Nishimune Y. 1997. 'Green mice' as a source of ubiquitous green cells. *FEBS letters* 407: 313-9

Orthmann-Murphy JL, Abrams CK, Scherer SS. 2008. Gap junctions couple astrocytes and oligodendrocytes. *J Mol Neurosci* 35: 101-16

Osterhout DJ, Wolven A, Wolf RM, Resh MD, Chao MV. 1999. Morphological differentiation of oligodendrocytes requires activation of Fyn tyrosine kinase. *J Cell Biol* 145: 1209-18

Osterhout JA, Josten N, Yamada J, Pan F, Wu SW, et al. 2011. Cadherin-6 mediates axon-target matching in a non-image-forming visual circuit. *Neuron* 71: 632-9

Padovani-Claudio DA, Liu L, Ransohoff RM, Miller RH. 2006. Alterations in the oligodendrocyte lineage, myelin, and white matter in adult mice lacking the chemokine receptor CXCR2. *Glia* 54: 471-83

Paez PM, Fulton D, Colwell CS, Campagnoni AT. 2009. Voltage-operated Ca(2+) and Na(+) channels in the oligodendrocyte lineage. *J Neurosci Res* 87: 3259-66

Pastores GM. 2009. Krabbe disease: an overview. *Int J Clin Pharmacol Ther* 47 Suppl 1: S75-81

Patterson G, Day RN, Piston D. 2001. Fluorescent protein spectra. *J Cell Sci* 114: 837-8

Patzig J, Jahn O, Tenzer S, Wichert SP, de Monasterio-Schrader P, et al. 2011. Quantitative and integrative proteome analysis of peripheral nerve myelin identifies novel myelin proteins and candidate neuropathy loci. *J Neurosci* 31: 16369-86

References

Pedraza L, Huang JK, Colman D. 2009. Disposition of axonal caspr with respect to glial cell membranes: Implications for the process of myelination. *J Neurosci Res* 87: 3480-91

Pedraza L, Huang JK, Colman DR. 2001. Organizing principles of the axoglial apparatus. *Neuron* 30: 335-44

Peters A. 1960. The formation and structure of myelin sheaths in the central nervous system. *J Biophys Biochem Cytol* 8: 431-46

Pfeiffer SE, Warrington AE, Bansal R. 1993. The oligodendrocyte and its many cellular processes. *Trends Cell Biol* 3: 191-7

Piaton G, Aigrot MS, Williams A, Moyon S, Tepavcevic V, et al. 2011. Class 3 semaphorins influence oligodendrocyte precursor recruitment and remyelination in adult central nervous system. *Brain : a journal of neurology* 134: 1156-67

Piaton G, Gould RM, Lubetzki C. 2010. Axon-oligodendrocyte interactions during developmental myelination, demyelination and repair. *J Neurochem* 114: 1243-60

Pollard TD, Borisy GG. 2003. Cellular motility driven by assembly and disassembly of actin filaments. *Cell* 112: 453-65

Potter GB, Rowitch DH, Petryniak MA. 2011. Myelin restoration: progress and prospects for human cell replacement therapies. *Arch Immunol Ther Exp (Warsz)* 59: 179-93

Privat A, Jacque C, Bourre JM, Dupouey P, Baumann N. 1979. Absence of the major dense line in myelin of the mutant mouse "shiverer". *Neuroscience letters* 12: 107-12

Raff MC, Abney ER, Cohen J, Lindsay R, Noble M. 1983a. Two types of astrocytes in cultures of developing rat white matter: differences in morphology, surface gangliosides, and growth characteristics. *J Neurosci* 3: 1289-300

Raff MC, Miller RH, Noble M. 1983b. Glial cell lineages in the rat optic nerve. *Cold Spring Harbor symposia on quantitative biology* 48 Pt 2: 569-72

Raff MC, Miller RH, Noble M. 1983c. A glial progenitor cell that develops in vitro into an astrocyte or an oligodendrocyte depending on culture medium. *Nature* 303: 390-6

Rasband MN. 2006. Neuron-glia interactions at the node of Ranvier. *Results Probl Cell Differ* 43: 129-49

Raval-Fernandes S, Rome LH. 1998. Role of axonal components during myelination. *Microsc Res Tech* 41: 379-92

References

Readhead C, Popko B, Takahashi N, Shine HD, Saavedra RA, et al. 1987. Expression of a myelin basic protein gene in transgenic shiverer mice: correction of the dysmyelinating phenotype. *Cell* 48: 703-12

Remahl S, Hildebrand C. 1982. Changing relation between onset of myelination and axon diameter range in developing feline white matter. *Journal of the neurological sciences* 54: 33-45

Remahl S, Hildebrand C. 1990. Relations between axons and oligodendroglial cells during initial myelination. II. The individual axon. *J Neurocytol* 19: 883-98

Remahl S, Hilderbrand C. 1990. Relation between axons and oligodendroglial cells during initial myelination. I. The glial unit. *J Neurocytol* 19: 313-28

Reynolds BA, Rietze RL. 2005. Neural stem cells and neurospheres--re-evaluating the relationship. *Nat Methods* 2: 333-6

Reynolds BA, Weiss S. 1992. Generation of neurons and astrocytes from isolated cells of the adult mammalian central nervous system. *Science* 255: 1707-10

Reynolds BA, Weiss S. 1996. Clonal and population analyses demonstrate that an EGF-responsive mammalian embryonic CNS precursor is a stem cell. *Dev Biol* 175: 1-13

Reynolds R, Wilkin GP. 1988. Development of macroglial cells in rat cerebellum. II. An in situ immunohistochemical study of oligodendroglial lineage from precursor to mature myelinating cell. *Development* 102: 409-25

Richardson WD, Smith HK, Sun T, Pringle NP, Hall A, Woodruff R. 2000. Oligodendrocyte lineage and the motor neuron connection. *Glia* 29: 136-42

Ridley AJ. 2006. Rho GTPases and actin dynamics in membrane protrusions and vesicle trafficking. *Trends Cell Biol* 16: 522-9

Ridley AJ. 2011. Life at the leading edge. *Cell* 145: 1012-22

Rios JC, Melendez-Vasquez CV, Einheber S, Lustig M, Grumet M, et al. 2000. Contactin-associated protein (Caspr) and contactin form a complex that is targeted to the paranodal junctions during myelination. *J Neurosci* 20: 8354-64

Rivers LE, Young KM, Rizzi M, Jamen F, Psachoulia K, et al. 2008. PDGFRA/NG2 glia generate myelinating oligodendrocytes and piriform projection neurons in adult mice. *Nat Neurosci* 11: 1392-401

Roach A, Takahashi N, Pravtcheva D, Ruddle F, Hood L. 1985. Chromosomal mapping of mouse myelin basic protein gene and structure and transcription of the partially deleted gene in shiverer mutant mice. *Cell* 42: 149-55

References

Rodriguez-Pena A. 1999. Oligodendrocyte development and thyroid hormone. *J Neurobiol* 40: 497-512

Rosenberg SS, Kelland EE, Tokar E, De la Torre AR, Chan JR. 2008. The geometric and spatial constraints of the microenvironment induce oligodendrocyte differentiation. *Proc Natl Acad Sci U S A* 105: 14662-7

Rosenbluth J. 1980. Central myelin in the mouse mutant shiverer. *J Comp Neurol* 194: 639-48

Rowitch DH. 2004. Glial specification in the vertebrate neural tube. *Nat Rev Neurosci* 5: 409-19

Saher G, Brugger B, Lappe-Siefke C, Mobius W, Tozawa R, et al. 2005. High cholesterol level is essential for myelin membrane growth. *Nat Neurosci* 8: 468-75

Saher G, Quintes S, Nave KA. 2011. Cholesterol: a novel regulatory role in myelin formation. *Neuroscientist* 17: 79-93

Salzer JL, Brophy PJ, Peles E. 2008. Molecular domains of myelinated axons in the peripheral nervous system. *Glia* 56: 1532-40

Sarret C, Combes P, Micheau P, Gelot A, Boespflug-Tanguy O, Vaurs-Barriere C. 2010. Novel neuronal proteolipid protein isoforms encoded by the human myelin proteolipid protein 1 gene. *Neuroscience* 166: 522-38

Sasaki M, Black JA, Lankford KL, Tokuno HA, Waxman SG, Kocsis JD. 2006. Molecular reconstruction of nodes of Ranvier after remyelination by transplanted olfactory ensheathing cells in the demyelinated spinal cord. *J Neurosci* 26: 1803-12

Schindler P, Luu B, Sorokine O, Trifilieff E, Van Dorsselaer A. 1990. Developmental study of proteolipids in bovine brain: a novel proteolipid and DM-20 appear before proteolipid protein (PLP) during myelination. *J Neurochem* 55: 2079-85

Schnadelbach O, Ozen I, Blaschuk OW, Meyer RL, Fawcett JW. 2001. N-cadherin is involved in axon-oligodendrocyte contact and myelination. *Mol Cell Neurosci* 17: 1084-93

Seggie J, Berry M. 1972. Ontogeny of interhemispheric evoked potentials in the rat: significance of myelination of the corpus callosum. *Experimental neurology* 35: 215-32

Sherman DL, Brophy PJ. 2005. Mechanisms of axon ensheathment and myelin growth. *Nat Rev Neurosci* 6: 683-90

Sidman RL, Conover CS, Carson JH. 1985. Shiverer gene maps near the distal end of chromosome 18 in the house mouse. *Cytogenet Cell Genet* 39: 241-5

References

Silver J, Miller JH. 2004. Regeneration beyond the glial scar. *Nat Rev Neurosci* 5: 146-56

Simons M, Trajkovic K. 2006. Neuron-glia communication in the control of oligodendrocyte function and myelin biogenesis. *J Cell Sci* 119: 4381-9

Simons R, Alon N, Riordan JR. 1987. Human myelin DM-20 proteolipid protein deletion defined by cDNA sequence. *Biochemical and biophysical research communications* 146: 666-71

Simpson PB, Armstrong RC. 1999. Intracellular signals and cytoskeletal elements involved in oligodendrocyte progenitor migration. *Glia* 26: 22-35

Sobottka B, Ziegler U, Kaech A, Becher B, Goebels N. 2011. CNS live imaging reveals a new mechanism of myelination: The liquid croissant model. *Glia*

Sofroniew MV, Vinters HV. 2010. Astrocytes: biology and pathology. *Acta Neuropathol* 119: 7-35

Sommer I, Schachner M. 1981. Monoclonal antibodies (O1 to O4) to oligodendrocyte cell surfaces: an immunocytological study in the central nervous system. *Dev Biol* 83: 311-27

Sommer I, Schachner M. 1982. Cell that are O4 antigen-positive and O1 antigen-negative differentiate into O1 antigen-positive oligodendrocytes. *Neuroscience letters* 29: 183-8

Sorensen A, Moffat K, Thomson C, Barnett SC. 2008. Astrocytes, but not olfactory ensheathing cells or Schwann cells, promote myelination of CNS axons in vitro. *Glia* 56: 750-63

Spassky N, de Castro F, Le Bras B, Heydon K, Queraud-LeSaux F, et al. 2002. Directional guidance of oligodendroglial migration by class 3 semaphorins and netrin-1. *J Neurosci* 22: 5992-6004

Steinman L, Martin R, Bernard C, Conlon P, Oksenberg JR. 2002. Multiple sclerosis: deeper understanding of its pathogenesis reveals new targets for therapy. *Annu Rev Neurosci* 25: 491-505

Stevens B, Porta S, Haak LL, Gallo V, Fields RD. 2002. Adenosine: a neuron-glial transmitter promoting myelination in the CNS in response to action potentials. *Neuron* 36: 855-68

Storts RW, Koestner A. 1969. Development and characterization of myelin in tissue culture of canine cerebellum. *Zeitschrift fur Zellforschung und mikroskopische Anatomie* 95: 9-18

References

Suetsugu S, Yamazaki D, Kurisu S, Takenawa T. 2003. Differential roles of WAVE1 and WAVE2 in dorsal and peripheral ruffle formation for fibroblast cell migration. *Dev Cell* 5: 595-609

Sugaya K. 2005. Possible use of autologous stem cell therapies for Alzheimer's disease. *Curr Alzheimer Res* 2: 367-76

Suzuki M, Raisman G. 1994. Multifocal pattern of postnatal development of the macroglial framework of the rat fimbria. *Glia* 12: 294-308

Svoboda K, Yasuda R. 2006. Principles of two-photon excitation microscopy and its applications to neuroscience. *Neuron* 50: 823-39

Tait S, Gunn-Moore F, Collinson JM, Huang J, Lubetzki C, et al. 2000. An oligodendrocyte cell adhesion molecule at the site of assembly of the paranodal axo-glial junction. *J Cell Biol* 150: 657-66

Talbott JF, Cao Q, Bertram J, Nkansah M, Benton RL, et al. 2007. CNTF promotes the survival and differentiation of adult spinal cord-derived oligodendrocyte precursor cells in vitro but fails to promote remyelination in vivo. *Experimental neurology* 204: 485-9

Taveggia C, Zanazzi G, Petrylak A, Yano H, Rosenbluth J, et al. 2005. Neuregulin-1 type III determines the ensheathment fate of axons. *Neuron* 47: 681-94

Thomson CE, Hunter AM, Griffiths IR, Edgar JM, McCulloch MC. 2006. Murine spinal cord explants: a model for evaluating axonal growth and myelination in vitro. *J Neurosci Res* 84: 1703-15

Thomson CE, McCulloch M, Sorenson A, Barnett SC, Seed BV, et al. 2008. Myelinated, synapsing cultures of murine spinal cord--validation as an in vitro model of the central nervous system. *The European journal of neuroscience* 28: 1518-35

Thurnherr T, Benninger Y, Wu X, Chrostek A, Krause SM, et al. 2006. Cdc42 and Rac1 signaling are both required for and act synergistically in the correct formation of myelin sheaths in the CNS. *J Neurosci* 26: 10110-9

Timsit SG, Bally-Cuif L, Colman DR, Zalc B. 1992. DM-20 mRNA is expressed during the embryonic development of the nervous system of the mouse. *J Neurochem* 58: 1172-5

Trajkovic K, Dhaunchak AS, Goncalves JT, Wenzel D, Schneider A, et al. 2006. Neuron to glia signaling triggers myelin membrane exocytosis from endosomal storage sites. *J Cell Biol* 172: 937-48

References

Trapp BD, Nishiyama A, Cheng D, Macklin W. 1997. Differentiation and death of premyelinating oligodendrocytes in developing rodent brain. *J Cell Biol* 137: 459-68

Tress O, Maglione M, Zlomuzica A, May D, Dicke N, et al. 2011. Pathologic and phenotypic alterations in a mouse expressing a connexin47 missense mutation that causes Pelizaeus-Merzbacher-like disease in humans. *PLoS Genet* 7: e1002146

Tsai HH, Frost E, To V, Robinson S, Ffrench-Constant C, et al. 2002. The chemokine receptor CXCR2 controls positioning of oligodendrocyte precursors in developing spinal cord by arresting their migration. *Cell* 110: 373-83

Tsien RY. 1998. The green fluorescent protein. *Annu Rev Biochem* 67: 509-44

Tyler WA, Gangoli N, Gokina P, Kim HA, Covey M, et al. 2009. Activation of the mammalian target of rapamycin (mTOR) is essential for oligodendrocyte differentiation. *J Neurosci* 29: 6367-78

Udvadia AJ, Koster RW, Skene JH. 2001. GAP-43 promoter elements in transgenic zebrafish reveal a difference in signals for axon growth during CNS development and regeneration. *Development* 128: 1175-82

Ullian EM, Sapperstein SK, Christopherson KS, Barres BA. 2001. Control of synapse number by glia. *Science* 291: 657-61

Uzman BG. 1964. The Spiral Configuration of Myelin Lamellae. *Journal of ultrastructure research* 11: 208-12

van Diepen MT, Eickholt BJ. 2008. Function of PTEN during the formation and maintenance of neuronal circuits in the brain. *Dev Neurosci* 30: 59-64

Wake H, Lee PR, Fields RD. 2011. Control of local protein synthesis and initial events in myelination by action potentials. *Science* 333: 1647-51

Wang Z, Colognato H, Ffrench-Constant C. 2007. Contrasting effects of mitogenic growth factors on myelination in neuron-oligodendrocyte co-cultures. *Glia* 55: 537-45

Warrington AE, Pfeiffer SE. 1992. Proliferation and differentiation of O4+ oligodendrocytes in postnatal rat cerebellum: analysis in unfixed tissue slices using anti-glycolipid antibodies. *J Neurosci Res* 33: 338-53

Watkins TA, Emery B, Mulinyawe S, Barres BA. 2008. Distinct stages of myelination regulated by gamma-secretase and astrocytes in a rapidly myelinating CNS coculture system. *Neuron* 60: 555-69

Waxman SG, Black JA. 1985. Membrane structure of vesiculotubular complexes in developing axons in rat optic nerve: freeze-fracture evidence for sequential

References

membrane assembly. *Proceedings of the Royal Society of London. Series B, Containing papers of a Biological character. Royal Society* 225: 357-63

Webster HD. 1971. The geometry of peripheral myelin sheaths during their formation and growth in rat sciatic nerves. *J Cell Biol* 48: 348-67

Werner HB, Jahn O. 2010. Myelin matters: proteomic insights into white matter disorders. *Expert Rev Proteomics* 7: 159-64

Werner HB, Kuhlmann K, Shen S, Uecker M, Schardt A, et al. 2007. Proteolipid protein is required for transport of sirtuin 2 into CNS myelin. *J Neurosci* 27: 7717-30

Williams A, Piaton G, Lubetzki C. 2007. Astrocytes--friends or foes in multiple sclerosis? *Glia* 55: 1300-12

Williams RW, Bastiani MJ, Lia B, Chalupa LM. 1986. Growth cones, dying axons, and developmental fluctuations in the fiber population of the cat's optic nerve. *The Journal of comparative neurology* 246: 32-69

Windrem MS, Nunes MC, Rashbaum WK, Schwartz TH, Goodman RA, et al. 2004. Fetal and adult human oligodendrocyte progenitor cell isolates myelinate the congenitally dysmyelinated brain. *Nat Med* 10: 93-7

Windrem MS, Schanz SJ, Guo M, Tian GF, Washco V, et al. 2008. Neonatal chimerization with human glial progenitor cells can both remyelinate and rescue the otherwise lethally hypomyelinated shiverer mouse. *Cell Stem Cell* 2: 553-65

Winterstein C, Trotter J, Kramer-Albers EM. 2008. Distinct endocytic recycling of myelin proteins promotes oligodendroglial membrane remodeling. *J Cell Sci* 121: 834-42

Wolswijk G, Noble M. 1992. Cooperation between PDGF and FGF converts slowly dividing O-2Aadult progenitor cells to rapidly dividing cells with characteristics of O-2Aperinatal progenitor cells. *J Cell Biol* 118: 889-900

Wood P, Okada E, Bunge R. 1980. The use of networks of dissociated rat dorsal root ganglion neurons to induce myelination by oligodencrocytes in culture. *Brain research* 196: 247-52

Wood PM, Bunge RP. 1986a. Evidence that axons are mitogenic for oligodendrocytes isolated from adult animals. *Nature* 320: 756-8

Wood PM, Bunge RP. 1986b. Myelination of cultured dorsal root ganglion neurons by oligodendrocytes obtained from adult rats. *Journal of the neurological sciences* 74: 153-69

References

Wood PM, Williams AK. 1984. Oligodendrocyte proliferation and CNS myelination in cultures containing dissociated embryonic neuroglia and dorsal root ganglion neurons. *Brain research* 314: 225-41

Wu E, Raine CS. 1992. Multiple sclerosis. Interactions between oligodendrocytes and hypertrophic astrocytes and their occurrence in other, nondemyelinating conditions. *Lab Invest* 67: 88-99

Wu H, Feng W, Chen J, Chan LN, Huang S, Zhang M. 2007. PDZ domains of Par-3 as potential phosphoinositide signaling integrators. *Mol Cell* 28: 886-98

Yamada M, Ivanova A, Yamaguchi Y, Lees MB, Ikenaka K. 1999. Proteolipid protein gene product can be secreted and exhibit biological activity during early development. *J Neurosci* 19: 2143-51

Ye F, Chen Y, Hoang T, Montgomery RL, Zhao XH, et al. 2009. HDAC1 and HDAC2 regulate oligodendrocyte differentiation by disrupting the beta-catenin-TCF interaction. *Nat Neurosci* 12: 829-38

Yoshida M, Macklin WB. 2005. Oligodendrocyte development and myelination in GFP-transgenic zebrafish. *J Neurosci Res* 81: 1-8

Zeller R. 2001. Fixation, embedding, and sectioning of tissues, embryos, and single cells. *Curr Protoc Mol Biol* Chapter 14: Unit 14 1

Zhang H, Jarjour AA, Boyd A, Williams A. 2011. Central nervous system remyelination in culture--a tool for multiple sclerosis research. *Experimental neurology* 230: 138-48

Zhang SC, Lipsitz D, Duncan ID. 1998a. Self-renewing canine oligodendroglial progenitor expanded as oligospheres. *J Neurosci Res* 54: 181-90

Zhang SC, Lundberg C, Lipsitz D, O'Connor LT, Duncan ID. 1998b. Generation of oligodendroglial progenitors from neural stem cells. *J Neurocytol* 27: 475-89

Zhao X, He X, Han X, Yu Y, Ye F, et al. 2010. MicroRNA-mediated control of oligodendrocyte differentiation. *Neuron* 65: 612-26

Zipfel WR, Williams RM, Webb WW. 2003. Nonlinear magic: multiphoton microscopy in the biosciences. *Nat Biotechnol* 21: 1369-77

Zonta B, Tait S, Melrose S, Anderson H, Harroch S, et al. 2008. Glial and neuronal isoforms of Neurofascin have distinct roles in the assembly of nodes of Ranvier in the central nervous system. *J Cell Biol* 181: 1169-77